

# Oil & Natural Gas Technology

DOE Award No.: DE-FC26-04NT15516

## Final Scientific/Technical Report

### Evaluating the Influence of Pore Architecture and Initial Saturation on Wettability and Relative Permeability in Heterogeneous, Shallow-Shelf Carbonates

Submitted by:  
University of Kansas Center for Research, Inc.  
2385 Irving Hill Road  
Lawrence, KS 66044

Prepared for:  
United States Department of Energy  
National Energy Technology Laboratory

September 6, 2011



Office of Fossil Energy

***Solicitation Number: DE-PS26-04NT15450-4C***  
***Subtopic Area: 2C- Reservoir Characterization and Management***

***U.S. DOE Contract Number: DE-FC26-04NT15516***

***University of Kansas Center for Research, Inc.  
and the Kansas Geological Survey  
2385 Irving Hill Road  
Lawrence, KS 66044-7552***

***Technical Point of Contact - Alan P. Byrnes  
voice: 785-864-3965, Fax: 785-864-5317, e-mail: [apbyrnes@cox.net](mailto:apbyrnes@cox.net)  
Budgetary/Contractual Point of Contact- Tracie Watkins  
voice: 785-864-7288, Fax: 785-864-5025, e-mail: [twatkins@ku.edu](mailto:twatkins@ku.edu)***

***Title of Project:***

***Evaluating the Influence of Pore Architecture and Initial Saturation on  
Wettability and Relative Permeability in Heterogeneous, Shallow-Shelf  
Carbonates***

***University of Kansas-Kansas Geological Survey*  
*Alan P. Byrnes (Principal Investigator)*  
*Saibal Bhattacharya (co-investigator)***

***Murfin Drilling Company*  
*James R. Daniels***

***Supporting Team Members:***

***Kansas Geological Survey– John Victorine, Ken Stalder***

**ACKNOWLEDGMENT:**

This material is based upon work support by the Department of Energy (National Energy Technology Laboratory) under Contract Number DE-FC26-04NT15516.

**DISCLAIMER:**

This report was prepared as an account of work sponsored by an agency of the United States Government. Neither the United States Government nor any agency thereof, nor any of their employees, makes any warranty, express or implied, or assumes any legal liability or responsibility for the accuracy, completeness, or usefulness of any information, apparatus, product, or process disclosed, or represents that its use would not infringe privately owned rights. Reference herein to any specific commercial product, process, or service by trade name, trademark, manufacturer, or otherwise does not necessarily constitute or imply its endorsement, recommendation, or favoring by the United States Government or any agency thereof. The views and opinions of authors herein do not necessarily state or reflect those of the United States Government or any agency thereof.

# TABLE OF CONTENTS

DISCLAIMER .....	i
TABLE OF CONTENTS .....	ii
LIST OF TABLES .....	v
LIST OF FIGURES .....	v
LIST OF ACRONYMS .....	x
EXECUTIVE SUMMARY .....	xiii
INTRODUCTION .....	1
I.1 Statement of Problem .....	1
I.2 Study Objectives.....	1
I.3 Participants .....	2
I.4 Importance of Moldic, Transition-Zone Reservoirs .....	3
RESULTS AND DISCUSSION .....	6
1.0 Rock, Oil, and Wettability Properties .....	6
1.1 Oil Characterization.....	6
1.2 Wettability .....	19
1.2.1 Laboratory Method .....	20
1.2.2 Crude Oil Wettability .....	21
1.2.3 Isopar G Oil Wettability .....	25
1.3 Porosity and Permeability .....	26
1.3.1 Lansing-Kansas City .....	26
1.3.2 Mississippian.....	34
1.3.3 Arbuckle .....	42
1.4 Capillary Pressure .....	48
1.4.1 Capillary Pressure Measurement Methods .....	48
1.4.1.1 Mercury Injection Capillary Pressure Methods .....	48
1.4.1.2 Air-Brine Capillary Pressure Methods .....	48
1.4.2 Capillary Pressure Results .....	49
1.4.3 Capillary Pressure Model.....	66
1.5 Electrical Properties.....	68
1.5.1 Experimental Method.....	68
1.5.2 Results.....	68
1.5.2.1 Arbuckle .....	68
1.5.2.2 Mississippian.....	70
1.5.2.3 Lansing-Kansas City .....	71
1.5.2.4 Vertical Cementation Exponent Distribution .....	73
1.5.3 Thin-Bed Resistivity Log Issues .....	75
1.6 Relative Permeability.....	82
1.6.1 Experimental Methods .....	82
1.6.2 Results.....	82
2.0 Relative Permeability and Modeling .....	90
2.1 Introduction.....	90
2.2 Reservoir Geology .....	91
2.3 Core-Analysis Methodology.....	93
2.3.1 Porosity, Permeability, and Capillary Pressure .....	93

2.4 Residual Oil Saturation to Waterflood .....	98
2.5 Relative Permeability.....	106
2.6 Conclusions.....	110
3.0 Theoretical Geomodels .....	111
3.1 Overview	111
3.2 Key Findings.....	111
3.3 Geologic Setting .....	112
3.4 Rock Properties for General Model .....	113
3.4.1 Mississippian Lithofacies, Permeability, and Porosity .....	113
3.5 Comparison Among Flow Simulation Models .....	118
3.5.1 Predicted Oil Recovery .....	118
3.5.2 Predicted Water Recovery .....	125
3.6 Vertical Scaling of Water Saturation.....	132
3.7 Predicted Cumulative Water/Oil Ratio .....	136
3.8 Perforation Criteria and Upscaled Models .....	138
3.9 Upscaled System Response .....	143
3.10 Scaling of Transition Zone Effects with Permeability and Capillary Pressure .....	147
4.0 Reservoir Simulation .....	149
4.1 Lansing-Kansas City.....	149
4.1.1 Terry Unit #7-32.....	149
4.1.2 Austin #2-27.....	157
4.2 Arbuckle 161	
4.2.1 Hadley L#4.....	161
4.2.2 Keja #1-3.....	171
5.0 Coring the Lansing-Kansas City and Arbuckle .....	181
5.1 Lansing-Kansas City Core: Austin 2-27 .....	181
5.1.1 Well Location, Drilling and Testing.....	181
5.1.2 Core Description.....	206
5.1.3 Routine Core Analysis .....	208
5.1.4 Electrical Properties .....	212
5.1.5 Capillary Pressure Properties .....	215
5.2 Arbuckle Core: Keja #1-3, Hadlew Field .....	220
5.2.1 Well Location, Drilling and Testing.....	220
5.2.2 Core Description .....	228
5.2.3 Routine Core Analysis .....	230
REFERENCES .....	235

## ***LIST OF TABLES***

Table 1-1 Lansing-Kansas City, Mississippian, and Arbuckle crude oil sampled .....	7
Table 1-2 Summary statistics for oil properties .....	8
Table 1-3 Coefficients for equation 1-15 expressing power-law relationship .....	35
Table 2-1 Potential total oil recover from Mississippian reservoirs .....	105
Table 3-1 Summary of cumulative oil at 40 years for various models .....	124
Table 3-2 Summary of cumulative water at 40 years for various models.....	131
Table 4-1 Summary of core analysis for Murfin Terry Unit #7-32 .....	154
Table 5-1 Summary of core analysis porosity, permeability and grain density .....	208
Table 5-2 Summary of Archie porosity exponent measurements .....	213
Table 5-3 Mercury injection capillary pressure analysis for Austin #2-27, 2921.7 ft .....	216
Table 5-4 Mercury injection capillary pressure analysis for Austin #2-27, 2926.1 ft .....	218
Table 5-5 Summary of core analysis porosity, permeability and grain density for the Keja #1-3 Arbuckle interval core .....	231

## ***LIST OF FIGURES***

Figure I-1 Map of Kansas showing Central Kansas Uplift .....	3
Figure I-2 Location of Lansing-Kansas City Group oil production .....	4
Figure I-3 Location of Mississippian formation oil production.....	4
Figure I-4 Location of Arbuckle Group oil production .....	5
Figure I-5 Kansas cumulative oil by formation .....	5
Figure 1-1 Distribution of API gravity for eastern Kansas oils from the Lansing- Kansas City .....	8
Figure 1-2 Distribution of API gravity for eastern Kansas oils from the Mississippian.....	9
Figure 1-3 Distribution of API gravity for eastern Kansas oils from the Arbuckle .....	10
Figure 1-4 Distribution of viscosity for eastern Kansas oils from the Lansing-Kansas City .....	11
Figure 1-5 Distribution of viscosity for eastern Kansas oils from the Mississippian.....	12
Figure 1-6 Distribution of viscosity for eastern Kansas oils from the Arbuckle .....	13
Figure 1-7 Distribution of oil-water interfacial tension in the Lansing-Kansas City .....	14
Figure 1-8 Distribution of oil-water interfacial tension in the Mississippian .....	15
Figure 1-9 Distribution of oil-water interfacial tension in the Arbuckle .....	16
Figure 1-10 Crossplot of measured oil viscosity at 100°F for eastern Kansas oils .....	17
Figure 1-11 Crossplot of measured oil viscosity at 60°F for eastern Kansas oils .....	18
Figure 1-12 Amott-Harvey wettability index distribution .....	23
Figure 1-13 Crossplot of Amott-Harvey wettability index versus permeability.....	24
Figure 1-14 Amott-Harvey wettability index distribution for cores and Isopar G oil .....	25
Figure 1-15 Crossplot of in situ Klinkenberg permeability versus porosity .....	28

Figure 1-16 Crossplot of in situ Klinkenberg permeability versus textural property .....	29
Figure 1-17 Porosity, permeability, and rock texture profile for Carter-Colliver #CO2-1 .....	29
Figure 1-18 Porosity, permeability, and rock texture profile for Murfin Austin #2-27 .....	30
Figure 1-19 Porosity, permeability, and rock texture profile for Woodward 32 .....	31
Figure 1-20 Crossplot of porosity and permeability for Bethany Falls outcrop wells.....	31
Figure 1-21 Interval near top of Bethany Falls exhibiting highly porous and permeable grainstone .....	32
Figure 1-22 Interval near top of Bethany Falls, well-sorted oomoldic grainstone .....	33
Figure 1-23 Crossplot of in situ Klinkenberg permeability versus porosity for all Mississippian core plugs .....	36
Figure 1-24 Permeability versus porosity crossplot for various lithofacies in Mississippian .....	37
Figure 1-25 Crossplot of permeability versus porosity for Mississippian rocks from Bindley field.....	38
Figure 1-26 Crossplot of permeability versus porosity for Mississippian rocks from Ness field.....	39
Figure 1-27 Crossplot of permeability versus porosity for Mississippian rocks from Schaben field.....	40
Figure 1-28 Graph of permeability versus porosity for different lithofacies from Cheyenne wells Champlin Aldrich 3 and Klepper 4.....	41
Figure 1-29 Crossplot of core plug permeability versus porosity for Arbuckle dolomites .....	44
Figure 1-30 Crossplot of permeability versus porosity for all Arbuckle core plugw .....	45
Figure 1-31 Lithologic vertical heterogeneity and cyclicity of Arbuckle bedding .....	46
Figure 1-32 Vertical permeability profiles for Hadley L#4 and Keja 31-3 .....	47
Figure 1-33 Air-mercury capillary pressure curves for Lansing-Kansas City samples .....	53
Figure 1-34 Air-mercury capillary pressure curves for Mississippian samples.....	54
Figure 1-35 Air-mercury capillary pressure curves for Lansing-Kansas City samples in oil column height below 60 ft .....	55
Figure 1-36 Air-mercury capillary pressure curves for Mississippian samples in oil column height below 60 ft .....	56
Figure 1-37 Air-mercury capillary pressure curves for Lansing-Kansas City samples showing general logSw-logH linear relationship .....	57
Figure 1-38 Air-mercury capillary pressure curves for Lansing-Kansas City samples showing general logSw-logH linear relationship below 60-ft oil-brine level .....	58
Figure 1-39 Air-mercury capillary pressure curves for Mississippian samples showing general logSw-logH linear relationship .....	59
Figure 1-40 Air-mercury capillary pressure curves for Mississippian samples showing general logSw-logH linear relationship below 60-ft oil-brine level .....	60
Figure 1-41 Crossplot of principal pore throat diameter versus permeability .....	61
Figure 1-42 Crossplot of wetting-phase saturation by air-Hg (120 psi) and air-brine (24 psi) ....	62
Figure 1-43 Crossplot of wetting-phase saturation by air-Hg (350 psi) and air-brine (70 psi) ....	63
Figure 1-44 Crossplot of wetting-phase saturation by air-Hg (95 psi) and air-brine (20 psi) .....	64
Figure 1-45 Crossplot of wetting-phase saturation by air-Hg (350 psi) and air-brine (70 psi) for Lansing-Kansas City .....	65
Figure 1-46 Measured and modeled capillary pressure curves.....	67
Figure 1-47 Crossplot of in situ Archie cementation exponent versus porosity for Arbuckle.....	69
Figure 1-48 Crossplot of in situ Archie cementation exponent versus porosity for Mississippian.....	70

Figure 1-49 Crossplot of in situ Archie cementation exponent versus porosity for Lansing-Kansas City .....	72
Figure 1-50 Vertical profile of cementation in five Lansing-Kansas City wells .....	74
Figure 1-51 Histogram of Lansing-Kansas City interval with porosity >8% .....	76
Figure 1-52 Histogram of Lansing-Kansas City interval with porosity >20% .....	77
Figure 1-53 Crossplot of estimated gross thickness of Lansing-Kansas City interval and net thickness of interval with $\phi > 8\%$ .....	77
Figure 1-54 Calculated resistivity tool response, $R_t$ , as a function of the reservoir interval bed thickness, tool vertical resolution, for reservoir and bounding bed properties .....	78
Figure 1-55 Calculated water saturations for $R_t$ readings shown in fig. 1-54 .....	79
Figure 1-56 Calculated water saturations for a 2-ft-thick bed for three conditions .....	80
Figure 1-57 General workflow for quantitative, semi-quantitative, and qualitative estimation ...	81
Figure 1-58 Mississippian rock drainage oil relative permeability versus absolute permeability	84
Figure 1-59 Mississippian rock drainage oil relative permeability versus 24 psi air-brine pressure .....	85
Figure 1-60 Lansing-Kansas City rock drainage oil relative permeability versus absolute permeability .....	86
Figure 1-61 Lansing-Kansas City rock drainage oil relative permeability versus 24 psi air-brine capillary pressure .....	87
Figure 1-62 Composite of Mississippian imbibition oil-water relative permeability curve .....	88
Figure 1-63 Composite of Lansing-Kansas City imbibition oil-water relative permeability curves .....	89
Figure 2-1 Thin-section photomicrographs of two example Mississippian lithologies .....	92
Figure 2-2 Thin-section photomicrograph of typical Lansing-Kansas City limestone .....	93
Figure 2-3 Permeability versus porosity crossplot for various Mississippian lithologies .....	94
Figure 2-4 Permeability versus porosity crossplot for Lansing-Kansas City limestones .....	95
Figure 2-5 Measured and modeled capillary pressure curves .....	97
Figure 2-6 Crossplot of trapping Characteristic versus porosity .....	99
Figure 2-7 Crossplot of Sorw versus Soi for Mississippian and Lansing-Kansas City .....	100
Figure 2-8 Lansing-Kansas City oomoldic limestone measured and predicted .....	101
Figure 2-9 Comparison of potentially recoverable saturation .....	102
Figure 2-10 Difference in recoverable saturation for model .....	103
Figure 2-11 Difference between recoverable oil where saturation difference applied .....	104
Figure 2-12 Imbibition oil and water relative permeability curves .....	105
Figure 2-13 kro curves at different heights above free water level .....	108
Figure 2-14 Comparing kro curves for kro calculated using Sorwmax and kro calculated using Sorw(Soi) .....	109
Figure 3-1 Cross section across western flank of Central Kansas Uplift .....	113
Figure 3-2 Example of Mississippian lithofacies-specific permeability-porosity trend .....	115
Figure 3-3 Lithofacies-specific generalized trends for Mississippian rocks .....	116
Figure 3-4 Difference in recoverable saturation for model .....	117
Figure 3-5 Estimated cumulative oil production with time for 40-ft thick, 40-layer model .....	119
Figure 3-6 Estimated cumulative oil production with time for the bottom 20 ft of the model ...	120
Figure 3-7 Estimated cumulative oil production with time for 40-ft thick, 40-layer model for both fixed Sor and variable Sor .....	121
Figure 3-8 Estimated cumulative oil production with time for 40-ft thick model comparing 40-layer model with 4-layer model .....	122

Figure 3-9	Estimated cumulative oil production with time for 40-ft thick, model comparing 40-layer model results using variable Sor (Sorv) compared with 4-layer model results using fixed Sor (Sor <sub>c</sub> ) .....	123
Figure 3-10	Estimated cumulative water production with time for 40-ft thick, 40-layer model.	126
Figure 3-11	Estimated cumulative water production with time for the bottom 20 ft of model ...	127
Figure 3-12	Estimated cumulative water production with time for 40-ft thick, 40-layer model for both fixed Sor and variable Sor .....	128
Figure 3-13	Estimated cumulative water production with time for 40-ft thick model .....	129
Figure 3-14	Estimated cumulative water production with time for 40-ft thick model comparing 40-layer model results .....	130
Figure 3-15	Comparison of ratio of total average water saturation for entire reservoir interval to average saturations .....	134
Figure 3-16	Comparison calculated oil saturation for a 30-mD reservoir .....	135
Figure 3-17	Estimated water/oil ratio with time for 40-ft thick, 40-layer model for reservoir of different permeability .....	136
Figure 3-18	Estimated water/oil ration with time for 40-ft thick model comparing 40-layer model results .....	137
Figure 3-19	Water saturation distribution in 4-layer 120 mD model .....	139
Figure 3-20	Water saturation distribution in 4-layer 30 mD model .....	140
Figure 3-21	Water saturation distribution in 4-layer 7.5 mD model .....	141
Figure 3-22	Water saturation distribution in 40-layer 7.5 MD, 30 mD and 120 mD models .....	142
Figure 3-23	Sequence of saturation states for a reservoir modeled using a single layer and 10 layers .....	145
Figure 3-24	Two cases representing two different oil relative permeability curves .....	146
Figure 3-25	Comparison of generalized capillary pressure curves for the Mississippian and Niobrara in Kansas .....	148
Figure 4-1	Map location of Terry Unit #7-32 well .....	151
Figure 4-2	Standard wireline log analysis of Terry Unit #7-32 .....	152
Figure 4-3	Pickett plot of Terry Unit #7-32 reservoir interval .....	153
Figure 4-4	Permeability-porosity trend for peloidal packstone in Lansing-Kansas City .....	155
Figure 4-5	Estimated cumulative production for the Terry #7-32 .....	156
Figure 4-6	Tech Log dual-compensated porosity log for Austin #2-27 .....	158
Figure 4-7	Tech Log borehole-compensated sonic log for Austin #2-27 .....	158
Figure 4-8	Numerical flow simulation prediction of Austin #2-27 .....	159
Figure 4-9	Flow simulation estimation of potential performance of Austin #2-27 .....	160
Figure 4-10	Location of Hadley L#4 in Bemis-Shutts field .....	162
Figure 4-11	Log analysis of Hadley L#\$ well .....	162
Figure 4-12	Pickett plot analysis of Arbuckle interval in Hadley L#4 .....	163
Figure 4-13	Histogram of Arbuckle Archie cementation exponents .....	164
Figure 4-14	Porosity and permeability profiles showing high frequency cyclicity .....	165
Figure 4-15	Horizontal permeability distribution for Hadley L#4 .....	166
Figure 4-16	Simulation estimate of cumulative gas and oil rate for Hadley L#4 .....	167
Figure 4-17	Simulation estimate of cumulative water and water rate for Hadley L#4, P <sub>i</sub> = 1,500 psi .....	168
Figure 4-18	Simulation estimate of cumulative gas and oil and oil rate for Hadley L#4 .....	169
Figure 4-19	Simulation estimate of cumulative water and water rate for Hadley L#4, P <sub>i</sub> = 700 psi .....	170

Figure 4-20 Dual-compensated porosity log for Hadlew Unit #1-3 .....	173
Figure 4-21 Dual-induction log for the Hadlew Unit #1-3 .....	174
Figure 4-22 Flow simulation estimate of cumulative gas and oil and oil rates for Hadlew #1-3 .	175
Figure 4-23 Flow simulation estimate of cumulative water oil and oil rates for Hadlew #1-3 ....	176
Figure 4-24 Porosity distribution for Keja #1-3 .....	177
Figure 4-25 Horizontal permeability distribution for Keja #1-3 .....	178
Figure 4-26 Flow simulation estimate of cumulative gas and oil and oil rates for Keja #1-3 .....	179
Figure 4-27 FFlow simulation estimate of cumulative water oil and oil rates for Keja #1-3.....	180
Figure 5.1 Location of Murfin Drilling Co. Austin #2-27 .....	182
Figure 5-2 Close-up of location of Murfin Drilling Co. Austin #2-27 .....	183
Figure 5-3 Austin #2-27 core photo for Lansing-Kansas City core.....	207
Figure 5-4 Porosity profile for Austin #2-27.....	209
Figure 5-5 Permeability profile for Austin #2-27 .....	210
Figure 5-6 Comparison of Austin 32-27 permeability-porosity relationship.....	211
Figure 5-7 Pickett plot for Austin #2-27 .....	212
Figure 5-8 Crossplot of formation resistivity factor versus porosity .....	213
Figure 5-9 Crossplot of Archie porosity exponent versus porosity .....	214
Figure 5-10 Comparison of water saturation profiles .....	215
Figure 5-11 Mercury injection derived properties for Austin 32-27, 2921.7 ft .....	217
Figure 5-12 Mercury injection derived properties for Austin 32-27, 2926.1 ft .....	219
Figure 5-13 Location of Murfin Drilling Co. Keja 31-3 Hadlew field .....	221
Figure 5-14 Close-up of location of Murfin Drilling Co. Keja 31-3 Hadlew field .....	222
Figure 5-15 Murfin Keja #1-3 core photo for Arbuckle interval .....	229
Figure 5-16 Porosity profile for the Keja #1-3 through the cored Arbuckle interval .....	232
Figure 5-17 Permeability profile for the Keja #1-3 through the cored Arbuckle interval .....	233
Figure 5-18 Comparison of Keja #1-3 permeability-porosity relationship with other Arbuckle dolomites .....	234

## ***LIST OF ACRONYMS***

***a*** = Archie equation constant, dimensionless  
AAPG = American Association of Petroleum Geologists  
B = Conversion constant for capillary pressure function  
C = Land equation trapping characteristic, dimensionless  
cc = cubic centimeter, cm<sup>3</sup>  
CEC = Cation exchange capacity (mequivalents/liter)  
D = Fractal dimension  
*D* = pore throat diameter (microns)  
DOE = Department of Energy  
*D<sub>te</sub>* = Threshold entry pore diameter (microns)  
E = Euclidean dimension  
***F*** = Fraction of total network sites where gas nucleation occurs  
g = gram  
g/cc = density, gram/cubic centimeters, m/L<sup>3</sup>, g/cc  
GD = grain density (g/cm<sup>3</sup>)  
GUI = graphical user interface  
***H*** = height, L, feet  
Hg = mercury  
***H<sub>te</sub>*** = Threshold entry gas column height (ft)  
***K*** = Permeability, mD  
K = thousands, x1000  
KGS = Kansas Geological Survey  
kPa = Kilo Pascal, 1 kPa = 0.001 MPa =  
k = permeability, L<sup>2</sup>, md  
***k<sub>ik</sub>*** = *in situ* Klinkenberg permeability, millidarcies  
***k<sub>mk</sub>*** = geometric mean of *in situ* and routine Klinkenberg permeability (mD)  
***k<sub>rg</sub>*** = Relative permeability to gas, fraction (v/v)  
***k<sub>rg,S<sub>w</sub></sub>*** = Relative permeability to gas at a specific water saturation *S<sub>w</sub>*, fraction (v/v)  
KU = University of Kansas  
KUCR = University of Kansas Center for Research, Inc.  
KUEC = University of Kansas Energy Research Center  
L = Network size, number of nodes  
ln = natural logarithm  
log *R<sub>w<sub>x</sub></sub>* = log10 of resistivity of brine at salinity X  
log *R<sub>w<sub>40K</sub></sub>* = log10 of resistivity of 40K ppm NaCl = 0.758.  
***m*** = Archie cementation (porosity) exponent, (dimensionless)  
***m<sub>1</sub>*** = matrix porosity exponent  
***m<sub>2</sub>*** = fracture or touching vug porosity exponent  
***m<sub>40K</sub>*** = Archie porosity exponent at 40,000 ppm NaCl,  
mD = millidarcy, 1 mD = 9.87x10<sup>-4</sup> μm<sup>2</sup>  
MDCI = Murfin Drilling Company, Inc.  
MICP = mercury intrusion capillary pressure  
MPa = Mega Pascal, 1 MPa = 1000 kPa =  
***m<sub>x</sub>*** = ***m*** at salinity X

$n$  = Archie saturation exponent, dimensionless  
 n = number  
 NaCl = sodium chloride  
 NCS = net confining stress  
 NETL = National Energy Technology Laboratory  
 NMR = nuclear magnetic resonance  
 $^{\circ}\text{F}$  = temperature degrees Fahrenheit  
 $P$  = pressure,  $\text{m}/\text{L}^2$ , psi  
 $P$  = average net effective confining pressure (psi)  
 $P_c$  = capillary pressure, psia  
 $P_{ce}$  = Threshold capillary entry pressure,  $\text{m}/\text{L}^2$ , psi  
 $P_{cf}$  = Capillary pressure slope function, dimensionless  
 $P_{c_{lab}}$  = laboratory-measured capillary pressure (psia)  
 $P_{c_{res}}$  = capillary pressure (psia) at reservoir conditions  
 pdf = Adobe Acrobat portable document file  
 ppm = parts per million  
 PTTC = Petroleum Technology Transfer Council  
 PPTD = Principal pore throat diameter  
 psi = pound per square inch, 1 psi = 6.89 kPa = 0.00689 MPa  
 psia = pound per square inch absolute  
 $P_{te}$  = Capillary pressure threshold entry pressure, psi  
 $P_{te}$  = threshold entry pressure, psi  
 RBO = reservoir barrels of oil  
 $R_o$  = resistivity of brine saturated rock,  $\text{ohm}\cdot\text{m}^2/\text{m}$   
 $R_w$  = resistivity of brine,  $\text{ohm}\cdot\text{m}^2/\text{m}$   
 $S$  = saturation, fraction or percent  
 scc = standard cubic centimeter  
 $S_{nwc}$  = critical non-wetting phase saturation  
 $S_{nwi}$  = initial non-wetting phase saturation  
 $S_{nwi}$  = non-wetting saturation initial, fractional percent of pore volume  
 $S_{nwr}$  = non-wetting saturation residual to imbibition, fractional percent of pore volume  
 SPE = Society of Petroleum Engineers  
 $S_w$  = Water (or more generally wetting phase) saturation, fraction (v/v) or percent depending on context  
 $S_{wc}$  = Critical water saturation, fraction (v/v), saturation below which  $k_{rw} = 0$   
 $S_{wirr}$  = “irreducible” wetting phase saturation  
 $S_{wirr}$  = “irreducible” wetting saturation, fraction of pore volume  
 Tcf = trillion cubic feet  
 USDOE = United States Department of Energy  
 USEIA = United States Energy Information Administration  
 $V$  = System volume (v)  
 XML = Extensible Mark-up Language  
  
 $\beta$  = pore volume compressibility ( $10^{-6}/\text{psi}$ )  
 $\beta_0$  = linear regression intercept  
 $\beta_1$  = linear regression slope  
 $\phi$  = porosity, percent or fraction of bulk volume depending on context

$\phi_1$  = matrix porosity  
 $\phi_2$  = fracture or touching vug porosity  
 $\sigma$  = interfacial tension (dyne/cm)  
 $\theta$  = contact angle, degrees

***Subscripts***

gr = residual gas to wetting phase  
gi = initial gas  
o = oil  
oi = initial oil  
oih = initial oil saturation at height  $h$   
oimax = initial oil maximum  
or = residual oil to waterflood  
ormax = maximum residual oil to waterflood  
ro = relative to oil  
rw = relative to water  
w = water  
wc = critical water  
wirr = “irreducible” water

***SI Metric Conversion Factors***

md x 9.869 233 E-04 =  $\mu\text{m}^2$   
psi x 6.894 757 E-03 = MPa

## EXECUTIVE SUMMARY

Thin (1-10 m thick), heterogeneous, shallow-shelf carbonates of the Arbuckle (Arb), Mississippian (Miss), and Lansing-Kansas City (L-KC) formations in Kansas account for over 73% of the 6.3 BBO cumulative oil produced over the last century. For these reservoirs basic petrophysical properties (e.g., porosity, absolute permeability, capillary pressure, residual oil saturation to waterflood, resistivity, and relative permeability) vary significantly horizontally, vertically, and with scale of measurement. Many of these reservoirs produce from structures of less than 30-60 ft (10-20 m), and exhibit vertical variation in initial saturations and relative permeability properties. Being located in the capillary pressure transition zone, these reservoirs exhibit vertically variable initial saturations and relative permeability properties. Rather than being simpler to model because of their small size, these reservoirs challenge characterization and simulation methodology and illustrate issues that are less apparent in larger reservoirs where transition zone effects are minor and most of the reservoir is at saturations near “irreducible” water saturation. Understanding how capillary pressure properties change with rock lithology and, in turn, within transition zones, how relative permeability and residual oil saturation to waterflood change through the transition zone is critical to successful reservoir management as reservoirs mature and enhanced recovery methods are planned and implemented.

Major aspects of the proposed study involve a series of tasks to measure data to reveal the nature of how wettability, drainage and imbibition oil-water relative permeability, capillary pressure, and electrical properties change with pore architecture and initial water saturation. A second goal is to utilize the data to model shallow shelf carbonate reservoirs and to explore how the properties observed influence reservoir production in transition zone environments. Tasks involved collection of oil and rock samples from carbonate fields around the state (Task 1). Basic properties of the rocks and oils were measured. Comparison was performed between crude and synthetic oil wettability and evaluation made of how wettability is influenced by pore architecture (Task 2). Drainage and imbibition oil-water relative permeabilities were measured on rocks representing the range of porosity, permeability, and lithofacies (Task 3). New petrophysical models were developed and used to construct theoretical reservoir architecture models and geomodels for both analysis of the nature of production in transition zone environments for “type” reservoir architectures and for two reservoirs previously simulated using simpler models (Task 4). Using the theoretical and real geomodels, coring locations in a Lansing-Kansas City and Arbuckle field were selected (task 5). In these fields cores were obtained, analyzed, and evaluated within the context of the geomodels (Task 6). A technology transfer program for data and findings included providing data through a web-based database, publication, and talks given a several professional organization meetings.

Analysis of preserved oil samples collected from 31 wells across western Kansas indicates that oils from the L-KC (n = 34), Miss (n = 53) and Arb (n = 30) average 39 API, 36 API, and 35 API and these western and eastern Kansas oils are statistically similar. Utilizing an empirical relationship developed from previous work oil-water interfacial tension (@60oF) averages 31+1 dyne/cm (error represents 1 standard deviation). Utilizing a selection of these oils with core plugs from the three formations, Amott wettability tests indicate that the Arb and Miss exhibit neutral wettability and that the LKC can be characterized as exhibiting low intermediate oil-wetness. Testing using an isoparaffinic oil indicated similar wettability results.

Porosity and permeability data were compiled from previous work at the Kansas Geological Survey and loaded into a new Rock Catalog database for public access. To supplement these data new cores from wells in the L-KC (n = 7), Miss (n = 2) and Arb (n = 1) were analyzed in addition to the two new cores obtained in the study fields. These data provide the basis for robust permeability-po-

rosity trend relationships. Trends for all three formations exhibit variance in permeability at any given porosity of approximately a factor of 2-2.5 orders of magnitude. They also show that knowledge of lithofacies significantly improves predictive accuracy. Lithofacies-specific porosity-permeability relationships were examined and improved. Of perhaps greater importance, vertical porosity and permeability profiles in the Arb and L-KC wells were analyzed. In the Arbuckle the highly cyclic nature of the peritidal sequences results in similar high frequency cyclicity of high and low porosity and permeability intervals on a scale of 0.1-3 m. In the L-KC the relation between permeability (0.001-400 md) and porosity (0-34%) is significantly influenced by the connectivity of the oomoldic pores complicating the use of porosity as an effective predictor of permeability without information about lithology. The nature of the lithology and the permeability porosity relationship changes vertically through beds as thin as 2-3 m. Of equal importance, work in this study reveals that in the L-KC the Archie cementation exponent ( $m$ ), used in wireline resistivity log analysis, exhibits significant vertical change over bed thickness ( $2 < m < 5$ ). A new relationship between cementation exponent and porosity, parametric in permeability, aids in understanding cementation exponent in oomoldic limestones. This relationship can also be utilized to improve permeability prediction. Cementation exponents for the Arb and Miss equal  $2+0.1$ , in agreement with the commonly utilized value of the standard Archie model.

Air-mercury and air-brine capillary pressure relationships for the L-KC and Miss reveal that for typical reservoir structural closures in Kansas of less than 10-20 m all rocks except the most permeable are in a capillary transition zone over most or all of the reservoir thickness. These relationships indicate that initial oil saturations significantly vertically due to lithology, porosity, permeability, and height above the free water level. Capillary pressure curve models were developed for the L-KC and Miss that provide the ability to estimate capillary pressure properties based on input porosity. Capillary pressures for these carbonates can be modeled using modified Brooks-Corey equations where the threshold entry pressure and pore size heterogeneity dimension can be predicted using permeability. These models can be utilized to estimate vertical water saturation variation and aid in geomodel construction.

Drainage and imbibition oil-water relative permeability measurements were performed on L-KC oomoldic limestones and Miss moldic porosity mudstone to grainstone lime-dolomites. For these rocks, residual oil to waterflood ( $S_{orw}$ ) increases with increasing initial oil saturation ( $S_{oi}$ ) for a given rock type due to enhanced trapping by emplacement of oil in fine pores. The Land (1968) equation trapping characteristic,  $C$ , increases with increasing porosity resulting in less trapping with increasing porosity. This relationship, coupled with increasing "irreducible" water saturation ( $S_{wi}$ ) with decreasing porosity and permeability, results in a systematic change in  $S_{orw}$  with porosity/permeability and  $S_{oi}$ . With  $S_{oi}$  decreasing with depth in the transition zone, proper modeling of  $k_r$  in the transition zone requires a family of relative permeability ( $k_r$ ) curves that reflect changes in  $k_r$  with changing  $S_{oi}$ . Utilizing a family of  $k_r$  curves in reservoir simulation shows that both oil and water recovery are greater than predicted from models utilizing  $k_r$  curves with a constant  $S_{oi}$  and  $S_{orw}$ . Oil recovery is higher because  $S_{orw}(S_{oi})$  is lower and water recovery is higher because water saturation ( $S_w$ ) increases with proximity to the oil-water contact. These results validate and expand on use of the Land equation in shallow-shelf carbonates and help to explain both the high oil recovery and the high water production rates that are often evident in these reservoir systems. Oil relative permeability varies with  $k$  and  $S_{orw}(S_{oi})$ . Comparison of models utilizing  $S_{orw}(S_{oi})$  with models utilizing a constant  $S_{orw}$  values for the entire reservoir indicates that models using  $S_{orw}(S_{oi})$  predict more oil and more water production.

Comparison of numerical flow simulation of reservoirs modeled using fewer vertical cells and simpler relationships with the same reservoirs modeled using the relationships developed in this study indicates that reservoir performance prediction differs between the approaches and that models using

the relationships developed in this study may improve reservoir performance prediction and management.

A part of this study worked to improve the on-line database access and develop new and improved code for creation of web-based rock catalog pages based on queries of the data. This rock catalog ([http://abyss.kgs.ku.edu/Gemini/RockCatalog\\_v2.html](http://abyss.kgs.ku.edu/Gemini/RockCatalog_v2.html)) is available to the public and operators to utilize the tools developed in this study.

# INTRODUCTION

## I.1 Statement of Problem

Thin (3-40 ft thick), heterogeneous, limestone and dolomite reservoirs, deposited in shallow-shelf environments, represent a significant fraction of the reservoirs in the U.S. midcontinent and worldwide. In Kansas, reservoirs of the Arbuckle, Mississippian, and Lansing-Kansas City formations account for over 73% of the 6.3 BBO cumulative oil produced over the last century. For these reservoirs basic petrophysical properties (e.g., porosity, absolute permeability, capillary pressure, residual oil saturation to waterflood, resistivity, and relative permeability) vary significantly horizontally, vertically, and with scale of measurement. Many of these reservoirs produce from structures of less than 30-60 ft, and being located in the capillary pressure transition zone, exhibit vertically variable initial saturations and relative permeability properties. Rather than being simpler to model because of their small size, these reservoirs challenge characterization and simulation methodology and illustrate issues that are less apparent in larger reservoirs where transition zone effects are minor and most of the reservoir is at saturations near  $S_{wir}$ . These issues are further augmented by the presence of variable moldic porosity and possible intermediate to mixed wettability and the influence of these on capillary pressure and relative permeability. Understanding how capillary-pressure properties change with rock lithology and, in turn, within transition zones, and how relative permeability and residual oil saturation to waterflood change through the transition zone is critical to successful reservoir management and as advanced waterflood and improved and enhanced recovery methods are planned and implemented.

## I.2 Study Objectives

Major aspects of the proposed study involve a series of tasks to measure data to reveal the nature of how wettability and drainage and imbibition oil-water relative permeability change with pore architecture and initial water saturation. Focus is placed on carbonate reservoirs of widely varying moldic pore systems that represent the major of reservoirs in Kansas and are important nationally and worldwide. A goal of the project is to measure wettability, using representative oils from Kansas fields, on a wide range of moldic-porosity lithofacies that are representative of Kansas and midcontinent shallow-shelf carbonate reservoirs. This investigation will discern the relative influence of wetting and pore architecture. In the midcontinent, reservoir water saturations are frequently greater than “irreducible” because many reservoirs are largely in the capillary transition zone. This can change the imbibition oil-water relative permeability relations. Ignoring wettability and transition-zone relative permeabilities in reservoir modeling can lead to over- and under-prediction of oil recovery and recovery rates, and less effective improved recovery management. A goal of this project is to measure drainage and imbibition oil-water relative permeabilities for a large representative range of lithofacies at differ-

ent initial water saturations to obtain relations that can be applied everywhere in the reservoir. The practical importance of these relative permeability and wettability models will be demonstrated by using reservoir simulation studies on theoretical/generic and actual reservoir architectures. The project further seeks to evaluate how input of these new models affects reservoir simulation results at varying scales. A principal goal is to obtain data that will allow us to create models that will show how to accurately simulate flow in the shallow-structure, complex carbonate reservoirs that lie in the transition zone.

Tasks involved to meet the project objectives include collection and consolidation of available data into a publicly accessible relational digital database and collection of oil and rock samples from carbonate fields around the state (Task 1). Basic properties of these rocks and oils will be measured and used in wettability tests. Comparison will be performed between crude and synthetic oil wettability and evaluation made of how wettability is influenced by pore architecture (Task 2). Drainage and imbibition oil-water relative permeabilities will be measured on representative rock types obtained from across the state using crude and synthetic oil for a range of initial water saturations to evaluate the role that initial water saturation, wettability, and pore architecture play on relative permeability (Task 3). The new petrophysical models will be used to construct theoretical reservoir architecture models and new geomodels for two fields previously simulated using simpler models and for two new field locations in which native-state core will be obtained and analyzed (Task 4). Using the theoretical and real geomodels, simulations will both parametrically explore the influence of relative permeability differences and allow comparison with previous simulation models and results. In addition, predictions will be made for two targeted infill wells in pockets of remaining potential in the two new fields (Task 5). Upon drilling, representative cores will be obtained from these infill wells and analyzed (Task 6). Data obtained from core analyses will be compared with that predicted from simulation study to refine the geomodel and revisit the simulation. A web-based publication and short-course technology transfer program will be performed (Task 7).

### **I.3 Participants**

This project represents a collaboration of the Kansas Geological Survey (KGS), University of Kansas Center for Research (KUCR), the University of Kansas (KU), the Kansas University Energy Research Center (KUERC), and Murfin Drilling Company, Inc. (MDCI, a small independent Kansas operator). Individuals involved in the project include: KGS – Alan P. Byrnes (Principal Investigator), Saibal Bhattacharya, Ken Stalder; MDCI – James R. Daniels; U.S. DOE – Paul West (Project Manager).

## I.4 Importance of Moldic, Transition-Zone Reservoirs to Kansas Oil and Gas Production

Kansas reservoirs have produced nearly 6.3 billion barrels of oil (BBO) to date, with a significant majority of the past production coming from reservoirs in proximity to the Central Kansas Uplift (CKU; **Figures I-1, I-2, and I-3**). Of the 6.3 BBO, 73% (4.5 BBO) has been produced from Arbuckle Group, Mississippian, and Lansing-Kansas City Group reservoirs that are predominantly moldic-porosity systems.

Arbuckle Group reservoirs account for 37% of all production (2.4 BBO) but are declining in production and presently represent 20% of annual production. With declining Arbuckle Group production, Mississippian reservoirs account for 33% of the total state production over the last decade and are increasing in importance. Lansing-Kansas City Group reservoirs represent 16% of current production (**Figure I-5**).

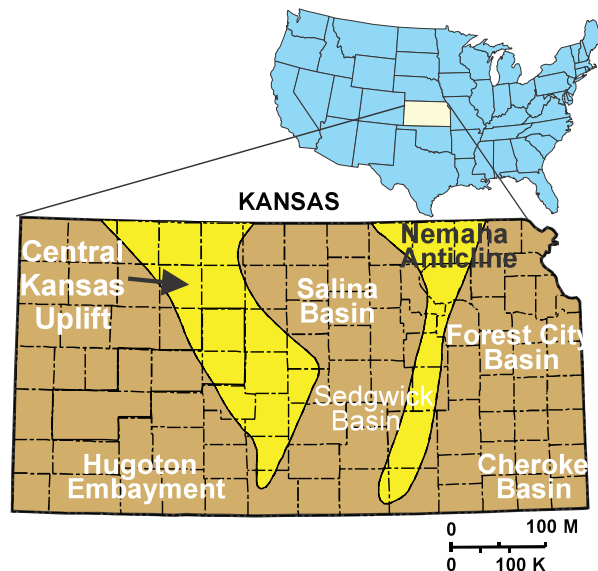


**Figure I-1.** Map of Kansas showing position of Central Kansas Uplift (CKU) where Arbuckle and Lansing-Kansas City reservoirs are principally located. Mississippian reservoirs are principally located on the flanks of the CKU.

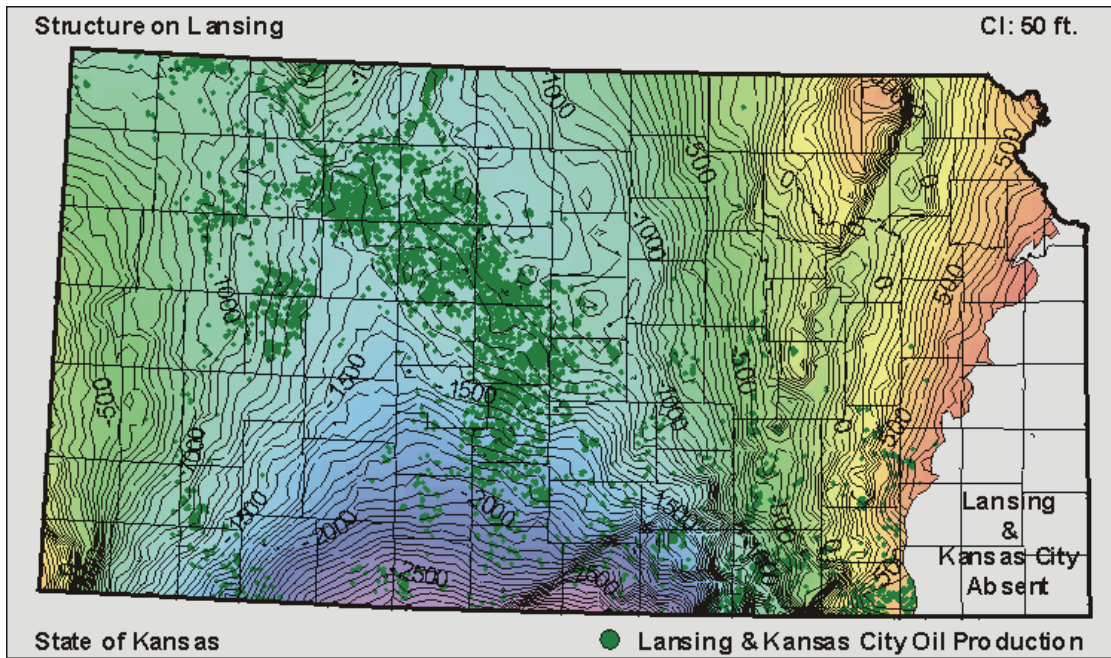


Figure I-2. Location of Lansing-Kansas City Group oil production (after Gerlach, 1998).

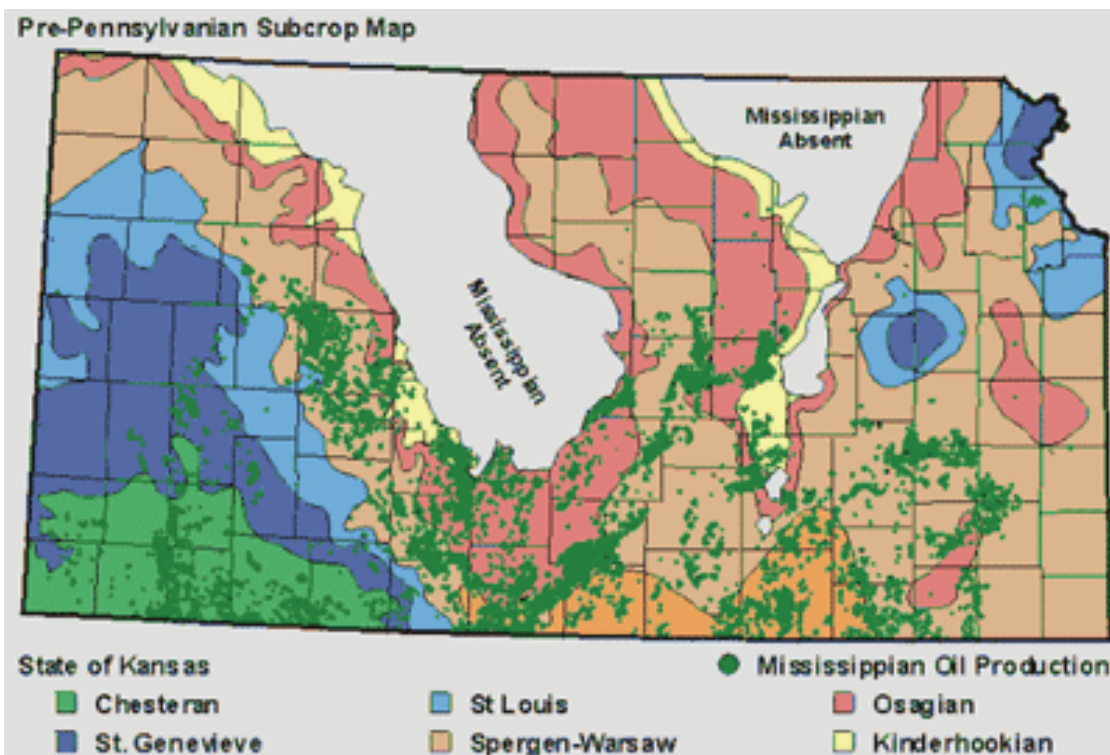


Figure I-3. Location of Mississippiian formation oil production (after Gerlach, 1998).

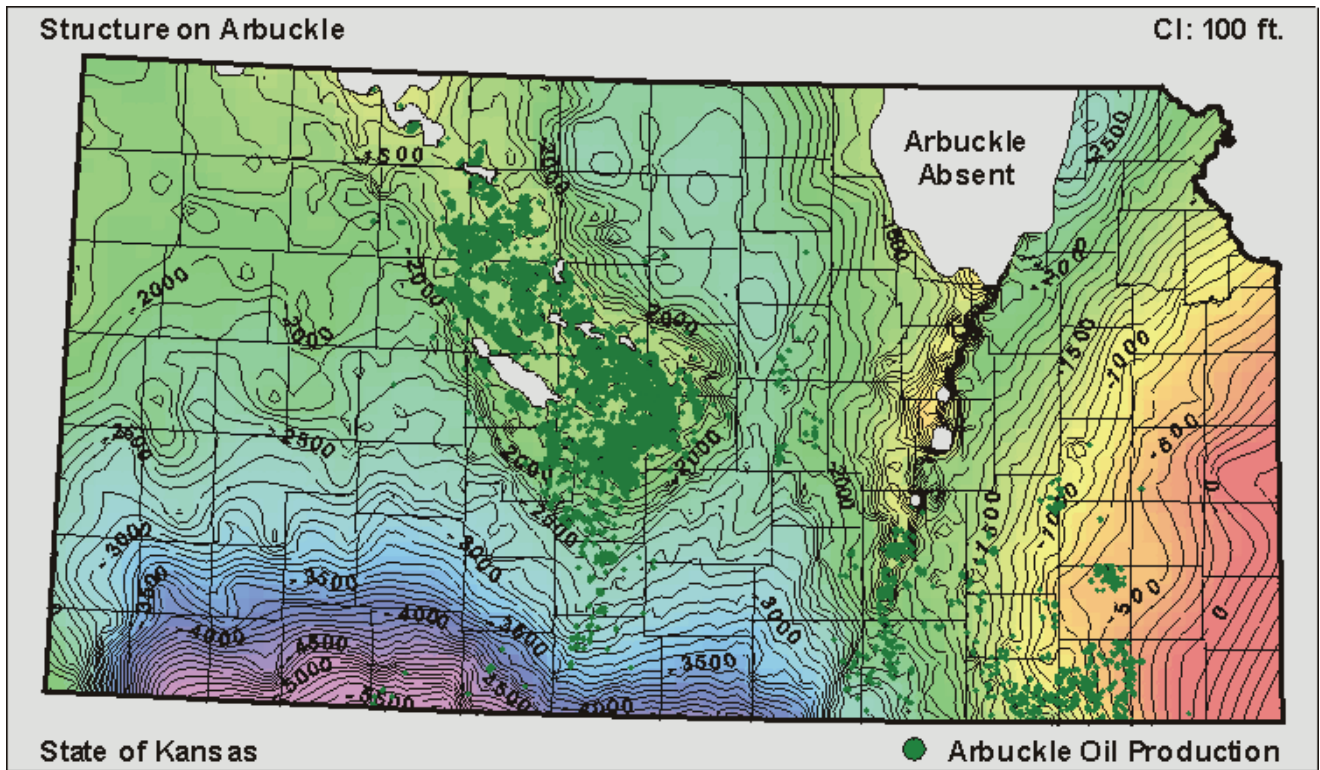


Figure I-4. Location of Arbuckle Group oil production (after Gerlach, 1998).

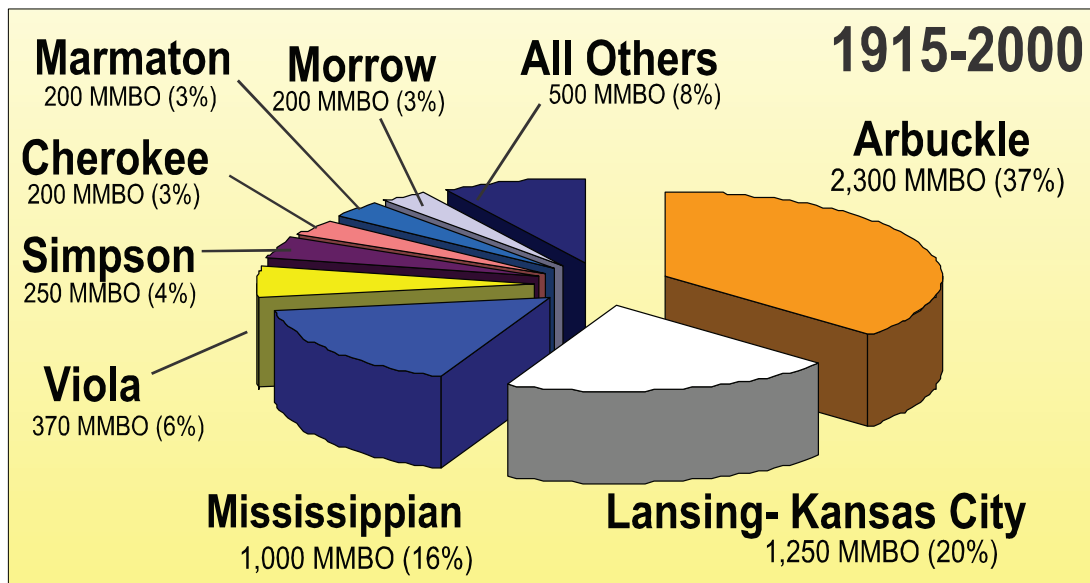


Figure I-5. Kansas cumulative oil by formation.

# RESULTS AND DISCUSSION

## 1.0 Rock, Oil, and Wettability Properties

### 1.1 Oil Characterization

Oil properties vary with formation and geographic locations across Kansas. Weinaug (1951) and Everett and Weinaug (1955) conducted comprehensive sampling of oils across eastern Kansas. Collecting primarily produced oil with some stock tank oil Weinaug sampled 54 wells and Everett and Weinaug (1955) sampled 446 wells. The wells sampled represent a wide range of formations including Arbuckle, Bartlesville, Burgess, Hays, Hoover, Hunton, Kansas City, Layton, Marmaton, Mississippian chat, Mississippian lime, Peacock, Peru, Simpson, Squirrel, Stalnaker, Viola, and Wayside. Collected oil samples from Lansing-Kansas City (n = 34), Mississippian (n = 53), and Arbuckle (n = 30) formations had basic properties measured (Everett and Weinaug, 1955). **Figures 1-1 through 1-3** illustrate the distribution of API values for the three formations. **Figures 1-4 through 1-6** illustrate the distribution of measured viscosities at 100 °F ( $\mu@100^\circ\text{F}$ , centipoise). **Figures 1-7 through 1-9** show the distribution of oil-water interfacial tension at 60°F ( $\sigma_{60}$ , dyne/cm). Everett and Weinaug (1955) graphically showed the relationship between viscosity ( $\mu$ ) and API gravity ( $\gamma_{\text{API}}$ ) but did not provide an empirical correlation equation. Utilizing their data, the relationship between viscosity (as measured at 100°F, which is close to reservoir temperatures) and API gravity can be expressed:

$$\log(\mu_{100}) = 77.75/\gamma_{\text{API}} - 1.52 \quad (1-1)$$

where viscosity ( $\mu_{100}$ ) is in centipoise. This relationship is similar to the Beal (1946) correlation (**Fig. 1-10**).

Oil-brine interfacial tension at 60°F ( $\sigma_{60}$ ) ranges from 20 to 48 dyne/cm and is weakly negatively correlated with API gravity (Fig. 1-7):

$$\sigma_{60} = 40.7 - 0.24 \gamma_{\text{API}} \quad (1-2)$$

where interfacial tension@60°F,  $\sigma_{60}$ , is in dyne/cm (**Fig. 1-11**).

K. David Newell, with the Kansas Geological Survey, sampled 158 western Kansas oil field oils and brines in 1983 and 1984. Oils from this sampling program were preserved in metal solvent cans and were made available to this study. From these samples, 31 samples represented Arbuckle, Mississippian, and Lansing-Kansas City reservoirs. For these 31 oil samples density was measured using a volumetric flask and balance and API gravity was estimated using the standard relation (**Table 1-1**):

$$\text{API (60°F)} = (141.5 - 131.5 * \rho_{\text{oil}}) / \rho_{\text{oil}} \quad (1-3)$$

where  $\rho_{oil}$  is in units of g/cc. API gravities for these samples exhibited the same range as the earlier study (Figs. 1-1 through 1-3).

In each of the oil sample sets there are one to three samples exhibiting anomalously low API gravity. These samples may represent the reservoir crude but they may also be compromised by sampling, chemical additives to the wellbore, or a reservoir that is abnormal in its oil properties. Table 1-2 summarizes oil properties for the eastern and western Kansas oils both including all samples and excluding +2 standard deviation outlier low API gravity samples.

Some of the western Kansas oils were used for wettability testing. In addition, oil samples were obtained from the Colliver Lease in Hall-Gurney field and the Murfin Austin #1-27 from the Lansing-Kansas City formation, and from the Murfin Hadley #L-4 well producing from the Arbuckle.

**Table 1-1.** Table of Lansing-Kansas City, Mississippian, and Arbuckle crude oil sampled in Newell 1983 and 1984 western Kansas oil sampling study for which API was measured in this study. Calculated viscosity and oil-water interfacial tension values were derived from equations 1-1 and 1-2 in text. Select oil samples were used in wettability testing on core.

Operator	Well	Lease	Location	Sec	Twn	Rng	Depth (ft)	Formation	Field	County	Measured API @60°F	Calculated Viscosity @100 °F (cP)	Calculated Oil-Water Interfacial Tension @60°F (dyne/cm)
Drillers & Prod., Inc.	#1	Harvey County	NW NW SW	4	23 S	2 E	2436	KC	Walton	Harvey	34.4	5.5	31.9
Shields Production	#1	Hegarty	SE SW SW	30	11 S	12 W	2985	Lansing	Hegarty	Russell	38.1	3.3	31.1
Cambria Corp.	#1	Riedl	W2 NE SE	10	17 S	14 W	3214	Lansing	Larkin	Barton	42.5	2.0	30.0
Fell O&G	#1	Dueser	E2 SE NW	29	19 S	10 W		LKC	Chase-Silica	Rice	42.4	2.1	30.0
Bruce Oil	#1	Phillips	SE NE NW	2	15 S	1 E	2411	Miss	Holland Creek	Dickinson	27.7	19.3	33.6
Range Oil	#1	Cooper	SW SW SW	7	17 S	1 E	2790	Miss	Fanska South	Marion	29.2	13.8	33.2
Dieter Production	#2	Schroeder	N2 SE SE	22	19 S	1 E	2807	Miss	Lehigh North	Marion	25.4	34.3	34.1
Acme Oil	#1	Timmerkamp 'B'	SW NE SE	4	26 S	2 E	2899	Miss	Fairview NE	Sedgwick	38.0	3.3	31.1
Am. Petrofina of TX	#1	Guinty	SW SW SW	13	23 S	3 E	2490	Miss	Paulson	Butler	41.2	2.3	30.3
Dieter Production	#1	A. Kirch	NW SW NW	15	18 S	4 E	2375	Miss	Lost Springs	Marion	32.4	7.5	32.4
Range Oil	#1	Bohlin	N2 SW	6	24 S	4 E	2436	Miss	Mellor	Butler	41.9	2.2	30.1
Kan-Go	#1	Remy	SW SE NW	15	17 S	5 E	2222	Miss	Burdick	Morris	36.5	4.1	31.4
Te-Pe O&G & Bruce Oil	#2	Stucky	SE NE SW	32	22 S	5 E	2472	Miss	Burns	Marion	41.7	2.2	30.2
	#13	Maher	W2 NE	12	24 S	16 E	1325	Miss	Neosho Falls	Woodson	30.5	10.7	32.9
Douglas Loewen	#1	Nelson-Winslow	NE SE SE	29	15 S	1 W	2652	Miss	Mortimer	Saline	36.1	4.3	31.5
Mellan Drilling	#1	Bukey	SW SE NW	4	17 S	1 W	2606	Miss	Gypsum Creek	McPherson	34.6	5.4	31.9
White Hawk Oil	#2	Bishop	CSL SE NE	30	17 S	1 W	2688	Miss	Roxbury South	McPherson	33.4	6.4	32.2
National Oil	#1	Koehn	SW SW NE	2	19 S	1 W	2849	Miss	Koehn	McPherson	35.0	5.0	31.8
Hess Oil	#3	Maude Smith	SE SW	15	19 S	2 W	2937	Miss	Ritz-Canton	Marion	40.8	2.4	30.4
Big J Production	#1	Kaufman 'B'	NE NW SW	26	22 S	2 W		Miss	Sperling South	Harvey	37.6	3.5	31.2
Hess Oil	#1	Neufeldt	E2 SE NW	28	21 S	3 W	3104	Miss	Voshell	McPherson	38.7	3.1	30.9
Kaiser-Francis	#2	Peters	NE NE SW	31	22 S	3 W	3334	Miss	Burrtton	Harvey	41.1	2.4	30.3
Kaiser-Francis	#2	Peters	NE NE SW	31	22 S	3 W	3334	Miss	Burrtton	Harvey	38.5	3.2	31.0
Excalibur Production	#1	A.J. Becker	NE NW	28	23 S	3 W	3307	Miss	Burrtton East	Harvey	36.4	4.2	31.5
Brunson-Spines	#1	Robert Bacon	SW SE NW	36	23 S	5 W	3360	Miss	Bacon	Reno	35.9	4.4	31.6
Aurora Oil	#1	Maloney	NE SE	18	25 S	5 W	3414	Miss	Fishburn	Reno	43.7	1.8	29.7
Texaco	#1	Bertholf	NW SW	23	29 S	8 W	4189	Miss	Belmont Center	Kingman	34.5	5.5	31.9
Energy Reserves Group	#1	Tjaden 'A'	SW SW NW	24	30 S	8 W	4246	Miss	Spivey-Grabs	Kingman	32.5	7.5	32.4
Southern States Oil	#1	Peters 'A'	NW SW	31	22 S	3 W	3401	Miss	Hollow-Nikkel	Harvey	39.5	2.8	30.7
Aspen Drilling	#1	Grossardt	NW SW NW	16	17 S	11 W	3288	Arbuckle	Kraft-Prusa	Barton	38.5	3.2	31.0
Petroleum Management	#1	Boxberger 'C'	E2 SW SE	32	13 S	14 W	3306	Arbuckle	Gorham	Russell	31.5	8.9	32.6

**Table 1-2.** Summary statistics for oil properties.

Formation	Statistic	API Gravity	API Gravity	Viscosity	Viscosity	Oil-water Interfacial Tension	Oil-water Interfacial tension	Study
		@ 60oF All	@ 60oF no outliers	@ 100°F All	@ 100°F no outliers	@ 60°F All	@ 60°F no outliers	
Lansing-Kansas City	Count	34	32	34	32	34	32	Everett & Weinaugh, 1955
Lansing-Kansas City	Average	35.2	35.5	5.7	5.3	32.7	32.7	Everett & Weinaugh, 1956
Lansing-Kansas City	std dev	2.3	2.1	2.4	1.8	2.4	2.4	Everett & Weinaugh, 1957
Lansing-Kansas City	Count	4	4	4	4	4	4	this study
Lansing-Kansas City	Average	39.4	39.4	3.2	3.2	30.8	30.8	this study
Lansing-Kansas City	std dev	3.9	3.9	1.6	1.6	0.9	0.9	this study
Mississippian	Count	53	51	53	51	53	51	Everett & Weinaugh, 1958
Mississippian	average	36.2	36.5	6.1	5.6	31.3	31.2	Everett & Weinaugh, 1959
Mississippian	std dev	4.2	4.0	8.0	7.7	4.0	4.0	Everett & Weinaugh, 1960
Mississippian	Count	24	24	24	24	24	24	this study
Mississippian	average	36.1	36.1	6.5	6.5	31.5	31.5	this study
Mississippian	std dev	4.7	4.7	7.1	7.1	1.1	1.1	this study
Arbuckle	Count	30	27	30	27	30	27	Everett & Weinaugh, 1961
Arbuckle	average	33.9	34.9	9.8	5.1	30.8	30.5	Everett & Weinaugh, 1962
Arbuckle	std dev	4.1	2.8	16.3	2.4	3.4	3.5	Everett & Weinaugh, 1963
Arbuckle	Count	2	2	2	2	2	2	this study
Arbuckle	average	35.0	35.0	6.0	6.0	31.8	31.8	this study
Arbuckle	std dev	4.9	4.9	4.0	4.0	1.2	1.2	this study

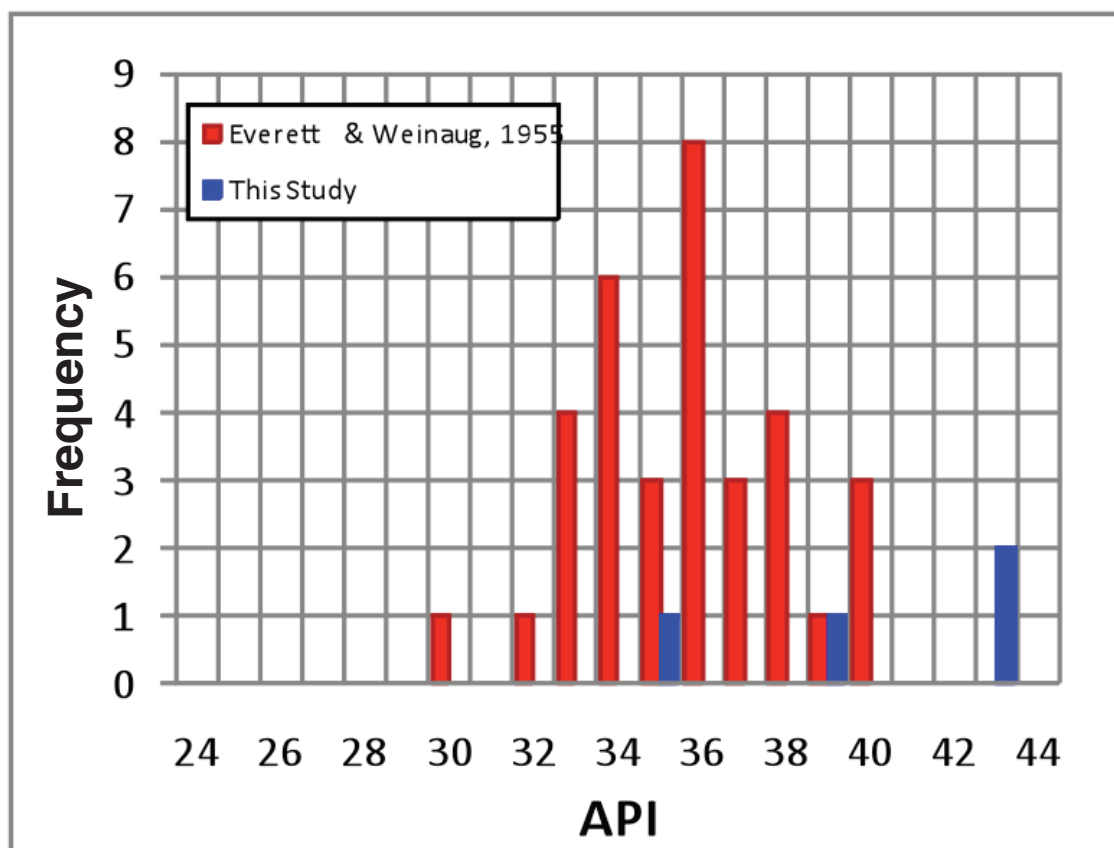


**Figure 1-1.** Histogram showing distribution of API gravity for eastern Kansas oils from the Lansing-Kansas City (red, n = 34, Everett and Weinaugh, 1955) and measured for western Kansas oils from the Lansing-Kansas City (blue, n = 4, this study).

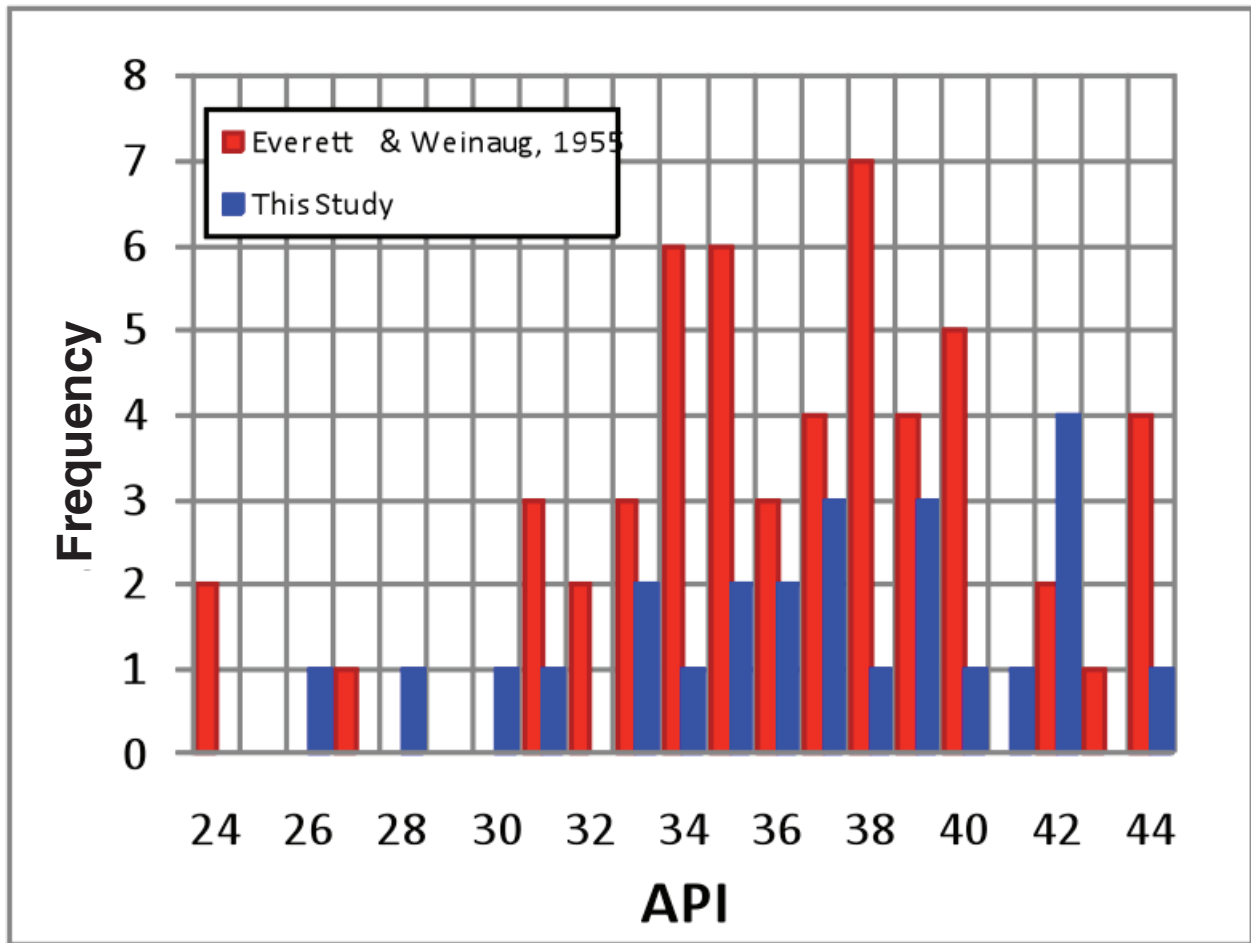


**Figure 1-2.** Histogram showing distribution of API gravity for eastern Kansas oils from the Mississippian (red, n = 53, Everett and Weinaug, 1955) and measured for western Kansas oils from the Mississippian (blue, n = 24, this study).

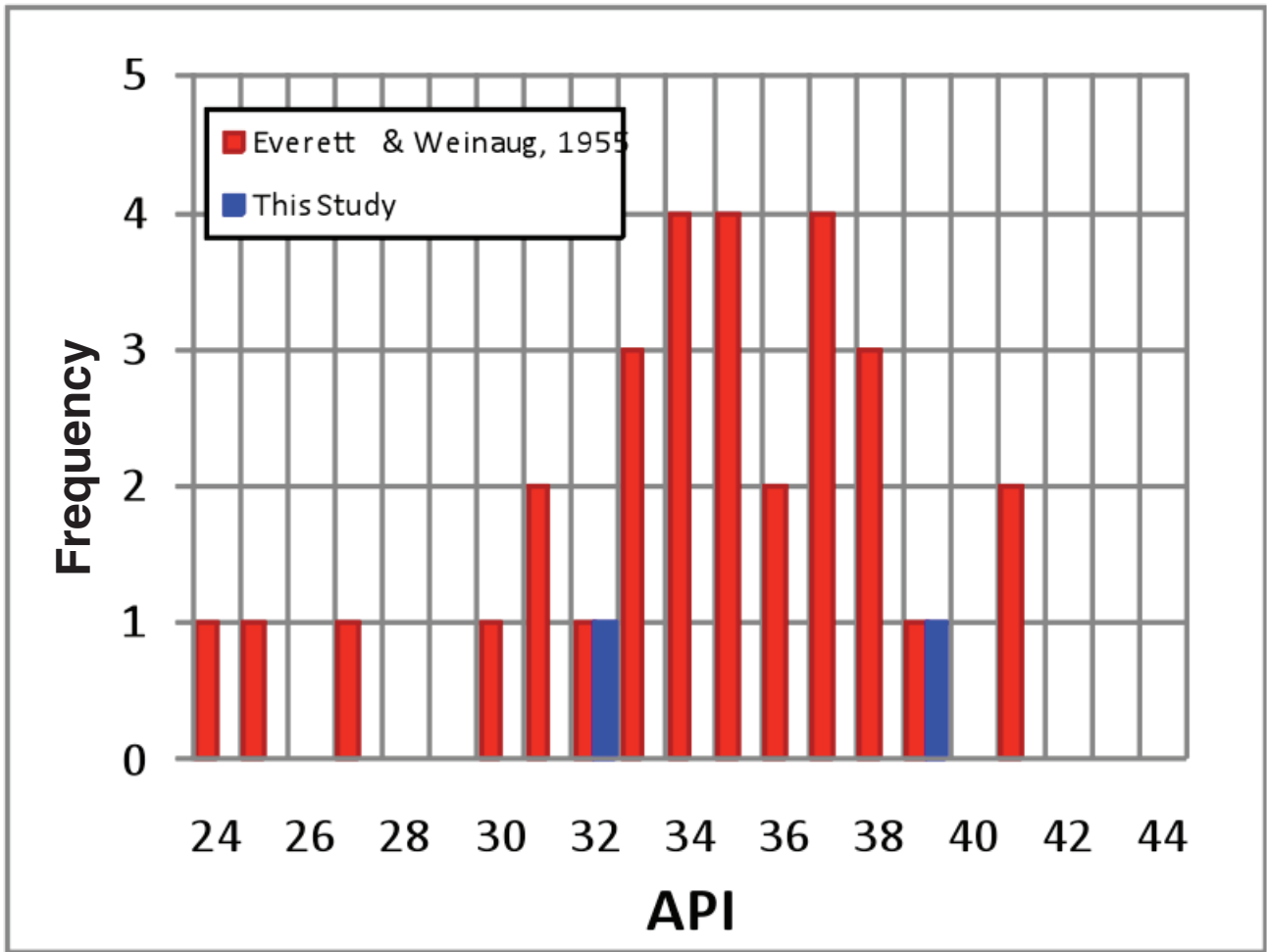


**Figure 1-3.** Histogram showing distribution of API gravity for eastern Kansas oils from the Arbuckle (red, n = 30, Everett and Weinaug, 1955) and measured for western Kansas oils from the Arbuckle (blue, n = 2, this study).

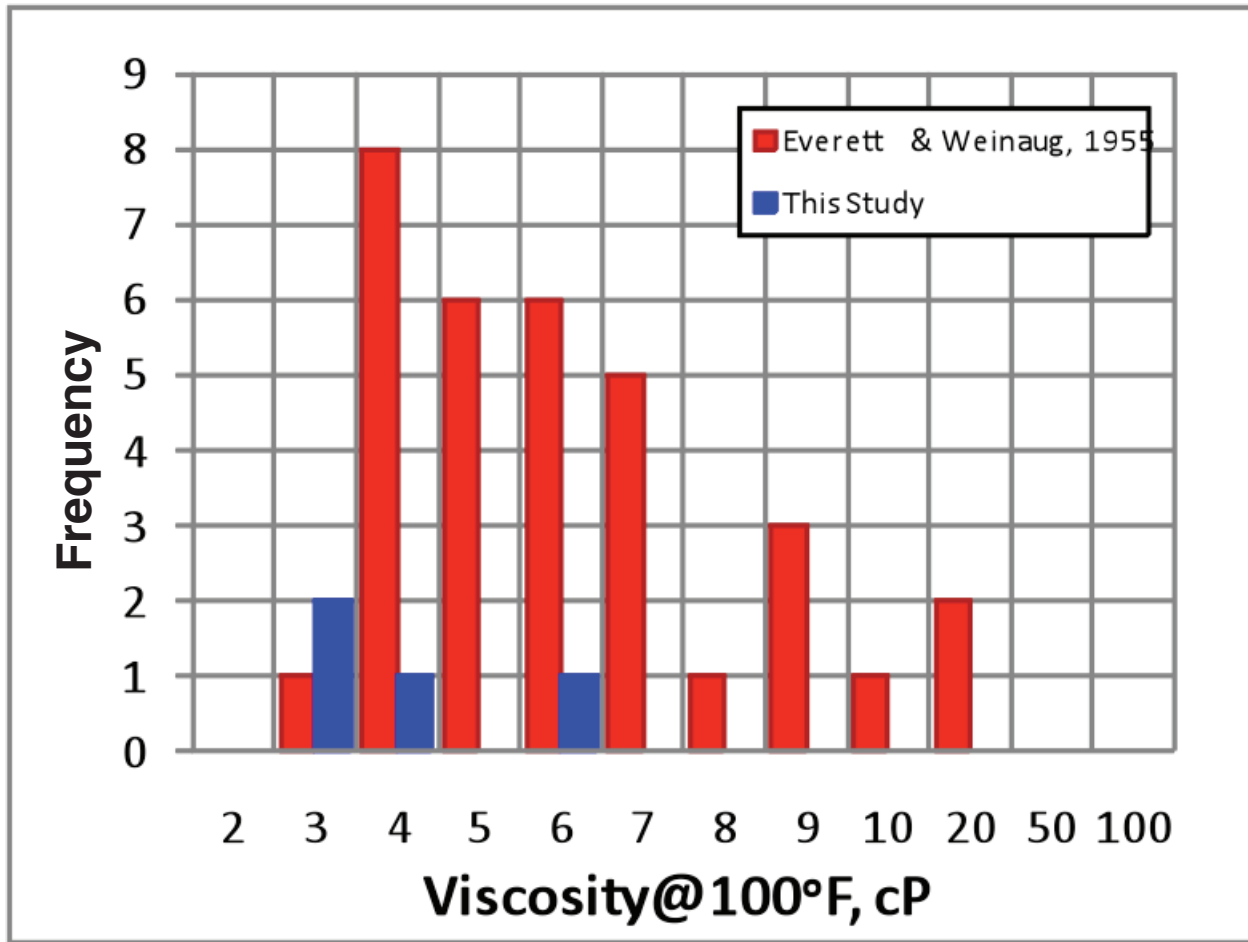


**Figure 1-4.** Histogram showing distribution of viscosity @100°F (centipoises) for eastern Kansas oils from the Lansing-Kansas City (red, n = 34, Everett and Weinaug, 1955) and estimated from equation 1-1 in the text for western Kansas oils from the Lansing-Kansas City (blue, n = 2, this study).

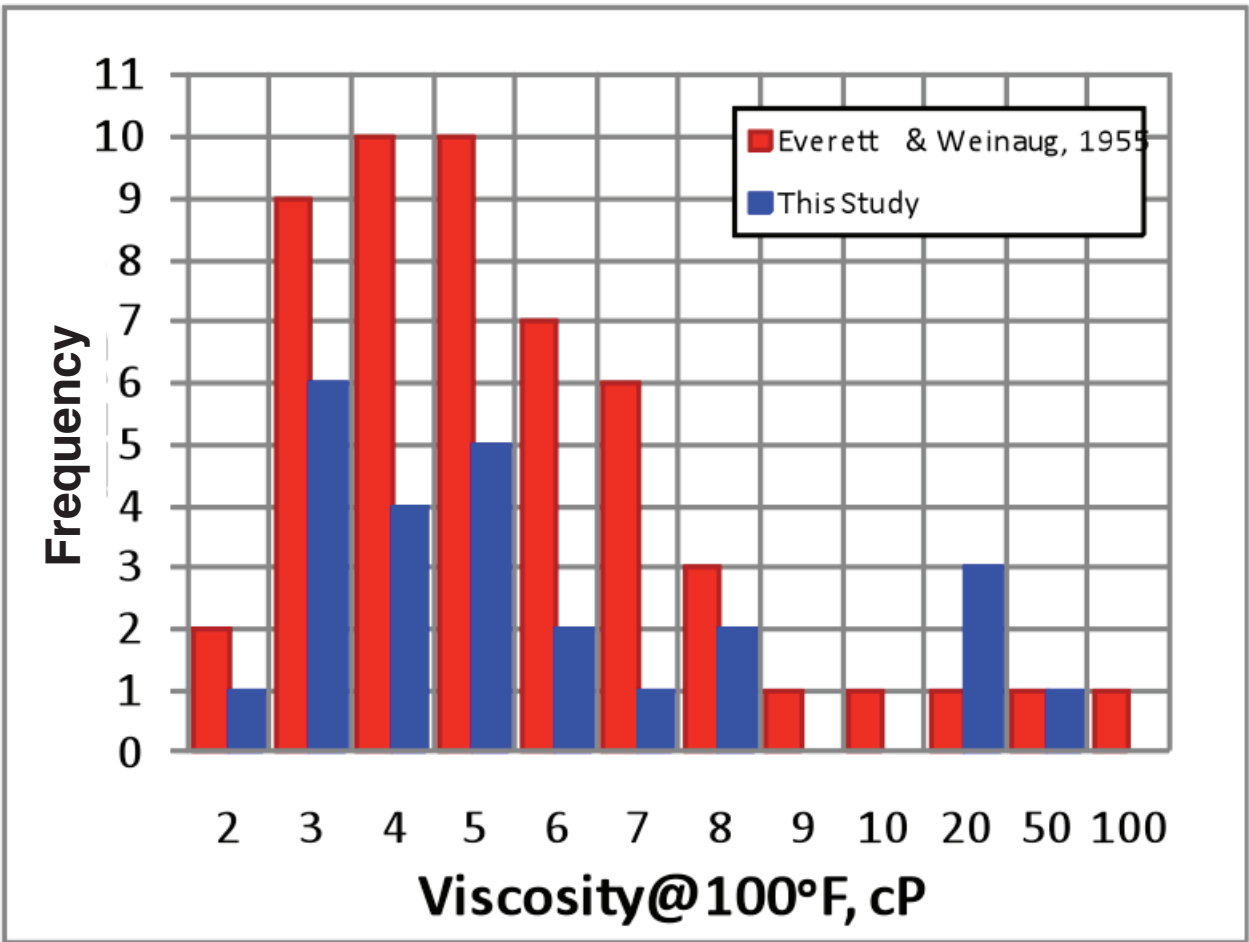


**Figure 1-5.** Histogram showing distribution of viscosity @100°F (centipoises) for eastern Kansas oils from the Mississippian (red, n = 53, Everett and Weinaug, 1955) and estimated from equation 1-1 in the text for western Kansas oils from the Mississippian (blue, n = 24, this study).

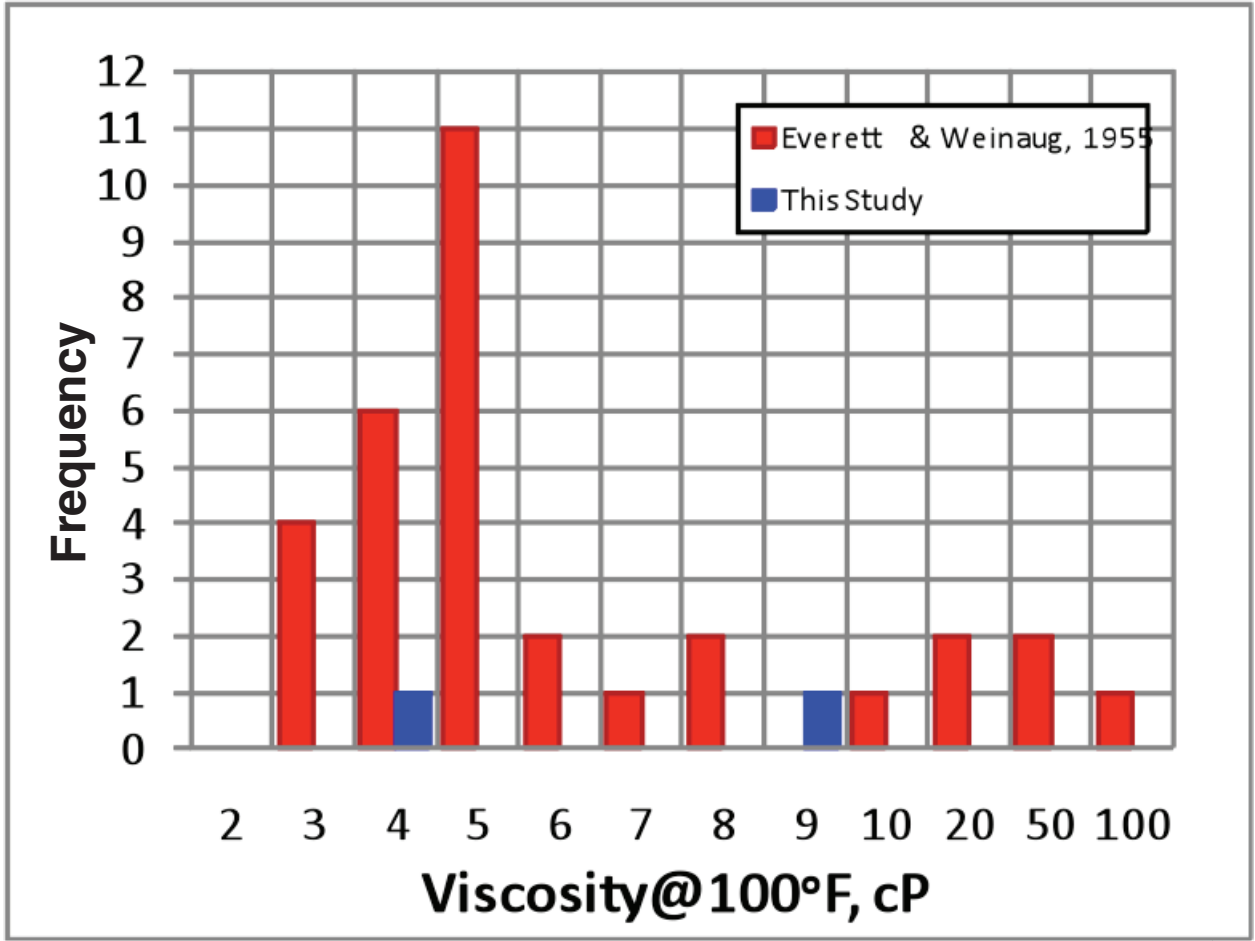


**Figure 1-6.** Histogram showing distribution of viscosity @100°F (centipoises) for eastern Kansas oils from the Arbuckle (red, n = 30, Everett and Weinaug, 1955) and estimated from equation 1-1 in the text for western Kansas oils from the Arbuckle (blue, n = 2, this study).

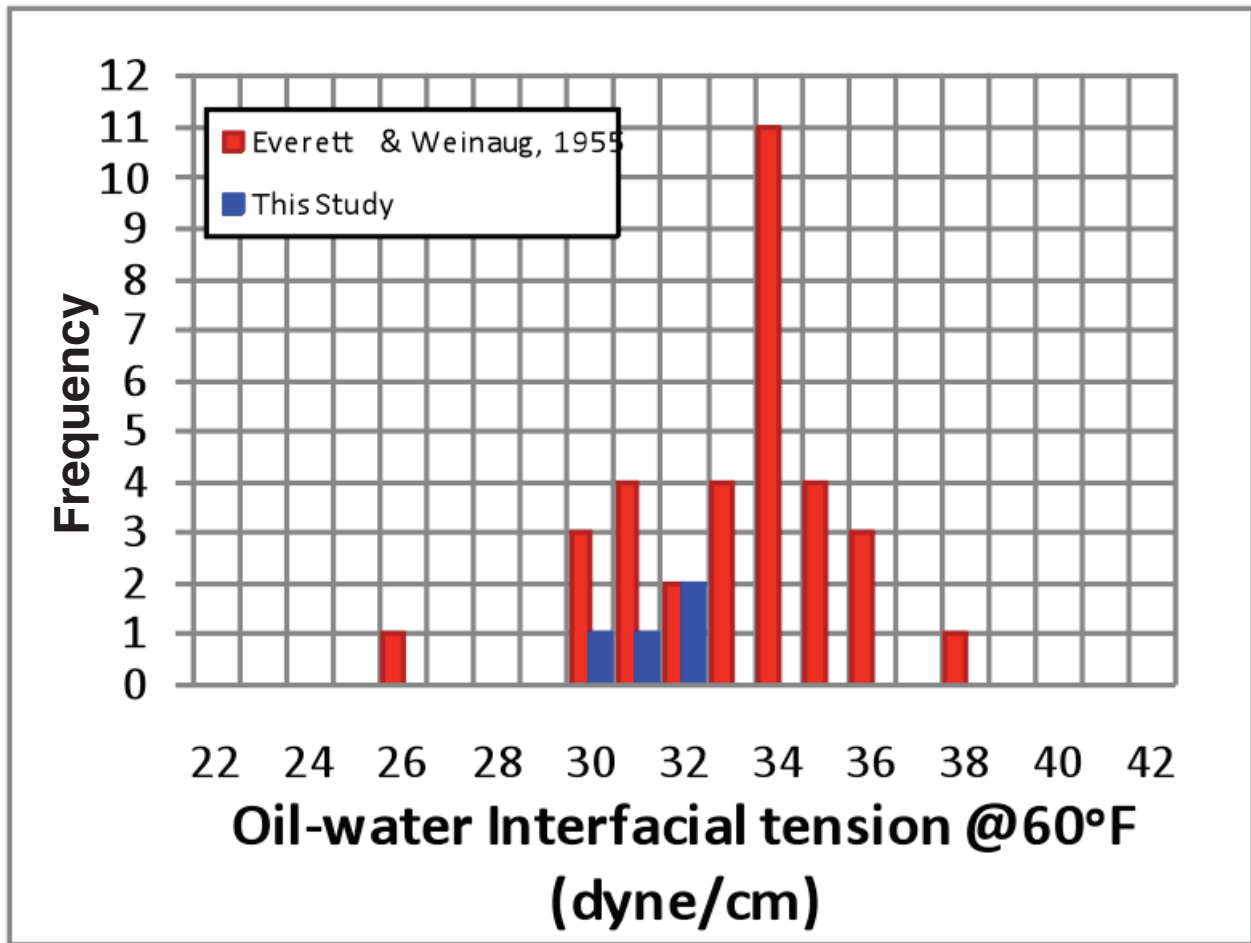


**Figure 1-7.** Histogram showing distribution of oil-water interfacial tension @60°F (dyne/cm) for eastern Kansas oils from the Lansing-Kansas City (red, n = 34, Everett and Weinaug, 1955) and estimated from equation 1-2 in the text for western Kansas oils from the Lansing-Kansas City (blue, n = 4, this study).

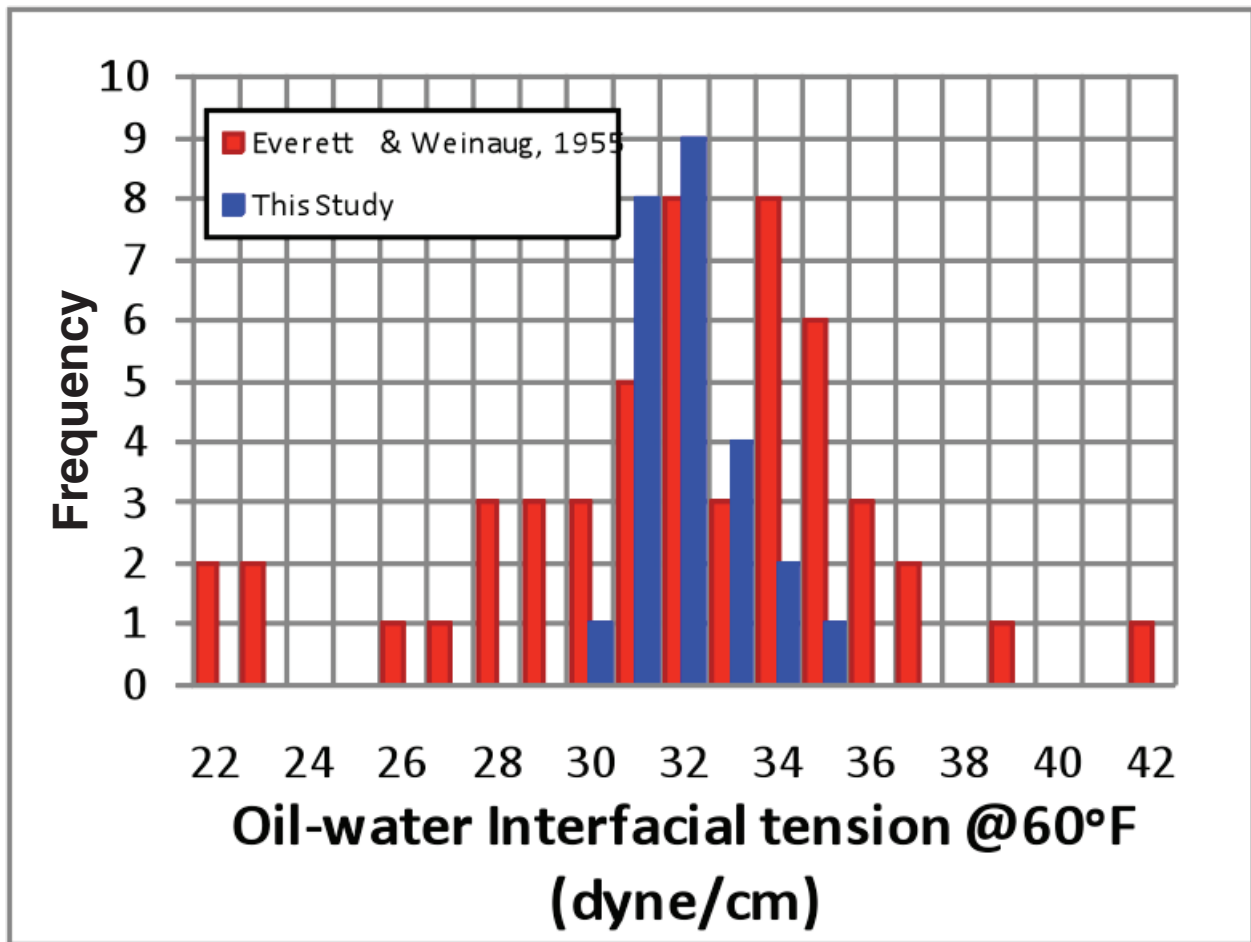


**Figure 1-8.** Histogram showing distribution of oil-water interfacial tension @60°F (dyne/cm) for eastern Kansas oils from the Mississippian (red, n = 53, Everett and Weinaug, 1955) and estimated from equation 1-2 in the text for western Kansas oils from the Mississippian (blue, n = 24, this study).

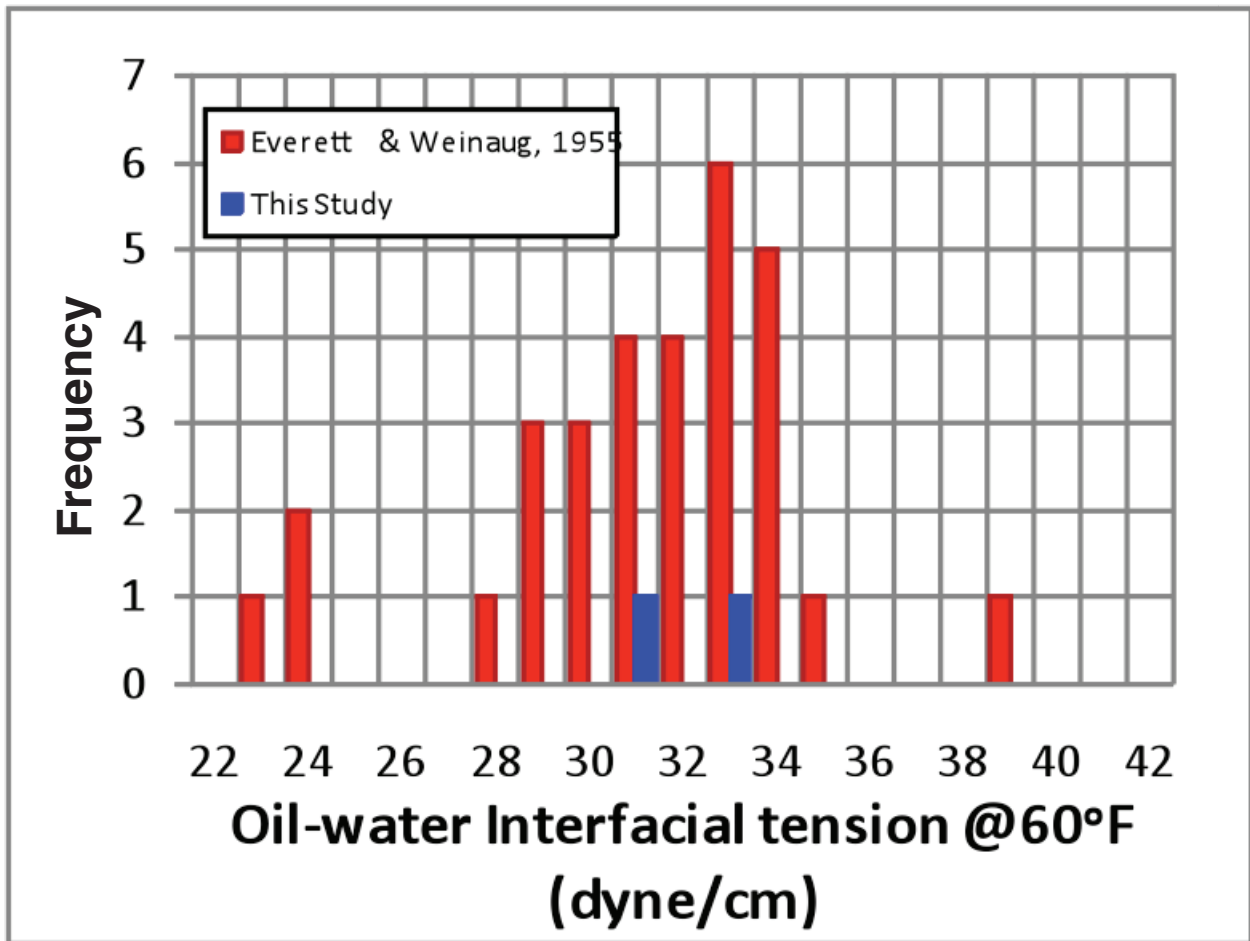


**Figure 1-9.** Histogram showing distribution of oil-water interfacial tension @60°F (dyne/cm) for eastern Kansas oils from the Arbuckle (red, n = 30, Everett and Weinaug, 1955) and estimated from equation 1-2 in the text for western Kansas oils from the Arbuckle (blue, n = 2, this study).

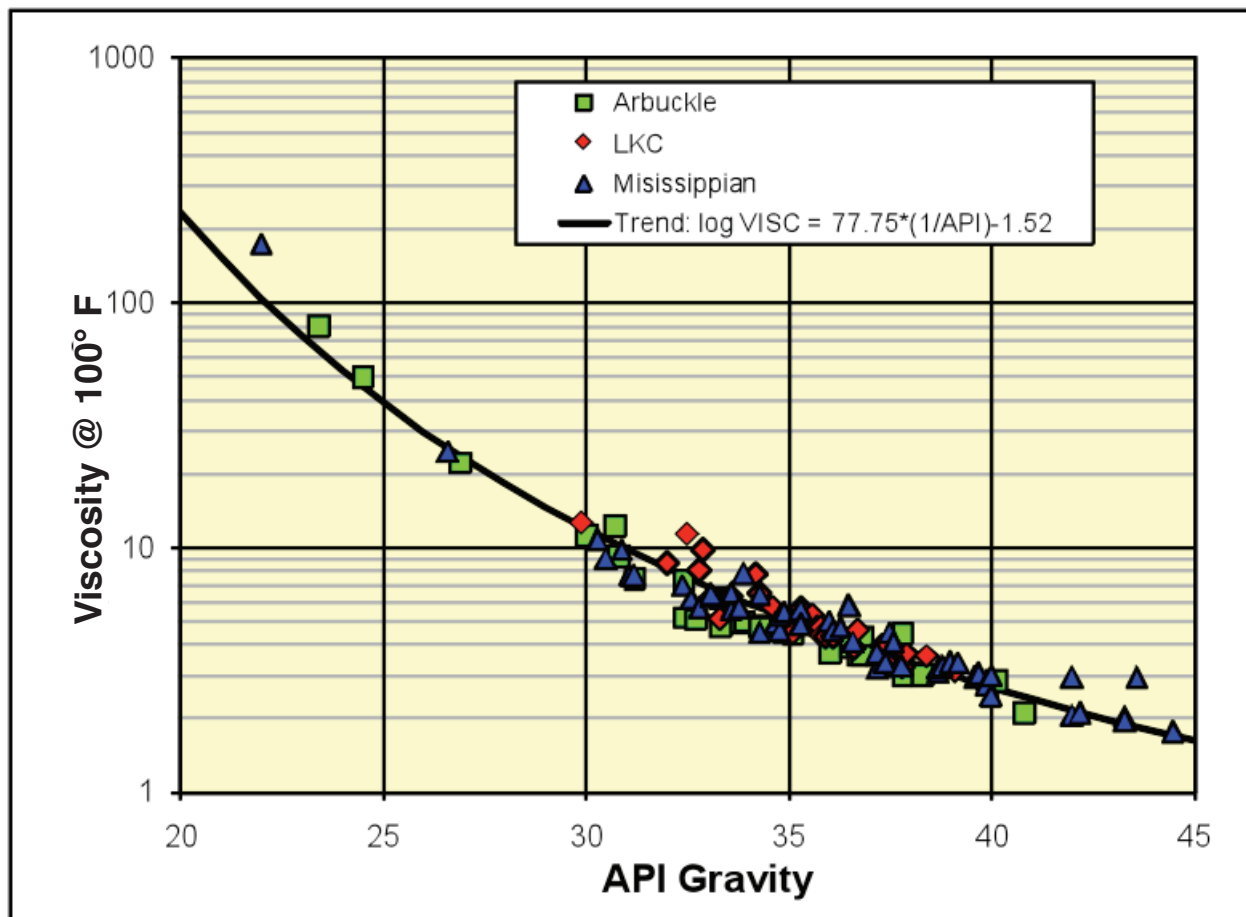


**Figure 1-10.** Crossplot of measured oil viscosity at 100 °F versus API gravity for eastern Kansas oils from the Arbuckle, LKC, and Mississippian formations (Everett and Weinaug, 1955). The correlation trendline developed in this investigation can be characterized as:  $\mu_{100F} = 10^{(77.75 * (1/API) - 1.52)}$ .

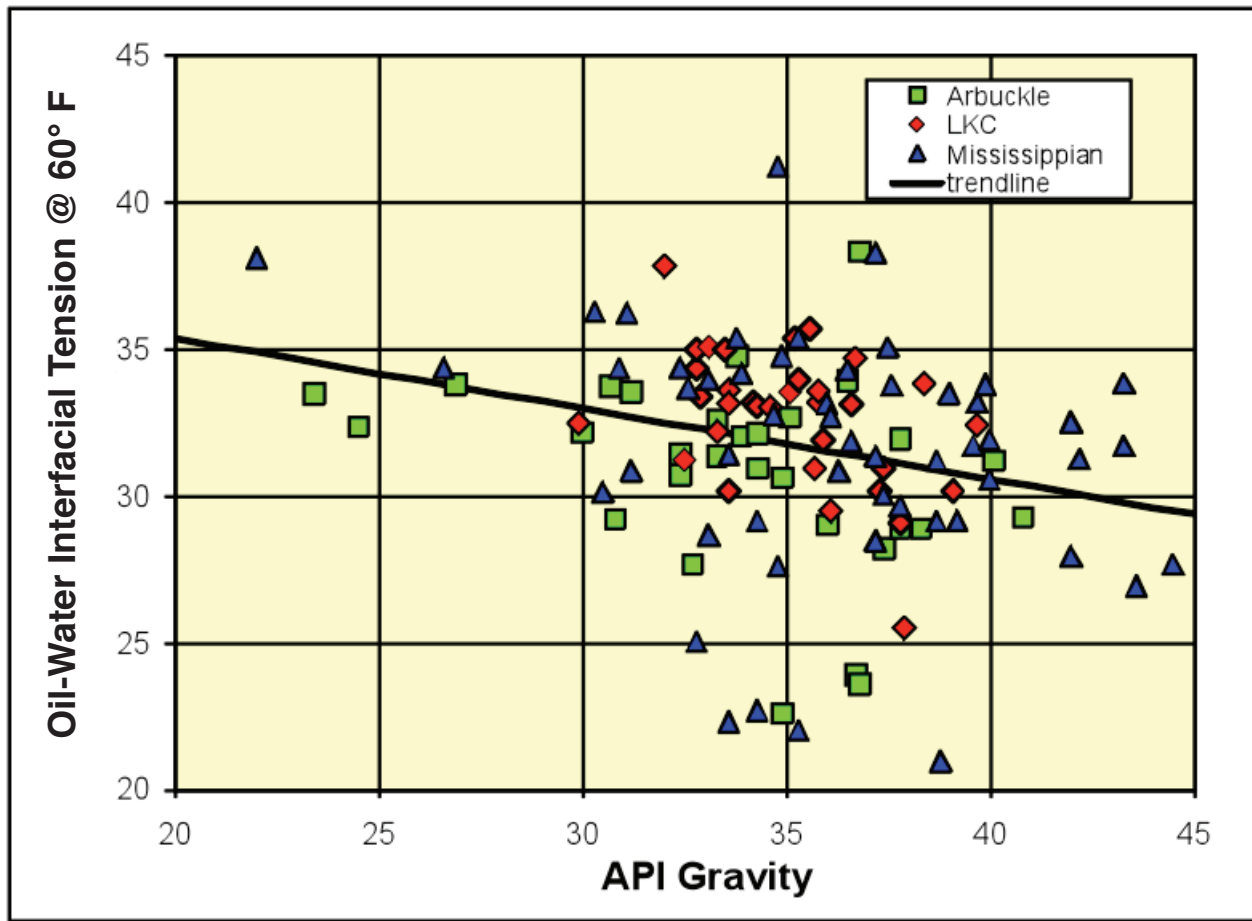


**Figure 1-11.** Crossplot of measured oil-water interfacial tension at 60°F versus API gravity for eastern Kansas oils from the Arbuckle, LKC and Mississippian formations (Everett and Weinaug, 1955). The weak correlation trendline can be characterized as:  $IFT_{60F} = -0.24 \text{ API} + 40.2$ .

## 1.2 Wettability

Wettability describes the relative preference of a rock pore surface to be covered by oil or water. By definition a rock is water-wet if a greater portion of the rock surface in the pores is covered with a water layer. Wettability is affected by the minerals present on the pore walls as well as the reservoir oil and brine chemistry, the pressure and temperature of the reservoir, and potentially by drainage and imbibition hysteresis. Clean sandstone or quartz is frequently water-wet, but sandstone reservoir rock is usually found to be intermediate-wet. Carbonates are often reported to be more oil-wet than siliciclastics. Extreme water-wetness or extreme oil-wetness is rare. Wettability can influence the distribution and flow of fluids in the pore space. Because of its influence on distribution and flow, changes in wettability have been demonstrated to affect capillary pressure, relative permeability, electrical properties, and reservoir performance. Anderson (1986a, 1986b, 1986c, 1987a, 1987b, 1987c) presented a thorough review of the effects of wettability on each of these properties. Rasmus (1986) characterized the influence of wettability on both intergranular- and vug-dominated rock pore systems.

Wettability affects the three-phase oil-water-rock contact angle. Studies indicate that that microscopic displacement efficiency increases as systems becomes less water-wet (Ma et al., 1999). Microscopic displacement efficiency for spontaneous imbibition and waterflooding is influenced by capillary phenomena related to stability of capillary structures and motion of the three phase (oil/brine/solid) lines of contact. In very strongly water-wet systems, trapping of oil is dominated by snap-off. In general, trapping of oil during water imbibition results from snap-off of oil droplets at pore throats leaving isolated oil blebs. Snap-off is inhibited as the systems become less strongly water-wet. Ma et al. (1999) report that maximum waterflood recoveries are obtained at intermediate wettability conditions or conditions close to very weakly water-wet conditions.

Research has shown that wettability strongly influences oil-water relative permeability (Owens and Archer, 1971; McCaffery and Bennion, 1974; Morrow et al., 1973; Watson and Boukadi, 1990; Haugen, 1990; Ringrose et al., 1996; Wang et al., 1997; van Dijke and Sorbie, 2001) and three-phase relative permeability (DiCarlo, 1998). These and other studies, which focus primarily on inter-particle porosity rocks, report that as oil-wetness increases in inter-particle-porosity sandstones and carbonates several characteristics change, including 1) relative permeability curves shift to lower water saturations, 2) water relative permeability increases, 3) oil relative permeability decreases, 4) residual oil saturation increases, and 5) “irreducible” water saturation decreases.

For shallow-shelf, dominantly moldic-porosity, carbonates in Kansas there are no known published studies reporting wettability test results and only a few unpublished tests. Recent Amott testing of the Lansing-Kansas City oomoldic limestone exhibited an Amott Wettability Index (using the Amott-Harvey -1-1 index described below,  $I_{AH}$ ) of  $I_{AH} = 0.35$  indicating intermediate oil-wetness. Few available measurements on Mississippian chat cores (Watney et al., 2001) and Lansing-Kansas City oomoldic limestone cores exhibit relative permeability curves that can be interpreted to result from intermediate wettability. While these limited results may indicate the existence of intermediate oil-wetness, the

unique pore architecture of moldic porosity rocks may produce results that for inter-particle porosity rocks can be interpreted as oil-wet but for these rocks is simply an expression of how water-wet moldic-porosity rocks behave under tests conditions.

To obtain data on wettability in Kansas shallow shelf carbonates, core plugs from the Lansing-Kansas City (n = 35), Mississippian (n = 16), and Arbuckle (n = 13) formations were selected from the library of core plugs created and discussed in Section 1.3. These core plugs generally represented the rocks with permeability equal to or greater than the average for the formations to facilitate Amott imbibition testing.

### 1.2.1 Laboratory Method

Samples were previously cleaned using soxhlet extraction using a methyl alcohol/toluene azeotrope. Helium porosity and *in situ* Klinkenberg gas permeability were measured. The samples were evacuated under a vacuum of  $< 10^{-3}$  torr and saturated with 100,000 ppm NaCl brine. To insure complete saturation, following ambient pressure filling of the pore space with brine, a pressure of 1,000 psi was applied to the brine for an 8 hour period. Each core plug was then placed in a Hassler core holder, subjected to 1,000 psi hydrostatic confining pressure on the sleeve, and flushed with Isopar G or crude oil to “irreducible” water saturation ( $S_{wi}$ ) and an effective oil permeability at  $S_{wi}$  measured. “Irreducible” saturation was defined as when no effluent water was observed for a 3 minute time period and over a 10 minute time period total displaced water did not change by greater than 1%. Generally this required 30-100 pore volumes throughput. Following the permeability measurement each sample was placed in an inverted graduated volumetric glass funnel in a covered beaker containing brine and placed in a convection oven at 110°F to approximate reservoir temperature. The samples were allowed to equilibrate and imbibe brine for a period of 7 days. After 7 days the volume of oil displaced by spontaneous imbibition of brine ( $V_{os}$ ) was measured by visual reading. The sample was then removed from the glass funnel, placed in a Hassler Cell, and flushed with 100,000 ppm NaCl brine to residual oil saturation ( $S_{orw}$ ) and a reading of the forced-displacement oil volume ( $V_{of}$ ) was recorded. Total oil displaced ( $V_{ot}$ ) was calculated from the sum of the spontaneously displaced oil and the forced-displacement oil volumes ( $V_{ot} = V_{os} + V_{of}$ ). The sample was then placed in a graduated volumetric glass funnel filled with oil and stoppered lightly to minimize evaporation. The sample was placed in an oven at 110°F for a period of 7 days and the volume of water displaced by spontaneous imbibition of oil was measured ( $V_{ws}$ ) by visual reading. The sample was then removed, placed in a Hassler cell, and flushed with oil to residual water saturation and a reading of the forced-displacement brine volume ( $V_{wf}$ ) was recorded. Total water displaced ( $V_{wt}$ ) was calculated as the sum of the spontaneously displaced brine and the forced-displacement brine ( $V_{wt} = V_{ws} + V_{wf}$ ).

The Amott wettability index to water ( $I_w$ ) and to oil ( $I_o$ ) were calculated using the ratio of the spontaneous and total displacement volumes:

$$I_w = (V_{ws} / V_{wl}) \quad (1-4)$$

$$I_o = (V_{os} / V_{ot}) \quad (1-5)$$

The Amott-Harvey index ( $I_{AH}$ ) provides a continuous index from -1 to +1 and is commonly defined by the difference between  $I_o$  and  $I_w$ :

$$I_{AH} = I_o - I_w \quad (1-6)$$

Using this method cores that are strongly water-wet exhibit  $I_{AH}$  values of approximately  $-1.0 < I_{AH} < -0.5$ . Cores that are strongly oil-wet exhibit  $I_{AH}$  values that are approximately  $1.0 > I_{AH} > 0.5$ . Cores exhibiting  $-0.1 < I_{AH} < 0.1$  are characterized as exhibiting neutral or intermediate wettability. This condition can also occur in cores containing both silicate and carbonate minerals. In these cores some oils may wet the carbonate surface and not wet the silicate surface. At the scale of measurement of the Amott test the combined influence of these processes can result in no indication of preferential wetness though at the pore scale the rock can be characterized as exhibiting mixed wettability. Cores exhibiting  $-0.5 < I_{AH} < -0.1$  can be characterized as exhibiting intermediate water-wetness and cores exhibiting  $0.5 > I_{AH} > 0.1$  can be characterized as exhibiting intermediate oil-wetness.

## 1.2.2 Crude Oil Wettability

Amott testing utilized crude oils native to the three formations. For all LKC cores located in wells near the Hall-Gurney Field oil from the Carter-Colliver lease was used. Arbuckle samples near the Hadley #L-4 utilized the oil from this well. Mississippian samples used oils obtained from the Newell 1983-1984 sampling program. In addition select LKC and Arbuckle samples used oils obtained from the Newell 1983-1984 sampling program.

Amott-Harvey wettability index ( $I_{AH}$ ) values for the Lansing-Kansas City oomoldic limestones can be interpreted to indicate this formation exhibits low intermediate oil-wetness to LKC crude oils (**Fig. 1-12**). Values range from  $0.10 < I_{AH} < 0.41$  with average  $I_{AHavg} = 0.26$ . Mississippian rocks have less oil wetness tendency exhibiting a range of  $0.19 > I_{AH} > -0.09$  with average  $I_{AHavg} = 0.03$ . This can be interpreted as indicating neutral-wettability. Arbuckle rocks also have less oil-wetness tendency exhibiting a range of  $0.23 > I_{AH} > -0.09$  with average  $I_{AHavg} = 0.02$ . This can be interpreted as indicating neutral-wettability.

The Mississippian cores contain variable amounts of chert and dolomite. Because of this mixed mineralogy the intermediate  $I_{AH}$  values may partially reflect mixed wetting conditions. However, the cores tested were not highly siliceous and did not have sufficient potentially water-wet chert to balance the presence of more oil-wet calcite supporting an interpretation that the rock exhibits neutral wettability.

Although  $I_{AH}$  values are shown to two decimal places, and are binned to two decimal places in Figure 1-12, the accuracy of the measurement only strictly supports interpretation to one decimal place.

For over half the samples, spontaneously-displaced oil and water volumes were small and could only be measured to an accuracy of  $\pm 10-40\%$ . Limited experiments with longer equilibration times than 7 days indicated additional fluid was expelled but incremental volumes were insufficient to support the added time and would not significantly change the wetness classification. More research is needed using significantly larger core plug samples but these were not easy to obtain in the core available. Though additional work may help reveal trends in wettability, it is unlikely that it will significantly change the ranking nature of the results presented in this study.

To evaluate how the wettability testing method may be influenced by rock pore geometry, Amott  $I_{AH}$  is cross-plotted against permeability in **Figure 1-13**. It can be conjectured that within a given rock pore system exhibited by a formation change in permeability would reflect some systematic pore geometry change (e.g., increasing pore throat diameter). The absence of correlation between Amott  $I_{AH}$  and permeability partially supports an interpretation that pore geometry, as measured by permeability, does not strongly influence the wettability results.

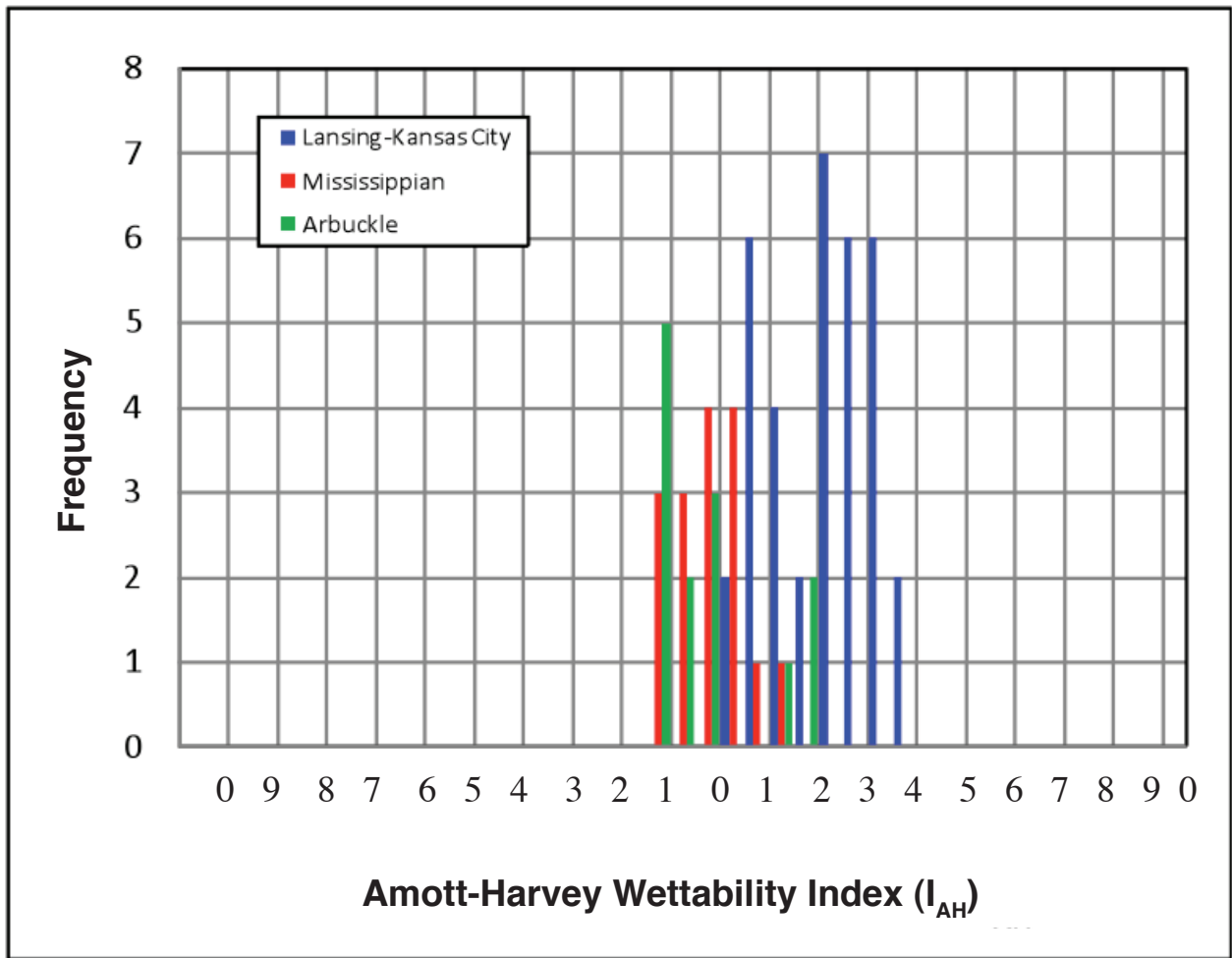


**Figure 1-12.** Amott-Harvey wettability index ( $I_{AH}$ ) distribution for Lansing-Kansas City, Mississippian, and Arbuckle cores and crude oils tested. LKC rocks can be characterized as exhibiting low intermediate oil wetness. Arbuckle and Mississippian rocks can be interpreted to exhibit neutral wettability.

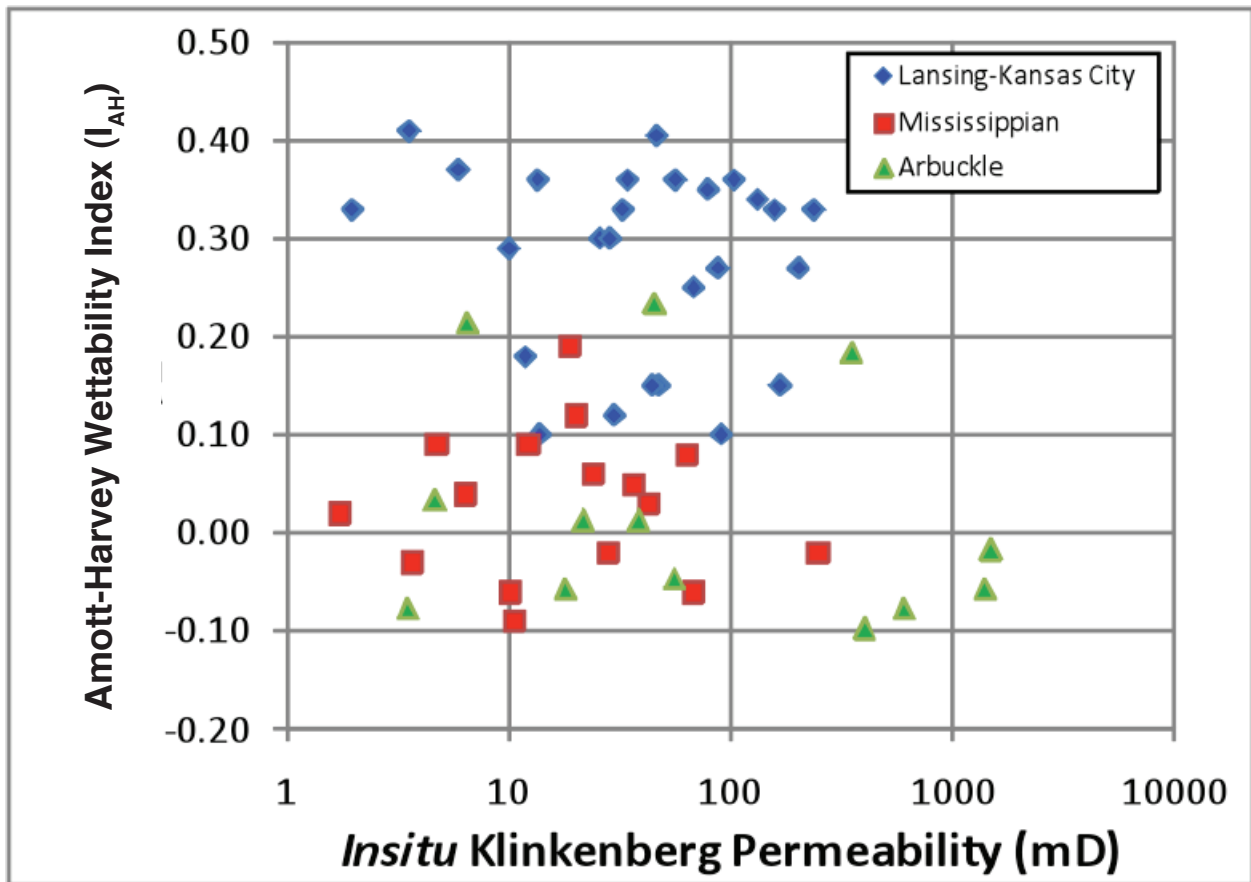


**Figure 1-13.** Crossplot of Amott-Harvey wettability index ( $I_{AH}$ ) versus permeability. The absence of correlation can be interpreted to indicate that pore geometry does not exert significant influence of the wettability testing results.

### 1.2.3 Isopar G Oil Wettability

Subsequent to crude testing select samples were Soxhlet extracted to remove fluids and the wettability testing repeated using an isoparaffinic oil, Isopar G. Being composed a narrow range of paraffinic oil, this oil is interpreted to not contain the surface active agents potentially present in crude oils which might influence wettability. Use of an oil without surface active molecules could aid in interpreting the role of pore geometry on wettability testing results. **Figure 1-14** shows the distribution of Amott-Harvey wettability index values for the Isopar G wettability tests. For the Lansing-Kansas City  $I_{AH}$  for Isopar G averaged 64% of  $I_{AH}$  for crude values, with a range of 49%-88%. Arbuckle and Mississippian  $I_{AH}$  values for Isopar G were randomly greater than and less than  $I_{AH}$  values for crude and can be interpreted to indicate no significant difference.

The difference between Isopar G and crude  $I_{AH}$  values for the LKC may indicate that the oils simply have differing amounts of surface active agents. General classification of wetness for these rocks is unchanged for Isopar G.

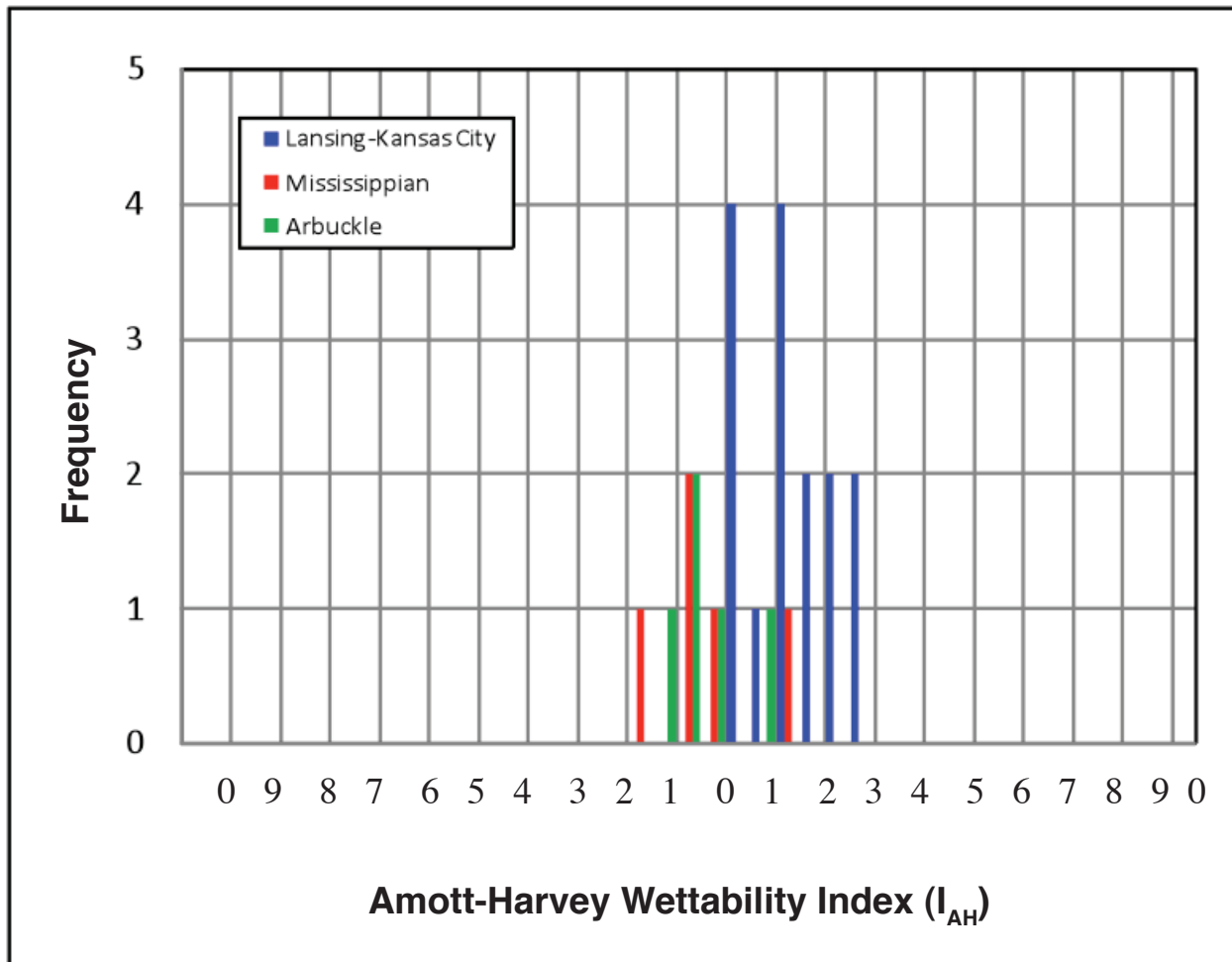


**Figure 1-14.** Amott-Harvey wettability index ( $I_{AH}$ ) distribution for Lansing-Kansas City, Mississippian, and Arbuckle cores and Isopar G oil. Comparison with Figure 1.3 shows that LKC cores exhibit  $I_w$  values that average 64% of the values exhibited for crude oils.

## 1.3 Porosity and Permeability

Fundamental to reservoir characterization and performance prediction is an understanding of porosity and permeability. For the three shallow shelf carbonates that are the focus of this study, efforts to characterize porosity and permeability have been an area of investigation. To support the efforts in this study core plugs were obtained from previous studies and some of the tests performed in this study were performed on core plugs previously obtained and for which porosity and permeability data existed. In addition, new cores were sampled in each of the three formations to supplement the existing database and to obtain better representative samples for testing.

### 1.3.1 Lansing-Kansas City

In the Lansing-Kansas City, a core was taken in the Murfin Terry Unit #7-32 (API 15-023-20503, T2S R41W Sec. 32, SE SW SW NW), Raile Field, and provided to this study. Most Lansing-Kansas City rock is oomoldic limestone. The Terry Unit #7-32 represented the LKC in northwest Kansas where the lithology also includes peloidal packstone in addition to the commonly observed oomoldic limestone. Core was also described, sampled, and analyzed from the Kansas Geological Survey Bethany Falls outcrop Woodward wells; W1, W2, W3, W4, W5, and W6 (T25S R22E Sec. 6) that were part of previous study of the Victory Field but did not have detailed porosity, permeability, or electrical properties data. This core provided important integration of petrophysical properties with oolite shoal geometry and vertical distribution of properties that formed the basis for reservoir geomodel construction discussed in Section 4. The Austin #2-27 was cored for this study and is discussed in Section 5.1. **Figure 1-15** shows the permeability-porosity trend for the Lansing-Kansas City with the data measured in this study included.

The Lansing-Kansas City rocks were deposited in a shallow shelf carbonate environment. Interaction of changing sea level and local episodic processes, such as tidal currents along a broad topographically high shelf area, led to accumulation and local reworking and redeposition of elongate stacked, shingled, and cross-cutting oolite sand bars (0.5-10 m thick). Subaerial exposure and meteoric water percolation led to microporous cementation around the aragonite ooids and often dissolution of the ooids and variable development of vuggy porosity. Resulting oomoldic grainstones, the principal reservoir lithofacies, underwent variable degrees of early or later touching oomold-oomold dissolution, fracturing, and crushing, providing connection between otherwise largely isolated oomolds. Grain size variation, location on oolite buildups and local topography, and interbedded carbonate mud (aquifers) influenced the nature and extent of diagenetic overprinting and resulting permeability-porosity, and capillary pressure properties.

Porosities in LKC oomoldic limestones range up to 35% and permeabilities principally range from 0.001-400 md. The relation between permeability (0.001-400 md) and porosity (0-34%) is significantly influenced by the connectivity of the oomoldic pores complicating the use of porosity as an effective predictor of permeability without information about lithology. Permeability is principally

controlled by porosity, oomold connectivity, and connection created by matrix crushing and fracturing. Permeability is also influenced by oomold diameter, oomold packing, and matrix properties. Increasing bioclastic constituents within and bounding oolite beds are often associated with increasing mud matrix and decreasing porosity and permeability.

Previous investigation (Byrnes et al, 2000, 2003) showed the relationship between permeability and rock textural parameters (**Fig. 1-16**) including:

- Connectivity Index - An index ranging from 1 to 4 representing the degree of connection between oomolds as observed at 10X-20X:
- Packing Index - An index from 1 to 4 representing the packing density of oomolds:
- Size - An estimate of the average oomold diameter in phi units
- Archie Matrix Porosity Index - base on Archie's (1952) second parameter for describing matrix  $\phi$ .

Individual wells exhibit porosity-permeability trends with less variance than the overall trend exhibited by LKC oomoldic limestones. Of significant importance to modeling permeability and porosity distribution is that within a given LKC interval 4<sup>th</sup> order sequence stratigraphic cycle porosity and permeability generally increase with the base to top of the interval. Within the LKC 'C' zone in the Hall-Gurney field, permeability decreases from the top of the bottom of the LKC 'C' interval (**Fig. 1-17**). Lower permeability with increasing depth in the reservoir interval is attributed to increased dense bioclastic limestone content and decreasing moldic porosity. Work in this study for the Murfin Austin #2-27 shows that permeability increases from the base to top of the LKC interval but that the highest porosities for the interval are below the highest permeability interval (**Fig. 1-18**). This is attributed to the presence of isolated oomolds within a micritic matrix. The high porosity portion of this reservoir exhibits permeability values that lie outside the general permeability-porosity trend for LKC oomoldic limestones.

The Woodward #2 core reveals the complexity of petrologic and petrophysical properties that can exist within an LKC interval at fine scale (e.g., < 0.5 ft). **Figure 1-19** shows the porosity, permeability, and rock texture profile for the Woodward #2 (W2) outcrop well. Porosity and permeability correlate with depositional trends but the relationship is complex and is strongly overprinted by diagenesis. The upper Mound Valley interval exhibits significantly lower permeability than the underlying Bethany Falls interval for similar porosities (Rankey et al, 2006). Wells generally exhibit a relatively unique permeability-porosity trend for each LKC cycle within the well (Fig. 1-20). In the Woodward #2 both the Mound Valley member and the underlying Bethany Falls are present and were sampled. Each LKC cycle exhibits a relative unique permeability-porosity trend (**Fig. 1-20**).

Although permeability-porosity trends for wells are often well defined and reflect a consistent pattern of oomold porosity development and connectivity, both the Austin #2-27 and the Woodward #2 indicate that multiple trends, reflecting different depositional and diagenetic patterns, may exist within a given LKC cycle. Trends often reflect; 1) a trend representing well-connected oomoldic porosity that is frequently observed at near the top of the cycle, and 2) a separate trend representing a lower

porous interval in which oomold connectivity and permeability are low. Fine-scale vertical lithologic and diagenetic heterogeneity can strongly influence permeability and porosity. An interval near top of Bethany Falls (**Fig. 1-21**) exhibits highly porous and permeable oomoldic grainstone layers measuring approximately 1-2 inches in thickness, finely interbedded with beds of very low-permeability patchy oomolds with abundant microspar. Three feet below this interval is a thick (4-foot) oomoldic grainstone interval that exhibits uniformly good porosity (14-21%) and permeability (3.5-10.2 mD) (**Fig. 1-22**).

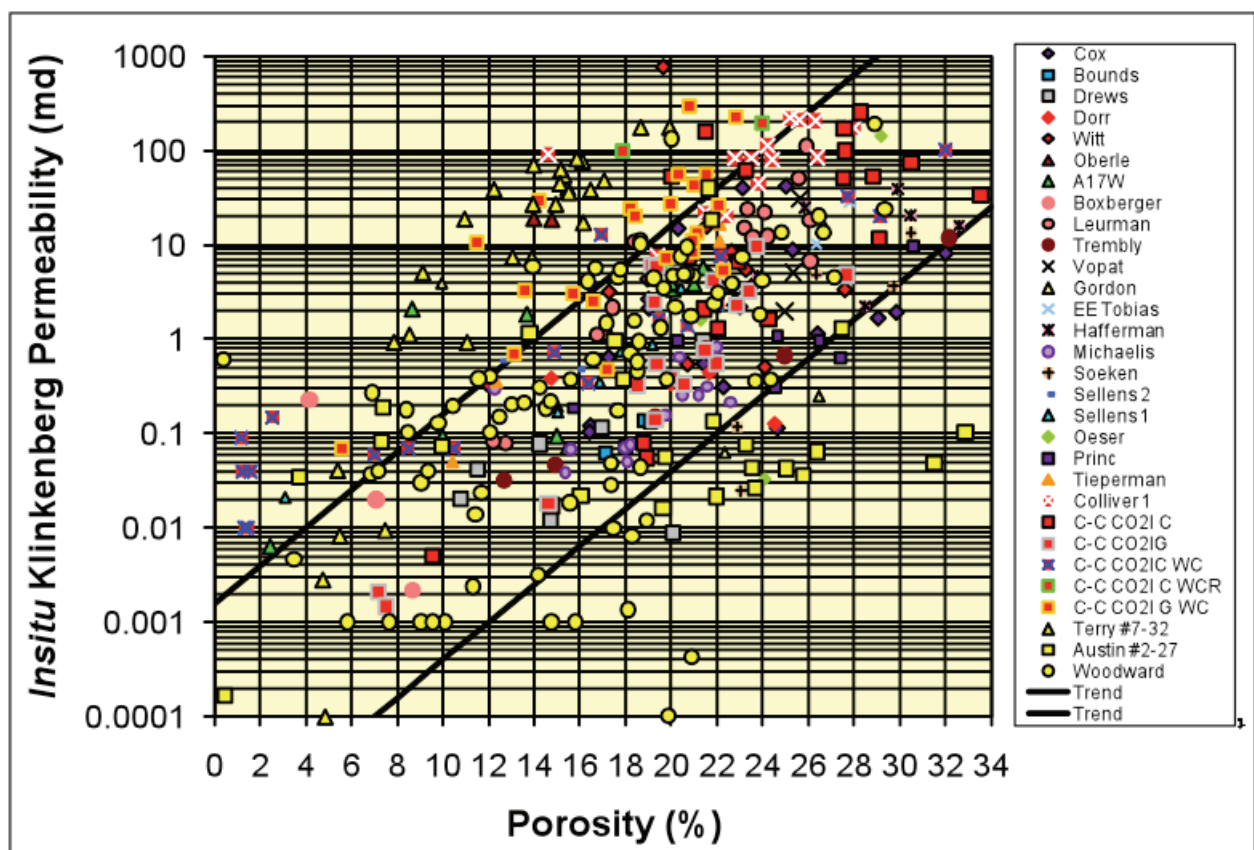


**Figure 1-15.** Crossplot of *in situ* Klinkenberg permeability versus porosity for all Lansing-Kansas City core plugs. The three data sets measured in this study (bottom three solid yellow symbols) increased the variance in permeability for a given porosity. Higher permeabilities in the Terry #7-32 are for peloidal packstone lithology cores and not oomoldic limestones which represent the majority of LKC rocks. Low permeability in the Woodward outcrop samples may reflect overprinting near-surface diagenetic overprinting.

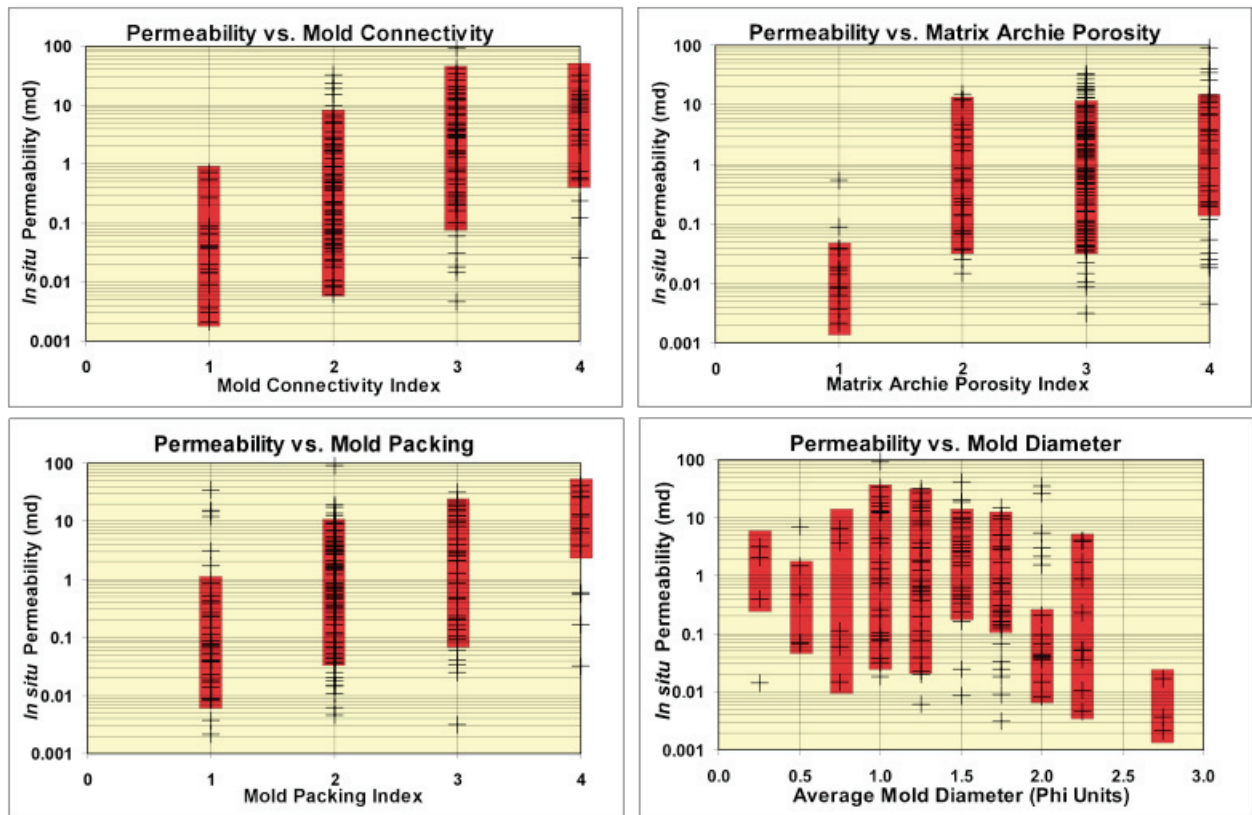


Figure 1-16. Crossplot of *in situ* Klinkenberg permeability versus textural property for Lansing-Kansas City oomoldic limestones (after Byrnes et al, 2000).

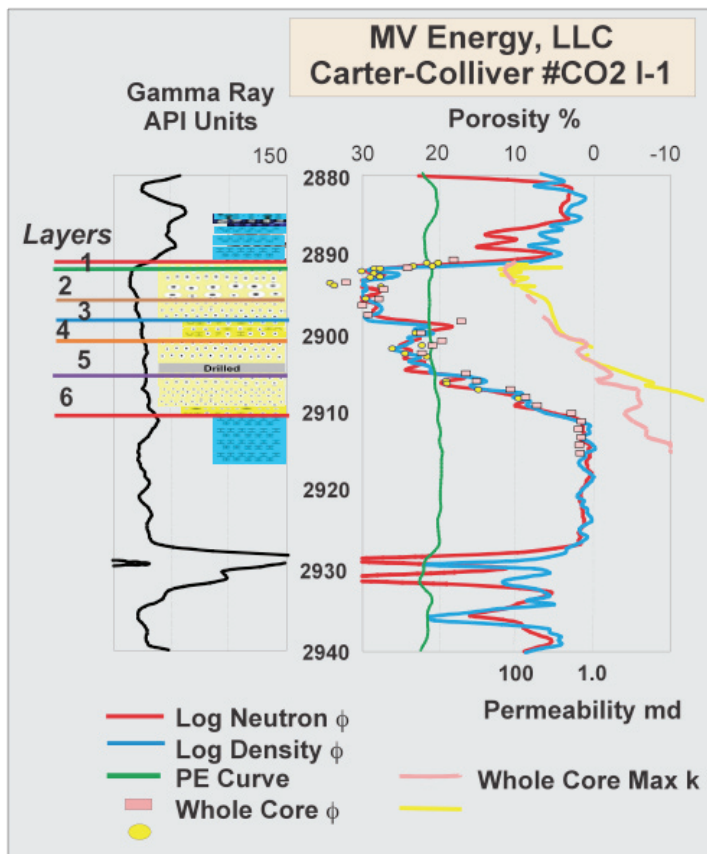
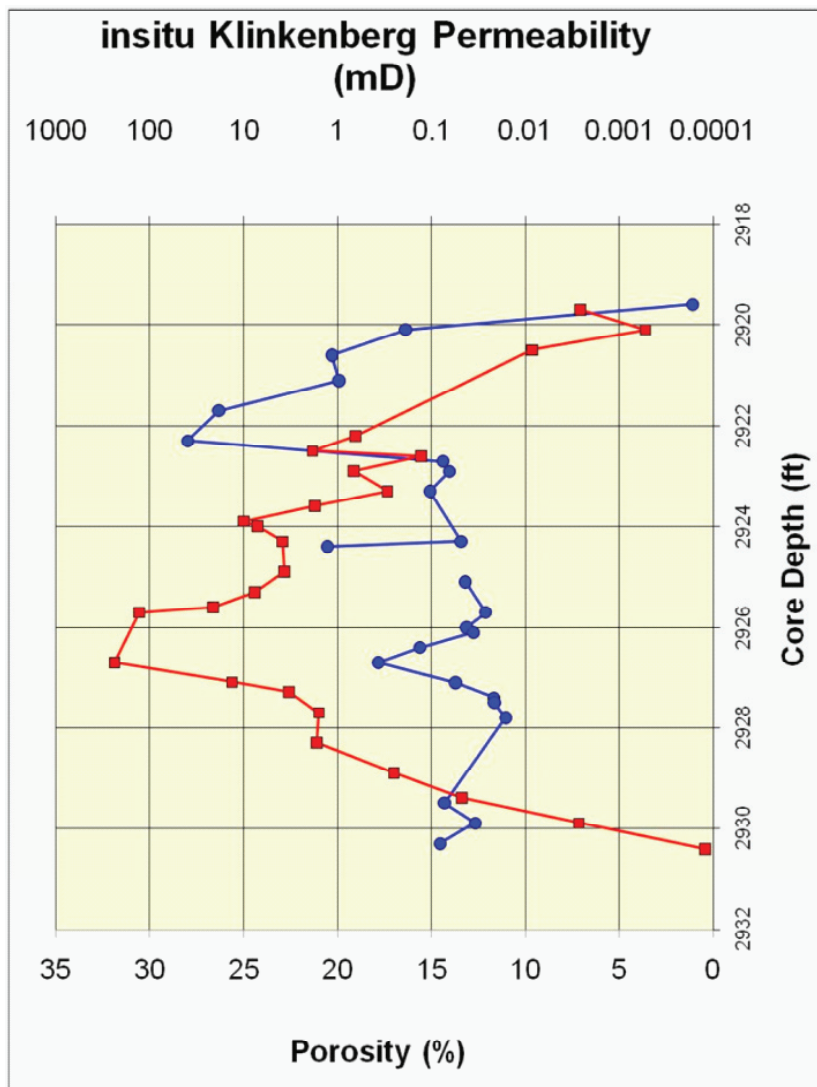
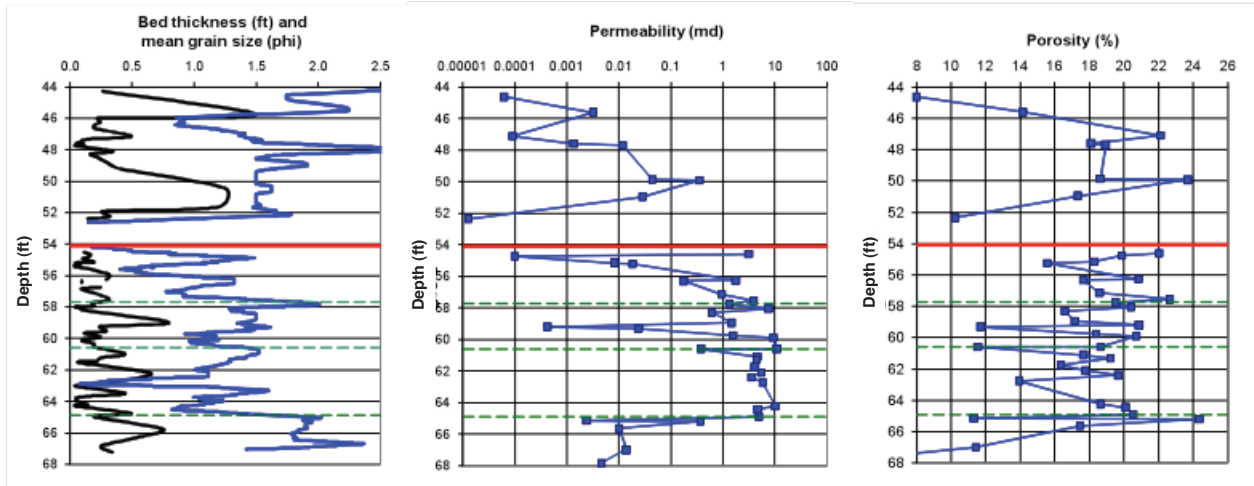


Figure 1-17. Porosity, permeability, and rock texture profile for the Carter-Colliver #CO2-1, Hall-Gurney field showing vertical increase in porosity, permeability and oomold size (after Dubois et al, 2001).



**Figure 1-18.** Porosity, permeability, and rock texture profile for the Murfin Ausitn #2-27, cored in this study. Showing vertical porosity and permeability profile. The role of rock texture on permeability is illustrated by the low permeability of the maximum porosity interval. High permeability at the uppermost portion of the reservoir interval is commonly observed in L-KC reservoirs.



**Figure 1-19.** Porosity, permeability, and rock texture profile for the Woodward #2 (W2) outcrop well. Porosity and permeability correlate with depositional trends but the relationship is complex and is strongly overprinted by diagenesis. The upper Mound Valley interval exhibits significantly lower permeability than the underlying Bethany Falls interval for similar porosities (modified after Rankey et al., 2007).

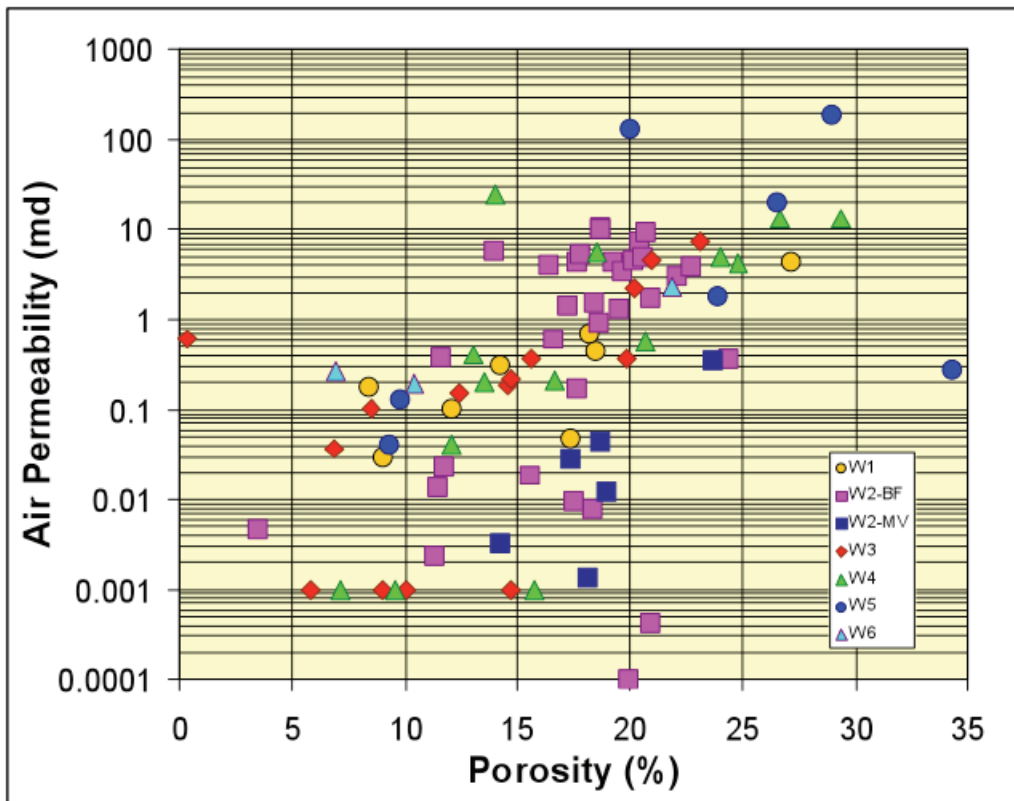


**Figure 1-20.** Crossplot of porosity and permeability for the Bethany Falls outcrop wells. Each well tends to exhibit a unique trend but can exhibit multiple trends. In the Woodward #2 the Mound Valley (W2-MV) interval exhibits a different trend than the underlying Bethany Falls (W2-BF). Low permeability samples within the W2-BF reflect fine-scale heterogeneity shown in Figures 1-21 and 1-22.

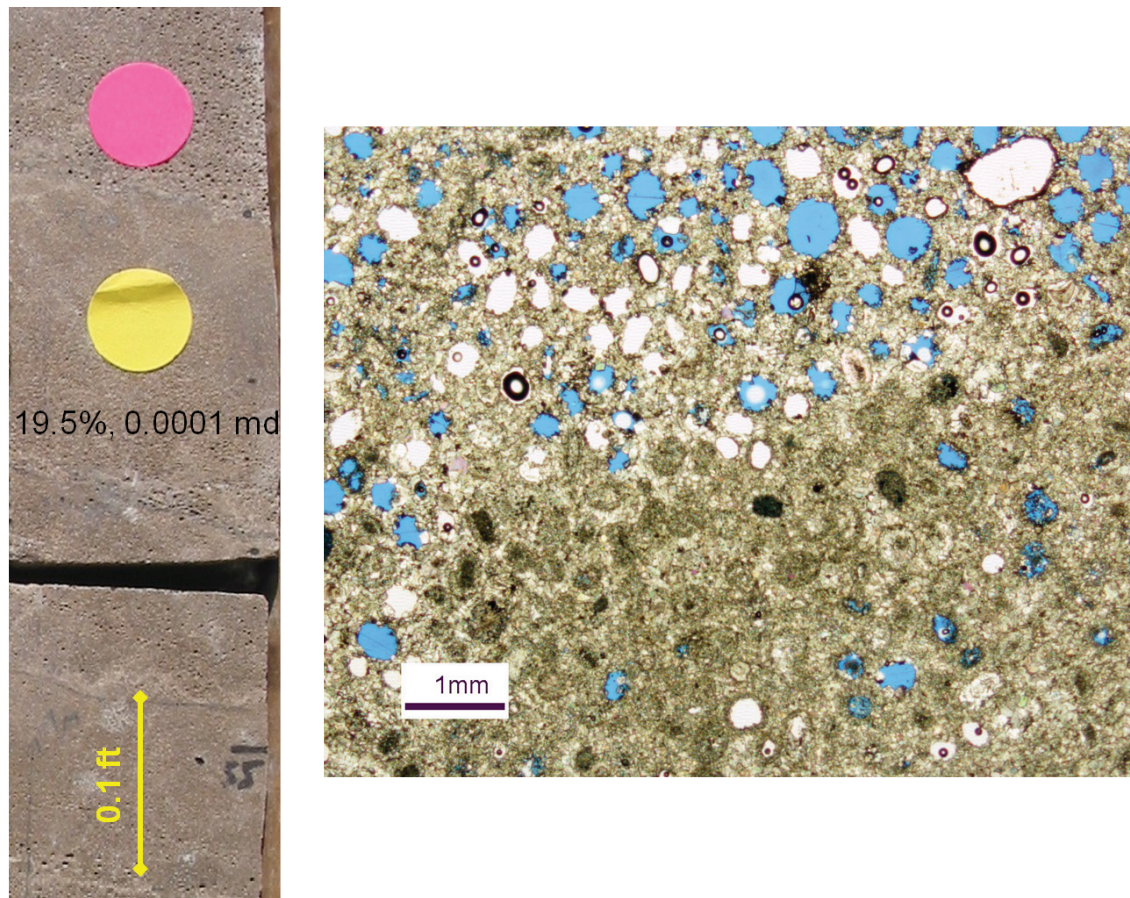


**Figure 1-21.** Interval near top of Bethany Falls (yellow dot marks core sample at 54.75 ft) exhibiting highly porous and permeable oomoldic grainstone layers measuring approximately 1-2 inches in thickness, finely interbedded with beds of patchy oomolds with abundant microspar. Images are plane polarized light with blue dye epoxy impregnation of porosity. (After Rankey et al, 2006.)

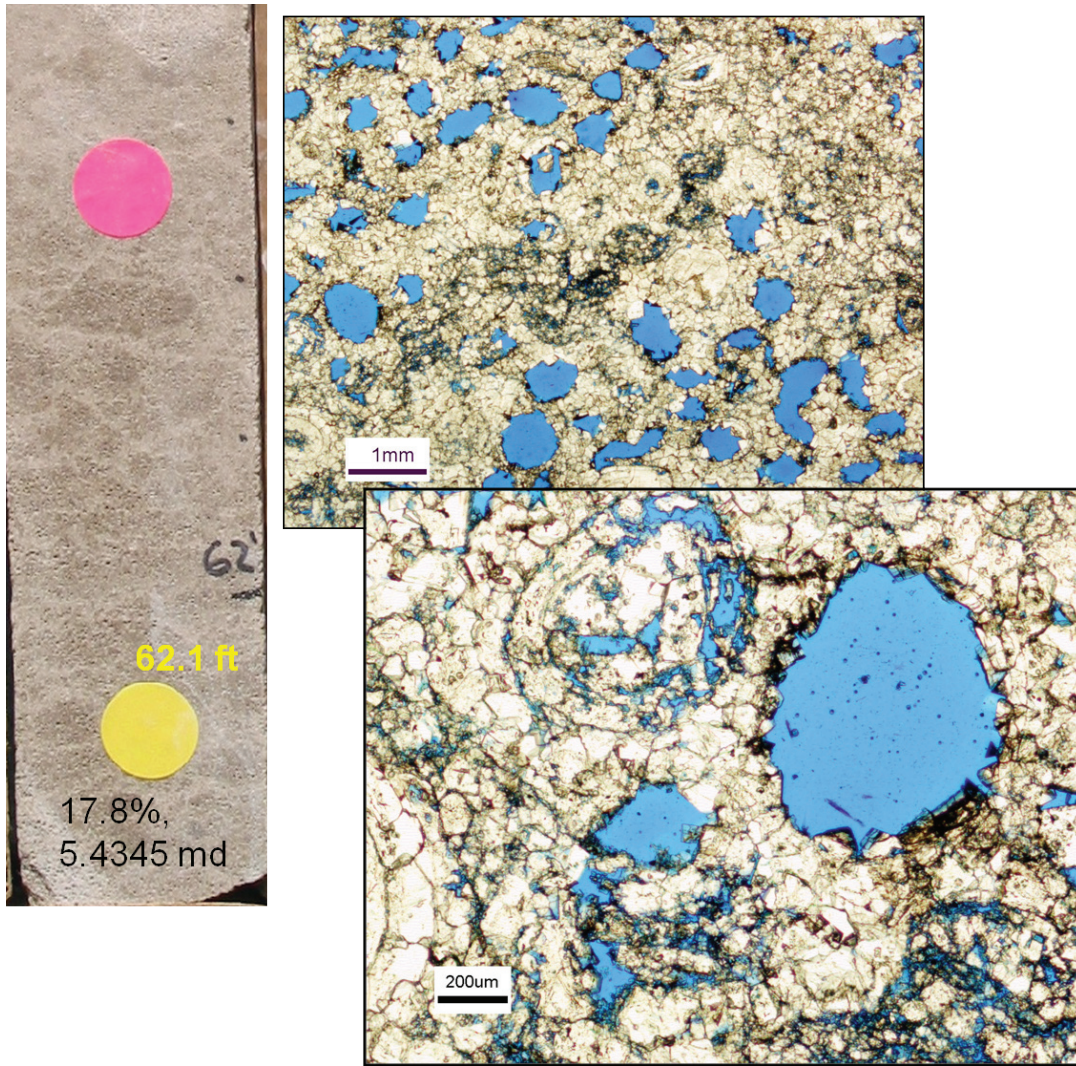


**Figure 1-22.** Interval near top of Bethany Falls (yellow dot marks sample at 62.1 ft). Uniformly thick interval of well sorted oomoldic grainstone. Two thin section images at different magnifications show partial dissolution of some ooids and local crushing. Images are plane polarized light with blue dye epoxy impregnation of porosity. (After Rankey et al, 2006.)

### 1.3.2 Mississippian

In the Mississippian core was made available from the Cheyenne Wells field in eastern Colorado. Core plugs (n=208) were taken from the Champlin Aldrich #3 and Klepper #4 cores. These data provided integration with a thesis study (Givens, 2007) characterizing the core lithology and mineralogy. **Figure 1-23** shows the permeability-porosity trend for the Mississippian with the data measured in this study included.

Franseen (2006) thoroughly reviewed the nature of carbonate facies deposition in the Mississippian system in Kansas.

Lithofacies and early diagenesis are major controls on permeability (k) and porosity ( $\phi$ ) despite complex diagenetic overprinting by sub-Pennsylvanian subaerial exposure and burial processes. Permeability and porosity decrease significantly and continuously with decreasing grain/mold size from packstone to mudstone (a trend exhibited by many other carbonates) and from echinoderm-rich to spicule-rich facies. An exception is the echinoderm grainstone facies which is silica cemented and exhibits very low permeability and porosity.

The *insitu* Klinkenberg permeability ( $k_{ik}$ )- *insitu* porosity ( $\phi_i$ ) trend for all lithofacies are approximately bounded within two orders of magnitude by trendlines defined by:

$$\log k_{ik} = 0.25 \phi_i - 2.5 \quad (1-7)$$

$$\log k_{ik} = 0.25 \phi_i - 4.5 \quad (1-8)$$

where  $k_{ik}$  is in millidarcies (md) and porosity is in percent.

Between these bounding trends each lithofacies exhibits a generally unique range of permeability and porosity which together define a continuous trend, with permeability decreasing with decreasing grain/mold size for any given porosity. Each individual lithofacies exhibits a unique sub-parallel trend to the general trend.

Subtrends for clusters of facies or individual facies may also be defined and are significantly more accurate with standard error of prediction of permeability decreasing with increasing selectivity of lithofacies characteristics. Standard error for a specific lithofacies is generally less than a factor of 3. Linear regression trends for spicule- and echinoderm-rich facies are:

$$\log k_{ik} = 0.19 \phi_i - 2.88 \text{ [Spicule-rich]} \quad (1-9)$$

$$\log k_{ik} = 0.12 \phi_i - 1.04 \text{ [Echinoderm-rich]} \quad (1-10)$$

where  $k_{ik}$  is in millidarcies (md) and porosity is in percent.

Mississippian fields' permeability (k)-porosity ( $\phi$ ) trends are similar for similar lithofacies. One significant difference is that calcite cementation of spicule-rich pack-wackestones significantly occludes porosity and reduces permeability. The bounding trends can be considered to define the range of porosity for a given lithofacies trend. The low k- $\phi$  slopes of individual lithofacies trends indicate that increas-

ing porosity does not significantly increase permeability compared with the influence of grain size. This is consistent with porosity development through dissolution of pores surrounded by permeability-controlling matrix.

Trends for echinoderm-rich and spicule-rich facies are significantly different:

$$\log k_{ik} = 0.157 \phi_i - 1.87 \quad [\text{Echinoderm-Bindley Field}] \quad (1-11)$$

$$\log k_{ik} = 0.147 \phi_i - 1.50 \quad [\text{Echinoderm-Ness City Field}] \quad (1-12)$$

$$\log k_{ik} = 0.230 \phi_i - 4.04 \quad [\text{Spicule-Bindley Field}] \quad (1-13)$$

$$\log k_{ik} = 0.170 \phi_i - 2.76 \quad [\text{Spicule-Ness City Field}] \quad (1-14)$$

Standard error of prediction of  $k$  ranges from a factor of 2X to 4.8X. For all fields the lowest  $k$ - $\phi$  slope and highest predictive accuracy is obtained for a single lithofacies. With successive addition of more lithofacies into a statistical analysis the resulting trend-line slope approaches that of the bounding trends. The intercept varies as a function of the nature of the population grain/mold size.

Where lithofacies are well defined the permeability porosity trend can also be expressed using a power law relation. Each individual lithofacies exhibits a unique sub-parallel trend to the general trend where the relationship between  $k$  and  $\phi$  for each lithofacies can be represented by a power-law function of the form:

$$k_{ik} = A \phi_i^{3.5} \quad (1-15)$$

where porosity is in % and permeability is in md, and where the coefficient,  $A$ , varies with lithofacies (Table 1-3). Increasing moldic content, and associated increasing  $\phi$ , increase  $k$  at a lower rate than the overall  $k$ - $\phi$  trend indicating that matrix properties dominate control of flow in these rocks.

**Table 1-3.** Coefficients for equation 1-15 expressing the power-law relationship between permeability and porosity as a function of lithofacies and shown in Figure 1-24.

Lithofacies	A
Packstone	0.00489
Pack-Wackestone	0.00142
Wackestone	0.00041
Mud-Wackestone	0.00012
Mudstone	0.00003
Shaly Mudstone	0.00001

Although equation 1-15 generally characterizes the  $k$ - $\phi$  relationship for lithofacies in Kansas, analysis of the Cheyenne Wells field cores, indicates a modified form of equation 1-15 is required:

$$k_{ik} = A \phi_i^{3.25} \quad (1-16)$$

where  $A = 10^{(-5.51 + 0.4 * lith)}$ , porosity (%) and *lith* represents an integer classification of the lithofacies (1- mudstone, 2- mud-wackestone, 3- wackestone, 4- wacke-packstone, 5- packstone, 6- pack-grainstone, grainstone, fine to medium crystalline dolomite).

Figures 1-25 through 1-28 illustrate the lithologic differences that can exist among Mississippian reservoirs that are characterized using the Dunham lithofacies classification. These differences can result in required modification of the coefficient in equation 1-15 to appropriately represent textural and diagenetic differences between rocks of similar Dunham classification.

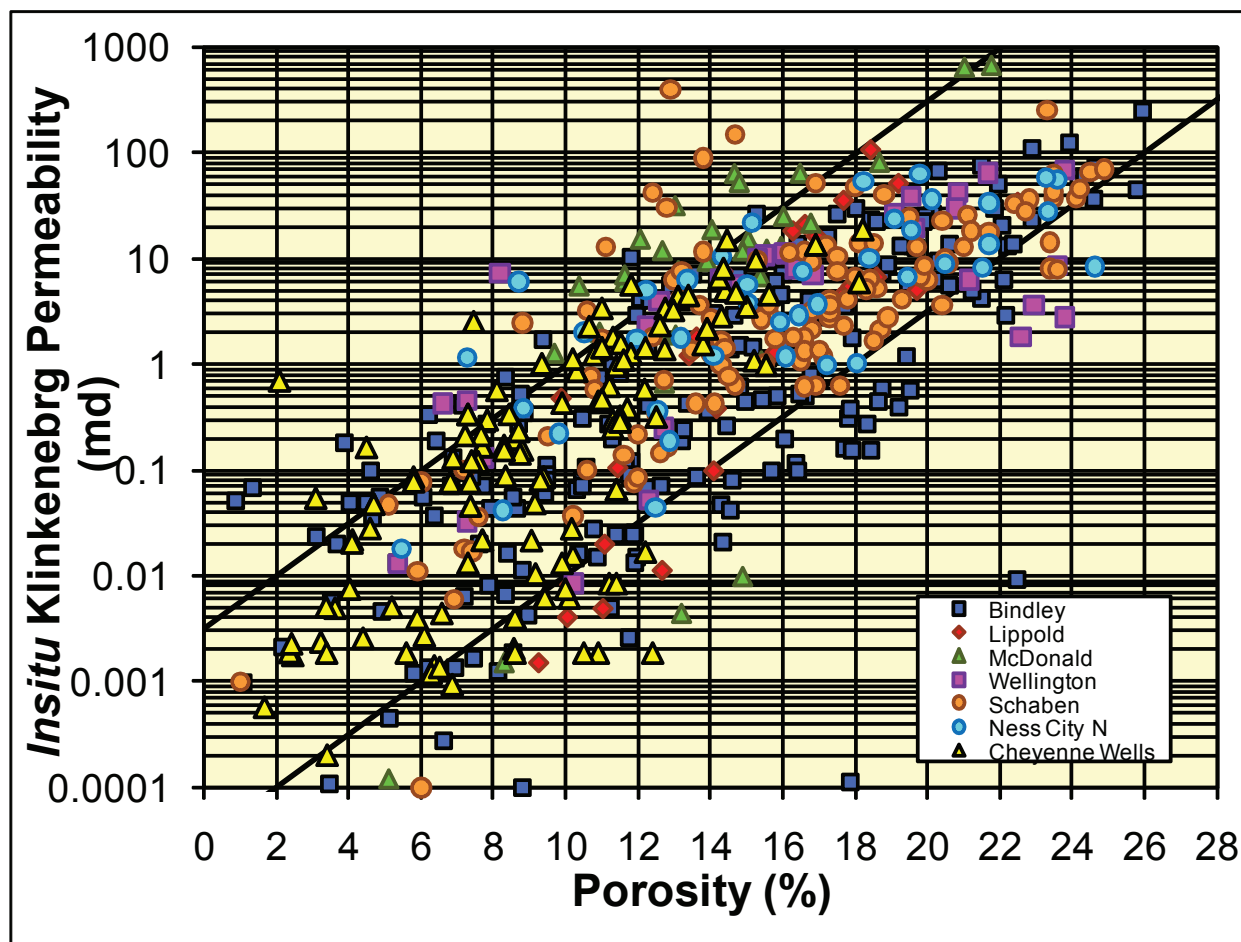
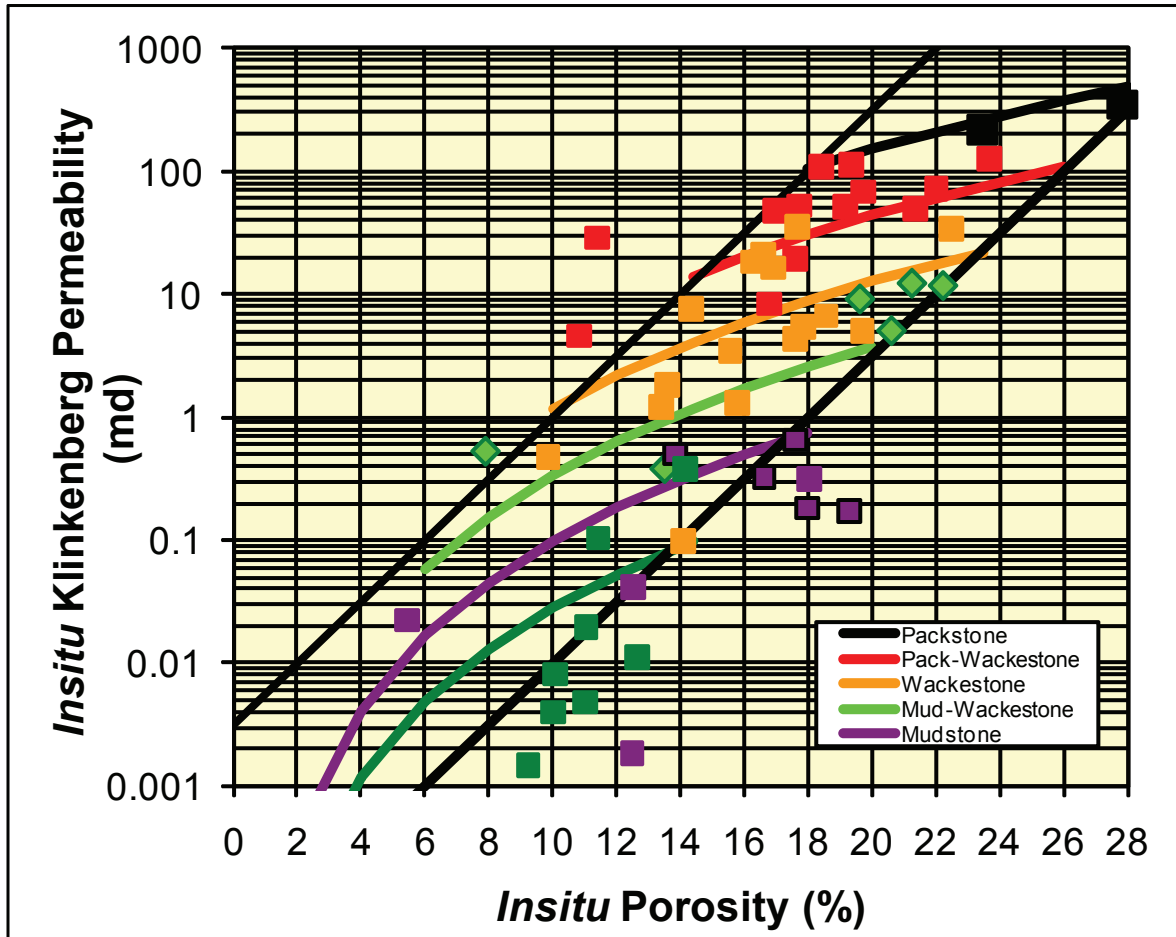
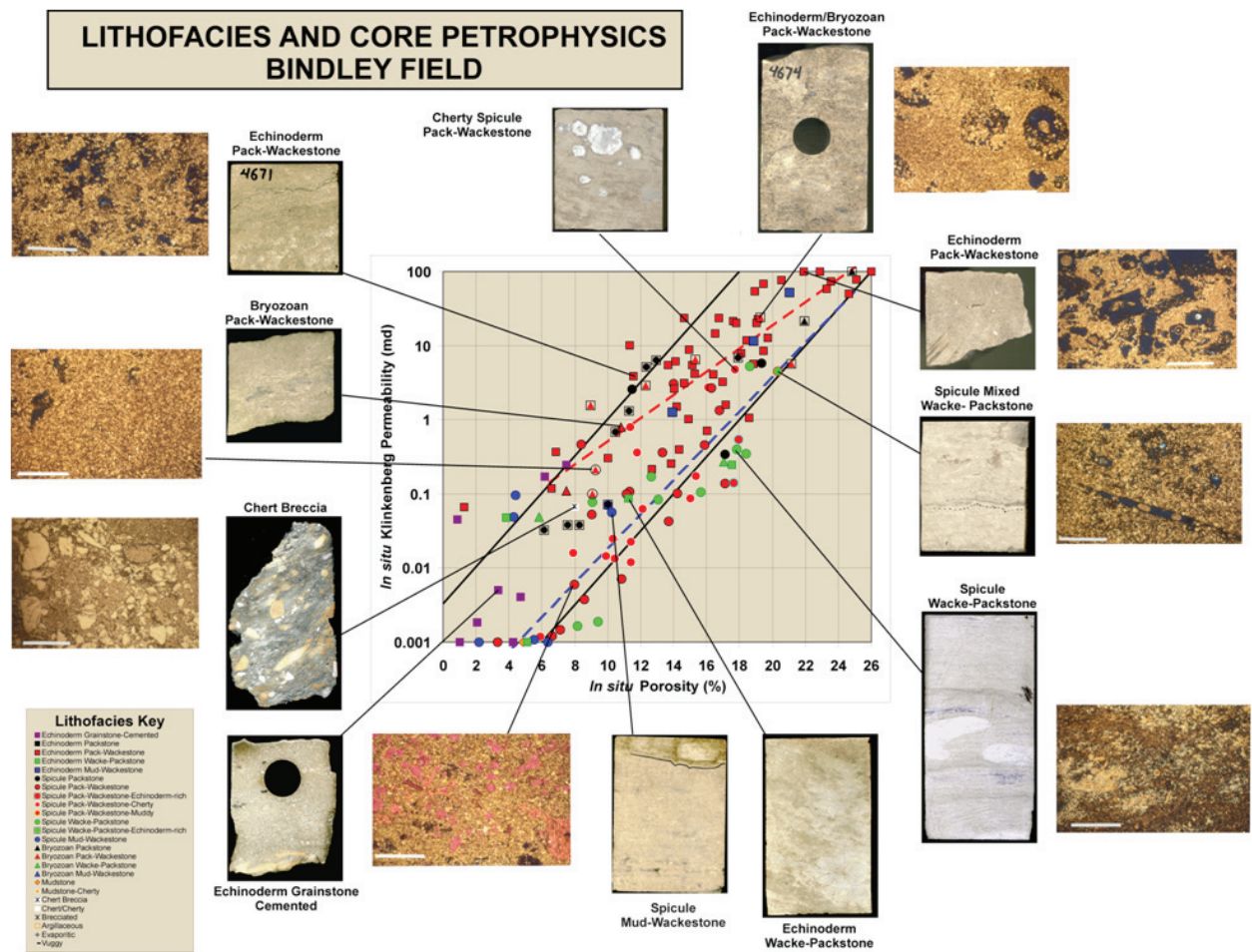


Figure 1-23. Crossplot of *insitu* Klinkenberg permeability versus porosity for all Mississippian core plugs. The eastern Colorado Cheyenne Wells data set measured in this study (solid yellow symbols) exhibited a consistent trend with central Kansas rocks but integration with lithofacies indicates that these rocks require a higher energy lithofacies to exhibit the same permeability for a given porosity. General bounding trendlines represent equations 1-7 and 1-8 in text.



**Figure 1-24.** Permeability versus porosity crossplot for various lithofacies in the Mississippian in Kansas. Each individual lithofacies exhibits a unique sub-parallel trend to the general trend where the relationship between  $k$  and  $\phi$  for each lithofacies can be represented by a power-law function of the form:  $k = A \phi^{-3.5}$  where the coefficient,  $A$ , varies with lithofacies. Values for  $A$  for each lithofacies are shown in the Table 1-3.



**Figure 1-25.** Crossplot of *in situ* Klinkenberg permeability versus porosity for Mississippian rocks from various wells in the Bindley field. Lithofacies are shown parametrically on plot. Images of representative cores and thin sections point to sample results for core shown.

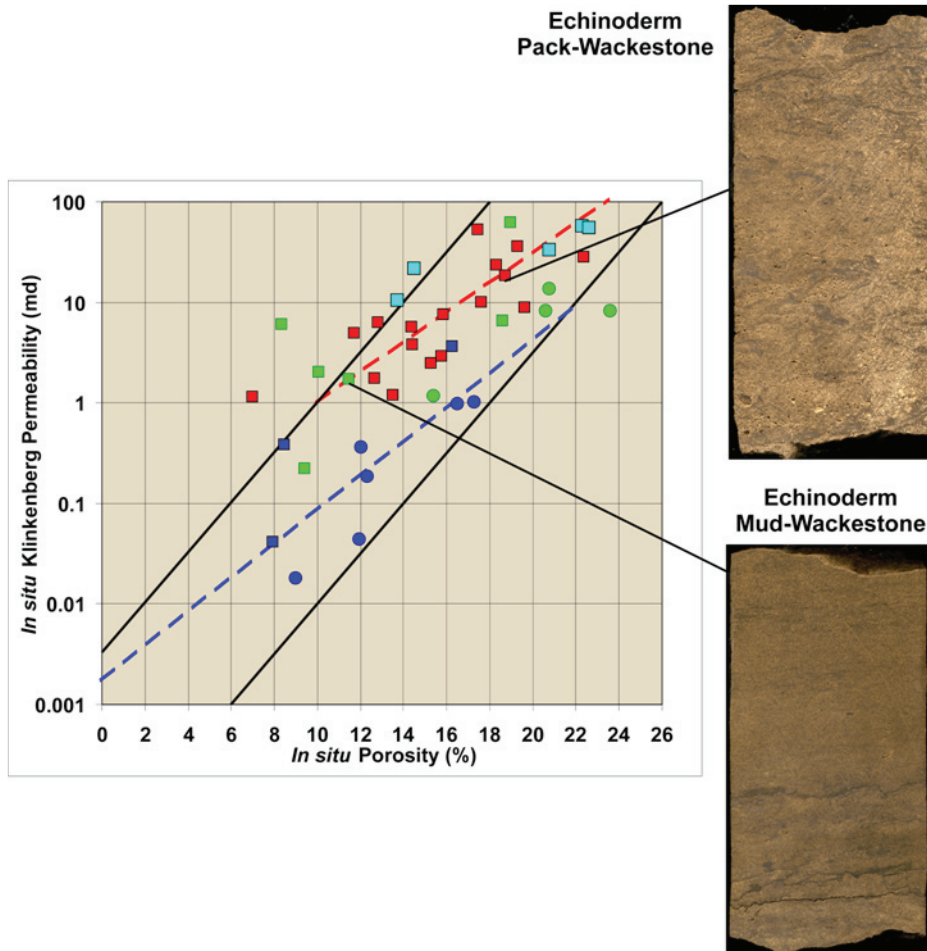


**Figure 1-26.** Crossplot of *in situ* Klinkenberg permeability versus porosity for Mississippian rocks from various wells in the Ness field. Lithofacies are shown parametrically on plot. Images of representative cores point to sample results for core shown.

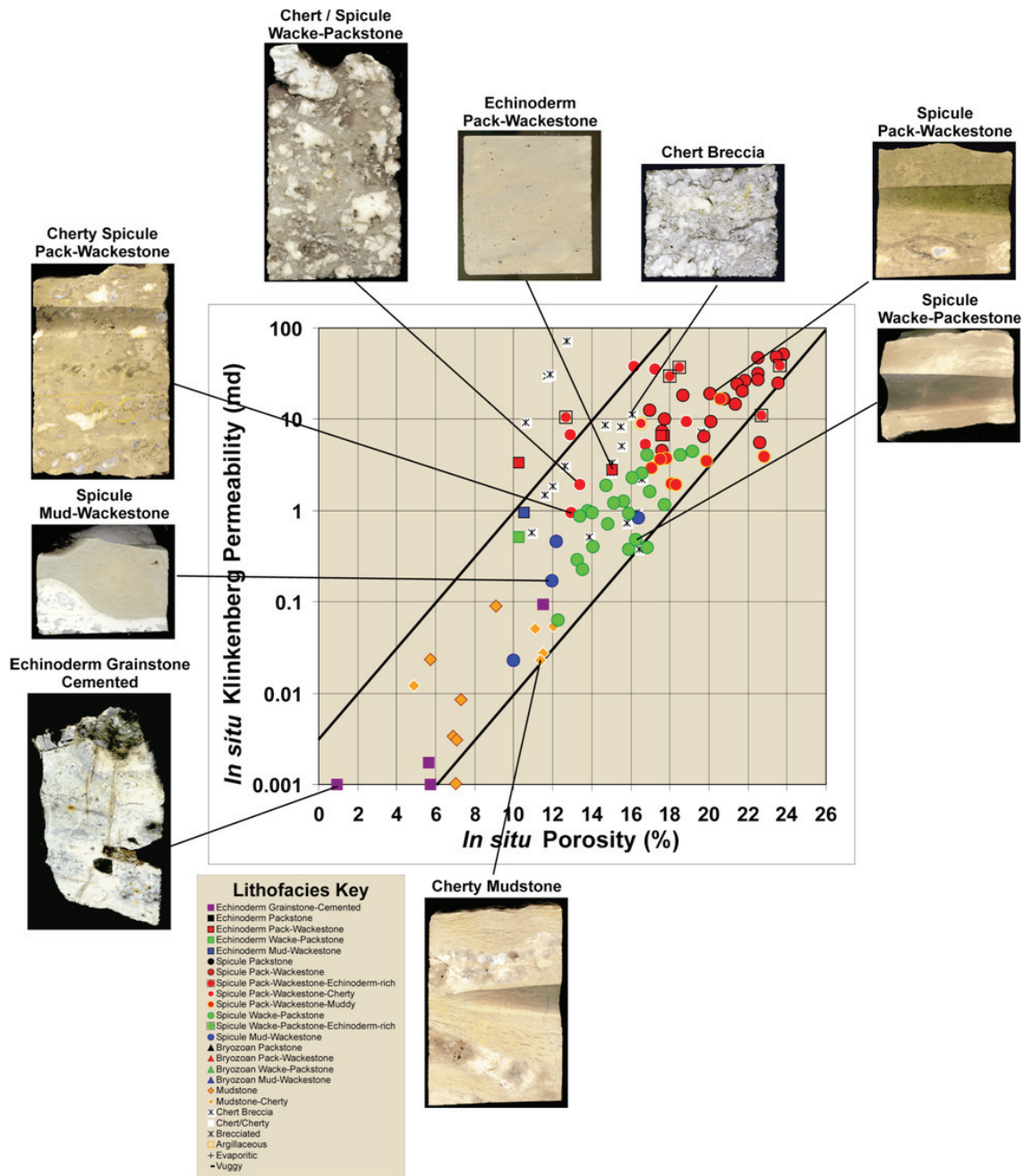


**Figure 1-27.** Crossplot of *in situ* Klinkenberg permeability versus porosity for Mississippian rocks from various wells in the Schaben field. Lithofacies are shown parametrically on plot. Images of representative cores point to sample results for core shown

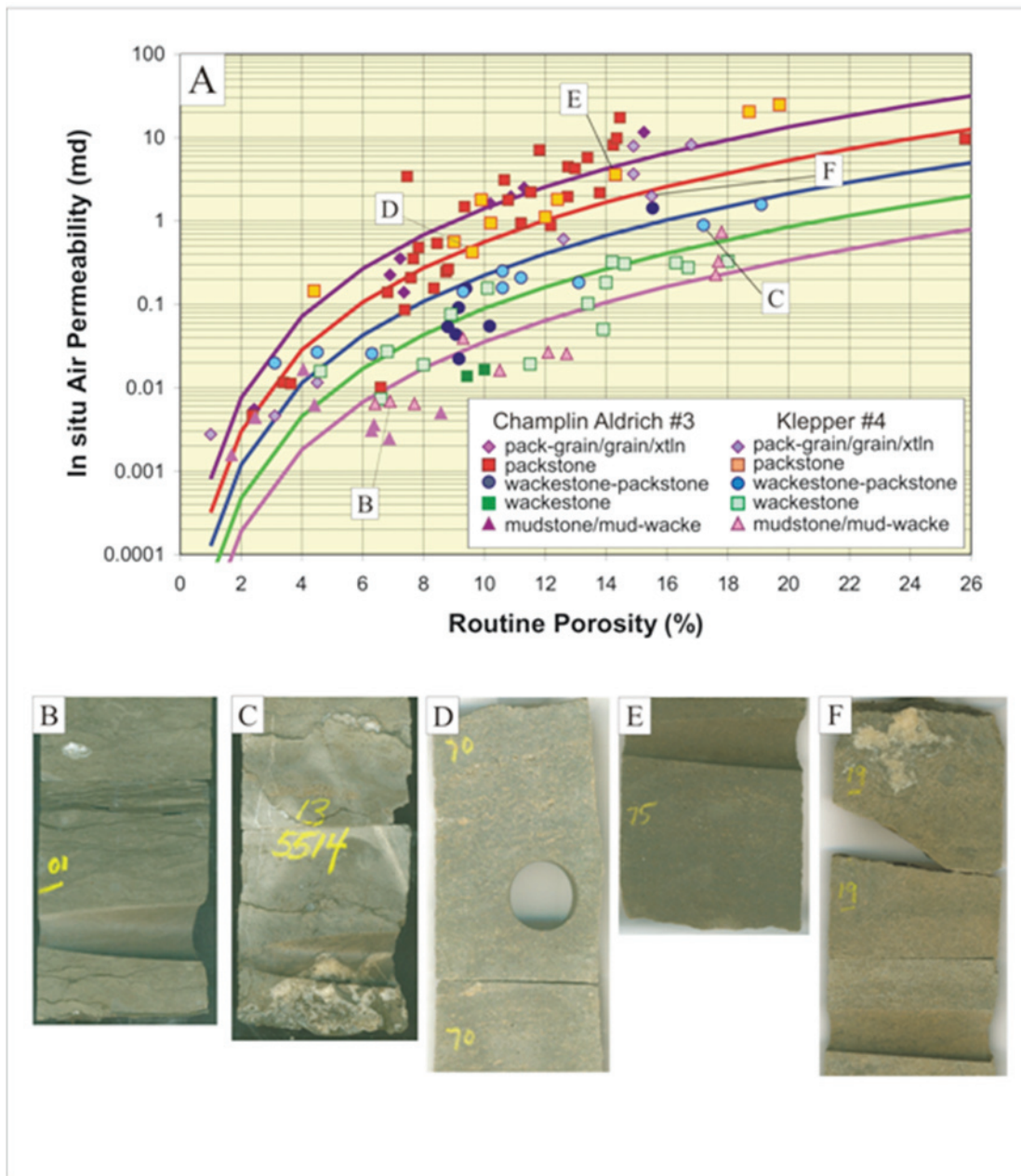


**Figure 1-28.** A. Graph of permeability versus porosity for different lithofacies from Cheyenne wells Champ- lin Aldrich 3 and Klepper 4. Trendlines are described by equation 1-16. Klepper core images show various lithofacies: B. Mudstone. C. Wacke-packstone and coarsely crystalline fractured interval where core plug was taken. D. Moldic packstone. E. Oil stained moldic packstone. F. Oil stained moldic pack-grainstone (after Givens, 2007).

### 1.3.3 Arbuckle

In the Arbuckle new core plug samples were obtained in and characterized in the Hadley L#4 (API 15-051-25131; W/2 SE sec. 30, T. 11 S., R. 17 W.) located in Bemis-Shutts Field. Oil was also obtained from the Haldey L#4. In addition, analyses were conducted on the Murfin Keja #1-3 core obtained as part of this study and discussed in Section 5.

Arbuckle strata are interpreted to have been deposited on a broad shallow shelf in shallow subtidal to peritidal environments. The stratigraphic section consists of up to hundreds of feet of largely dolomitized subtidal to peritidal cyclic carbonates ranging in thickness from one to several tens of feet with karst overprinting in the upper portion as a result of prolonged exposure related to the overlying post- Arbuckle (Sauk-Tippecanoe) unconformity. There is a marked relative absence of karst associated fracture, breccia, and dissolution porosity in most cores, despite their location on the flanks or tops of structural highs where karst processes would likely have been most extensive. Matrix porosity comprises intercrystalline, moldic, fenestral, and vuggy pores related to depositional facies, early diagenesis, and dolomitization. Major facies include: (1) Clotted algal boundstone, (2a) laminated muddy algal boundstone, (2b) laminated grainy algal boundstone, (3) peloidal packstone-grainstone, (4) packstone-grainstone, (5) ooid packstone-grainstone, (6) mudstone, (7) wackestone, (8) intraclastic conglomerate and breccia, (9) cave fill shale and depositional shale, and (10) chert. In the cores studied the first seven lithologies account for more than 85% of the cored intervals.

Petrophysics of lithofacies at the core-plug scale, and for many lithologies at the whole-core scale, are dominantly controlled by grain size. Each lithology exhibits a generally unique range of petrophysical properties modified by the presence of fractures, vuggy porosity, and grain size variation within the lithologic class. Facies comprising multiple lithologies of differing grain size exhibit bulk properties that are scale-dependent and are a function of the architecture of the constituent facies.

Variance in permeability at any given porosity is approximately 2.5 orders of magnitude and may be primarily attributed to the influence of such lithologic variables as the ratio and distribution of matrix and fenestral/vuggy porosity, grain size variations, and subtle mixing or interlamination of lithologies. Fracturing enhances permeability but does not add significantly to porosity. Vuggy porosity is largely isolated in mudstones, even up to vuggy porosities as high as 8%, but is better connected in wackestones. Vuggy pores can be well connected where vuggy porosity is extensive near the unconformity surface.

Figure 1-29 shows the permeability-porosity trend for Arbuckle core plugs by lithofacies. Key lithofacies in the Arbuckle as described in Franseen and Byrnes (2008), Franseen (1994; 2000), and Steinhaff et al. (1998) include:

**Clotted Algal Boundstones** are characterized by abundant carbonate mud and peloids; a mottled texture and abundant clotted fabrics strongly suggest binding by algae. Local burrow mottling is present in this facies. Clotted algal boundstones typically have a tightly bound matrix consisting of anhedral, euhedral, and polyhedral dolomite (< 0.5 mm) with peloidal cement; locally sheet-like vuggy and

fenestral porosity and rare intercrystalline porosity occur. Clotted algal boundstones exhibit porosities generally less than 6% and permeabilities below 0.1md.

**Laminated Algal Boundstones** consists of wavy laminated algal boundstones and stromatolites with muddy to grainy textures. Brecciated stromatolite facies typically grades upward to non-brecciated, in-place stromatolites. The stromatolites are locally tightly cemented but commonly contain abundant and distinctive differentially developed intercrystalline, fenestral, keystone vug, and solution enlarged porosity that closely follows laminations. Muddy textures exhibit porosities generally less than 6% and permeabilities below 0.1md. Grainy textures represent some of the best reservoir rock ranging in porosity up to 32% and permeability up to 1,500md.

**Peloidal Packstone-Grainstones** are typically massive, horizontally laminated or bedded, and commonly interbedded with coarser-grained lithologies. Locally, it contains wispy lenses of shale and interbedded shale layers. Burrow traces and mottling are common. Peloids are abundant and rare interclasts, lumps, and skeletal grains (gastropods) are present. This rock is tightly bound consisting of anhedral, euhedral, and polyhedral dolomite (< 0.5 mm) and peloidal cement. Porosities range from 0% to 4% and absolute permeabilities range from 0.0003md to 0.1md but are generally below 0.005md.

**Mixed Packstone-Grainstones** are typically massive, horizontally bedded or crossbedded, and interbedded with ooid packstone-grainstone and wackestone-packstone facies. Grains include intraclasts, skeletal and algal fragments, ooids, peloids, and lumps. This facies typically has good intercrystalline porosity. In some rocks the original cement between grains has been leached creating interparticle porosity that is open or filled with chalky chert. Porosities range from 6%, for finer-grained rock and where packstone is mottled with wackestone, to 18% for cleaner more coarse-grained rock. Permeabilities in the packstone lithology range from 0.1md to 50md.

**Ooid Packstone-Grainstones** are massive, horizontally bedded or crossbedded, and typically interbedded with wackestone-packstone facies. Dominant grains are ooids, but other grains including intraclasts, skeletal and algal fragments, peloids, and lumps occur in varying abundance. This facies typically has good inter-crystalline porosity, but locally is tightly cemented by euhedral dolomite (< 0.5 mm). Generally these contain little to no vuggy porosity but exhibit intercrystalline and moldic porosities ranging from 11% to 30%; associated permeabilities range from 10 md to 1,500 md. The highest porosity and permeability values are exhibited by clean, homogeneous, medium-grained moldic packstones.

**Wackestone-Mudstones** are massive to horizontally laminated and frequently burrowed. This facies typically is composed of euhedral dolomite (< 0.05 mm) with little or no porosity. Without vugs, wackestones exhibit porosities ranging from 2% to 11% and permeabilities ranging from 0.01md to 1md. Where vugs are present, porosities can range from 9% to 17%, and permeabilities can range from 1md to 1,000md.

**Intra-Arbuckle Shales** occur interbedded with carbonate rocks.

**Conglomerate and Breccias** consist of rip-up clasts derived from underlying lithologies and typically overlie a sharp erosional surface and are commonly associated desiccation and mud cracks, dewa-

tering structures, sheet cracks, and incipient tepee structures. Conglomerate permeabilities are difficult to measure accurately at the plug or full-diameter scale and generally reflect fracture permeabilities.

**Figure 1-30** shows the *insitu* Klinkenberg permeability ( $k_{ik}$ )- *insitu* porosity ( $\phi_i$ ) trend for all lithofacies are approximately bounded within 2.5 orders of magnitude by trendlines defined by:

$$\log k_{ik} = 0.28 \phi_i - 1.7 \quad (1-17)$$

$$\log k_{ik} = 0.28 \phi_i - 4.3 \quad (1-18)$$

where  $k_{ik}$  is in millidarcies (md) and porosity is in percent.

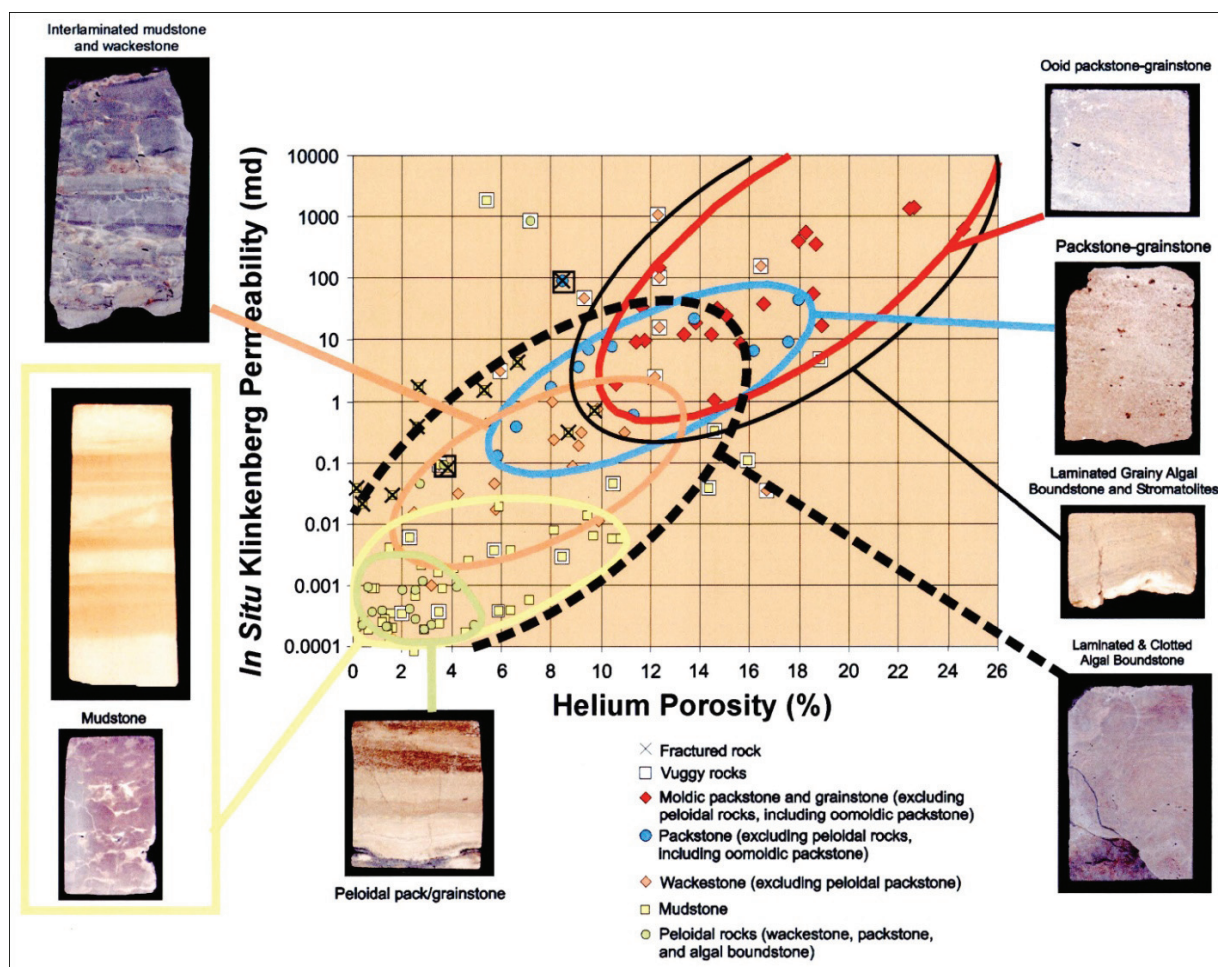


**Figure 1-29.** Crossplot of core plug *insitu* Klinkenberg permeability versus porosity for Arbuckle dolomites parametric with lithofacies. Petrophysical properties of the facies at the core-plug scale are generally controlled by matrix grain size. Each lithology exhibits a generally unique range of petrophysical properties. Fracturing of lithologies enhances permeability but does not add significantly to porosity. Vuggy pores can be well connected where vuggy porosity is extensive near the unconformity surface.

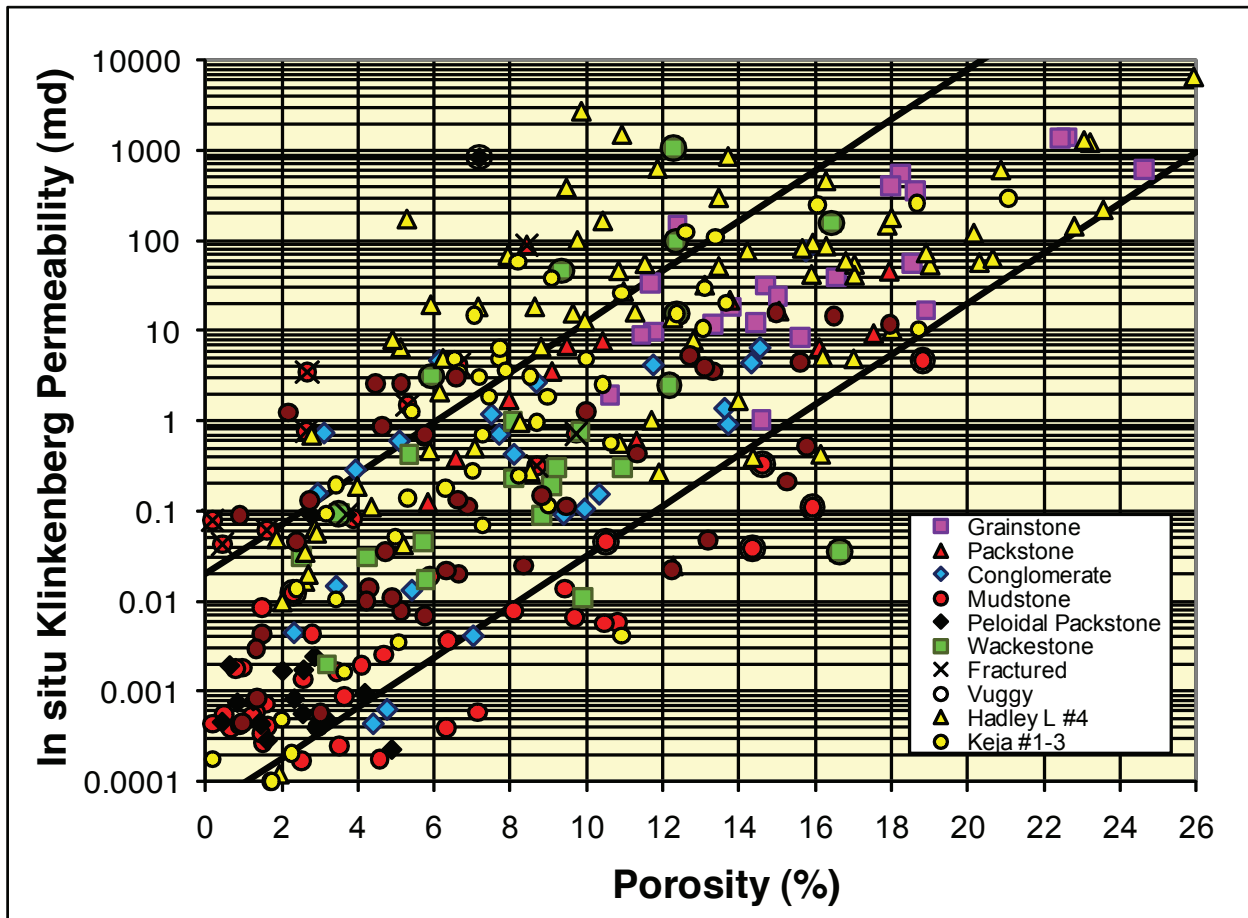


**Figure 1-30.** Crossplot of *insitu* Klinkenberg permeability versus porosity for all Arbuckle core plugs. The Hadley L#4 (solid yellow triangle) and Keja #1-3 (solid yellow circle) cores, measured in this study, generally fall within the Arbuckle trend though some better-quality grainstones lie above the trend. General bounding trendlines represent equations 1-17 and 1-18 in text.

The vertically heterolithic nature of the Arbuckle exerts a very strong control on the vertical distribution of permeability. Lithologies are stacked into cycles and cycle bundles that affect vertical and lateral heterogeneity and variable connectivity to the underlying Arbuckle aquifer. Individual cycles can be as thin as 1-3 feet in thickness (**Figure 1-31**). This thin-bedded lithofacies architecture results in high frequency changes in porosity and permeability vertically in the reservoir. The permeability profiles for both the Hadley L#4 and the Keja #1-3 show alternating high and low permeability beds stacked vertically in the reservoir interval (**Figure 1-32**).

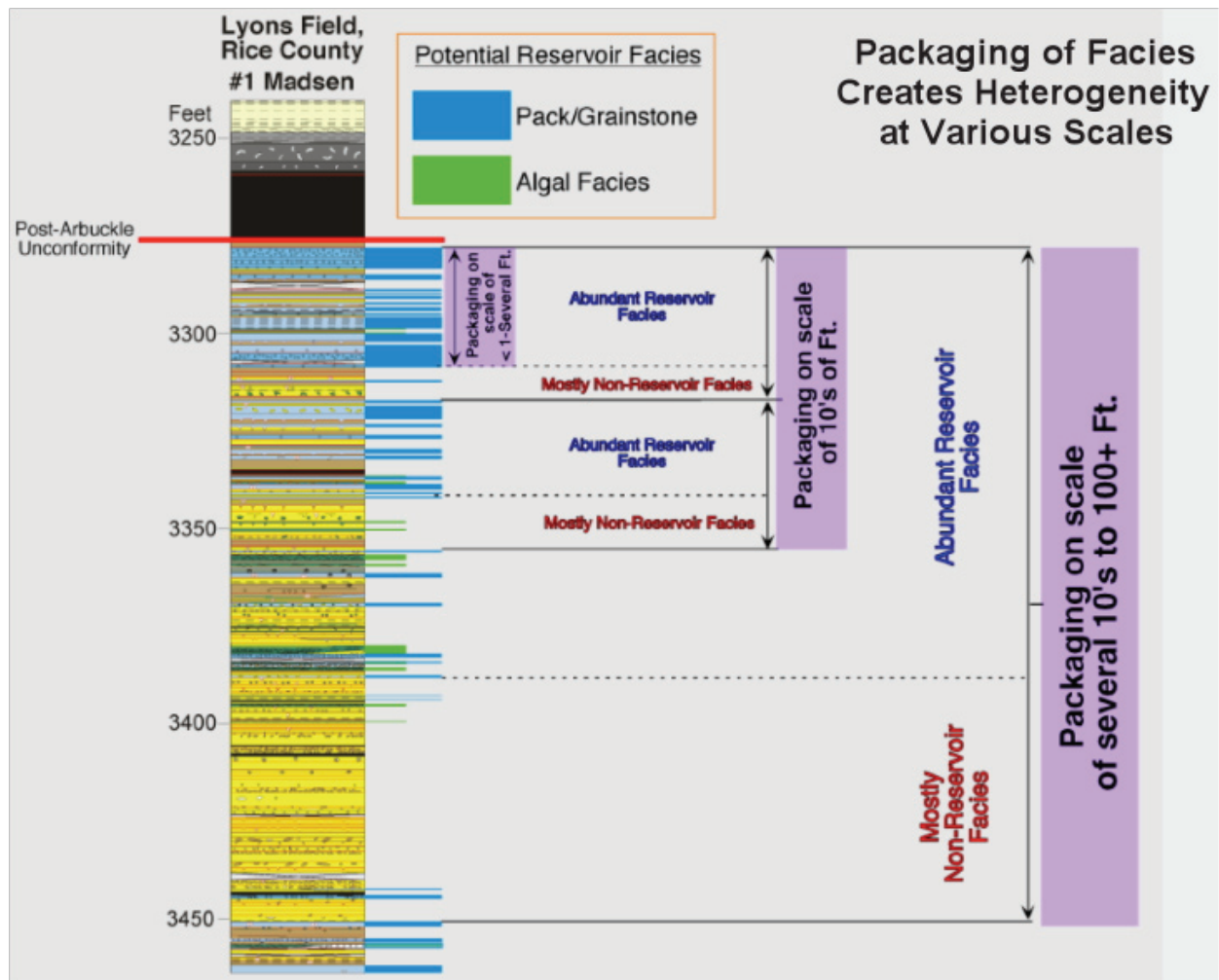


**Figure 1-31.** Example of lithologic vertical heterogeneity and cyclicity of Arbuckle bedding. High frequency changes in lithofacies results in associated high frequency changes in porosity and permeability.

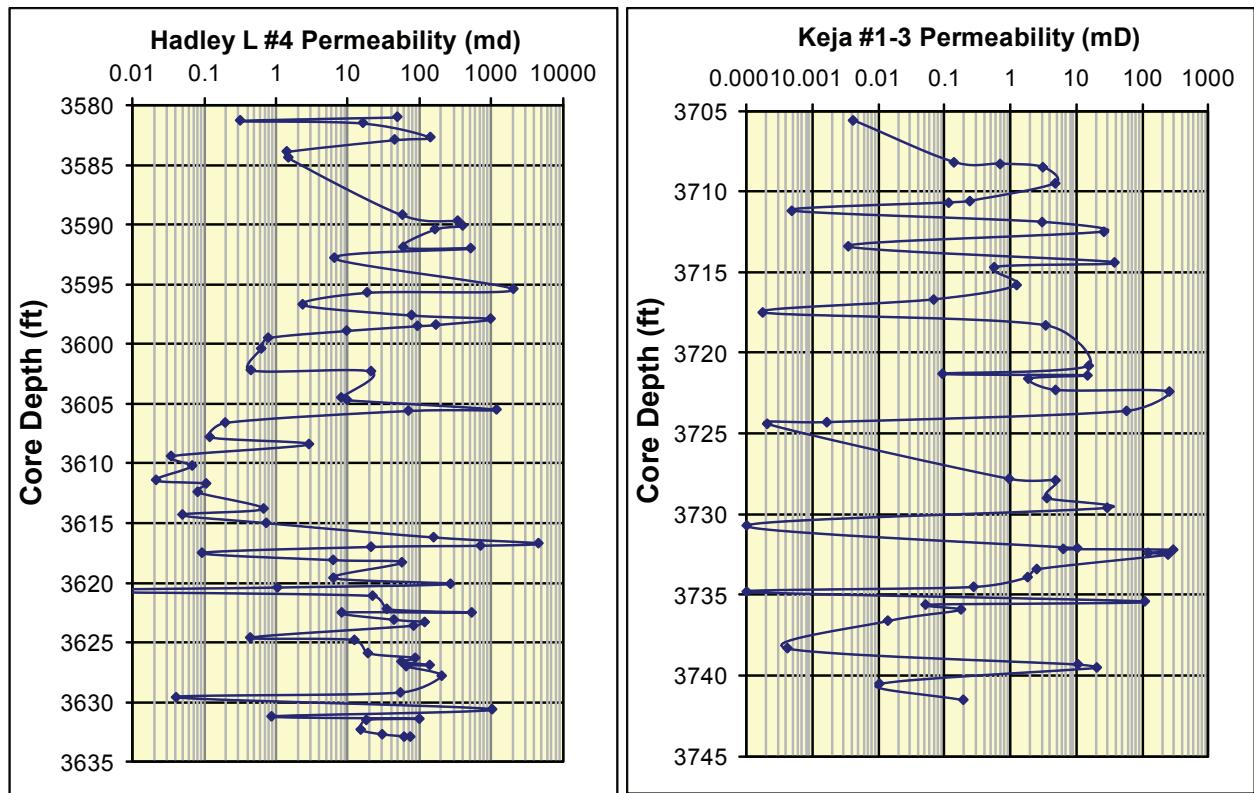


**Figure 1-32.** Vertical permeability profiles for the Hadley L#4 and Keja #1-3 Arbuckle wells showing the high frequency changes in permeability resulting from lithologic vertical heterogeneity and cyclicity of Arbuckle bedding and high frequency changes in lithofacies.

## 1.4 Capillary Pressure

Capillary pressure properties of Mississippian and L-KC carbonates differ between lithofacies. With structural closure in many Kansas fields less than 60 feet, it is also important to note that these values represent the maximum oil column height and that much of the volume of a field lies in the transition zone below these oil column heights (water-free zone). At these lower oil column heights, understanding the exact capillary pressure relationship becomes important. Utilizing over 50 air-brine and air-mercury drainage capillary pressure curves, measured on a range of lithofacies, equation parameters to construct generalized capillary pressure curves were developed using: 1) capillary threshold entry pressure, and 2) the slope of the  $\log P_c$ - $\log S_w$  curve, reflecting pore size distribution, using a modification (Angulo, 1992) of the Brooks and Corey (1964, 1966) method.

### 1.4.1 Capillary Pressure Measurement Methods

#### 1.4.1.1 Mercury Injection Capillary Pressure Methods

Subsequent to lithologic description and porosity and permeability analysis core plugs were selected for mercury injection capillary pressure analysis. Samples were selected to represent the range in lithofacies, and range in porosity and permeability. The selected cores were dried at 90°C, transferred to a vacuum desiccators, and maintained at vacuum conditions for a period of not less than 8 hours until ready for analysis. Each sample was transferred from the vacuum desiccator to the capillary pressure instrument and evacuated to a pressure of less than 0.01 torr for a period of 15 minutes. The sample was then subjected to increasing incremental mercury injection pressures ranging from 2 to 9,300 psia (14 - 64,124 kPa)). At each pressure, saturation equilibrium was assumed to have been established when the volume of mercury injected was less than 0.1% of the pore volume for a three minute period. Injected mercury volumes were corrected for system and mercury compressibility effects. Pore volume was corrected for sample compressibility to the threshold entry pressure. Accuracy and precision vary with sample pore volume and outer pore sizes and surface roughness. Pump injection volumes are readable to 0.001 cc. Based on pore volumes from 1 to 3 cc, estimated precision for the measurement is 0.5% for pore sizes less than 107 $\mu$ m.

#### 1.4.1.2 Air-Brine Capillary Pressure Methods

In addition to air-mercury capillary pressure measurement select samples were also analyzed for air-brine capillary pressure relations. A select population of samples was tested for “irreducible” brine saturation.

Clean, dry samples were evacuated for a period of eight (8) hours and then vacuum saturated with a de-aerated solution of 100,000 ppm NaCl brine. After vacuum saturation, complete saturation was obtained by applying a pressure of 1,000 psi for a period of 8 hours to the saturating brine and samples.

Complete saturation was confirmed by agreement between helium determined porosity and gravimetric saturation porosity values. The core plugs were placed on semi-permeable ceramic membrane in a multi-core capillary pressure cell. Each was then subjected to incremental capillary pressure increases of 2 to 100 psi. Samples selected for just “irreducible” water saturation measurements were exposed only to a capillary pressure of 100 psi. Initial equilibrium was established by monitoring the expelled fluid with a micropipette. Once the cores had established initial equilibrium each was removed from the cell and the saturation determined gravimetrically. The sample was then returned to the porous plate capillary cell and subjected to the same pressure. Equilibrium was established if subsequent gravimetric measurements agreed within 2 percent following a pattern of declining effluent volume consistent with equilibrium.

### 1.4.2 Capillary Pressure Results

To examine the lithofacies dependence of threshold-entry pressure, oil-column height, and pore-throat size, laboratory capillary pressure data were converted to reservoir oilbrine capillary pressure data using the standard equation (Purcell, 1949; Berg, 1975):

$$Pc_{res} = Pc_{lab} (\sigma \cos \theta_{res} / \sigma \cos \theta_{lab}) \quad (1-19)$$

where  $Pc_{res}$  is the oilbrine capillary pressure (psia) at reservoir conditions,  $Pc_{lab}$  is the laboratory-measured capillary pressure (psia), and  $\sigma \cos \theta_{res}$  and  $\sigma \cos \theta_{lab}$  is the interfacial tension ( $\sigma$ , dyne/cm) times the cosine of the contact angle ( $\theta$ , degrees) at reservoir and laboratory conditions, respectively. Contact angle measurements are not available for Kansas crude oils but are assumed to be similar to other crudes and a value of  $\theta = 0.87$  was used. Average oil-water interfacial tension for Kansas crude oils is  $\sigma_{60F} = 31 \pm 4$  dyne/cm (Table 1-2, Section 1.1). Correcting the average interfacial tension to the average pressure (1,500  $\pm$  200 psi) and temperature (110  $\pm$  10 °F) conditions present in central Kansas Lansing-Kansas City, Mississippian, and Arbuckle fields, the average oil-brine interfacial tension  $\sigma_{110F,1,500psi} = 27.9 \pm 4$  dyne/cm. Conversion of capillary pressure to height above free-water level to determine the water saturation in any given rock type as a function of height above the free-water level requires conversion of capillary-pressure data to height above free-water level. This conversion was performed using the standard relation (Hubbert, 1953; Berg, 1975):

$$H = Pc_{res} / (C(\rho_{brine} - \rho_{oil})) \quad (1-20)$$

where  $H$  is the height (ft) above free-water level,  $Pc_{res}$  is the capillary pressure (psia) at reservoir conditions,  $\rho_{brine}$  and  $\rho_{oil}$  are the density of brine and oil at reservoir conditions. Brine densities vary with salinity with a typical value being  $\rho_{brine} = 1.04 + 0.02$  g/cc. Average oil gravity is  $35 \pm 10$  (2 sd) API (Table 1-2). Correcting to 1,500 psi, with a temperature of 110 °F, and assuming a solution gas content of 300 scf/bbl, the average oil density is approximately  $\rho_{oil} = 0.75$  g/cc. In equation 1-20  $C$  is a constant (0.433(psi/ft)/(g/cc)) for converting density to pressure gradient in psia/ft.

Ignoring the small uncertainty in laboratory air-mercury interfacial tension and contact angle, from equation 1-19, height calculations are sensitive to uncertainty in reservoir oil-brine interfacial tension (IFT, which controls  $Pc_{res}$ ), oil density, and brine density. For the LKC through Arbuckle systems the estimated range for each of these variables is

$$\begin{array}{ll} 24 \text{ dyne/cm} < \text{IFT} < 32 \text{ dyne/cm}; & \text{for } P = 1,300 \text{ psi} - 1,700 \text{ psi}; T=100-120^\circ\text{F} \\ 0.67 \text{ g/cc} < \rho_{oil} < 0.85 \text{ g/cc}; & \text{for } P = 1,300 \text{ psi} - 1,700 \text{ psi}; T=100-120^\circ\text{F} \\ 1.02 \text{ g/cc} < \rho_{brine} < 1.06 \text{ g/cc}; & \text{for } P = 1,300 \text{ psi} - 1,700 \text{ psi}; T=100-120^\circ\text{F} \end{array}$$

For this range in variance of properties, the height above free-water level conversions exhibit an maximum variance from the average of +95% for the extreme case of maximum IFT, maximum  $\rho_{oil}$ , and minimum  $\rho_{brine}$ . For an assumed range in properties of one standard deviation, average variance from the average conditions is error is  $\pm 20\%$ . For this uncertainty a calculated height of 60 ft might be 72 feet or 48 feet or a height of 30 ft might be 24 feet or 36 feet at different interfacial tension, oil density, and brine density conditions.

From the air-mercury capillary pressure data, pore-throat diameter was calculated using the modified Washburn (1921) relation:

$$d = 4C\sigma\cos\theta/Pc \quad (1-21)$$

where  $Pc$  = capillary pressure (psia),  $C = 0.145$  ((psia·cm· $\mu\text{m}$ )/dyne),  $\theta$  = contact angle (140 degrees),  $\sigma$  = interfacial tension (484 dyne/cm), and  $d$  = pore-throat diameter ( $\mu\text{m}$ , microns). This relation assumes that the non-wetting phase (i.e., oil) enters the pores through circular pore-throats.

For the purpose of converting air-mercury capillary pressure data to oil-brine capillary pressure data and oil-brine height above free-water level at reservoir conditions, the following properties were assumed:  $\rho_{oil} = 0.75$  g/cc,  $\rho_{brine} = 1.104$  g/cc,  $\text{CH}_4$ -brine IFT = 27.9 dyne/cm, air-mercury IFT = 484 dyne/cm, cosine air-mercury contact angle = 0.766 degrees, cosine oil-brine contact angle = 0.87. These values are appropriate for the saturated brine present in the formations studied and for the crude oils in these formations at reservoir conditions.

**Figure 1-33** shows the composite of air-mercury capillary pressure curves for the Lansing-Kansas City samples and **Figure 1-34** shows the composite for Mississippian samples. Air-mercury capillary pressures are converted to oil-brine height above free water level using the average values presented above. Wetting phase in the air-mercury measurement is formally mercury vapor. The figures present this as wetting phase. In the oil-brine system this would correspond to brine. Both sets of samples exhibit the commonly observed pattern of increasing threshold entry pressure with decreasing permeability resulting in the need for higher oil-column heights to achieve the same wetting phase saturation with decreasing permeability.

Lansing-Kansas City curves exhibit both continuous curves, with little or no distinct inflections, and curves that show an inflection at some saturation. Continuous curves can be interpreted to indicate that the pore-throat size distribution is unimodal and that there are not distinctly different populations of pore throats. This does not preclude the presence of a distinct matrix pore system separate from the pore throat system connecting the principal pore bodies which comprise the large oomolds in these oomoldic limestones. A continuous curve does indicate that any matrix pores either represent a minor portion of the pore volume, and therefore do not influence the curve significantly, or represent a continuum with the pores connecting the oomoldic pore bodies. It can also result from the pore architecture where the only connection between oomolds is the matrix pore system. For these conditions the capillary pressure curve represents the volume of oomoldic pores that are accessed through the matrix pore throat size invaded at a given oil column height and corresponding pressure. Although oomoldic rocks may exhibit uni-modal, bi-modal, or multi-modal pore throat size distributions, the general curve shape can be modeled using a unimodal model with the understanding that for some samples the estimated saturation at a given oil column height has an error associated with the difference between the unimodal model and the actual curve shape.

The Mississippian curves (Fig. 1-34) exhibit no significant inflections and can therefore be interpreted to represent a unimodal pore throat size distribution. The two exceptions to this are the highest permeability samples ( $k_{ik} = 401$  md) and the lowest permeability sample ( $k_{ik} = 0.077$  md). Both samples are likely to have contained large external pores relative to the remainder of the pores in the samples. For the high permeability sample the large pores must have been spanning, resulting in the measured permeability. The steep curve after initial low-pressure entry at  $S_w = 53\%$  indicates the remaining pore system is very low permeability. Conversely, the lowest permeability sample shows a low threshold entry oil-column height and pressure characteristic of samples with  $k_{ik} > 10$  mD. The sample did not exhibit this permeability and it can therefore be postulated that the pores entered at low pressures were not connected through the sample.

It is important to note that the capillary pressure relationships shown in figures 1-33 and 1-34 show the complete pore volume relationships to capillary pressures equivalent to oil-column heights that do not exist in nature. These are helpful to understand the pore system but extend to oil-column heights significantly greater than exist in Kansas. In the region of Kansas in which the Lansing-Kansas City, Mississippian, and Arbuckle are productive maximum oil columns heights are generally 40-60 feet and can be considered to not exceed 100 feet. **Figures 1-35 and Figure 1-36** show the capillary pressure curves presented in Figures 1-33 and 1-34 but limited to the oil column heights found in Kansas and therefore representative of the wetting phase saturation range that would be encountered in these reservoirs. It is evident from these figures that Kansas reservoirs are in the transition zone over most or all of the oil-column height. Only the highest permeability samples can be considered to be at “irreducible” water saturation. For the many reservoirs that only have a oil-column height of 40-feet above free water level generally only Lansing-Kansas City oomoldic

limestones with permeability greater than 50 md are desaturated to  $S_w < 30\%$ . For LKC rocks with  $1 \text{ md} < k_{ik} < 50 \text{ md}$  water saturations range from  $30\% < S_w < 60\%$ .

Comparison of Figures 1-37 and 1-39 shows that Mississippian rocks exhibit generally higher threshold entry heights (entry pressures) than similar permeability LKC rocks and also exhibit lower  $\log S_w$ - $\log H$  slopes indicating a narrow pore throat size distribution. The higher threshold entry pressures, even with similar pore throat size distributions, result in Mississippian rocks exhibiting higher water saturations at the same oil-column height for a similar permeability. The difference in threshold entry pressure is evident in **Figure 1-40**. Figure 1-40 shows a crossplot of the principal pore throat diameter versus permeability. Principal pore throat diameter ( $D_{ppt}$ ) can be defined as the pore throat diameter that corresponds to the sample spanning cluster and not just to the first pore entered in the capillary pressure experiment. The  $D_{ppt}$  is representative of the pore throat size that limits entry to a connected path of oil throughout the rock (i.e., sample spanning). A threshold entry pore size can also be calculated from the  $\log P_c$ - $\log S_w$  intercept at  $S_w = 100\%$ . Either method provides a consistent reference frame for examining pore size-permeability questions.

Figure 1-40 shows a  $D_{ppt}$ - $k_{ik}$  trend for samples of many lithologies including principally interparticle-pore dominated quartzose sandstone, lithic sandstone, and inter-particle pore dominated lime mudstone-packstones. The  $D_{ppt}$ - $k_{ik}$  trends for the Mississippian and LKC rocks are different than these other rock lithologies and differ from each other. The Niobrara chalk samples illustrate that lithologies of unique pore geometry can exhibit trends very different than inter-particle. The  $D_{ppt}$ - $k_{ik}$  trends can be expressed:

$$D_{ppt} = 5.479 k_{ik}^{0.411} \quad [\text{LKC}] \quad (1-22)$$

$$D_{ppt} = 0.629 k_{ik}^{0.771} \quad [\text{MISS}] \quad (1-23)$$

where  $D_{ppt}$  is in units of microns and  $k_{ik}$  is in millidarcies.

The  $D_{ppt}$ - $k_{ik}$  can be transformed into a threshold entry oil-brine column height using equations 1-19 through 1-21. The development of saturation prediction models is discussed below.

In addition to air-mercury capillary pressure measurement, air-brine capillary pressure measurements were conducted including both single-pressure and multi-pressure measurements. Single-point air-brine capillary pressure data for Mississippian rocks shows that wetting phase saturation increases with decreasing permeability (**Fig. 1-41**). Air-Hg and air-brine capillary pressure measurements for equivalent pressures corresponding to 60-feet of oil-column height show a similar  $S_{w60ft}$ - $k_{ik}$  relationship which can be expressed:

$$S_{w60ft} = -24.5 \log k_{ik} + 55.9 \quad [\text{MISS}] \quad (1-24)$$

where  $S_{w60ft}$  is in percent (%) and  $k_{ik}$  is in millidarcies (md).

In comparison to the higher water saturations associated with 60-ft oil-column heights capillary pressure curves for and “extreme” oil-column height for Kansas of 175 ft (**Figure 1-42**) shows that

water saturations are decreased by approximately 20% for most permeabilities indicating that this range of oil-column heights can be considered as approaching “irreducible” conditions.

Single-point air-brine capillary pressure data for Lansing-Kansas City rocks shows that wetting phase saturation increases with decreasing permeability (**Fig. 1-43**). Air-Hg and air-brine capillary pressure measurements for equivalent pressures corresponding to 50-feet of oil-column height show a similar  $S_{w60ft} - k_{ik}$  relationship which can be expressed:

$$S_{w60ft} = -19.8 \log k_{ik} + 44.9 \quad [LKC] \quad (1-25)$$

where  $S_{w60ft}$  is in percent (%) and  $k_{ik}$  is in millidarcies (md).

In comparison to the higher water saturations associated with 50-ft oil-column heights capillary pressure curves for and “extreme” oil-column height for Kansas of 175 ft (**Figure 1-44**) shows that water saturations are decreased significantly for many samples.

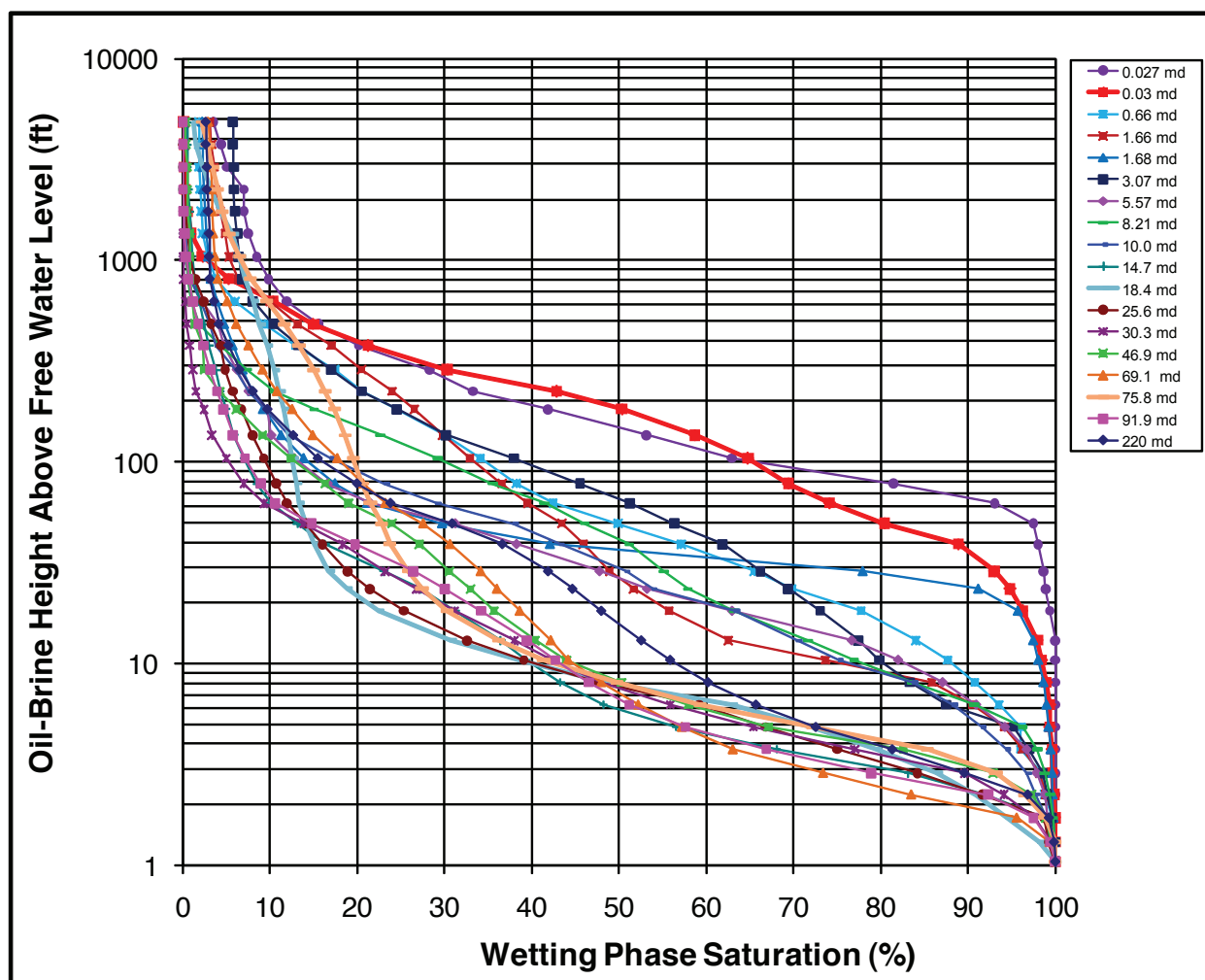


**Figure 1-33.** Air-mercury capillary pressure curves for Lansing-Kansas City samples. Air-mercury pressures were converted to oil-brine height above free water level using equations in text. Curves exhibit commonly observed trend that threshold entry pressures increase with decreasing permeability.

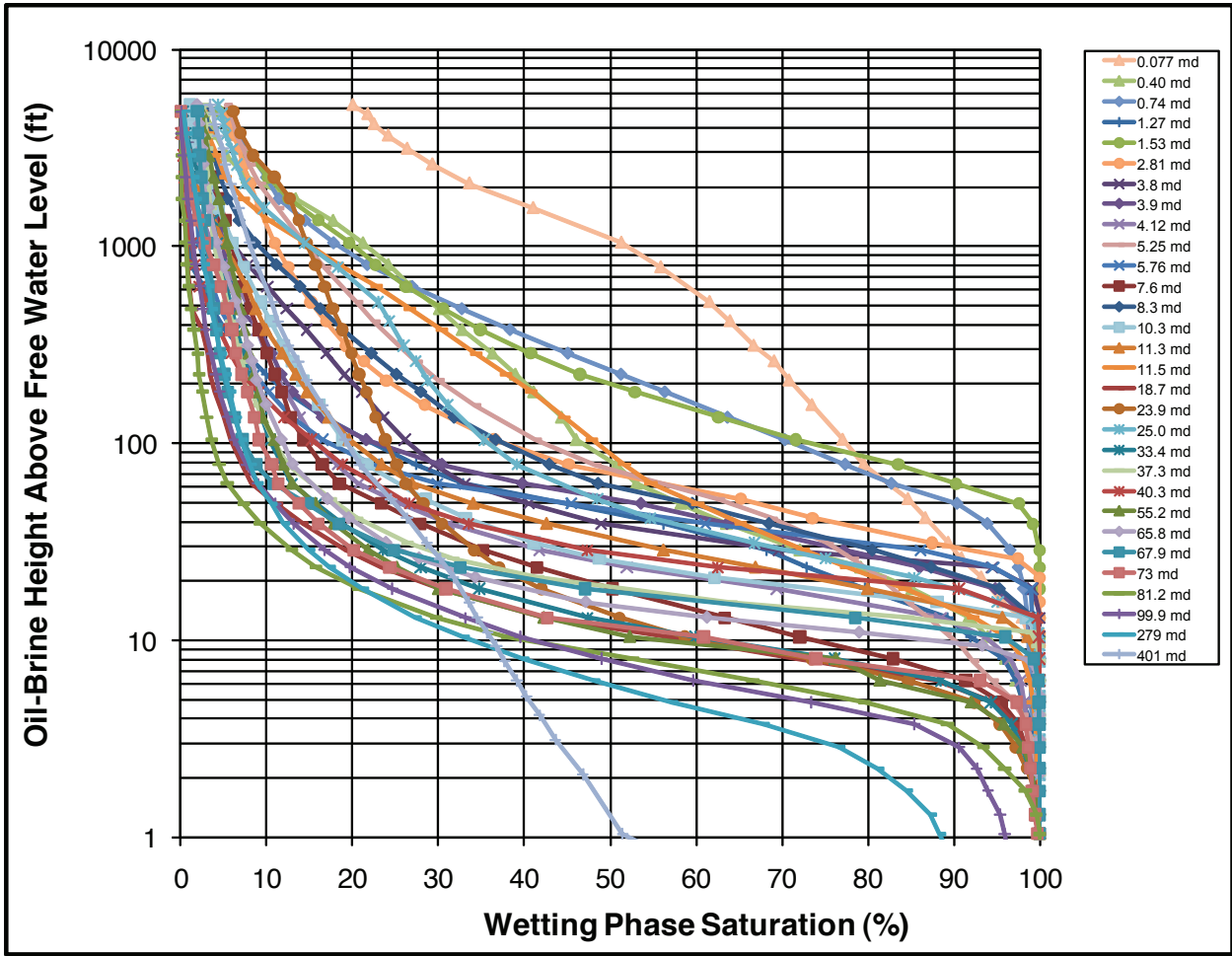


**Figure 1-34.** Air-mercury capillary pressure curves for Mississippian samples. Air-mercury pressures were converted to oil-brine height above free water level using equations in text. Curves exhibit commonly observed trend that threshold entry pressures increase with decreasing permeability.

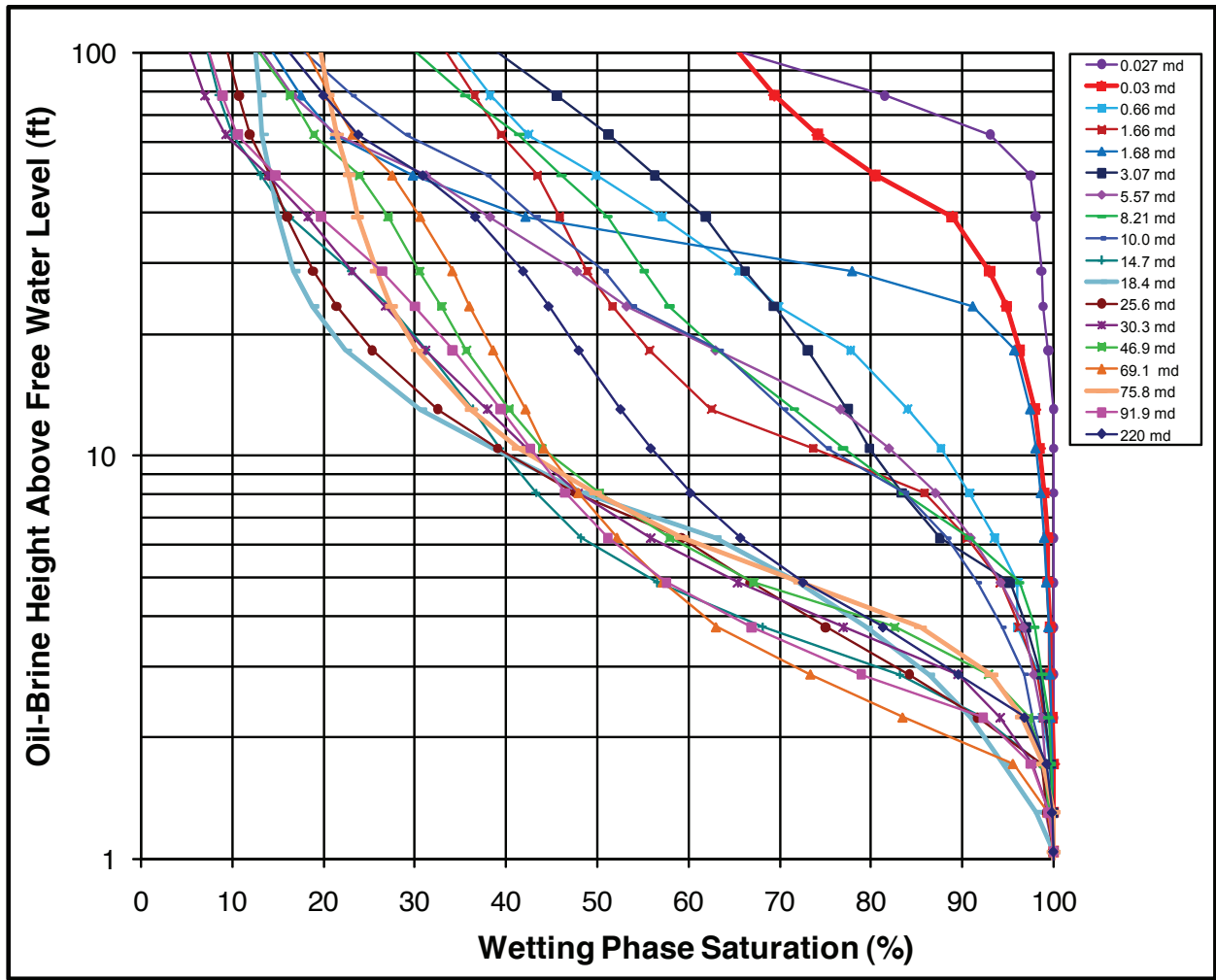


**Figure 1-35.** Air-mercury capillary pressure curves for Lansing-Kansas City samples examining just the range in oil column height found in Kansas which usually range below 60 ft. Air-mercury pressures were converted to oil-brine height above free water level using equations in text. Curves exhibit commonly observed trend that threshold entry pressures increase with decreasing permeability

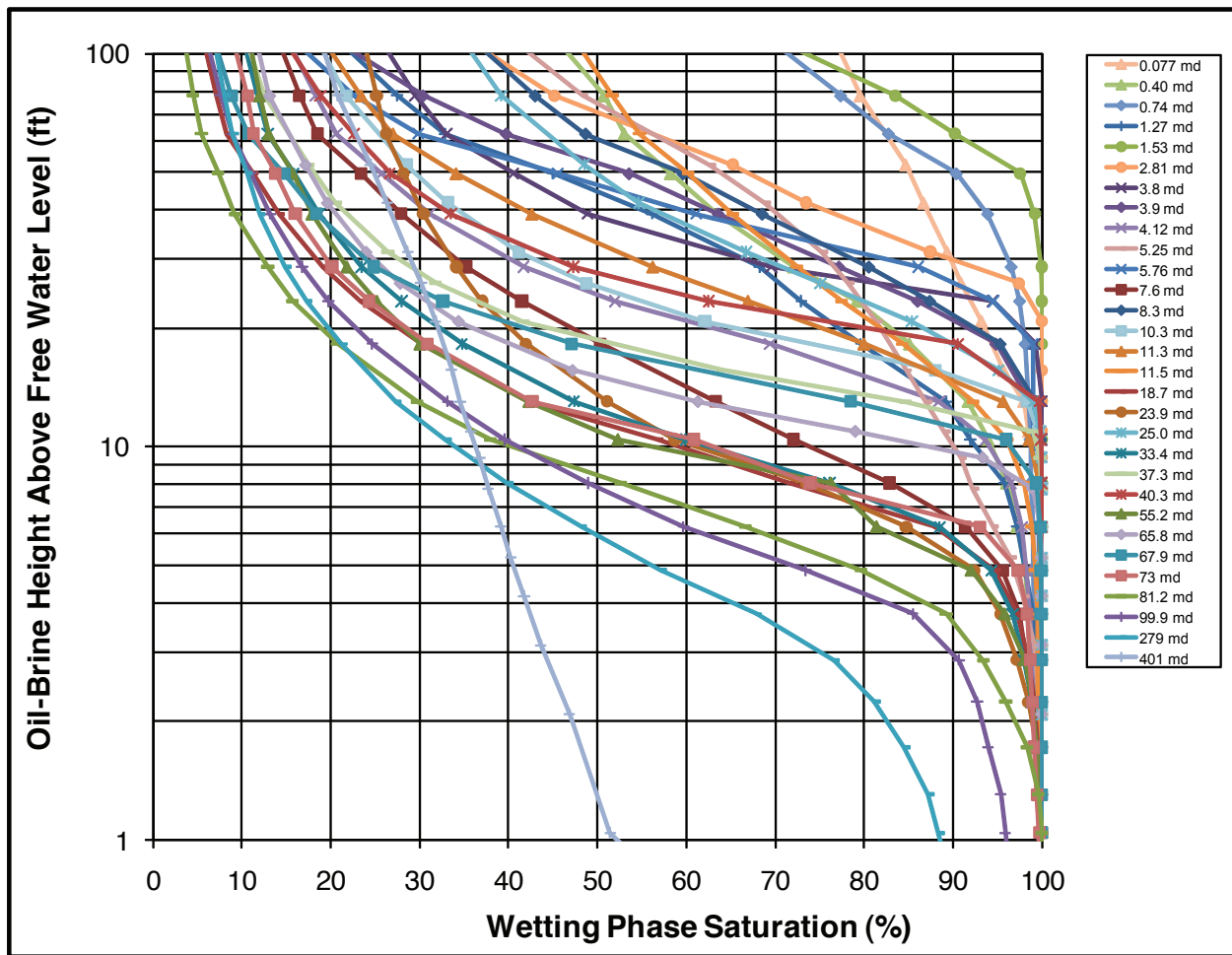


**Figure 1-36.** Air-mercury capillary pressure curves for Mississippian samples examining just the range in oil column height found in Kansas which usually range below 60 ft. Air-mercury pressures were converted to oil-brine height above free water level using equations in text. Curves exhibit commonly observed trend that threshold entry pressures increase with decreasing permeability.

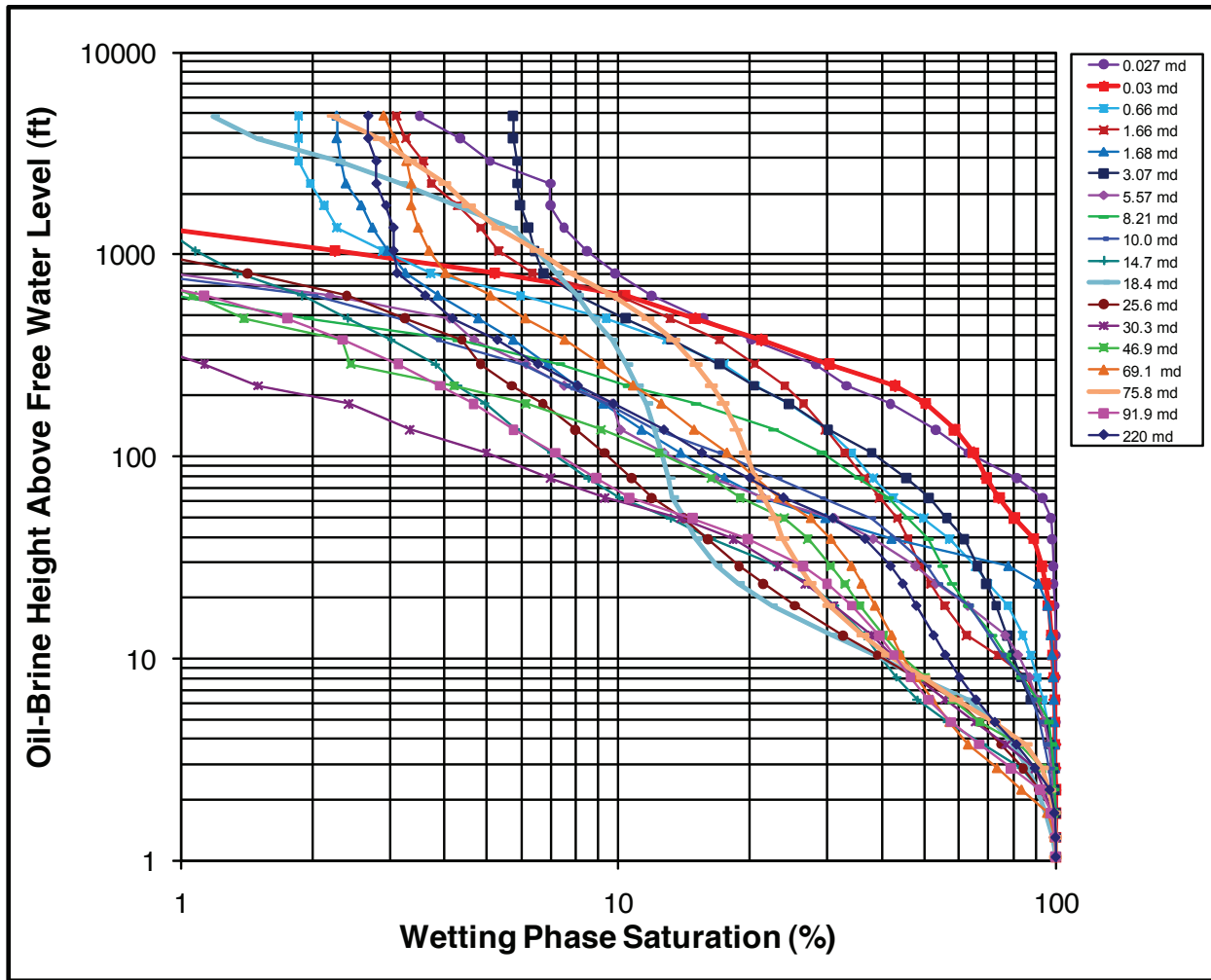


**Figure 1-37.** Air-mercury capillary pressure curves for Lansing-Kansas City samples showing the general  $\log S_w$ - $\log H$  linear relationship. Some samples exhibit an inflection in the slope at saturations greater than 60%-80%. These inflections can be the result of several conditions including; 1) a bimodal pore throat size distribution, 2) invasion of large external pores on a small pore volume sample, or 3) invasion of a portion of the pore system comprising a non-sample spanning cluster of larger pores. Air-mercury pressures were converted to oil-brine height above free water level using equations in text. Curves exhibit commonly observed trend that threshold entry pressures increase with decreasing permeability.

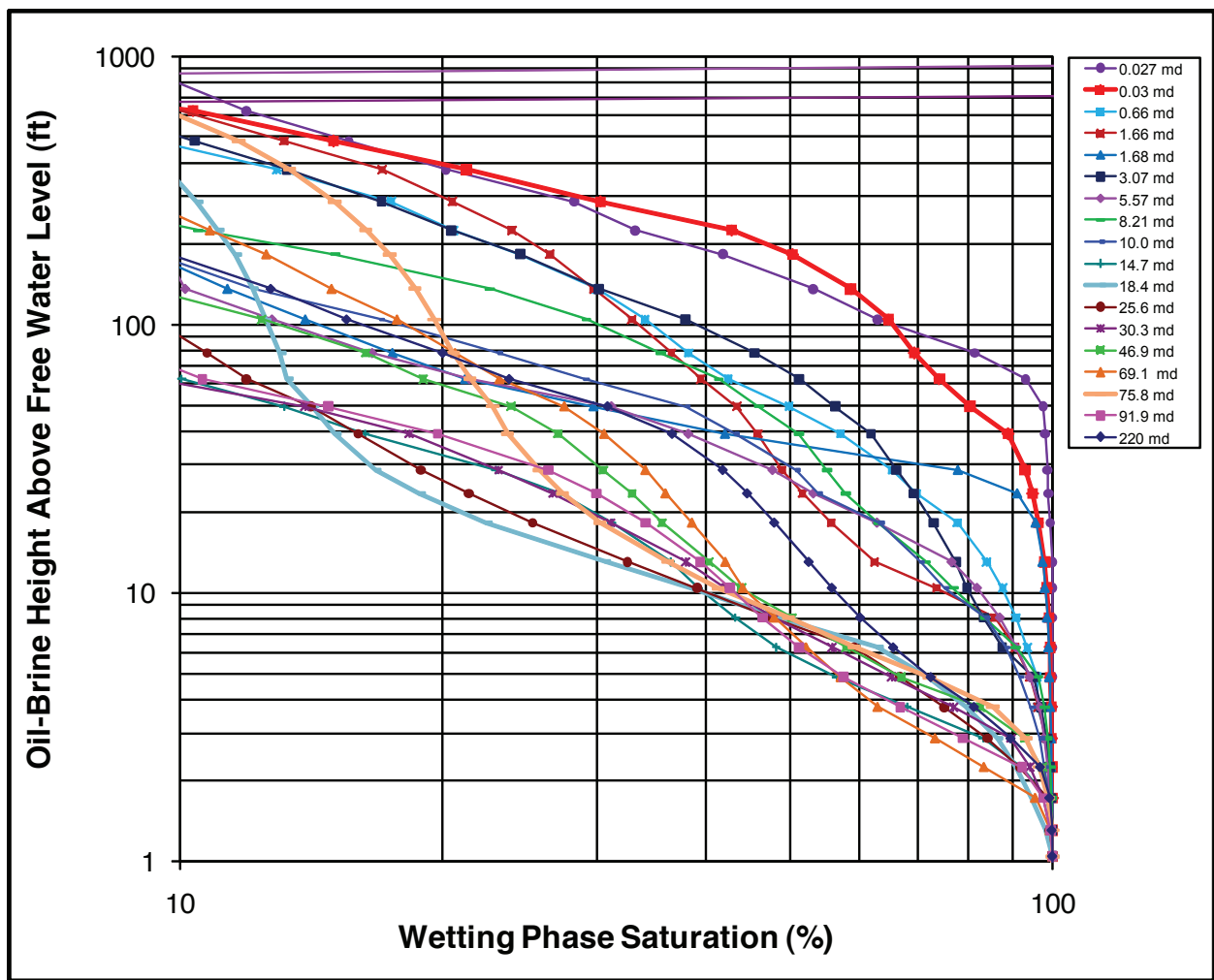


**Figure 1-38.** Air-mercury capillary pressure curves for Lansing-Kansas City samples showing the general  $\log S_w$ - $\log H$  linear relationship examining just the range in wetting phase saturation commonly found in Kansas reservoirs which usually range below 60 ft oil-brine height above free water level. Some samples exhibit an inflection in the slope at saturations greater than 60%-80%. These inflections can be the result of several conditions including; 1) a bimodal pore throat size distribution, 2) invasion of large external pres on a small pore volume sample, or 3) invasion of a portion of the pore system comprising a non-sample spanning cluster of larger pores. Air-mercury pressures were converted to oil-brine height above free water level using equations in text. Curves exhibit commonly observed trend that threshold entry pressures increase with decreasing permeability.

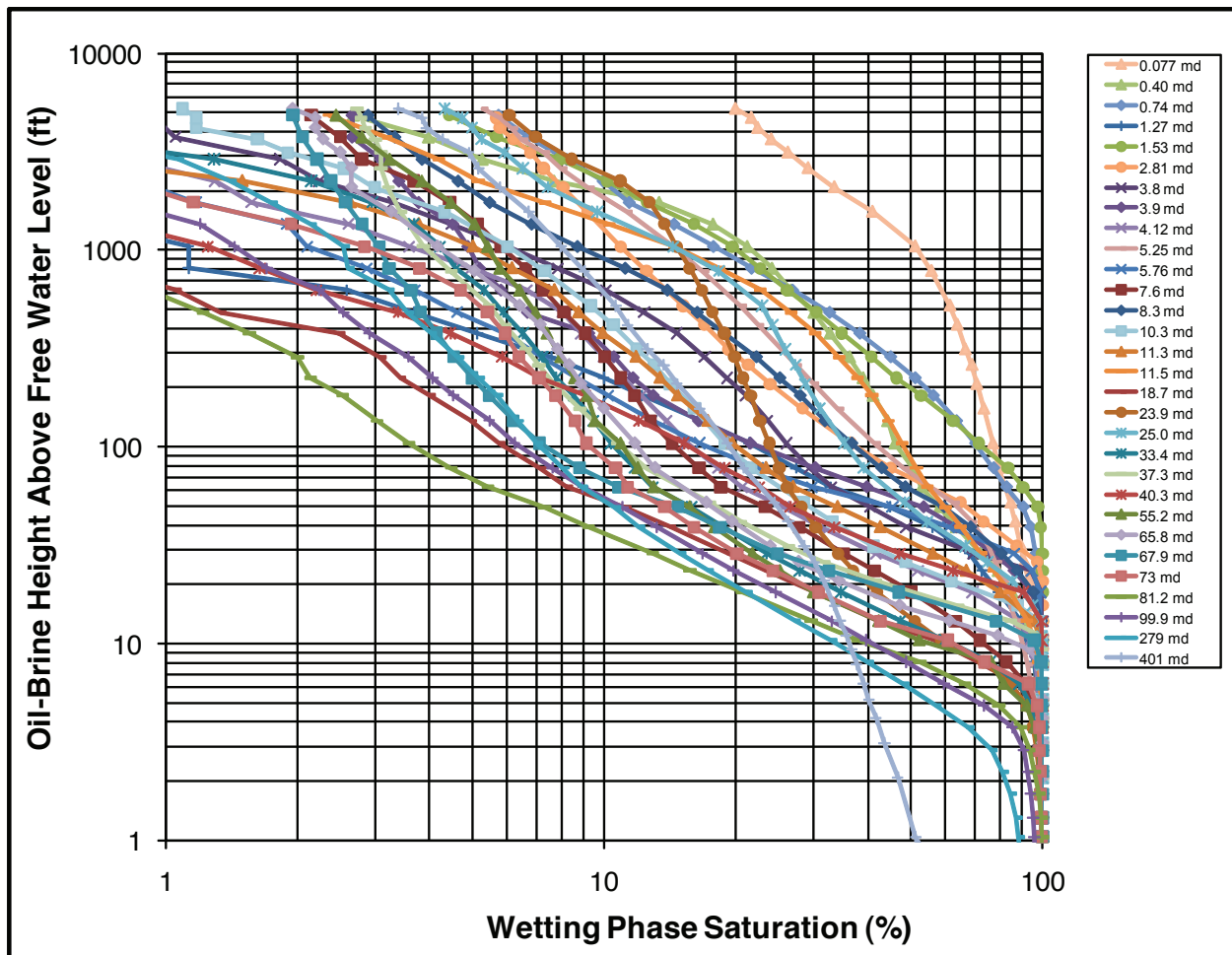


**Figure 1-39.** Air-mercury capillary pressure curves for Mississippian samples showing the general  $\log S_w$ - $\log H$  linear relationship. Some samples exhibit an inflection in the slope at saturations greater than 60%-80%. These inflections can be the result of several conditions including; 1) a bimodal pore throat size distribution, 2) invasion of large external pres on a small pore volume sample, or 3) invasion of a portion of the pore system comprising a non-sample spanning cluster of larger pores. Air-mercury pressures were converted to oil-brine height above free water level using equations in text. Curves exhibit commonly observed trend that threshold entry pressures increase with decreasing permeability.

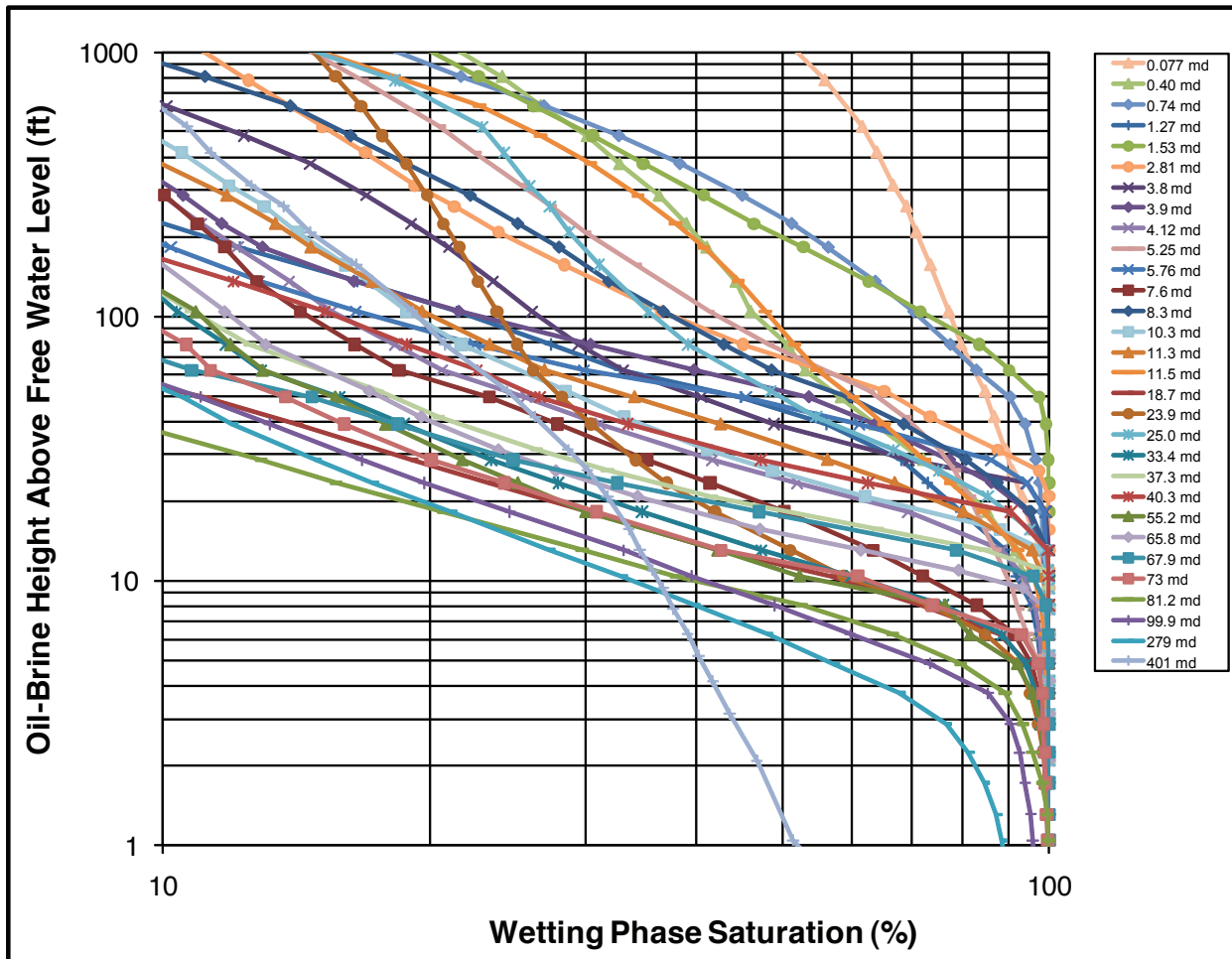


**Figure 1-40.** Air-mercury capillary pressure curves for Mississippian samples showing the general  $\log S_w - \log H$  linear relationship examining just the range in wetting phase saturation commonly found in Kansas reservoirs which usually range below 60 ft oil-brine height above free water level. Some samples exhibit an inflection in the slope at saturations greater than 60%-80%. These inflections can be the result of several conditions including; 1) a bimodal pore throat size distribution, 2) invasion of large external pres on a small pore volume sample,, or 3) invasion of a portion of the pore system comprising a non-sample spanning cluster of larger pores. Air-mercury pressures were converted to oil-brine height above free water level using equations in text. Curves exhibit commonly observed trend that threshold entry pressures increase with decreasing permeability.

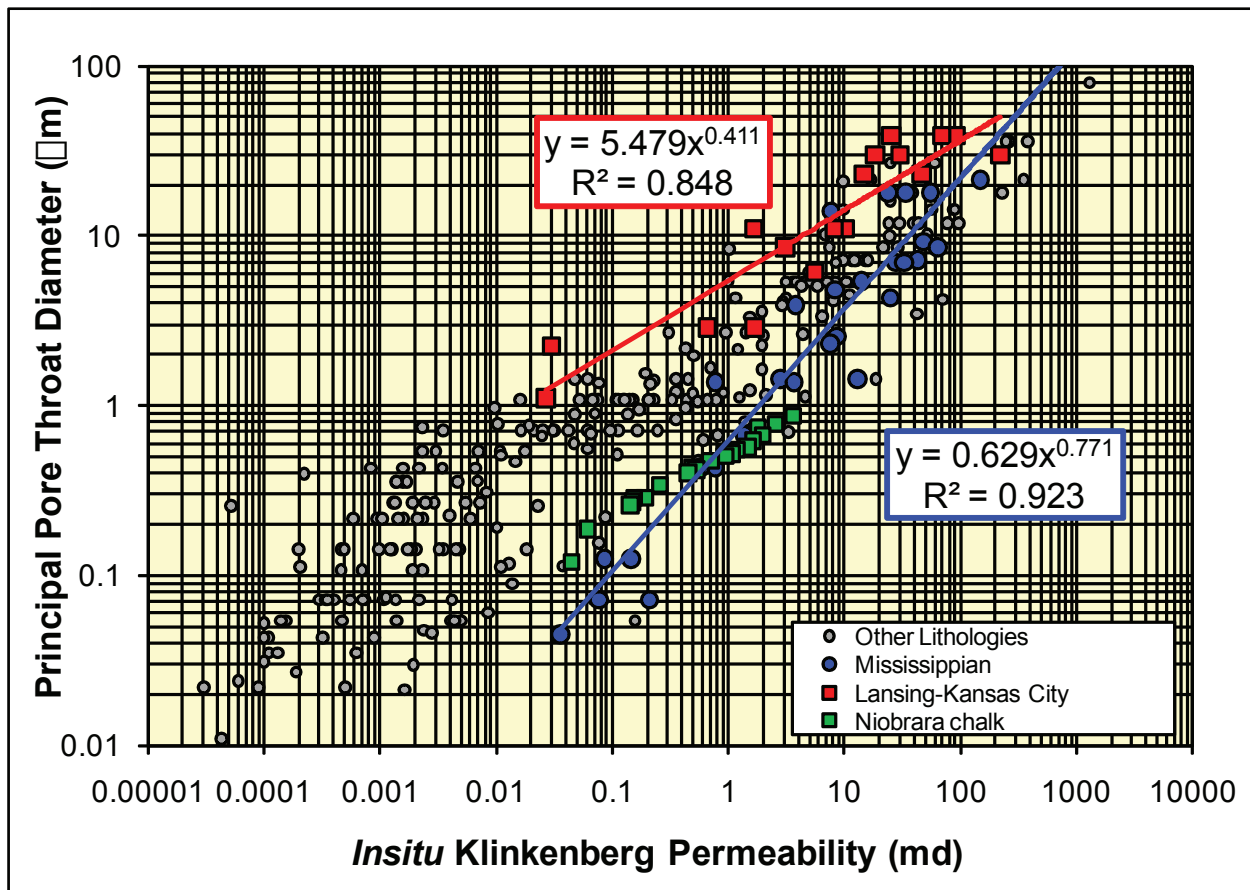


**Figure 1-41.** Crossplot of principal pore throat diameter versus insitu Klinkenberg permeability of Mississippian and Lansing-Kansas City rocks compared to a wide range of other lithologies (grey solid circles) including sandstones and interparticle-porosity dominated limestones. Niobrara chalk (green squares) are singled out to illustrate how unique lithofacies can exhibit unique trends similar.

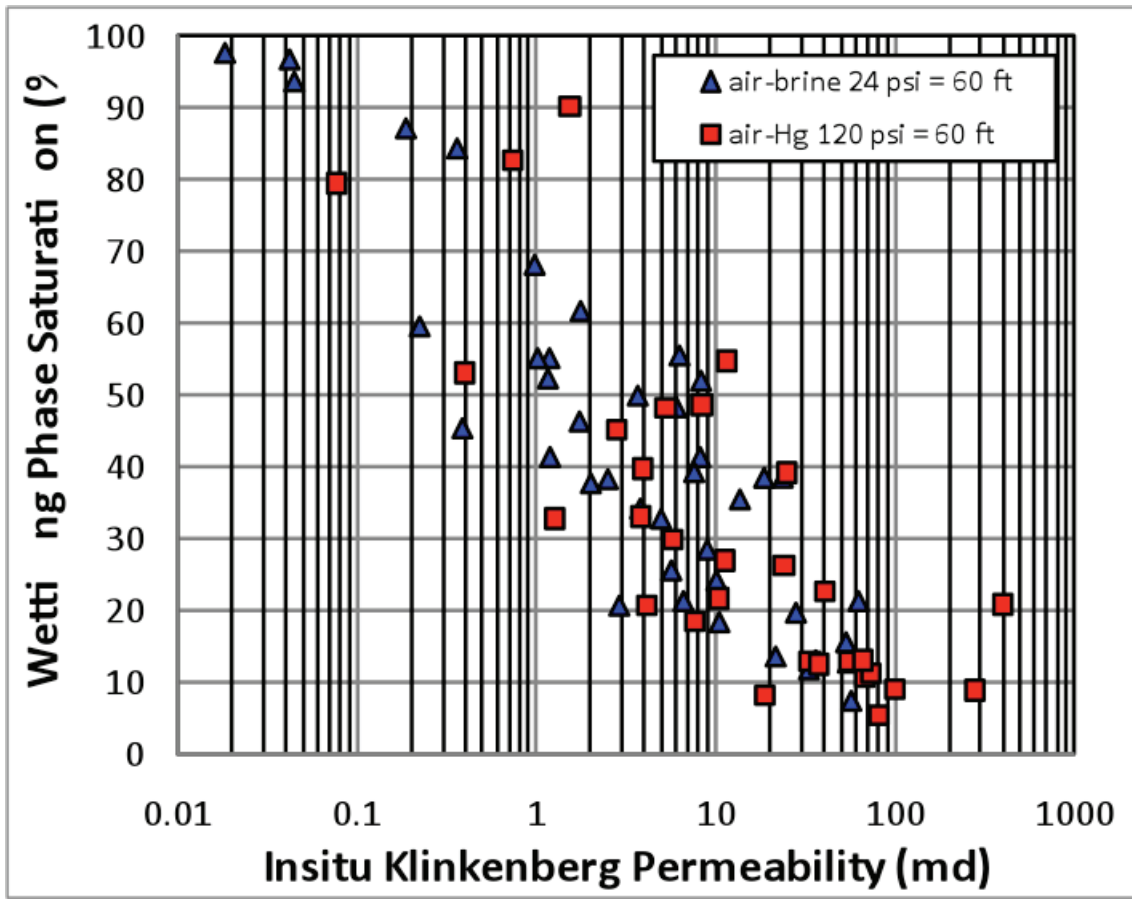


**Figure 1-42.** Crossplot of wetting-phase saturation achieved by air-Hg (120 psi) and air-brine (24 psi) capillary pressure for Mississippian rocks. The capillary pressures for each set of fluids correspond to an approximate oil-brine height above free water level of 60 feet, which is generally the maximum oil-column height in Kansas reservoirs.

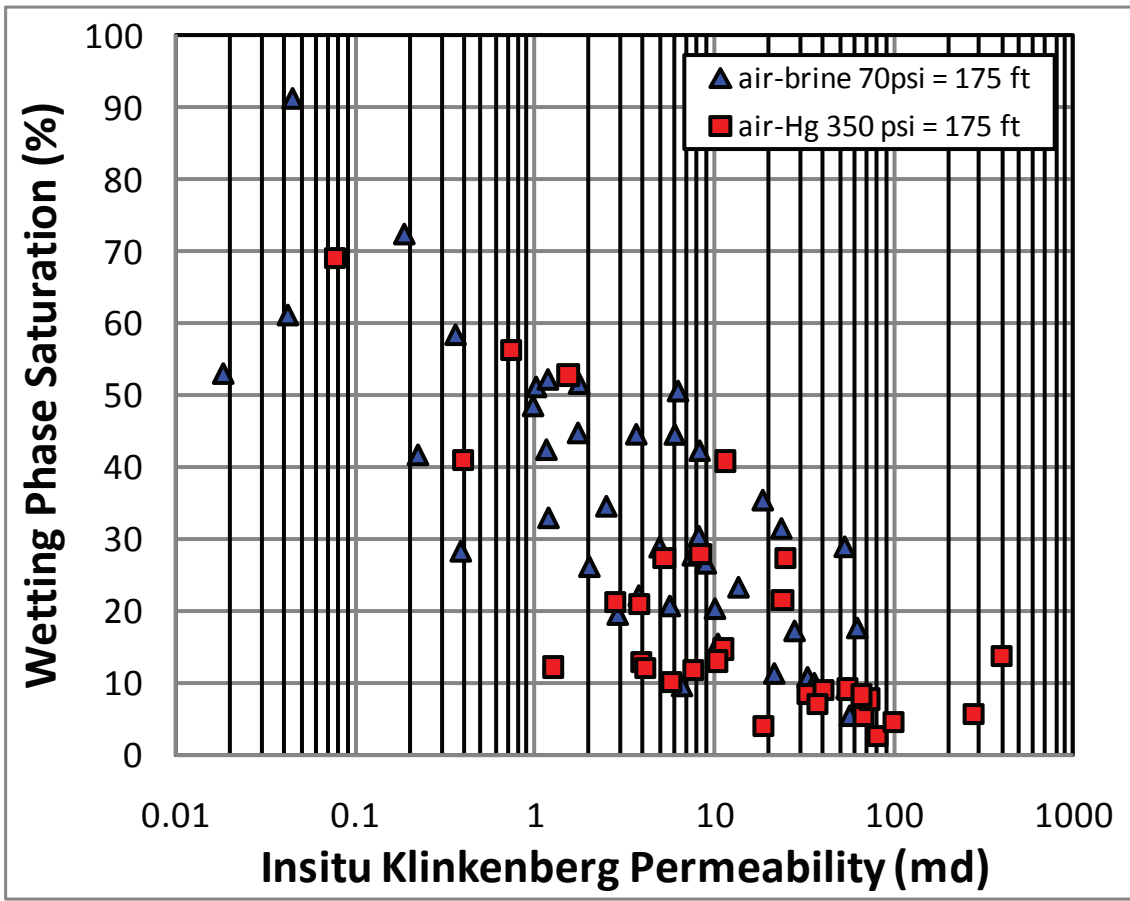


**Figure 1-43.** Crossplot of wetting-phase saturation achieved by air-Hg (350 psi) and air-brine (70 psi) capillary pressure for Mississippian rocks. The capillary pressures for each set of fluids correspond to an approximate oil-brine height above free water level of 175 feet, which is significantly greater than maximum oil-column heights in Kansas reservoirs.

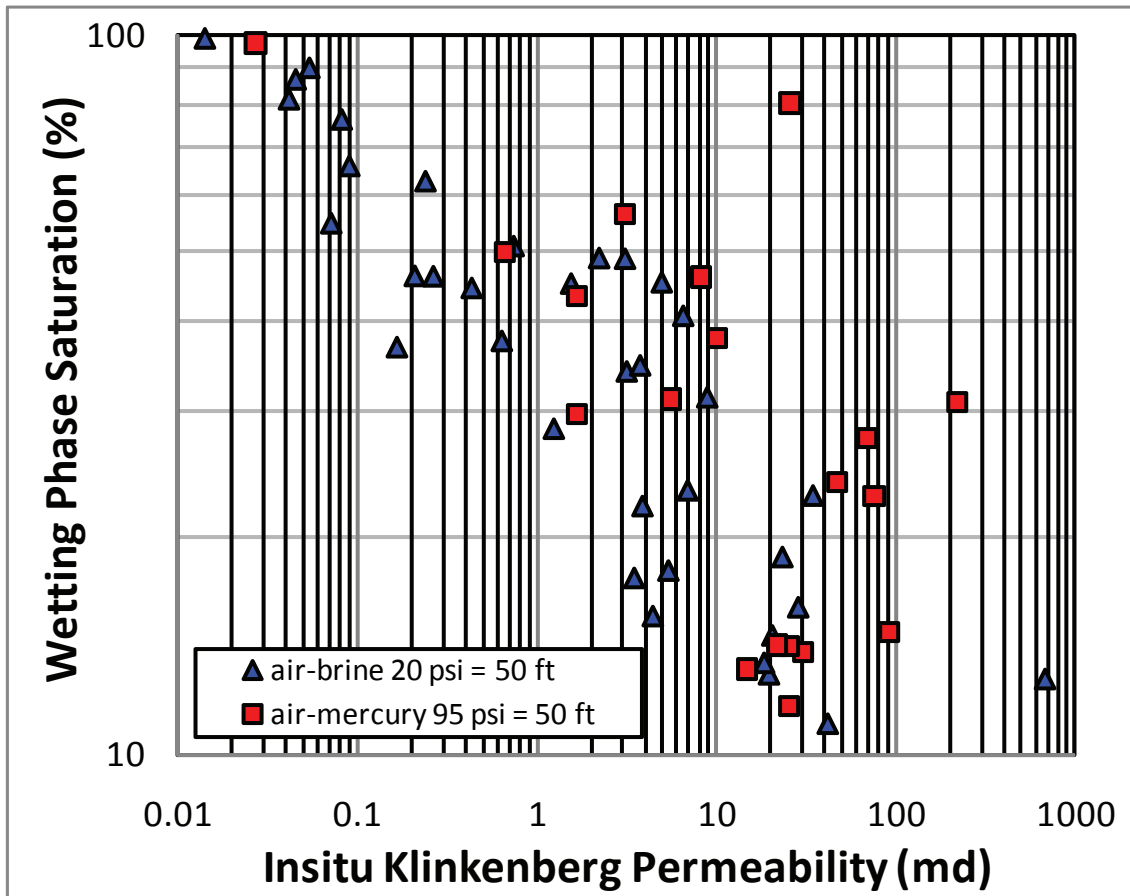


**Figure 1-44.** Crossplot of wetting-phase saturation achieved by air-Hg (95 psi) and air-brine (20 psi) capillary pressure for Lansing-Kansas City rocks. The capillary pressures for each set of fluids correspond to an approximate oil-brine height above free water level of 50 feet.

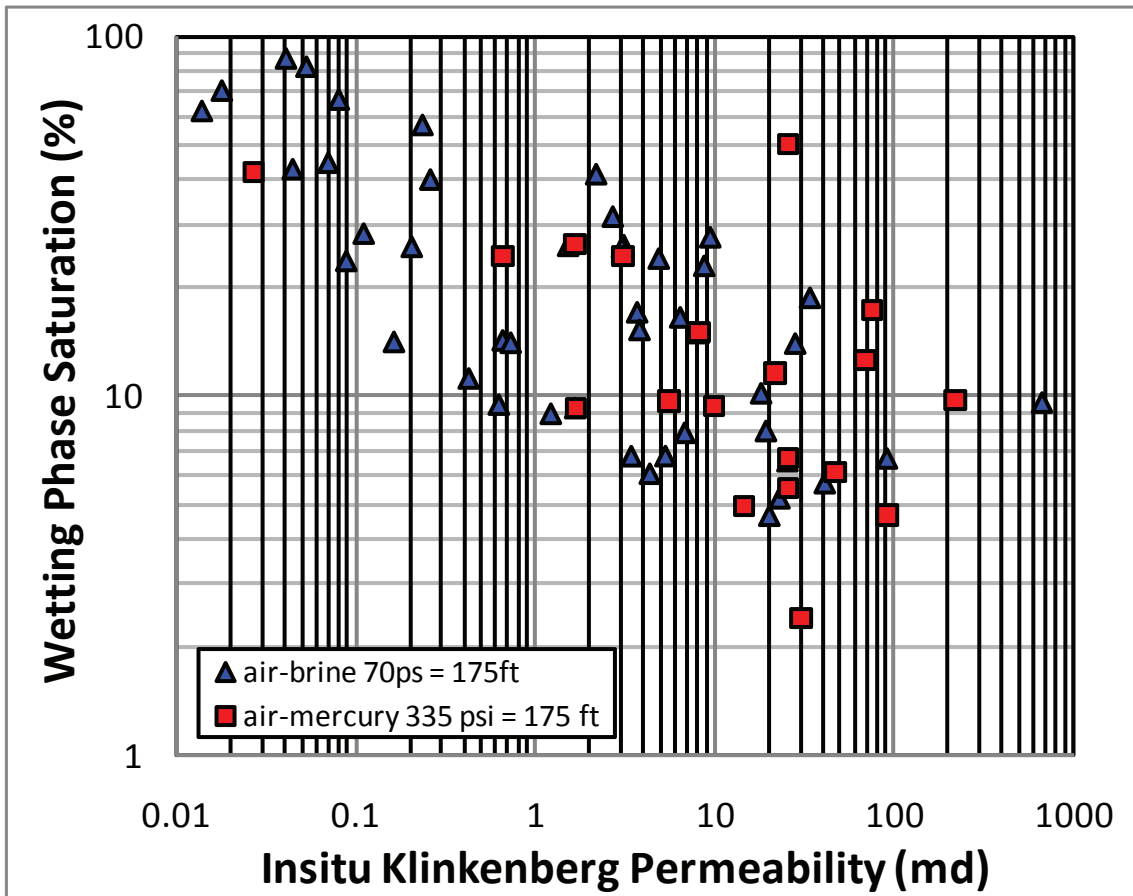


**Figure 1-45.** Crossplot of wetting-phase saturation achieved by air-Hg (350 psi) and air-brine (70 psi) capillary pressure for Lansing-Kansas City rocks. The capillary pressures for each set of fluids correspond to an approximate oil-brine height above free water level of 175 feet, which is significantly greater than maximum oil-column heights in Kansas reservoirs.

### 1.4.3 Capillary Pressure Model

Utilizing the threshold entry pressure and the  $\log S_w$ - $\log P_c$  slopes of the curves shown in Figures 1-37 and 1-39, Oil-water capillary threshold entry pressure (psi),  $P_{ce}$ , and a dimensionless measure of the pore size heterogeneity fractal dimension,  $P_{cf}$ , represented by the slope of the  $\log P_c$ - $\log S_w$  curve, correlate with  $k_i$  and can be predicted using:

Mississippian:

$$P_{ce} = 2.30 k^{-0.42} \quad (1-26)$$

$$P_{cf} = 0.168 \ln k - 1.985 \quad (1-27)$$

Lansing-Kansas City

$$P_{ce} = 1.05 k^{-0.394} \quad (1-28)$$

$$P_{cf} = -0.061 \ln k - 1.46 \quad (1-29)$$

Using the capillary pressure parameters defined in equations 1-19 to 1-22 the water saturation can be calculated for any given oil column height using:

$$S_w = \left[ \frac{[Bh(\rho_w - \rho_o)]}{\frac{P_{ce}}{100^{P_{cf}}}} \right]^{1/P_{cf}} \quad (1-30)$$

Where B is a proportionality constant (= 0.433 psi cc/ft g),  $h$  is the oil column height (ft),  $\rho_w$  and  $\rho_o$  are the water and oil specific gravity (g/cc),  $P_{ce}$  is the oil-water capillary threshold entry pressure (psi),  $P_{cf}$  is the dimensionless measure of pore size heterogeneity, and  $S_w$  is the water saturation at height,  $h$ . Complete capillary pressure curves for any given permeability are constructed by calculations at multiple heights (**Fig. 1-46**).

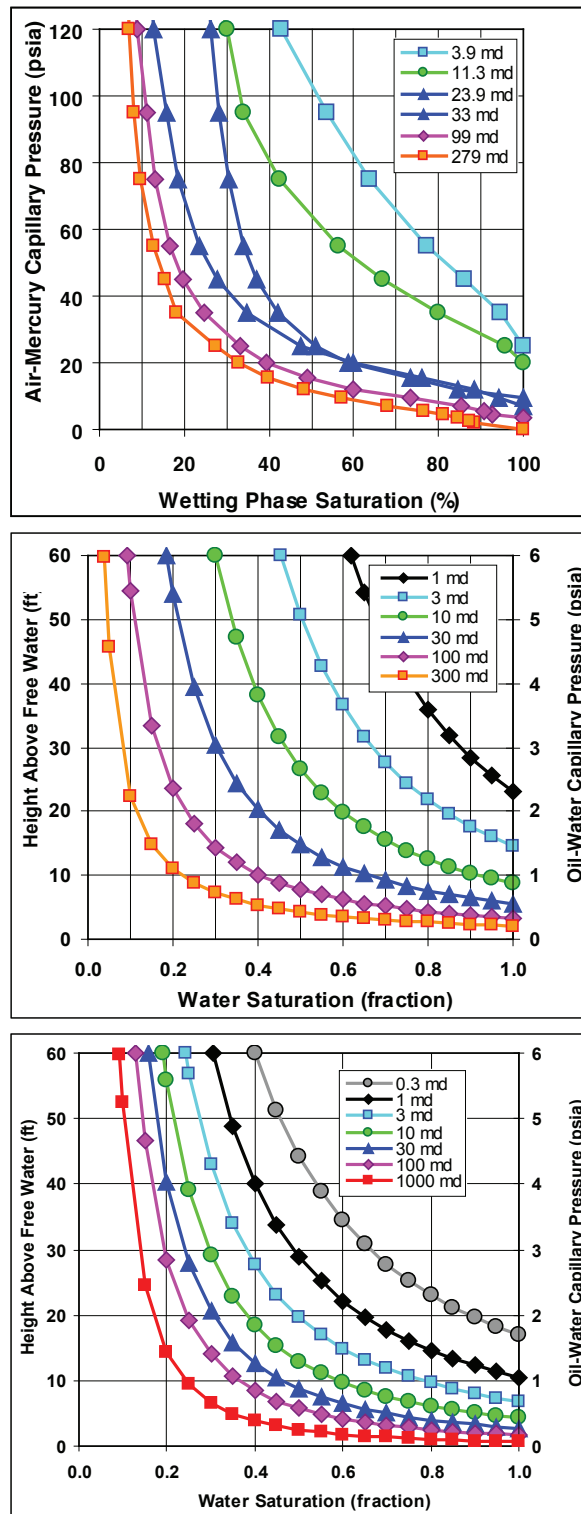


**Figure 1-46.** Measured (top) and modeled (middle) capillary pressure curves for Kansas Mississippian mudstones to grainstones and modeled curves for Lansing-Kansas City oomoldic limestones (bottom). Curves were constructed using equations 1-19 through 1-22 in text. Representative fluid densities used were  $\rho_w = 1.04 \text{ g/cc}$  and  $\rho_o = 0.75 \text{ g/cc}$ .

## 1.5 Electrical Properties

In Kansas the commonly used form of the modified Archie equation for both limestones and dolomites is:

$$S_w = (aR_w / (R_t \phi^m))^n \quad (1-31)$$

where  $S_w$  is water saturation,  $R_w$  is the formation brine resistivity (ohm-m),  $R_t$  is the true formation resistivity (ohm-m),  $\phi$  is fractional porosity ( $\phi$ ), and  $m$  is the Archie “cementation” or porosity exponent, and  $n$  is the Archie saturation exponent. Commonly in limestone and dolomites values adopted for  $a$  and  $m$  are  $a=1$  and  $m=2$ . These values are reasonably robust in carbonates with predominantly interparticle or intercrystalline porosity. However, in vuggy rocks, and in particular, oomoldic rocks, the Archie porosity exponent can have values significantly different than  $m=2$ . The Lansing-Kansas City limestones are predominantly oomoldic porosity and the variation in Archie parameters can cause significant problems for conventional log analysis of water saturation because of the difference in properties between the large oomolds and the fine interparticle porosity. Without meaningful Archie parameters the ability to accurately estimate water saturations in these rocks is hampered.

During the process of the electrical measurements, and the vertical profiles in several cores, the problem posed by thin-bed effects became apparent. This issue has as significant an influence on log interpretation as the porosity exponent. This is discussed below.

To evaluate the Archie cementation exponent, data were compiled and measured on Lansing-Kansas City (223), Mississippian (41), and Arbuckle (14) cores. In addition, to better understand oomoldic porosity exponent properties 106 modern carbonate oomoldic rocks from Ocean Cay, Bahamas also had Archie porosity exponent measurements.

### 1.5.1 Experimental Method

Subsequent to vacuum/pressure saturation with a 100,000 ppm NaCl brine, the cores were allowed to equilibrate with the brine for a minimum of a period of five (5) days. Once a plug had reached equilibration with the brine it was placed in a Hassler-type core holder and subjected to hydrostatic confining stress equal in psi to of one half the sample depth ( $\text{psi} = 0.5 * \text{depth (ft)}$ ). Electrical resistivity was measured at 10 kHz using a two electrode configuration using gold plated end electrodes. Resistivity was recorded only after the core had achieved equilibrium with the confining stress as determined by no change in the pore volume over a period of ten (10) minutes.

### 1.5.2 Results

#### 1.5.2.1 Arbuckle

Measurements on 14 core plugs from the Hadley L#4 provided to this study show that Arbuckle cementation exponents are not correlated with porosity (**Fig. 1-47**). Cementation exponent values average  $m_{\text{avg}} = 2.01 \pm 0.11$  (1 std dev). This value is consistent with the standard carbonate Archie model.

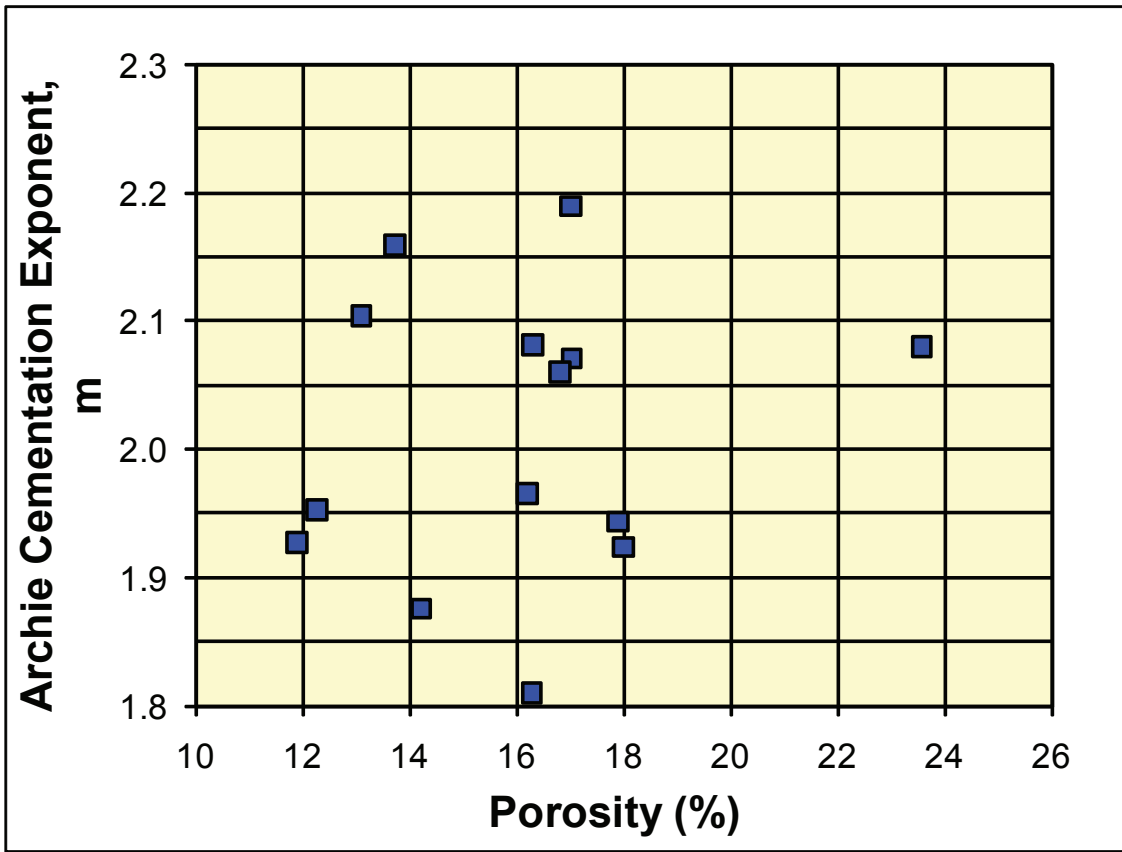
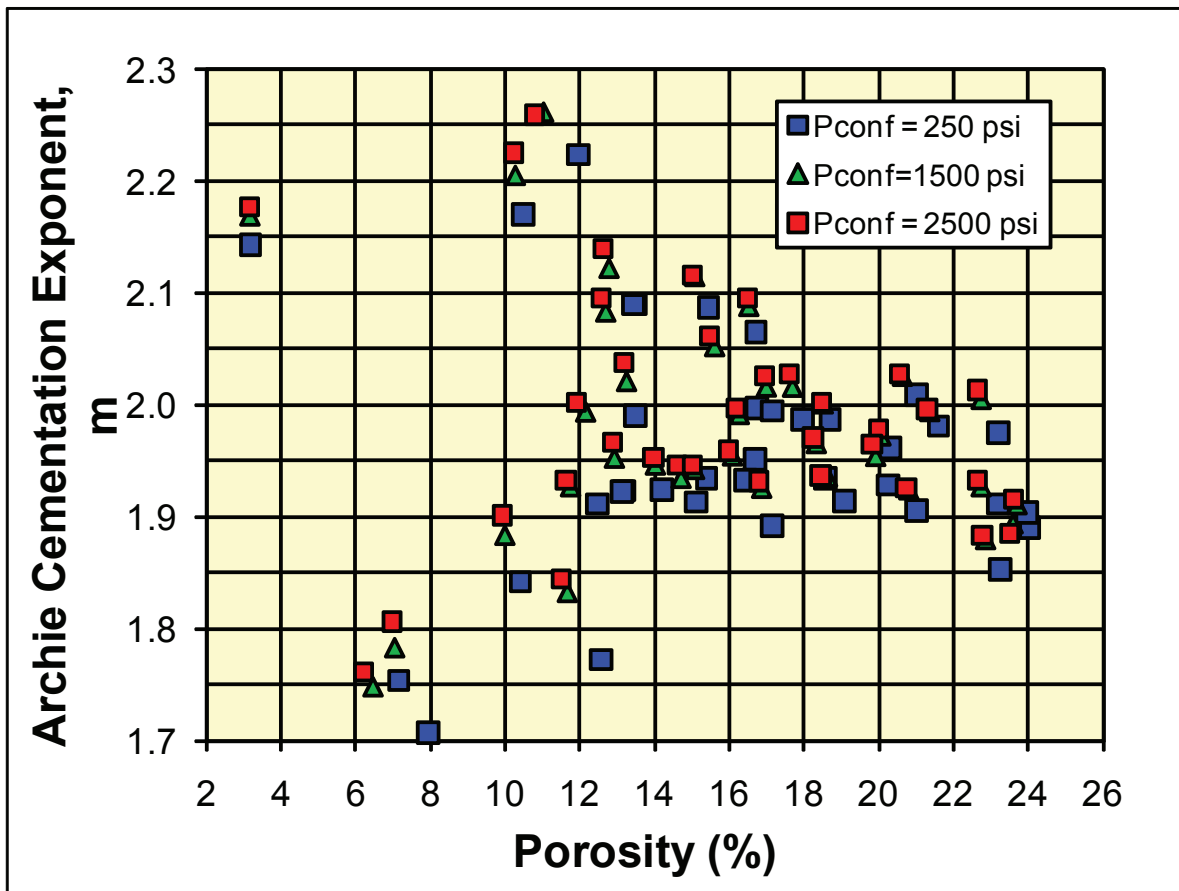


Figure 1-47. Crossplot of *in situ* Archie cementation exponent versus porosity for Arbuckle cores. The absence of correlation indicates the average cementation exponent,  $m = 2.01 \pm 0.11$ , can be used.

### 1.5.2.2 Mississippian

Measurements on 41 core plugs at both routine low confining stress conditions and at *in situ* stress conditions show that Mississippian cementation exponents are not correlated with porosity (**Fig. 1-48**). There is the possibility that cementation exponent increases slightly with decreasing porosity but anomalous low porosity values make interpretation ambiguous. *In situ* cementation exponent values average  $m_{\text{avg}2500} = 2.02 \pm 0.16$  (1 std dev). This value is consistent with the standard carbonate Archie model.



**Figure 1-48.** Crossplot of *in situ* Archie cementation exponent versus porosity for Mississippian cores. The lack of correlation indicates the average cementation exponent,  $m = 2.02 \pm 0.16$ , can be used.

### 1.5.2.3 Lansing-Kansas City

Measurements were performed on 223 core plugs from 32 wells at *insitu* stress conditions for the Lansing-Kansas City oomoldic limestone. To help in understanding of how and when oomoldic rock properties are developed an additional 106 analyses were performed on set of modern oomoldic limestone core plugs from Ocean Cay, Andros Island. **Figure 1-49** shows that cementation exponent values that can differ from the standard value of  $m = 2$  significantly. Previous studies have worked to model oomoldic cementation exponents (Rasmus, 1986; Watfa and Nurmi, 1987; Doveton, 2001). These investigations worked to resolve the relative contribution of moldic porosity to the total resistivity of the rock. Figure 1-50 presents these rocks in a different perspective. The cementation exponent is a function of porosity and pore architecture ( $A_{\text{pore}}$ ),  $m = f(\phi, A_{\text{pore}})$ . Using permeability as a proxy for pore architecture, cementation exponent can be considered as dependent on porosity and permeability. Empirical solution of a dependent relation provides an equation for estimation of oomoldic cementation of the form:

$$m = (-0.019 \log k_{\text{ik}} + 0.085) * \phi + 1.5 \quad (1-32)$$

where  $k_{\text{ik}}$  is in millidarcies and  $\phi$  is in percent.

Equation 1-32 can be used to estimate  $m$  but it a potentially more powerful use is the estimation of permeability. Using the wireline log analysis methods cited above (Rasmus, 1986; Watfa and Nurmi, 1987; Doveton, 2001), a value for  $m$  might be able to be estimated from log response. Given a value for  $m$  and  $\phi$  Figure 1-32 can be used to estimate the permeability of the oomoldic limestone being analyzed. Use of the more accurate cementation exponent values predicted using equation 1-32 result in correct log-calculated water saturations which vary by up to 80% from values calculated using  $m = 2$ .

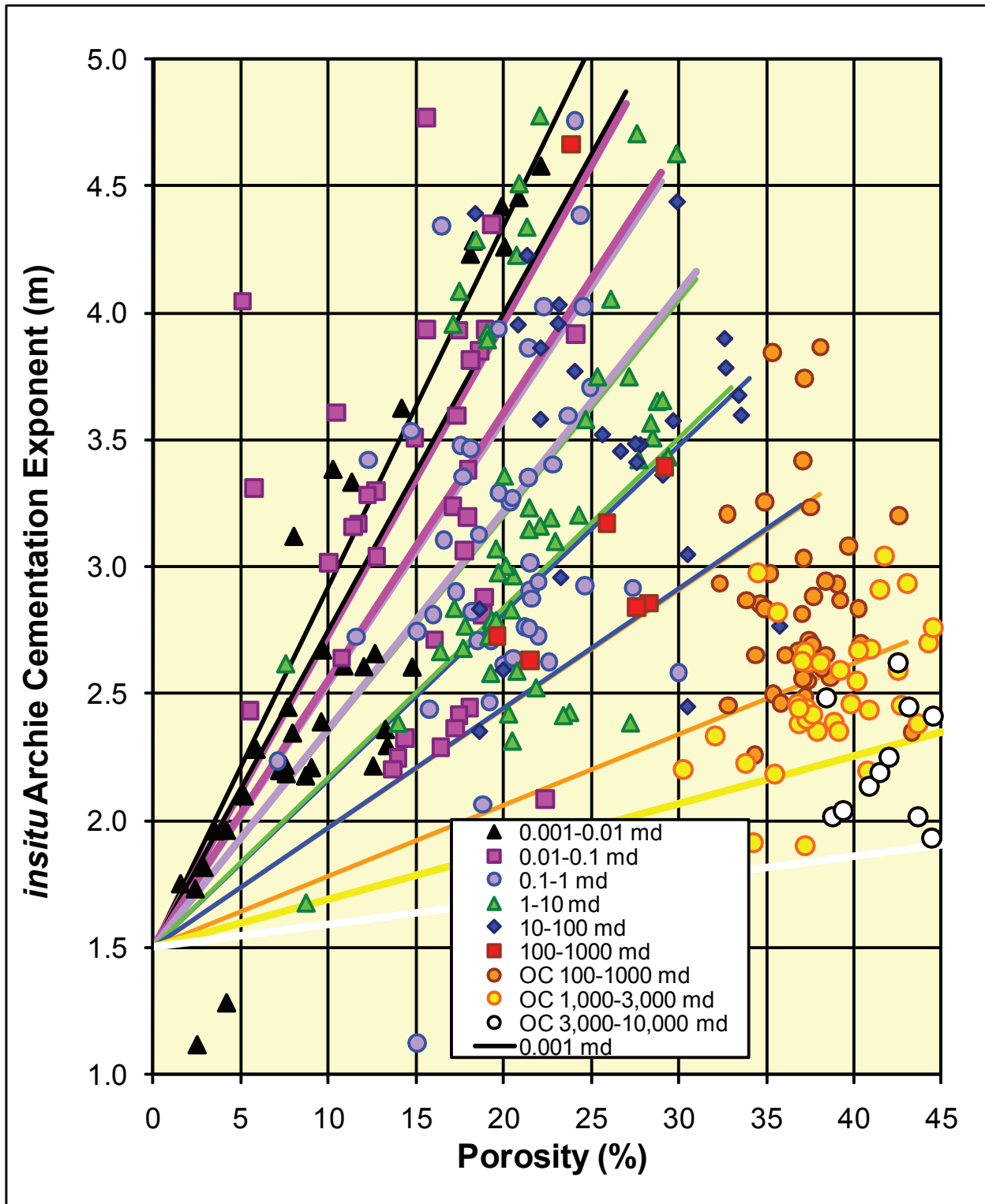


Figure 1-49. Crossplot of *in situ* Archie cementation exponent versus porosity for Kansas oomoldic Lansing-Kansas City limestones and modern oomoldic limestones from Ocean Cay, Andros Island (OC) cores. The lines shown are estimated using the empirical relation  $m = (-0.019 \log k_{ik} + 0.085) * \phi + 1.5$ .

#### 1.5.2.4 Vertical Cementation Exponent Distribution

Properties within meter-scale parasequences that comprise the LKC limestone reservoirs result from interaction of depositional architecture and particle texture with subsequent near-surface and deep diagenesis leading to oomoldic porosity. This exposure and paragenetic history can lead to significant changes in reservoir properties with depth from the unconformity surface. Frequently-observed micritized ooids and micritic calcite cements associated with terminal subaerial exposure at the top of the depositional sequence is associated with poorer reservoir quality. Underlying enhancement of permeability by improved oomoldic connectivity is common. A general decrease in permeability with depth, often associated with little decrease in porosity, frequently characterizes the lower portion of the oomoldic interval. These same changes can be associated with change in the electrical properties with depth for similar porosities.

Vertical cementation exponent profiles were developed for four LKC wells (**Fig. 1-50**) including 2 wells from previous investigation and three cores measured in this study. Depths for all wells were set on a datum of the top of the bed. All five wells exhibit significant vertical variation in cementation exponent. In all wells there is a general pattern of “normal”  $m = 2$  at the very top of the bed in the non-oomoldic limestone. Immediately underlying this cap cementation exponents increase rapidly in the 1-2 feet and may reach maximum values. With increasing depth  $m$  decreases but an interval of elevated  $m$  may exist within the over-all decreasing pattern. The basal portion of the interval is characterized by a return to normal  $m$  values and an absence of oomoldic porosity.

The vertical pattern shown in Figure 1-50 has important implication for log interpretation. It is clear that cementation is not constant over the interval even for intervals as thin as 10 ft to 16 ft. The highest  $m$  values are generally near the top of the interval where permeability is greatest.

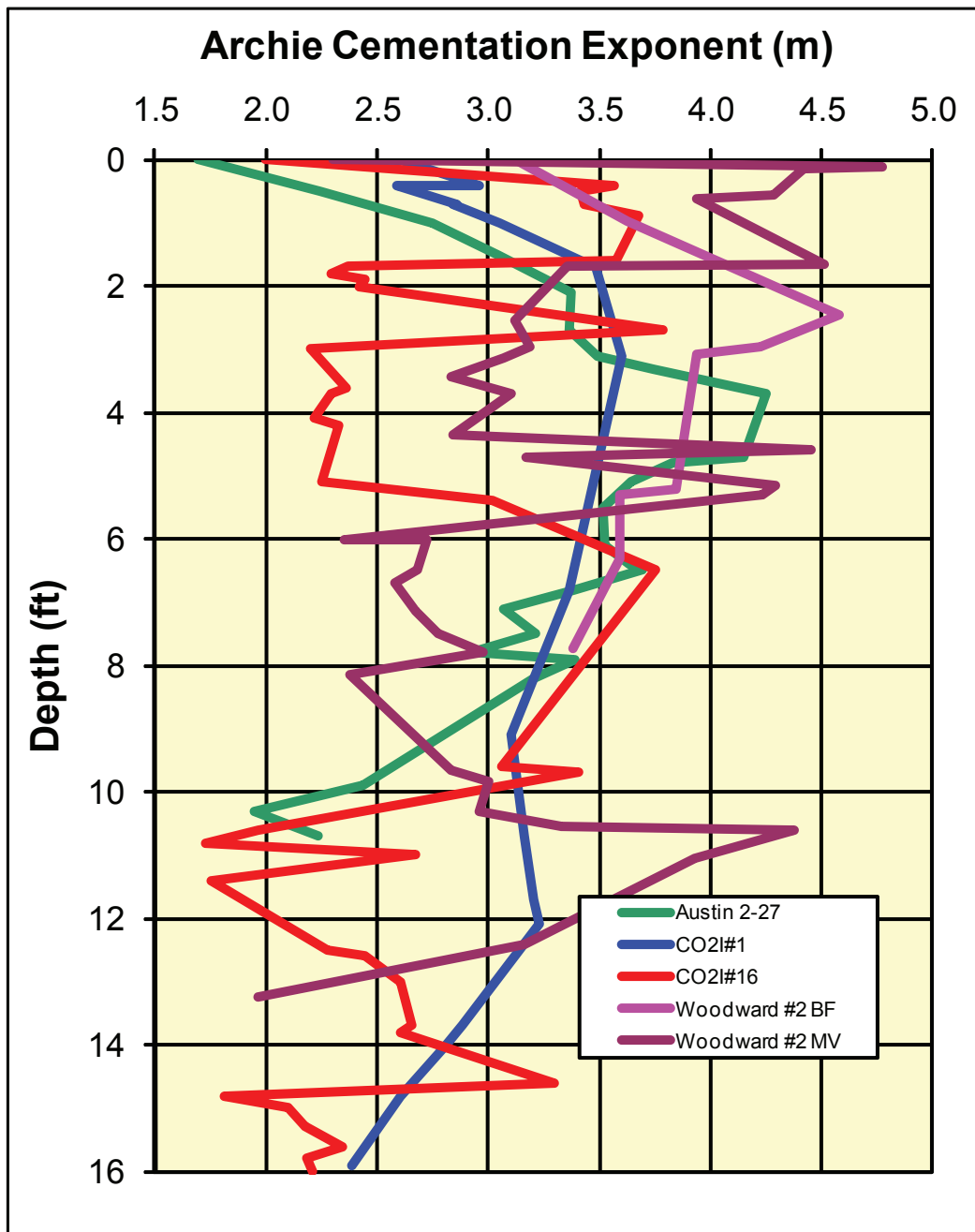


**Figure 1-50.** Vertical profile of cementation exponents in five Lansing-Kansas City oomoldic limestone wells. Profile represent one LKC cycle. Text discusses the vertical pattern.

### 1.5.3 Thin-Bed Resistivity Log Issues

The Lansing-Kansas City reservoirs vary in reservoir thickness. Though the total thickness of the combined stacked cycles can be several tens of feet, thickness of pay intervals can be considerably less. Because pay intervals are often thin (66% < 6 ft thick, 2 m; 45% < 4 ft, 1.3 m) and exhibit high porosity (8-30%), a single set of petrophysical properties is often assigned to the entire interval although petrophysical properties can vary significantly foot-by-foot.

Analysis of wireline logs for the Lansing-Kansas City interval across Kansas reveals that the LKC can be characterized as a thin-bed play. Analyzing 4,395 wells for LKC interval thickness with porosity > 8% provides an estimate of the distribution of LKC reservoir thicknesses (Fig. 1-52) Based on the method used over 50% of all LKC reservoir pay interval are less than 6-feet in thickness and over 80% are less than 9-feet in thickness. Given the permeability-porosity relationship for the Lansing-Kansas City a  $\phi > 8\%$  may include a significant fraction of non-pay interval. Using a more conservative interpretation that porosity must be  $\phi > 20\%$  for the same population of wells **Figure 1-53** shows that over 80% of reservoir pay intervals have thicknesses less than 5- feet. Increasing reservoir thickness is correlated with increasing quality. **Figure 1-54** indicates that as the reservoir interval increases in thickness the fraction of reservoir with  $\phi > 20\%$  increases.

The thin-bedded nature of the LKC can present a problem for electric log measurement and interpretation of saturation. If the pay interval is less than 5-feet in thickness then deep induction logs, and deep lateralogs, can be strongly influenced by over- and underlying bed properties leading to inability to accurately read  $R_t$  and therefore interpret  $S_w$ , even when an accurate  $m$  value is used.

**Figure 1-55** shows an example  $R_t$  response from wireline logs with vertical resolution ranging from 0.1 to 8 ft, representing the range in shallow to deep induction and lateral log investigation. It is assumed the reservoir interval ranges in thickness from 1 ft to 3 ft and the reservoir and bounding beds have the properties shown. For these conditions, if the reservoir interval is only 1-ft thick then it is only accurately visible to the shallow  $R_t$  tool. As the reservoir interval thickness increases the deeper-reading tools are influenced by the reservoir interval properties but only tools with vertical resolution less than half the bed thickness accurately measure  $R_t$  for some portion of the reservoir.

Using the observed  $R_t$  values in **Figure 1-55** and calculated water saturations using the correct reservoir electrical properties results in accurate estimation of the true water saturation for the reservoir interval only as shown in **Figure 1-56**. It is evident that only focused vertical resolution logs accurately read the reservoir bed saturations.

Comparing estimation using the correct cementation values with estimation using “standard” shows that if a reservoir interval were analyzed using the standard  $m = 2$  then the logs appear to be able to accurately estimate the reservoir saturation (Fig. 1-57B). However, **Figure 1-57C** shows that even if the reservoir interval were completely water saturated the logs would still predict the reservoir is hydrocarbon-bearing. This condition results because the resistivity log is effectively responding to porosity and is insensitive to water saturation.

These analyses indicate that accurate water estimation in the thin bedded Lansing-Kansas City requires advanced methods. **Figure 1-58** shows a general workflow to provide quantitative, semi-quantitative, and qualitative estimation of reservoir properties depending on whether tool resolution is finer than the reservoir interval thickness.

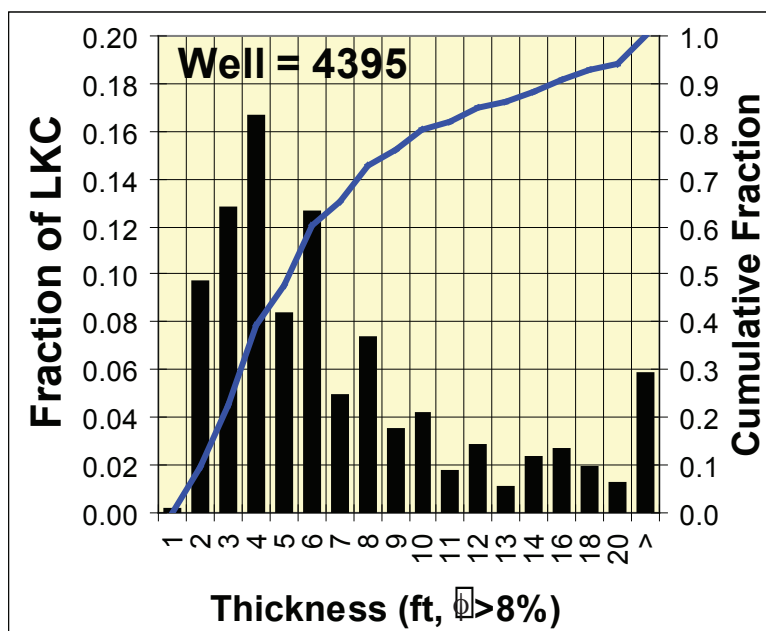


**Figure 1-51.** Histogram of Lansing-Kansas City interval thickness with porosity > 8% (n = 4,395)

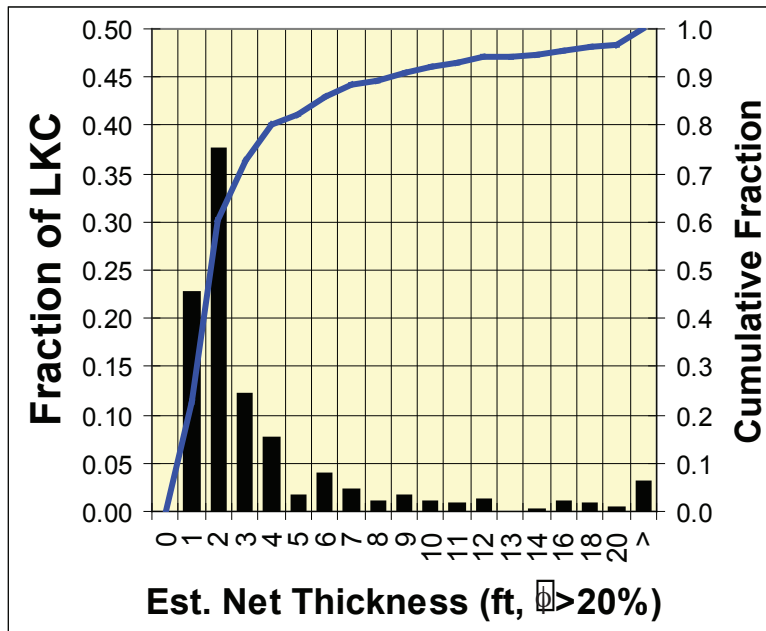


Figure 1-52. Histogram Lansing-Kansas City interval thickness with porosity > 20% (n=4,395).

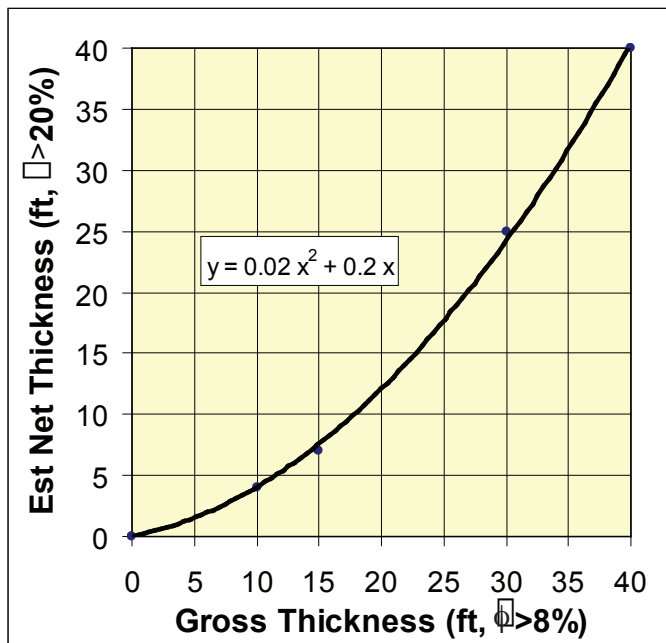
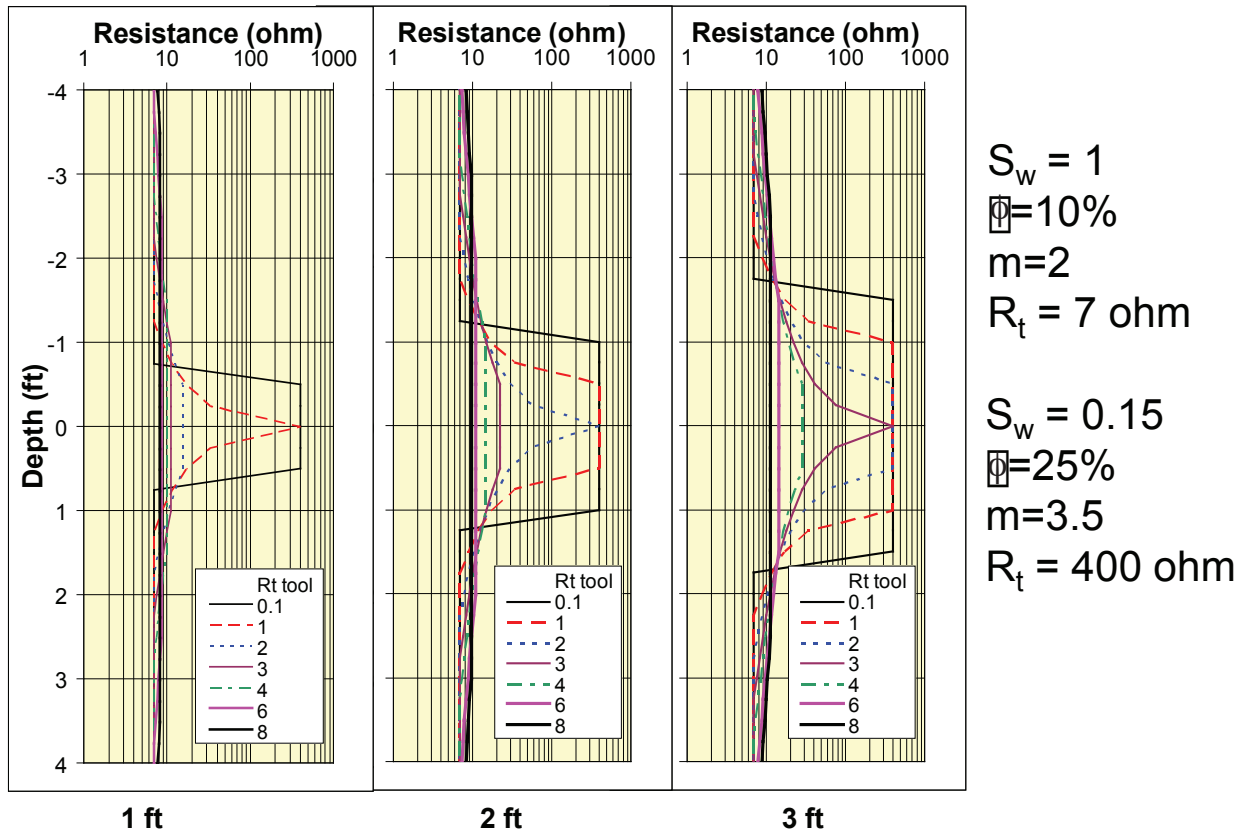


Figure 1-53. Crossplot of the estimated gross thickness of Lansing-Kansas City interval and the net thickness of the interval with  $\phi > 8\%$  (n=4,395). AS reservoir thickness increases the fractional of the total thickness that is higher quality increases.

# Average $R_t$ response



**Figure 1-54.** Example calculated resistivity tool response,  $R_t$ , as a function of the reservoir interval bed thickness (lower posted values), the tool vertical resolution (parametric values in graphs), for reservoir and bounding bed properties as noted on right. Note that only tools with vertical resolution less than half the bed thickness accurately measure  $R_t$  for some portion of the reservoir.

# Average $S_w$ response

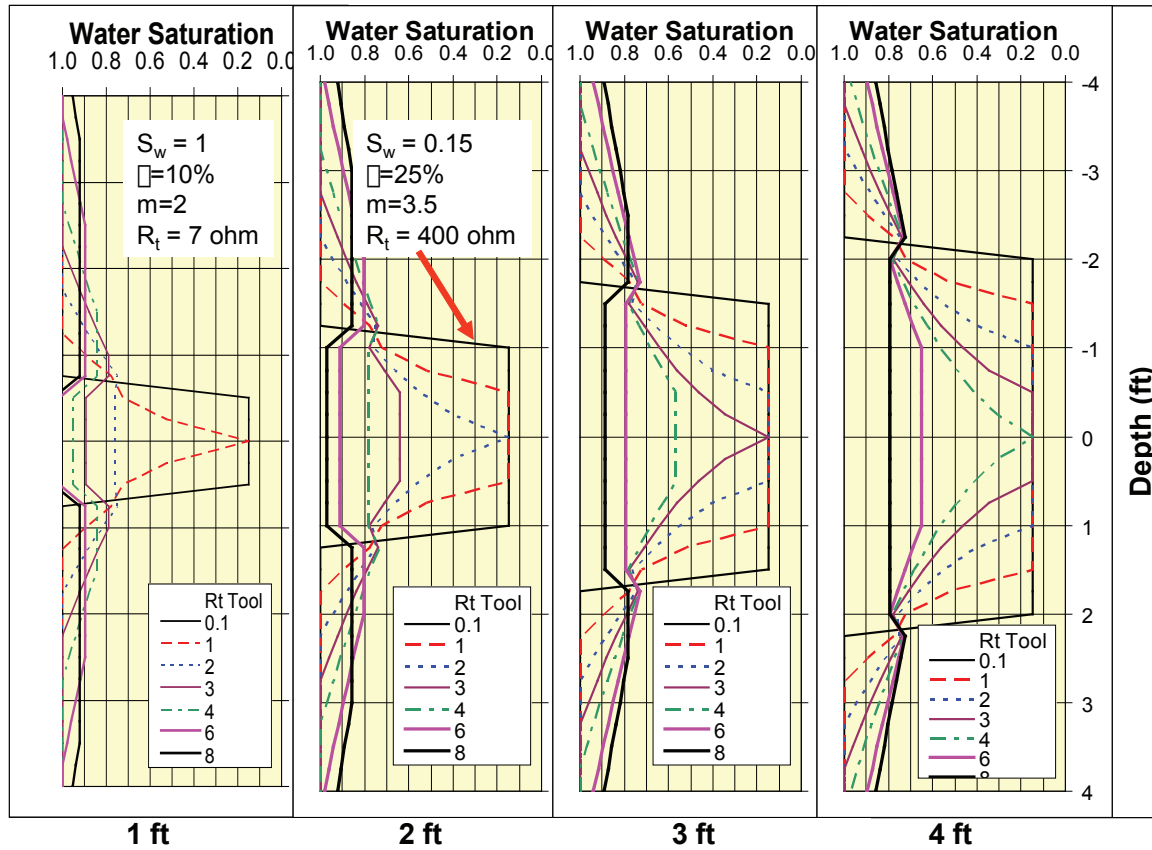
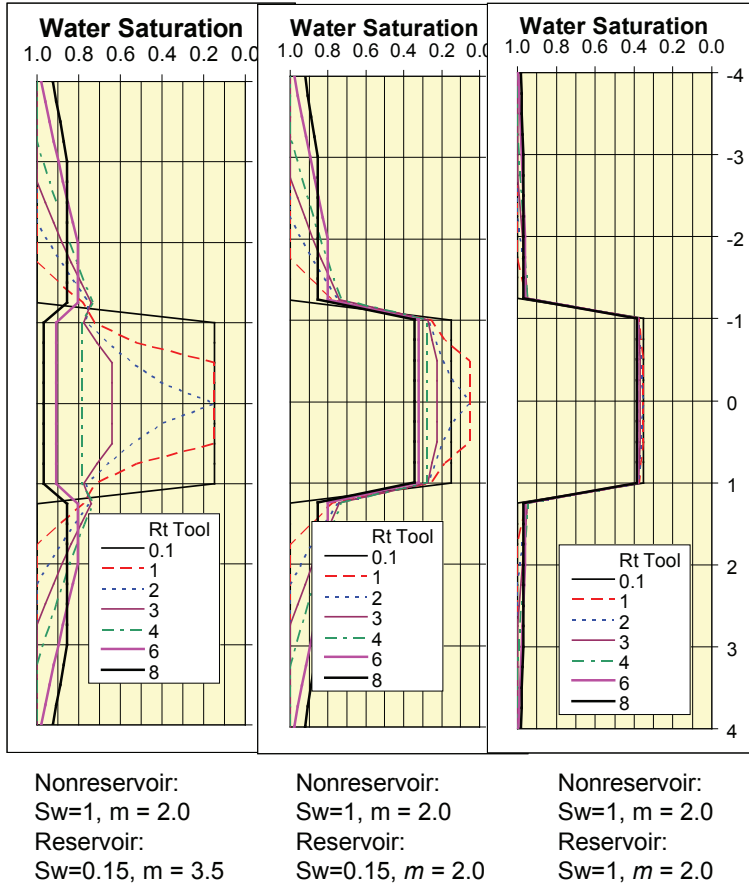


**Figure 1-55.** Example calculated water saturations for  $R_t$  readings shown in Figure 1-54. Estimated water saturations vary as a function of the reservoir interval bed thickness (lower posted values), the tool vertical resolution (parametric values in graphs), for reservoir and bounding bed properties as boxes. These water saturation estimates assume that the correct porosity and cementation exponent was used and only the  $R_t$  values change as shown in Figure 1-56. Note that only tools with vertical resolution less than half the bed thickness accurately measure  $S_w$  for some portion of the reservoir.



## Assigning $m=2$ is not the solution

Problem:

With correct  $m$   
 Ild sees  $S_w = 0$

Improper Solution:  
 When assign  $m = 2$   
 IIs sees  $S_w < 0.15$   
 Ild sees  $S_w = 0.34$

**but**

When  $S_w = 1$   
 Ild still sees  $S_w = 0.39$   
 $m$  is being used as a  
 porosity cut-off through  
 the Archie equation and  
 has nothing to do with oil

**Figure 1-56.** Example calculated water saturations for a 2-ft thick bed for three conditions: 1) Left - correct porosity and  $m$  are assigned to reservoir and bounding beds as shown in Figure 1-55; 2) Center -  $m$  is assigned a value of 2 for a reservoir where true  $m = 3.5$  and where true water saturation is  $S_w=0.15$ ; 3) Right -  $m$  is assigned a value of 2 for a reservoir where true  $m = 3.5$  and where true water saturation is  $S_w=1$ . Estimated water saturations with correct  $m$  for deep induction are incorrect. Use of  $m = 2$  gives the apparent correct estimation of water saturation (center), however, the example on the right shows that the log estimates low  $S_w$  even when the reservoir is 100% water saturated because the resistivity tool is more sensitive to porosity and is insensitive to saturation.

## Simplified Methodology for Oomoldic $k$ & $S_w$ Calculation

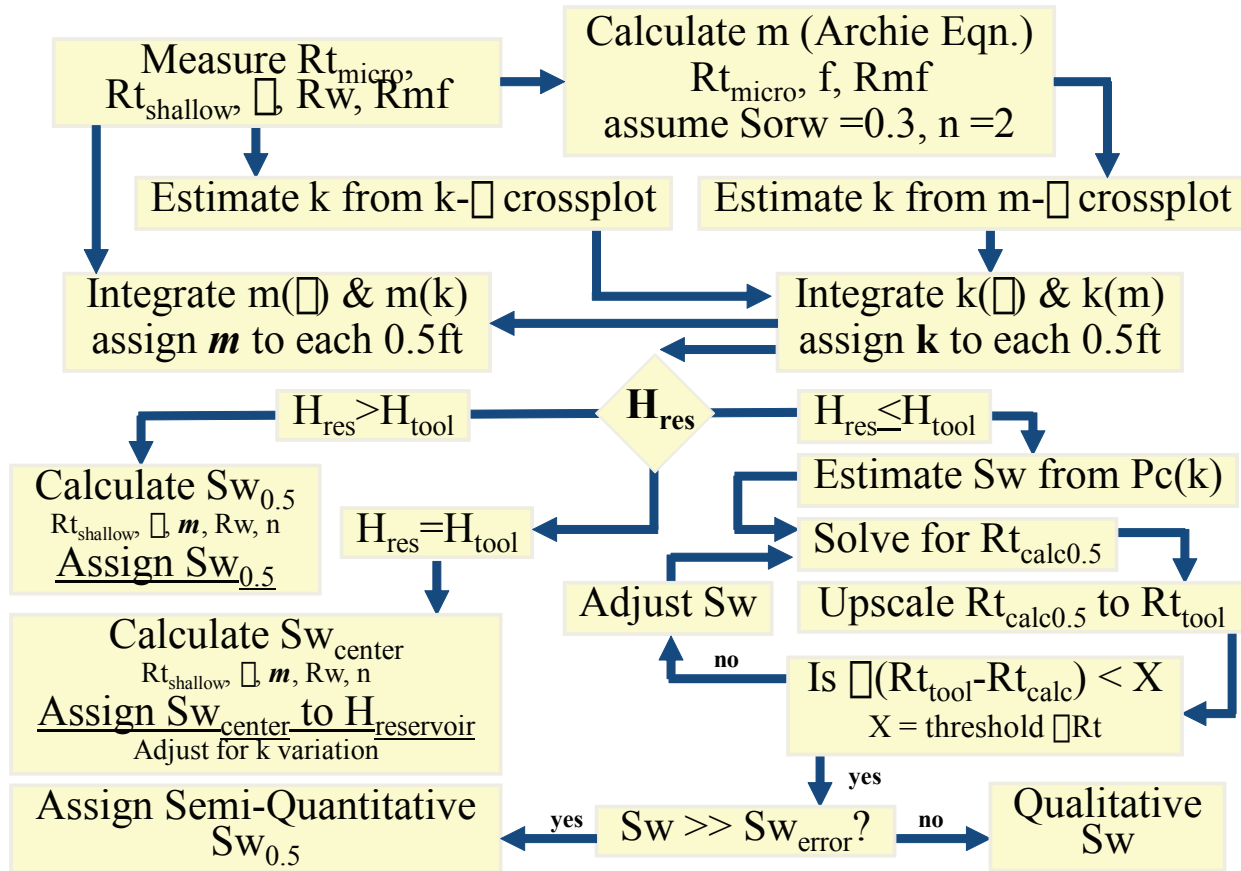


**Figure 1-57.** General workflow for quantitative, semi-quantitative, and qualitative estimation of reservoir properties depending on whether tool resolution is finer than the reservoir interval thickness.

## 1.6 Relative Permeability

Frequently only a few relative permeability ( $k_r$ ) curves are utilized to simulate a field, however,  $k_r$  curves can change with pore architecture changes associated with lithologic variables, absolute permeability, starting saturations, and saturation hysteresis. For the rocks presented in this study a suite of relative permeability curves exist as a function of the absolute permeability and the associated increase in  $S_{wirr}$  and  $S_{wc}$  with decreasing  $k$ . To better understand relative permeability relationships in the Lansing-Kansas City and Mississippian drainage and imbibition relative permeability measurements were performed.

### 1.6.1 Experimental Methods

For drainage relative permeability measurements it was desired to start the cores at the same water saturation as present in the reservoir. Frequently drainage relative permeability is performed by displacement to “irreducible” water saturation. Though this method is suitable to achieve low water saturation states, the saturations achieved may not represent reservoir saturations that were achieved by natural drainage capillary pressure conditions. In addition, fluid saturation distribution may not be the same as the saturation distribution achieved by capillary drainage. To achieve capillary equilibrium saturations, cleaned cores were saturated with brine as described in Section 1.4.1.2. The cores were placed in a porous-plate capillary pressure cell and desaturated at a pressure of 24 psi, which is equivalent to an oil-column height of 60 feet. Once the cores had reached equilibrium they were removed and the “irreducible” water saturation determined gravimetrically. The cores were then placed in a vacuum/pressure saturator and saturated with a isoparaffinic oil. The core plugs were removed for the saturator and placed in a Hassler cell at a confining pressure similar to that used for the *in situ* Klinkenberg permeability measurements. Drainage effective oil permeability at the “irreducible” saturation ( $k_{eo,S_{w60}}$ ) was measured at a low differential pressure using the single-phase stationary method. This method utilizes a low differential pressure across the core to avoid displacement of any possibly mobile water. For most cores no effluent water was observed. In a few cores minor water was expelled but volumes would not have changed the core saturation by more than 1-5%.

### 1.6.2 Results

Results of relative permeability testing are discussed in the modeling section. The following discussion briefly addresses results. Curve data are available on the website.

Relative permeability to oil at  $S_{w60}$  ( $k_{ro,S_{w60}}$ ) can be defined as:

$$k_{ro,S_{w60}} = k_{eo,S_{w60}}/k_{ik} \quad (1-33)$$

where  $k_{ik}$  is the *in situ* Klinkenberg permeability (md) and represents the absolute permeability. **Fig-**

**ures 1-58 and 1-59** show the measured drainage oil relative permeabilities for Mississippian cores as a function of the absolute permeability and water saturation. Oil relative permeabilities at  $S_{w60}$  for cores with permeability greater than approximately 10 md exhibit  $k_{ro,S_{w60}} > 95\%$  .

**Figures 1-60 and 1-61** show the measured drainage oil relative permeabilities for Lansing-Kansas City cores as a function of the absolute permeability and water saturation. Relative oil permeabilities at Sw60 for the LKC exhibit a weak positive correlation with permeability (Fig. 1-60) but exhibit no correlation with water saturation (Fig. 1-61)

Following drainage relative permeability testing select cores, representing a range in permeability and well location, were analyzed for unsteady-state imbibition oil-water relative permeability. Due to small pore volumes in some samples (pore volume < 5 cc) relative permeability curve data occasionally were erratic. To provide a continuous curve, for these samples minor data smoothing was performed. Testing was limited to cores with permeability greater than approximately 1 md because of experimental difficulty. This limits the range of the family of curves evaluated but provided sufficient range to define trends. Figures 1-63 and 1-64 show composite imbibitions oil-water relative permeability curves for the Mississippian and Lansing-Kansas City.

Generalized relative permeability curves can be used to illustrate comparative differences in relative permeability in response to changes in absolute permeability and  $S_{orw}$  ( $S_{oi}$ ) for the LKC and Mississippian carbonates studied. Relative permeability curves for any given permeability were modeled using modified Corey-type equations. The modified Corey relative permeability equations used were:

$$k_{ro} = k_{romax} (1 - S_{wD})^n \quad (1-34)$$

$$k_{rw} = k_{rwmmax} S_{wD}^m \quad (1-35)$$

$$S_{wD} = (S_w - S_{wc}) / (1 - S_{wc} - S_{orw}) \quad (1-36)$$

where  $S_{wc}$  was defined as the saturation achieved at an oil column height of 60 ft. Average values for Mississippian relative permeability parameters from this modeling were:  $k_{romax} = 1$ ,  $k_{rwmmax} = \sim 0.22$ ,  $n = 3.1$ ,  $m = 0.5$ . For L-KC rocks parameters were:  $k_{romax} = 1$ ,  $k_{rwmmax} = 0.24$ ,  $n = 3.7$ ,  $m = 1.1$ .

For both formation there is significant scatter in the relative permeability curves but general patterns are evident. Modeling of relative permeability is discussed in the following section.

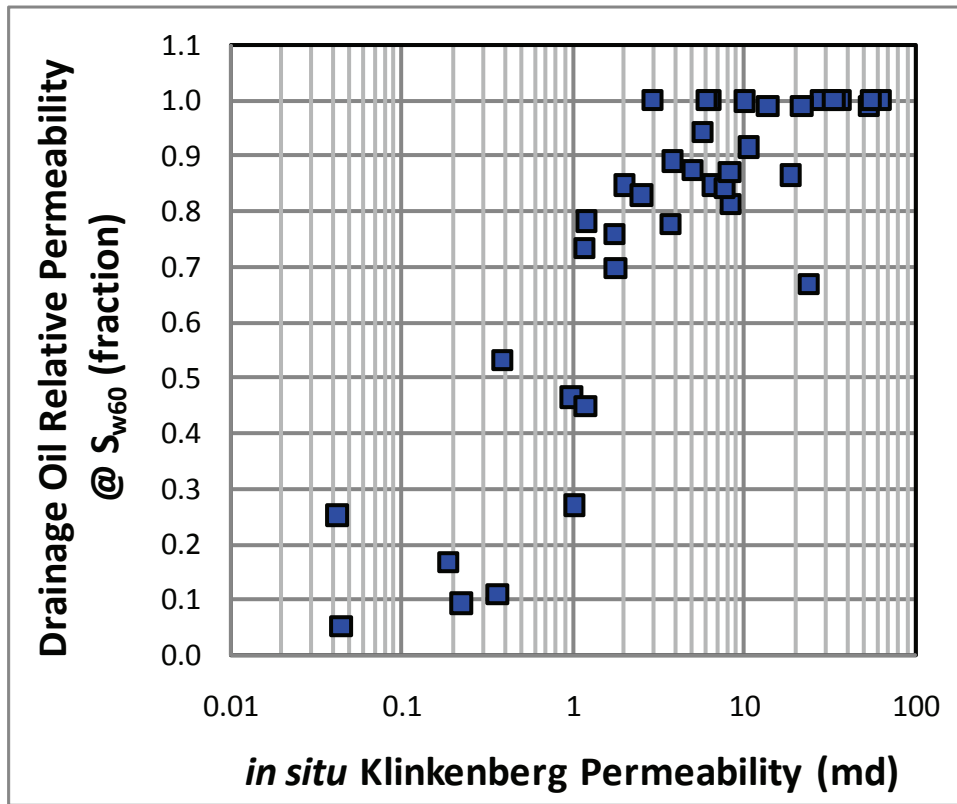


**Figure 1-58.** Mississippian rock drainage oil relative permeability measured at  $S_{w60}$  (water saturation achieved by capillary pressure desaturation at a pressure equivalent to a 60-ft oil column height) versus absolute permeability of the core. Core with  $K_{ik} > \sim 10$  md have  $k_{rg,S_{w60}} > 98\%$ .

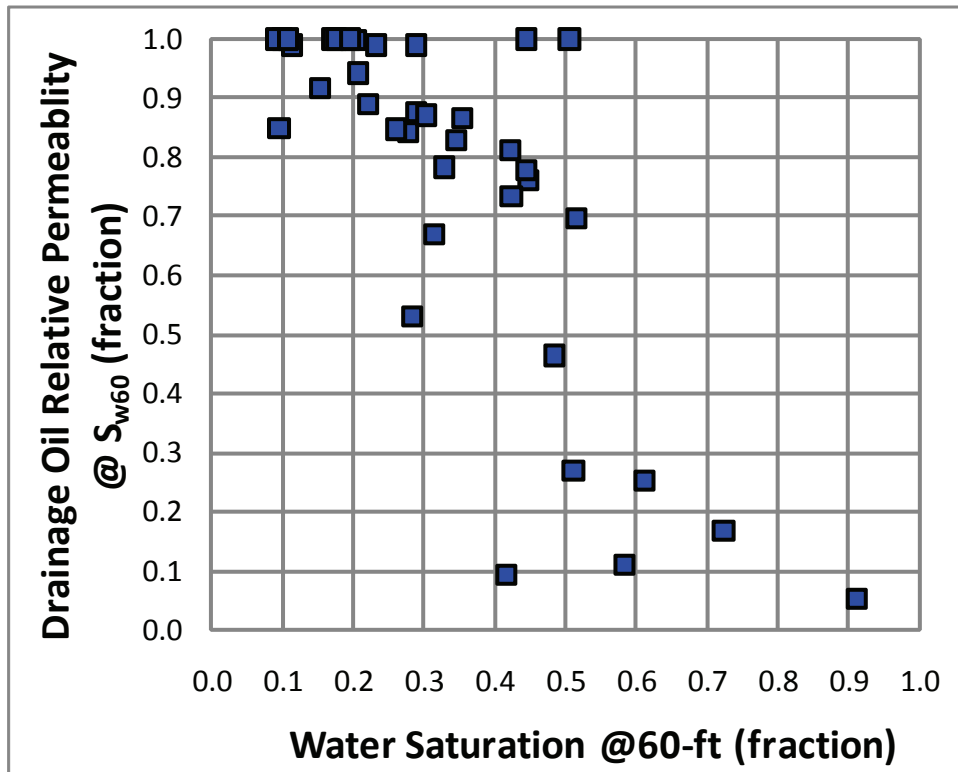


**Figure 1-59.** Mississippian rock drainage oil relative permeability measured at  $S_{w60}$  (water saturation achieved by capillary pressure desaturation at a pressure equivalent to a 60-ft oil column height) versus water saturation of the core as measured at 24 psi air-brine capillary pressure which is estimated to be equivalent to a 60-ft oil-brine column height. Core with  $S_{w60} < \sim 0.3$  have  $k_{rg,Sw60} > 98\%$ .

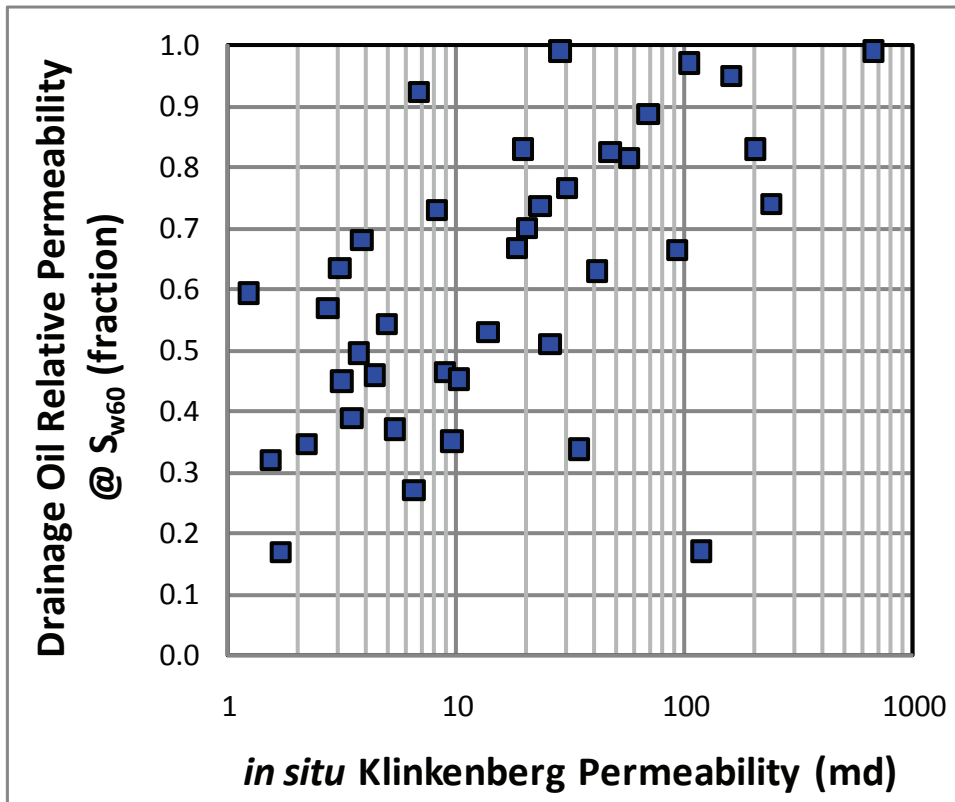


**Figure 1-60.** Lansing-Kansas City rock drainage oil relative permeability measured at  $S_{w60}$  (water saturation achieved by capillary pressure desaturation at a pressure equivalent to a 60-ft oil column height) versus absolute permeability of the core.

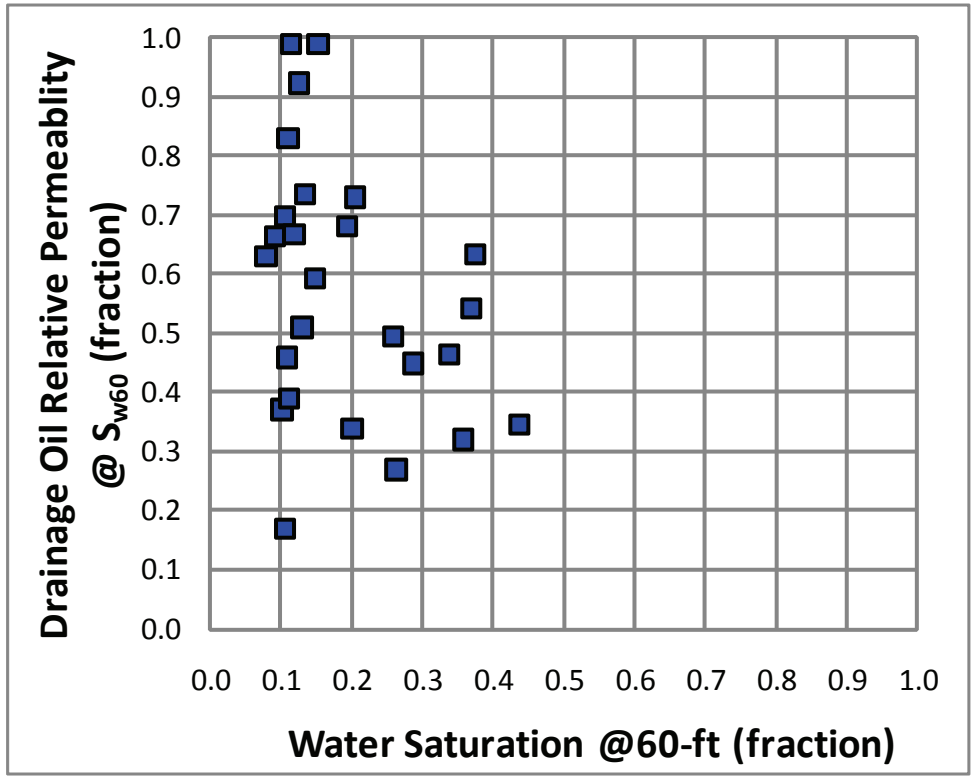


**Figure 1-61.** Lansing-Kansas City rock drainage oil relative permeability measured at  $S_{w60}$  (water saturation achieved by capillary pressure desaturation at a pressure equivalent to a 60-ft oil column height) versus water saturation of the core as measured at 24 psi air-brine capillary pressure which is estimated to be equivalent to a 60-ft oil-brine column height. Core with  $S_{w60} < \sim 0.3$  have  $k_{rg,S_{w60}} > 98\%$ .

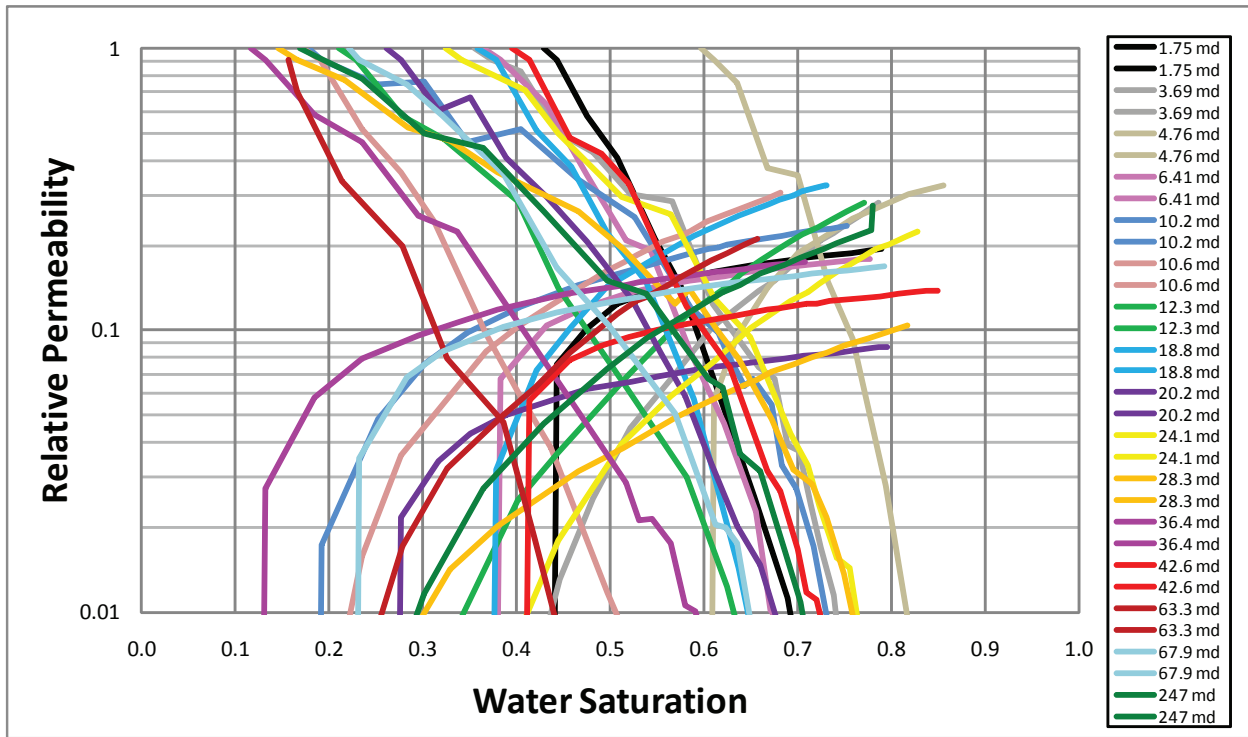


**Figure 1-62.** Composite of Mississippiian imbibition oil-water relative permeability curves. Curve set positions shift with  $S_{wi}$  and  $S_{orw}$ . In general sets shift to lower  $S_{wi}$  with increasing permeability. Relative permeability model is discussed in text.

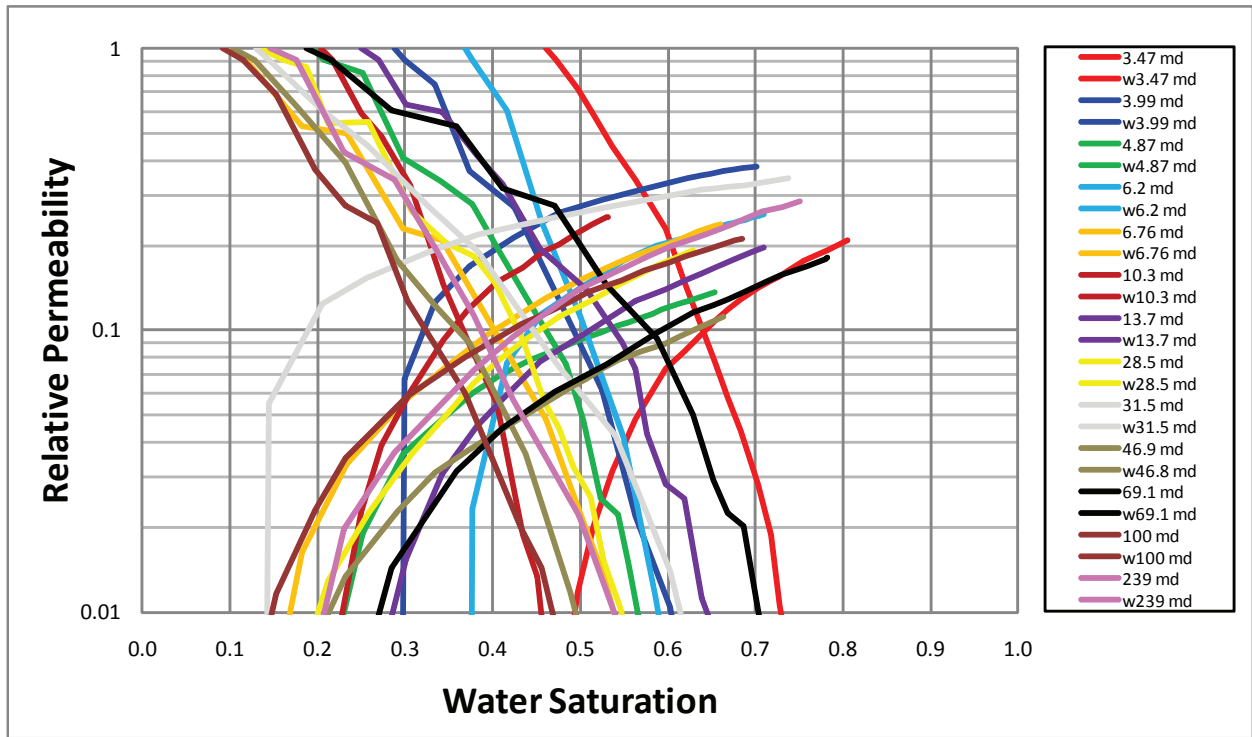


**Figure 1-63.** Composite of Lansing-Kansas City imbibition oil-water relative permeability curves. Curve set positions shift with  $S_{wi}$  and  $S_{orw}$ . In general sets shift to lower  $S_{wi}$  with increasing permeability. Relative permeability model is discussed in text.

## 2.0 Relative Permeability and Modeling

### 2.1 Introduction

Thin (3-40 ft thick), heterogeneous, limestone and dolomite reservoirs, deposited in shallow-shelf environments, represent a significant fraction of the reservoirs in the U.S. midcontinent and worldwide. In Kansas, reservoirs of the Arbuckle, Mississippian, and Lansing-Kansas City formations account for over 73% of the 6.3 BBO cumulative oil produced over the last century. For these reservoirs basic petrophysical properties (e.g., porosity, absolute permeability, capillary pressure, residual oil saturation to waterflood, resistivity, and relative permeability) vary significantly horizontally, vertically, and with scale of measurement. Many of these reservoirs produce from structures of less than 30-60 ft, and exhibit vertical variation in initial saturations and relative permeability properties being located in the capillary pressure transition zone exhibit vertically variable initial saturations and relative permeability properties. Rather than being simpler to model because of their small size, these reservoirs challenge characterization and simulation methodology and illustrate issues that are less apparent in larger reservoirs where transition zone effects are minor and most of the reservoir is at saturations near  $S_{wirr}$ . Understanding how capillary pressure properties change with rock lithology and, in turn, within transition zones, how relative permeability and residual oil saturation to waterflood change through the transition zone is critical to successful reservoir management as reservoirs mature and enhanced recovery methods are planned and implemented.

From early imbibition studies in gas-water and gas-oil systems (Holmgren and Morse, 1951; Dyes, 1954; Kyle et al, 1956; Crowell et al., 1966), and a single oil-water study (Pickell et al., 1966), all primarily conducted on sandstones, Land (1968, 1971) showed that  $S_{gr}^*$  increases with increasing  $S_{gi}^*$  following the relation:

$$C = 1/S_{gr}^* - 1/S_{gi}^* \quad (2-1)$$

where  $C$  was defined as the trapping characteristic and  $S_{gr}^*$  and  $S_{gi}^*$  are the effective residual and effective initial gas saturations, respectively, determined (e.g., for a gas-water system) from  $S_{grw}^* = S_{gr}/(1-S_{wirr})$  and  $S_{gi}^* = S_{gi}/(1-S_{wirr})$ . Testing this relationship on a range of limestone lithofacies for a gas-water system Keelan and Pugh (1975) reported for sucrosic, intercrystalline, chalk, and oomoldic carbonates lithofacies: 1) residual gas saturation to waterflood,  $S_{grw}$ , ranged from 23 to 68% in the carbonates studied, 2)  $S_{grw}$  increased with increasing  $S_{gi}$ , 3)  $S_{grw}$  was a function of rock lithology, 4)  $S_{grw}$  increased with increasing pore-size heterogeneity, 5)  $S_{grw}$  increased with decreasing porosity in oolitic rocks, 6)  $S_{grw}$  was independent of porosity in dense crystalline and chalky lithofacies, 7)  $S_{grw}$  did not vary significantly for  $S_{gi}$  greater than 70% in chinks and sucrosic dolomites, 8)  $S_{grw}$  exhibits hysteresis, and 9)  $S_{grw}$  is complex in carbonate reservoirs and to obtain accurate values data have to be measured on the formation of interest.

Stegemeier (1974) provided a pore doublet model analysis of the nature of trapping. Morrow (1987) reviewed the effects of  $S_{oi}$ , pore-size heterogeneity, and wettability on  $S_{orw}$  presenting conclusions consistent with Keelan and Pugh (1975). Recently, Heymans (1997), Christiansen and Heymans (2000), and Fanchi et al. (2002) have presented an analysis of the influence of variable  $S_{orw}$  and  $S_{oi}$  on oil recovery from oil-water transition zones and presented an analytical method for calculating oil reserves.

This study investigates the properties of moldic carbonate rocks from the Mississippian and Lansing-Kansas City (L-KC) formations in Kansas to better understand oil recovery from these transition-zone reservoirs. The paper first briefly reviews the reservoir geology and rock lithologic properties for the selected Mississippian and L-KC across Kansas. Measured basic properties, including porosity, permeability, capillary pressure are summarized. The relationships among  $S_{oi}$ ,  $S_{orw}$ , relative permeability and lithology are examined. Lastly, the application of these relationships is explored to illustrate how oil and water production are influenced.

## 2.2 Reservoir Geology

Properties of Kansas Mississippian and L-KC reservoirs are discussed in Byrnes et al. (2003). Multi-scale carbonate-dominated sequences were deposited in subtidal to supratidal environments on the broad shallow Kansas shelf throughout the Paleozoic. A repeating association of original depositional facies and early diagenesis for these rocks produced lithofacies ranging from mudstones to grainstones with abundant moldic porosity. The nature of the molds varied through time reflecting change in primary carbonate grain constituents: Upper Cambrian-Lower Ordovician Arbuckle peloid and ooid molds, Mississippian carbonate/siliceous sponge spicule and echinoderm/brachipod molds, and Pennsylvanian ooid and bioclast molds.

For Mississippian strata, post-depositional regional uplift, subaerial exposure, and differential erosion of the ramp strata at the pre-Pennsylvanian unconformity resulted in paleotopographic highs (buried hills) of low relief (generally <30-60 ft). The majority of production occurs at or near the top of the Mississippian section just below the sub-Pennsylvanian unconformity. Lansing-Kansas City oolitic/oomoldic reservoirs exhibit geometries and architectures similar to modern oolites. Reservoirs usually comprise multiple stacked, or *en echelon* shoals that formed in response to sea level fluctuations. Oomoldic reservoirs, ranging in thickness from several feet to several tens of feet, formed across the entire Kansas Pennsylvanian ramp; however, thicker, porous and permeable oolite deposits are commonly associated with the flanks or crests of paleostructural highs. These highs may have influenced the intensity of early diagenesis and may have been responsible for development of good reservoir properties. Grain size variation, location on oolite buildups and interbedded carbonate mud (aquitards) influenced the nature and extent of diagenetic overprinting.

For Mississippian rocks, early dissolution of grains and dolomitization created moldic, inter-crystalline, and vuggy porosity important for favorable reservoir conditions (**Fig. 2-1**). Very finely

crystalline (<10-50  $\mu\text{m}$ ) dolomite is characteristic of early reflux or mixing zone dolomitization. Despite overprinting by sub-Pennsylvanian subaerial exposure and burial processes, lithofacies and early diagenesis are the major controls on the nature and distribution of reservoir properties. For L-KC rocks subaerial exposure and meteoric water percolation led to cementation around the aragonite ooids and often dissolution of the ooids and variable development of matrix and vuggy porosity. Resulting oomoldic grainstones, the principal reservoir lithofacies, underwent variable degrees of early or later fracturing and crushing, providing connection between otherwise isolated oomolds. Reservoir oomoldic rocks range from wackestones with isolated oomolds to grainstones with close-packed oomolds (**Fig. 2-2**). Matrix properties range from dense crystalline to microporous micritic to sucrosic fine-medium crystalline.

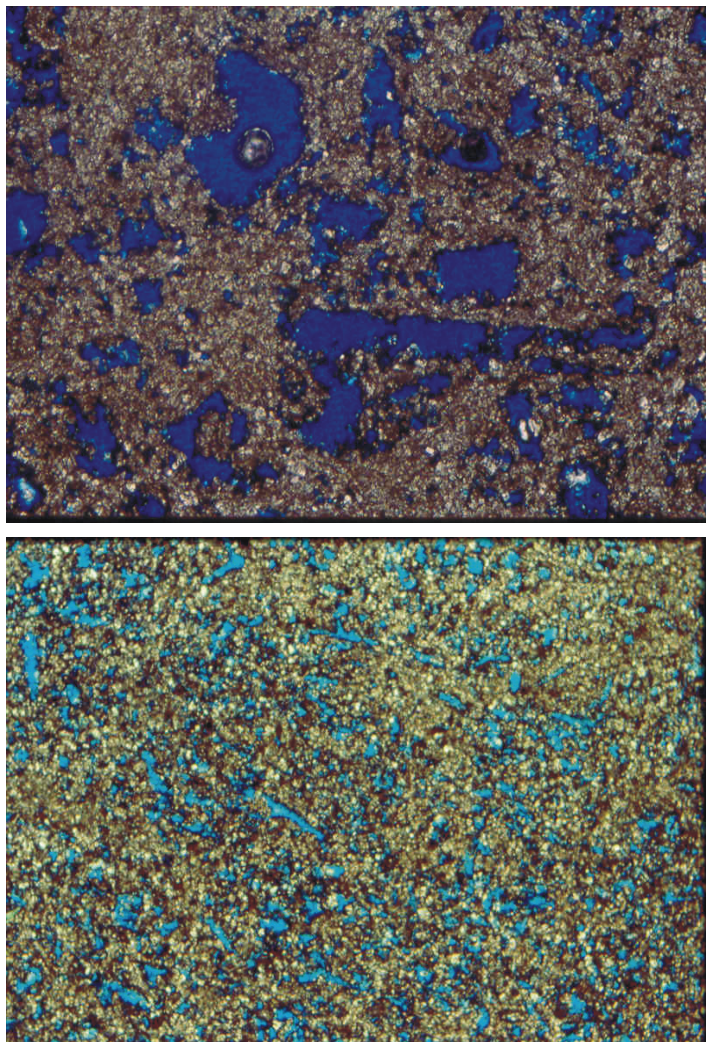


**Figure 2-1.** Thin-section photomicrographs of two example Mississippian lithologies showing nature of moldic porosity. Upper image – Echinoderm fragments and other skeletal fragments, including sponge spicules, have been dissolved leaving abundant moldic porosity (blue areas) in relatively tight dolomitic matrix. Lower image – Abundant sponge spicule moldic and intercrystalline porosity in dolomite matrix. Width 5 mm.

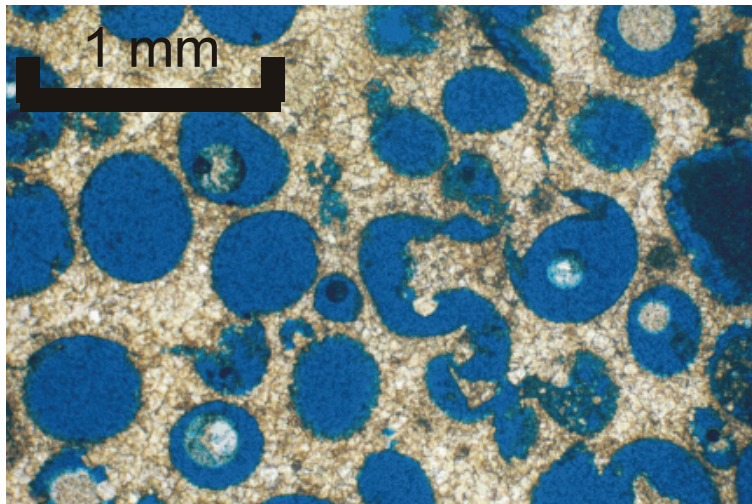


**Figure 2-2.** Thin section photomicrograph of typical Lansing-Kansas City oomoldic limestone with oomoldic porosity (blue) separated by crystalline matrix. Early crushing helped develop oomoldic connectivity.

## 2.3 Core-Analysis Methodology

The results of this investigation are based on petrophysical analyses of over 300 L-KC and 650 Mississippian core plugs obtained from fields across Kansas. Core plugs were approximately 1-inch in diameter and ranged from 1 to 3 inches long. Grain density, helium porosity, and routine air were measured on all samples. Helium porosity was measured unconfined, and routine air permeability was measured using a confining pressure of 400 psi. For many wells whole cores were slabbed, plugged, and photographed to facilitate description. Thin sections were prepared and examined for selected samples.

Advanced rock properties were measured on selected samples representing the range in porosity, permeability, and lithology observed in each formation. Advanced rock properties measured on various numbers of samples for each measurement included *in situ* porosity ( $\phi$ ), *in situ* Klinkenberg gas permeability ( $k$ ), air-mercury capillary pressure analysis to 10,000 psi, air-brine capillary pressure analysis to 200 psi, oil-water drainage, and imbibition relative permeability. Relative permeability measurements were performed unsteady-state and used synthetic brine and isoparaffinic *Isopar M* and *Isopar G* oil.

### 2.3.1 Porosity, Permeability, and Capillary Pressure

For Mississippian rocks, lithofacies and early diagenesis are major controls on permeability ( $k$ ) and porosity ( $\phi$ ) despite complex diagenetic overprinting by sub-Pennsylvanian subaerial exposure and burial processes. Permeability and  $\phi$  decrease significantly and continuously with decreasing grain/mold size from packstone to mudstone (a trend exhibited by many other carbonates) and from echinoderm-rich to spicule-rich facies (an exception is the echinoderm grainstone facies which may be silica cemented and exhibit very low  $k$  and  $\phi$ ).

Porosities range from 2% to 30% and permeabilities range from <0.001 md to 400 md. The  $k$ - $\phi$  trend for all Mississippian lithofacies (**Fig. 2-3**) is approximately bounded within two orders of magnitude by trendlines defined by:

$$\log k = 0.25 \phi - 2.5 \tag{2-2}$$

$$\log k = 0.25 \phi - 4.5 \tag{2-3}$$

Between these bounding trends each lithofacies exhibits a generally unique range of  $k$  and  $\phi$  which together define a continuous trend, with  $k$  decreasing with decreasing grain/mold size for any given porosity. Each individual lithofacies exhibits a unique sub-parallel trend to the general trend where the relationship between  $k$  and  $\phi$  for each lithofacies can be represented by a power-law function of the form:

$$k = A \phi^{-3.5} \tag{2-4}$$

where the coefficient,  $A$ , varies with lithofacies. Increasing moldic content, and associated increasing  $\phi$ , increase  $k$  at a lower rate than the overall  $k$ - $\phi$  trend indicating that matrix properties dominate control of flow in these rocks.

Porosity in L-KC oomoldic limestones ranges from 0 to 35% with rocks below 15% porosity exhibiting poor reservoir properties. Permeability (<0.001-400 md) is principally controlled by  $\phi$  and oomold connectivity created by dissolution of matrix at ooid-ooid contacts, crushing, and fracturing

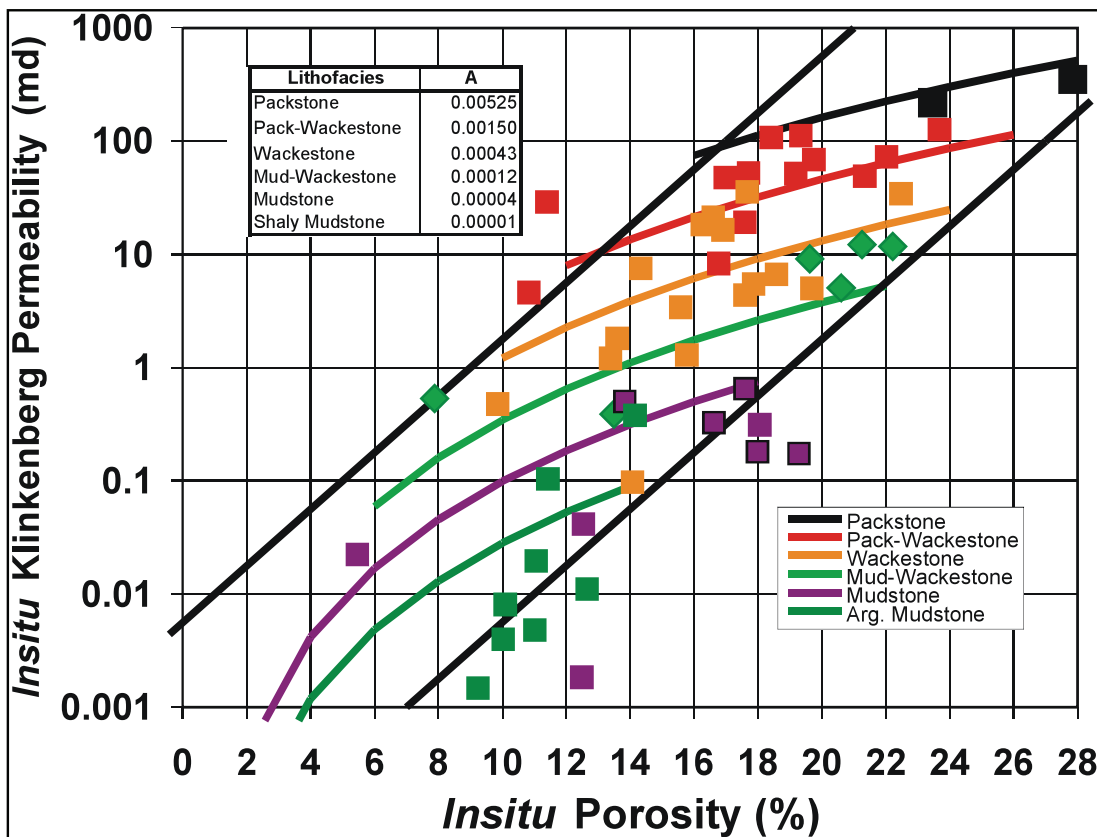


**Figure 2-3.** Permeability versus porosity crossplot for various lithologies in the Mississippian in Kansas. Each individual lithofacies exhibits a unique sub-parallel trend to the general trend where the relationship between  $k$  and  $\phi$  for each lithofacies can be represented by a power-law function of the form:  $k = A \phi^{-3.5}$  where the coefficient,  $A$ , varies with lithofacies. Values for  $A$  for each lithofacies are shown in the figure.

(Byrnes et al., 2000). The  $k$ - $\phi$  trend for all oomoldic lithofacies is approximately bounded within two orders of magnitude by trendlines defined by:

$$\log k = 0.2 \phi - 2.8 \quad (2-5)$$

$$\log k = 0.2 \phi - 5.4 \quad (2-6)$$

Between these bounding trends each lithofacies exhibits a generally unique range of  $k$  and  $\phi$  where variance is significant due to variable oomold connectivity and matrix properties. It is important to note that individual wells generally exhibit  $k$ - $\phi$  trends with less variance than the overall trend (Fig. 2-4). Other variables that exert influence on  $k$  but are colinear with  $\phi$  include oomold diameter, oomold packing, matrix properties, and matrix fracturing. Power-law function can be utilized for carefully defined oomold lithofacies such as the medium crystalline matrix oomoldic facies which can very generally be estimated using

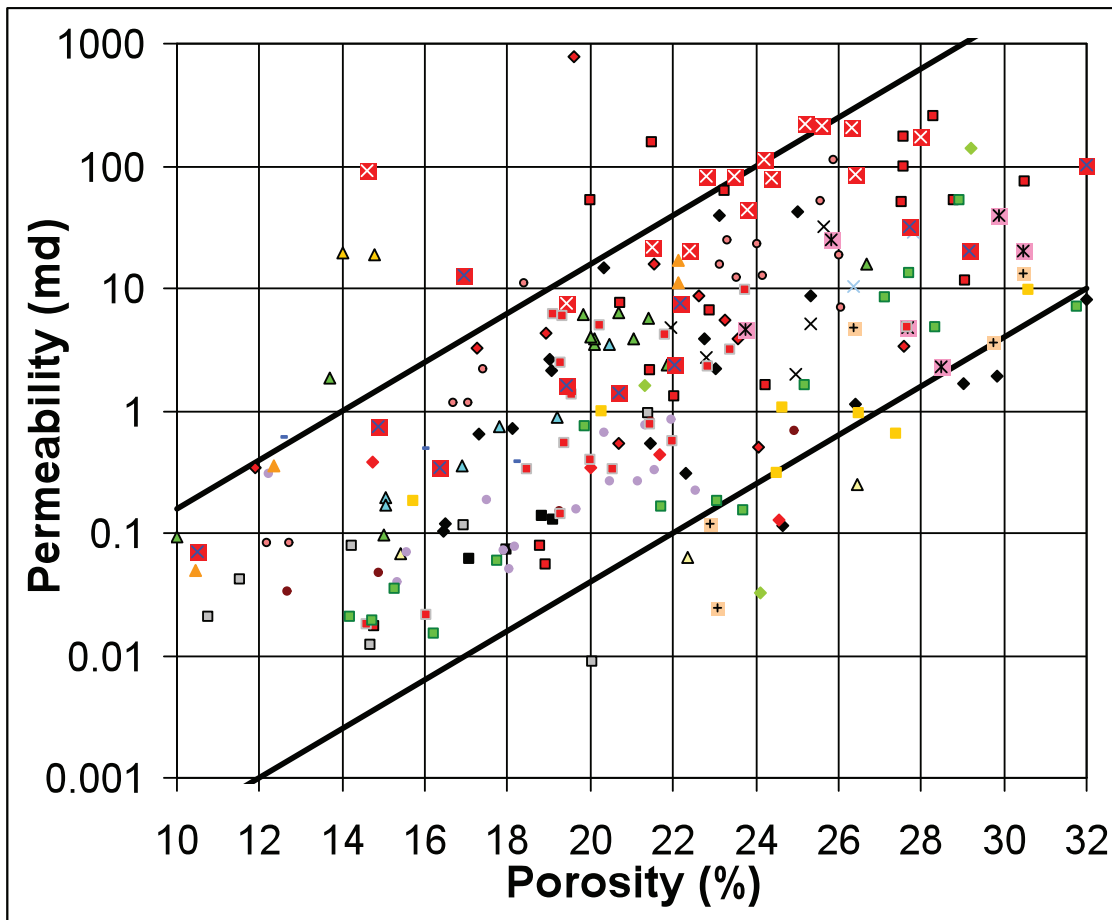


**Figure 2-4.** Permeability versus porosity crossplot for Lansing-Kansas City Group oomoldic limestones for reservoirs across Kansas. Permeability (<0.001-400 md) is principally controlled by  $\phi$  and oomold connectivity created by dissolution of matrix at ooid-ooid contacts, crushing, and fracturing (Byrnes et al., 2000). The  $k$ - $\phi$  trend for all oomoldic lithofacies is approximately bounded within two orders of magnitude by trendlines defined by:  $\log k = 0.2 \phi - 2.8$  and  $\log k = 0.2 \phi - 5.4$ . Between these bounding trends each lithofacies exhibits a generally unique range of  $k$  and  $\phi$  where variance is significant due to variable oomold connectivity, oomold diameter, oomold packing, matrix properties, and matrix fracturing. Symbols represent wells.

$$k = 4.894 \times 10^5 \phi^{6.21} \quad (2-7)$$

Precise relationships between oomoldic lithofacies texture characteristics and permeability have not been quantified to date though they have been investigated (Byrnes et al., 2000).

Capillary pressure properties of Mississippian and L-KC carbonates differ between lithofacies. With structural closure in many Kansas fields less than 60 feet, it is also important to note that these values represent the maximum oil column height and that much of the volume of a field lies in the transition zone below these oil column heights (water-free zone). At these lower oil column heights, understanding the exact capillary pressure relationship becomes important. Utilizing over 50 air-brine and air-mercury drainage capillary pressure curves, measured on a range of lithofacies, equation parameters to construct generalized capillary pressure curves were developed using 1) capillary threshold entry pressure, and 2) the slope of the  $\log P_c$ - $\log S_w$  curve, reflecting pore size distribution, using a modification<sup>16</sup> of the Brooks and Corey (1964, 1966) method. Oil-water capillary threshold entry pressure (psi),  $P_{ce}$ , and a dimensionless measure of the pore size heterogeneity fractal dimension,  $P_{cf}$ , represented by the slope of the  $\log P_c$ - $\log S_w$  curve, correlate with  $k_1$  and can be predicted using

Mississippian:

$$P_{ce} = 2.30 k^{-0.42} \quad (2-8)$$

$$P_{cf} = 0.168 \ln k - 1.985 \quad (2-9)$$

Lansing-Kansas City

$$P_{ce} = 1.05 k^{-0.394} \quad (2-10)$$

$$P_{cf} = -0.061 \ln k - 1.46 \quad (2-11)$$

Using the capillary pressure parameters defined in equations 2-8 to 2-11 the water saturation can be calculated for any given oil column height using:

$$S_w = \left[ \frac{[Bh(\rho_w - \rho_o)]}{\frac{P_{ce}}{100^{P_{cf}}}} \right]^{1/P_{cf}} \quad (2-12)$$

Where B is a proportionality constant (= 0.433 psi cc/ft g),  $h$  is the oil column height (ft),  $\rho_w$  and  $\rho_o$  are the water and oil specific gravity (g/cc),  $P_{ce}$  is the oil-water capillary threshold entry pressure (psi),  $P_{cf}$  is the dimensionless measure of pore size heterogeneity, and  $S_w$  is the water saturation at height,  $h$ . Complete capillary pressure curves for any given permeability are constructed by calculations at multiple heights (**Fig. 2-5**).

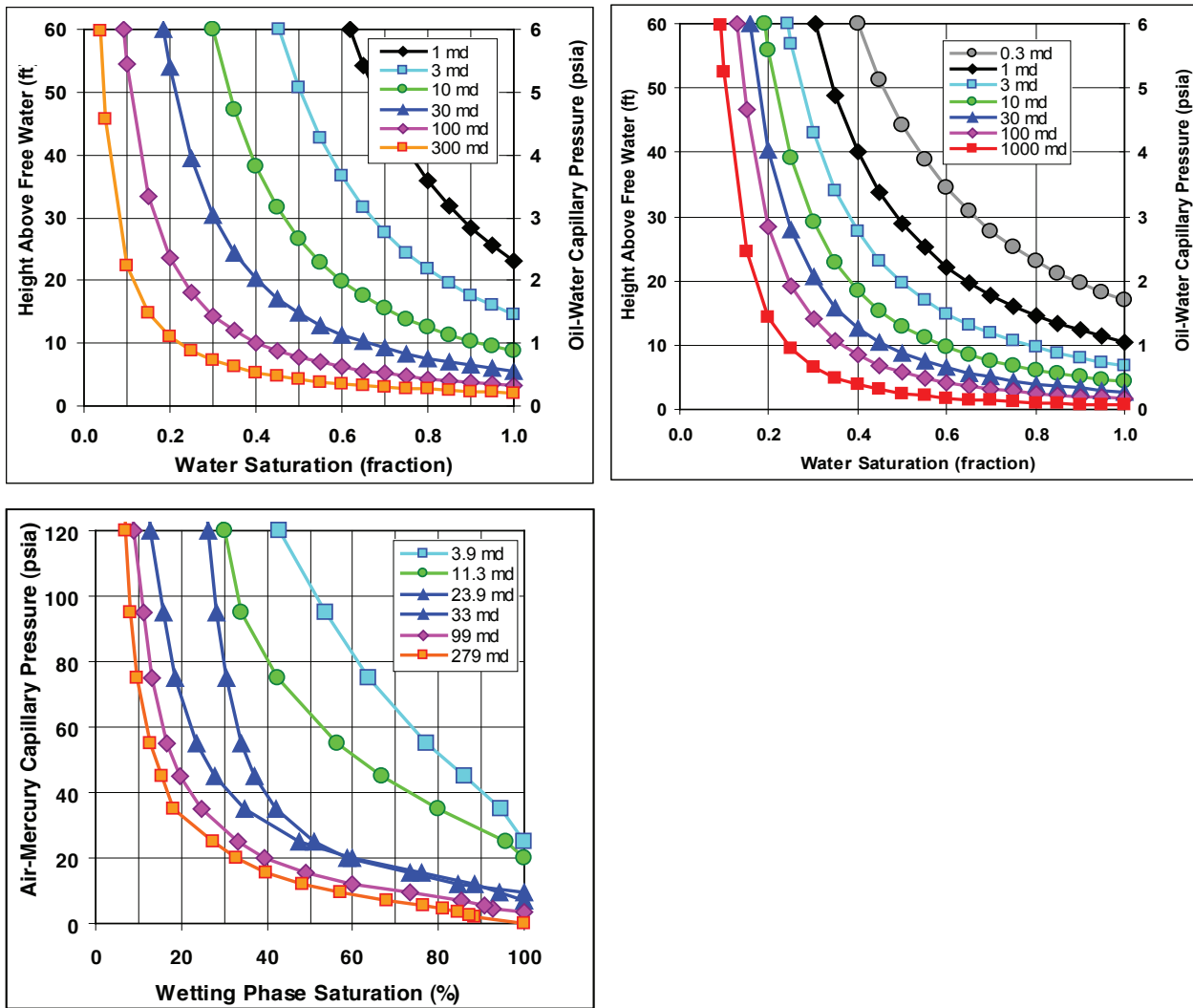


**Figure 2-5.** Measured (top) and modeled (middle) capillary pressure curves for Kansas Mississippian mudstones to grainstones and modeled curves for Lansing-Kansas City oomoldic limestones (bottom). Curves were constructed using equations 8-12 in text. Representative fluid densities used were  $\rho_w = 1.05$  g/cc and  $\rho_o = 0.82$  g/cc.

## 2.4 Residual Oil Saturation to Waterflood

From the capillary pressure curves shown in Figure 2-5, it is clear that for many thin Mississippian and L-KC reservoirs, many of which have  $k_i < 10-100$  md, there is considerable variation in  $S_{oi}$  (i.e.,  $1-S_{wirr}$ ) vertically through the reservoirs. Applying equation 1 to an oil-water system, it is clear that as  $S_{oi}$  changes vertically in the reservoir,  $S_{orw}$  would also change as noted and modeled in previous work (Heymans, 1997; Christiansen and Heymans, 2000; Fanchi et al., 2002). The amount of residual oil to waterflood is a function of the trapping characteristic. Cores representing a range of lithologies from each formation were flooded with oil to critical water saturation,  $S_{wc}$  ( $\sim S_{wirr}$ ) or were flooded to  $S_w > S_{wc}$  representing different  $S_{oi}$  conditions. Starting from different  $S_{oi}$  conditions the cores were then waterflooded to  $S_{orw}$ . Treating each flood individually, a value for the trapping characteristic,  $C$ , was calculated using equation 2-1 for an oil-water system and assuming  $S_{wc} = S_{wirr}$ . **Figure 2-6** illustrates the relationship between  $C$  and  $\phi$  for Mississippian and L-KC rocks of various lithologies. For the carbonate rocks studied here,  $S_{orw}$  increases with increasing  $S_{oi}$  which can be attributed to emplacement of oil in progressively finer pores with increasing  $S_{oi}$  and where trapping is increased. Figure 6 shows the Land trapping characteristic,  $C$ , increases with increasing porosity resulting in less trapping with increasing porosity and can be predicted using the relationships:

Mississippian:

$$C = 11.14\phi + 0.27 \quad (2-13)$$

Lansing-Kansas City

$$C = 11.70\phi - 0.51 \quad (2-14)$$

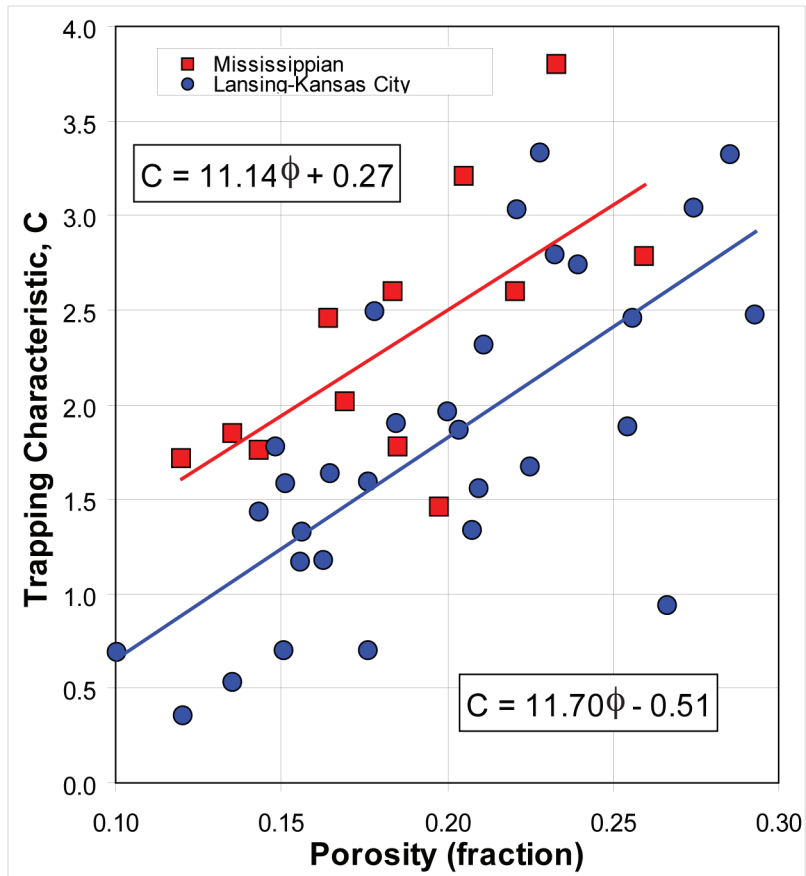


**Figure 2-6.** Crossplot of trapping characteristic,  $C$ , versus porosity for Mississippian and L-KC samples. Trapping characteristic was calculated using equation 2-1 in text substituting oil for gas. Linear regression for data of each formation provided predictive equations for  $C$ .

**Figure 2-7** illustrates the relationship derived from equations 2-13 and 2-14 between  $S_{orw}$  and  $S_{oi}$  for Mississippian and L-KC rocks exhibiting a range of porosity (and associated permeability). Maximum values of  $S_{oi}$  shown for each porosity curve were defined by  $S_w$  at  $h = 60$  ft and represent approximate  $S_{wirr}$  and  $S_{wc}$ . For each curve as  $S_{oi} \rightarrow 0$ :  $S_{orw} \rightarrow 0$  and for the suite of curves as  $\phi \rightarrow 0$ :  $S_{wirr} \rightarrow 1$  and  $S_{oi} \rightarrow 0$ . Though the slopes of the  $C$ - $\phi$  relationships for the two formations are similar, the lower intercept for L-KC rocks results in significantly greater  $S_{orw}$  at any given  $S_{oi}$ . High values of  $S_{grw}$  were also reported for oomoldic limestone by Keelan and Pugh (1975). The progressive shift of the curves to higher  $S_{orw}$  for any given  $S_{oi}$  with decreasing  $\phi$  result from the decrease in  $C$  with decreasing  $\phi$ .

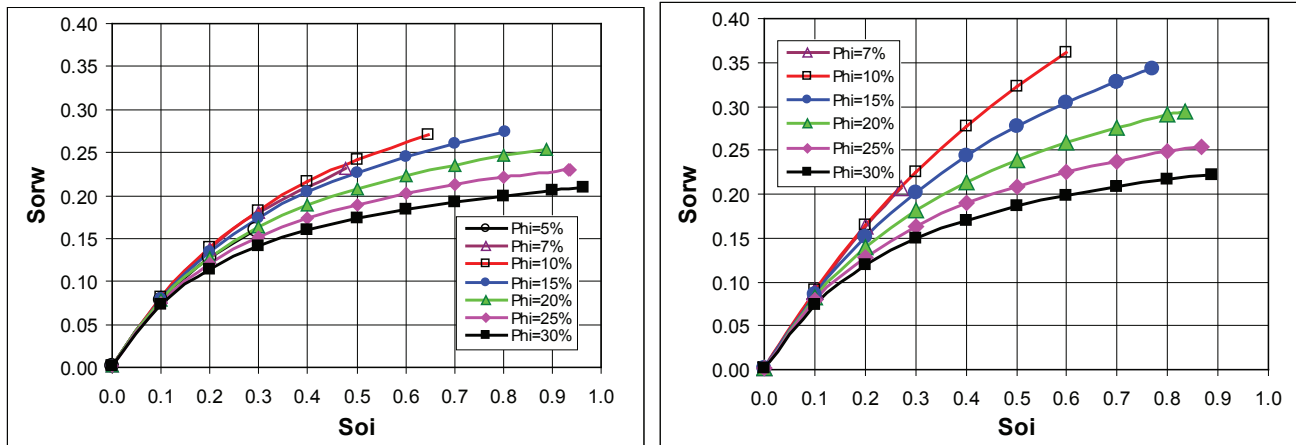


**Figure 2-7.** Crossplot of  $S_{orw}$  versus  $S_{oi}$  for Mississippian (top) and Lansing-Kansas City (bottom) derived from equations 2-13 and 2-14 in text. Maximum values of  $S_{oi}$  shown for each porosity curve were defined by  $S_w$  at  $h = 60$  ft and represent approximate  $S_{wirr}$  and  $S_{wc}$ . For each curve as  $S_{oi} \rightarrow 0$ :  $S_{orw} \rightarrow 0$  and for the suite of curves as  $\phi \rightarrow 0$ :  $S_{wirr} \rightarrow 1$  and  $S_{oi} \rightarrow 0$ . The progressive shift of the curves to higher  $S_{orw}$  for any given  $S_{oi}$  with decreasing  $\phi$  result from the decrease in  $C$  with decreasing  $\phi$  shown in Figure 6.

Uncertainty in the trapping characteristic predicted by equations 2-13 and 2-14 is approximately  $\pm 0.6$  for 1 standard deviation. **Figure 2-8** compares L-KC oomoldic limestone measured and predicted  $S_{orw}$ . The curves shown represent the predicted  $S_{orw}$  using  $C$  values calculated using equation 2-14 and  $S_{wirr}$  and  $S_{oi}$  values consistent with an oil column height of 60 ft and  $S_w$  values calculated from equation 2-12 using permeabilities predicted using equation 2-7. Figure 2-8 shows that as porosity decreases and  $S_{wirr}$  increases and  $S_{oi}$  decreases, it is predicted that  $S_{orw}$  increases with decreasing  $\phi$  until at low porosity values it decreases sharply and approaches zero where  $S_{wirr} = 1$ . The nature of the maximum in the  $S_{orw}$ - $\phi$  relations is a function of the  $C$ - $\phi$  trend and the porosity at which  $S_{wirr} = 1$ . In Figure 2-8  $S_{wirr}$  is defined as the saturation achieved at an oil column height of 60 ft and this value is generally consistent with measured  $S_{wc}$  values. However, lower values of  $S_w$  could be obtained at greater oil capillary pressures. This would result in the curve maximum shifting to lower porosity and higher  $S_{orw}$  values. Differences between measured and predicted values can be attributed to variance in  $C$ , and lower  $S_{oi}$  in some measured samples compared to assumed values for the curves. These predicted  $S_{orw}$  curves are consistent with reported trends of increasing  $S_{orw}$  with decreasing porosity and permeability (consistent with reported trends of increasing  $S_{orw}$  with decreasing porosity and permeability (Keelan and Pugh, 1975)).

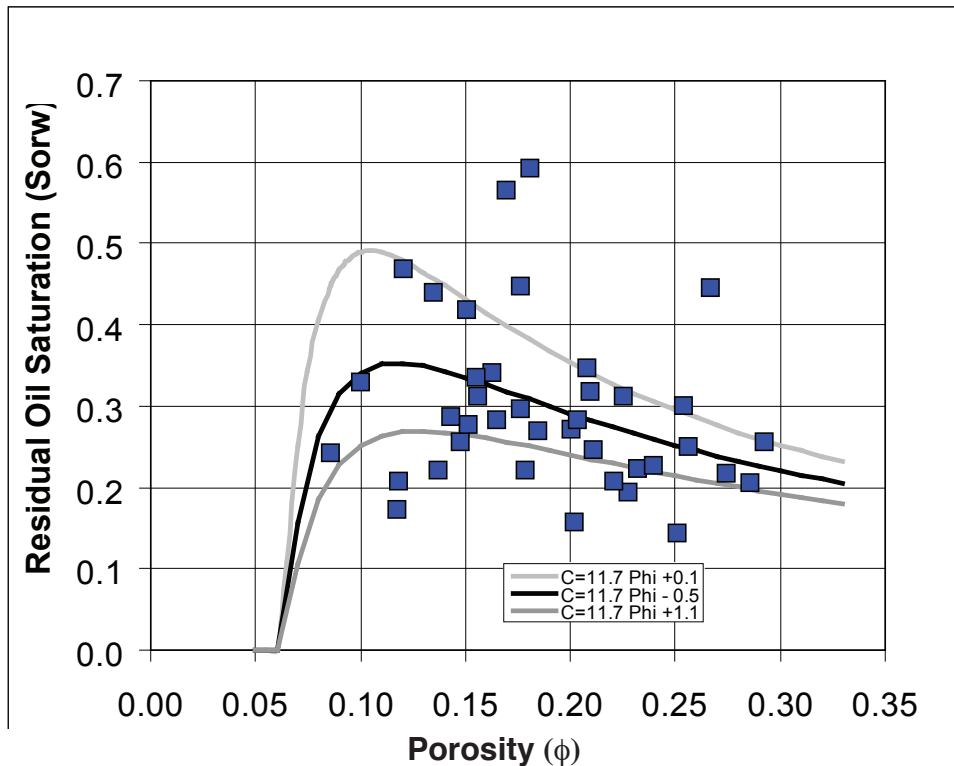


**Figure 2-8.** Lansing-Kansas City oomoldic limestone measured (blue squares) and predicted (curves)  $S_{orw}$  for  $S_{oi} = 1 - S_w$  ( $h = 60$  ft) versus porosity. At each porosity, the trapping characteristic,  $C$ , is defined by equation 2-14 in text and  $S_{oi}$  at  $h = 60$  ft is predicted using equations 2-8–2-12 in text. Standard error in  $C$  is approximately  $\pm 0.6$ . The upper and lower curves show  $S_{orw}$  using  $C$  values predicted using equation 2-14 with addition and subtraction of 0.6. With decreasing porosity  $S_{orw}$  rises to a maximum due to decreasing trapping characteristic,  $C$ , but with further decrease in porosity  $S_{orw}$  decreases to zero as  $S_{wirr} \rightarrow 1$  and  $S_{oi} \rightarrow 0$ . For  $h > 60$  ft  $S_{oi}$  increases and the curves are shifted to higher  $S_{orw}$  values and the maximum shifts to lower porosity.

Fanchi et al. (2002) presented an analytical method for estimating oil reserves in the transition zone. **Figure 2-9** illustrates, for Mississippian reservoirs of various permeability, the potentially recoverable saturation ( $S_{oi} - S_{orw}(S_{oi})$ ) for the condition where  $S_{orw}(S_{oi})$  varies vertically through the reservoir as a function of  $S_{oi}$  and the recoverable saturation  $S_{oi} - S_{orwmax}$  where  $S_{orw} = S_{orwmax} = S_{orw}$  at 40 ft. Variable  $S_{orw}(S_{oi})$  allows greater oil recovery in portions of the transition zone and approaches the fixed  $S_{orwmax}$  values at the maximum reservoir height. The difference between these two measures of recoverable oil represents the actual oil recovery versus that which is incorrectly estimated using a constant  $S_{orwmax}$  (**Fig. 2-10**). Maximum incremental recoverable oil occurs at a height slightly above the threshold entry height and at greater heights decreases as  $S_{orw}(S_{oih}) \rightarrow S_{orw}(S_{oimax})$ . At  $h_{max}$ ,  $S_{orw}(S_{oih}) = S_{orw}(S_{oimax})$ . Between the threshold entry height and the maximum incremental recoverable  $S_o$  the oil saturation increases but has not reached sufficient  $S_{oi}$  for large amounts of recoverable oil saturation. **Figure 2-11** illustrates the vertical distribution of additional oil recovery for a general Mississippian reservoir example where the region drained is 40 acres and the porosity is 16%. The incremental

barrels recovered varies through the height of the reservoir. For reservoirs of different height and permeability the fraction of incremental oil that would actually be recovered versus what would be estimated using Sorwmax can represent a significant fraction of estimated total recovery (**Table 2-1**).

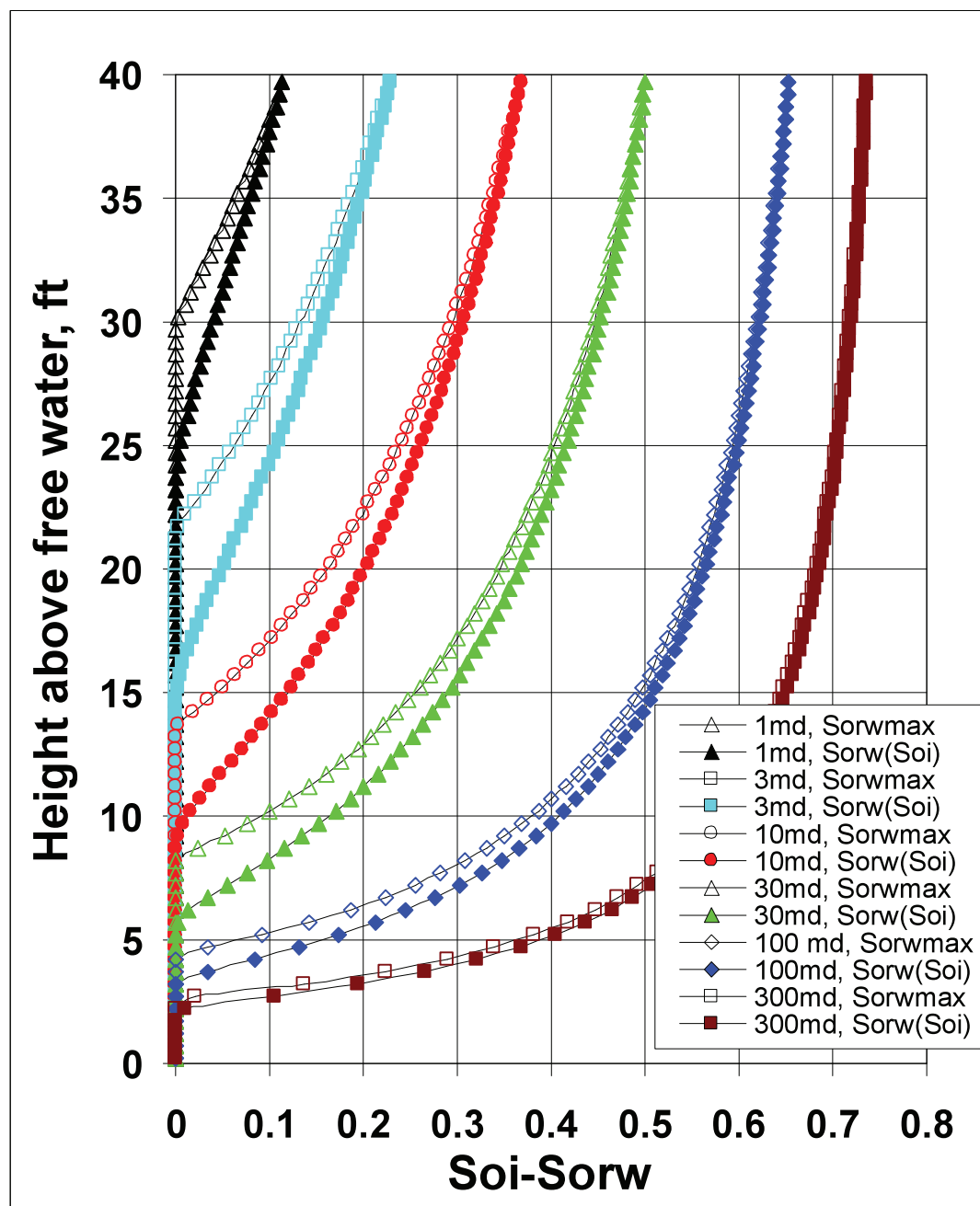


**Figure 2-9.** For Mississippian reservoir, comparison of potentially recoverable saturation ( $S_{oi}-S_{orw}(S_{oi})$ ) (solid symbols) for the condition where  $S_{orw}(S_{oi})$  varies vertically through the reservoir as a function of  $S_{oi}$  with the recoverable saturation  $S_{oi}-S_{orwmax}$  where  $S_{orw}=S_{orwmax}=S_{orw}$  at 40 ft (open symbols). Variable  $S_{orw}(S_{oi})$  allows greater oil recovery in portions of the transition zone and approaches the fixed  $S_{orwmax}$  values at the maximum reservoir height.

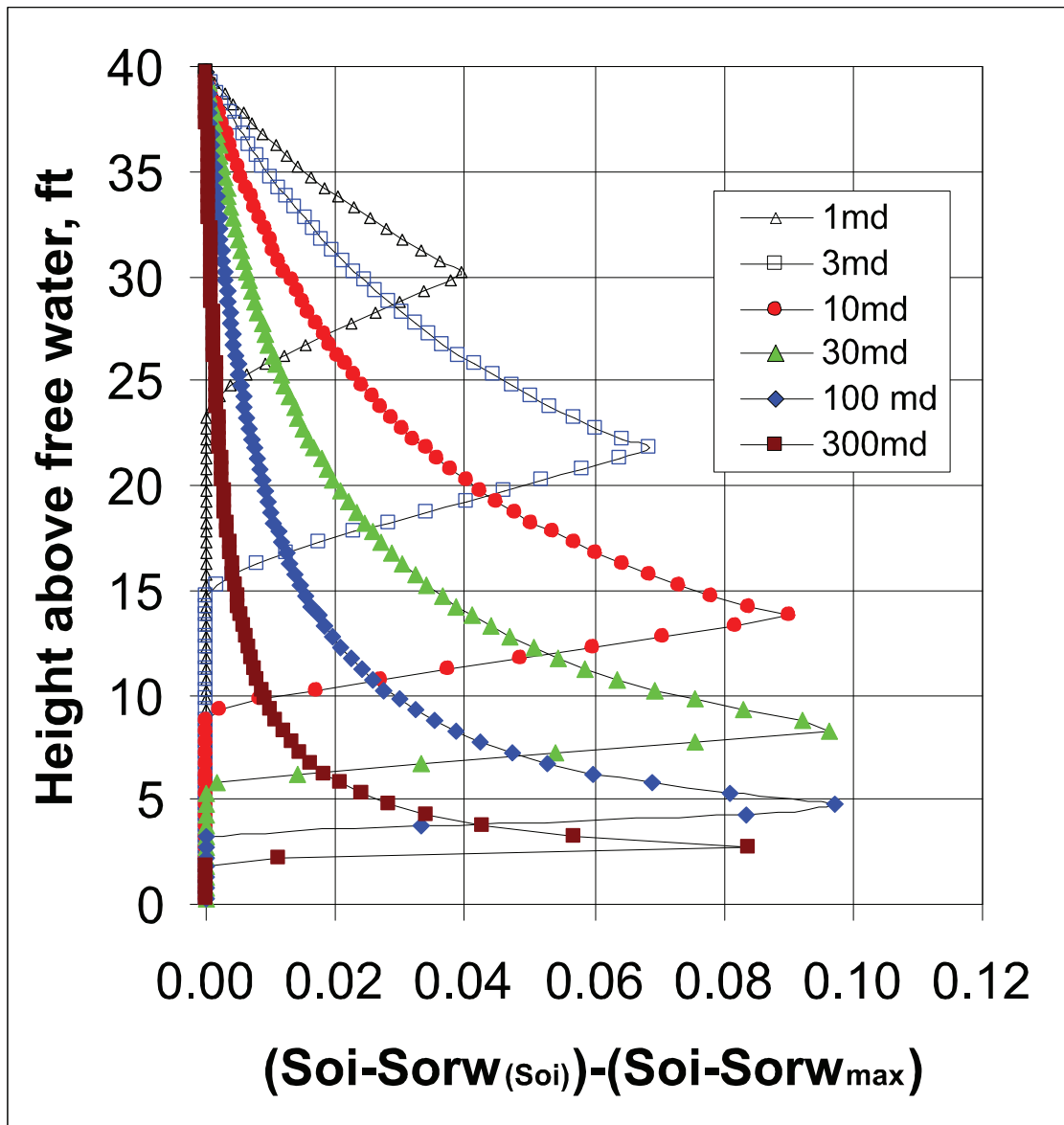


**Figure 2-10.** Utilizing data shown in Figure 2-9, difference in recoverable saturation for model with  $(S_{oi} - S_{orw}(S_{oi}))$ , for the condition where  $S_{orw}(S_{oi})$  varies vertically through the reservoir as a function of  $S_{oi}$ , and the recoverable saturation for a model with  $S_{oi} - S_{orw_{max}}$  where  $S_{orw} = S_{orw_{max}} = S_{orw}$  at 40 ft. Variable  $S_{orw}(S_{oi})$  allows greater oil recovery in portions of the transition zone and approaches the fixed  $S_{orw_{max}}$  values at the maximum reservoir height. Fluid densities assumed for capillary pressure relations were  $\rho_w = 1.05$  g/cc and  $\rho_o = 0.82$  g/cc.

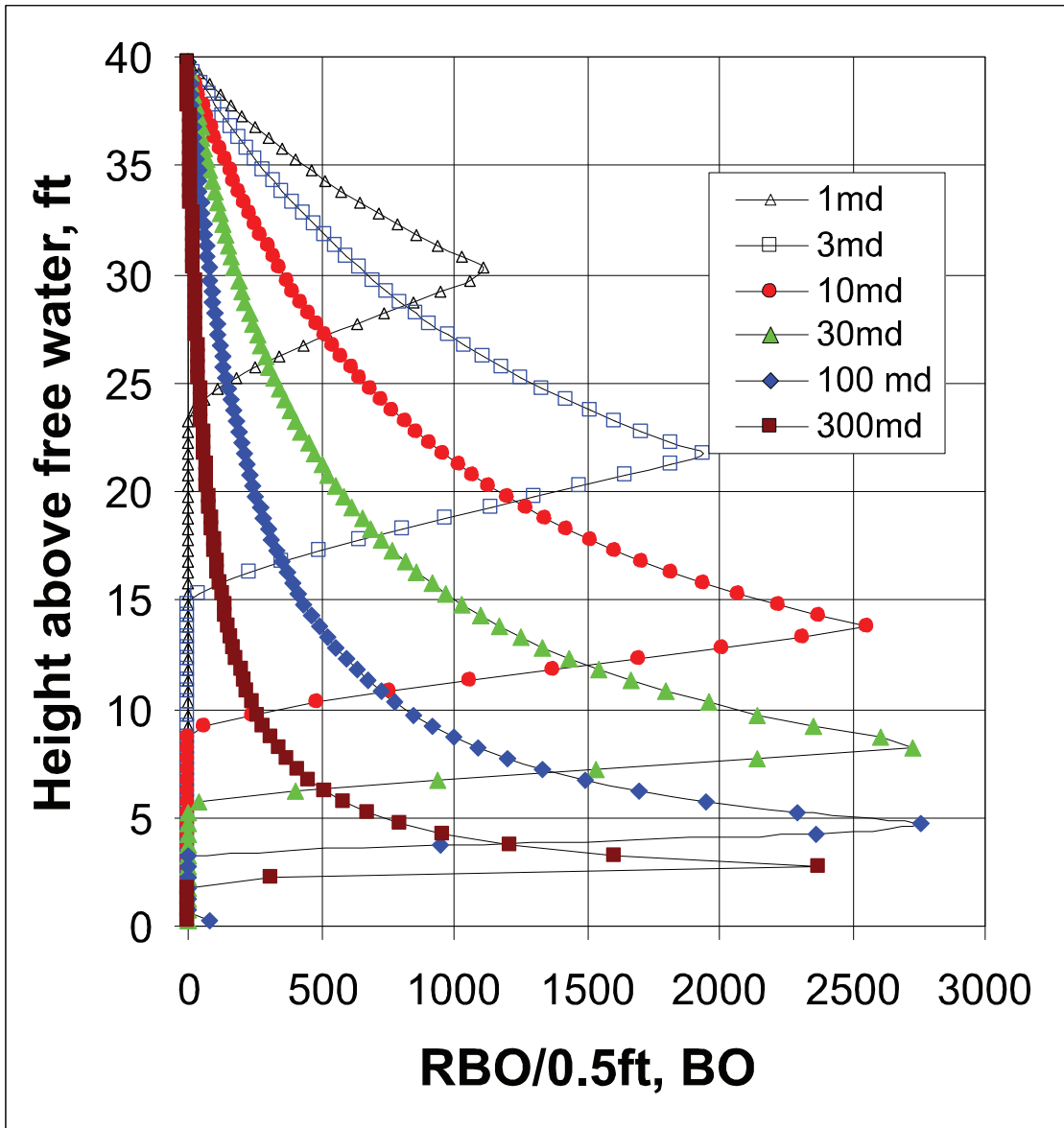


**Figure 2-11.** Difference between recoverable oil for  $S_{orw}(S_{oi})$  model and  $S_{orwmax}$  model shown in Figure 2-10 where saturation difference in Figure 2-10 is applied to a Mississippian reservoir with 16% porosity and 40-acre drainage area. Reservoir barrels of oil (RBO) in each 0.5 ft or reservoir are crossplotted with their height above free water level.

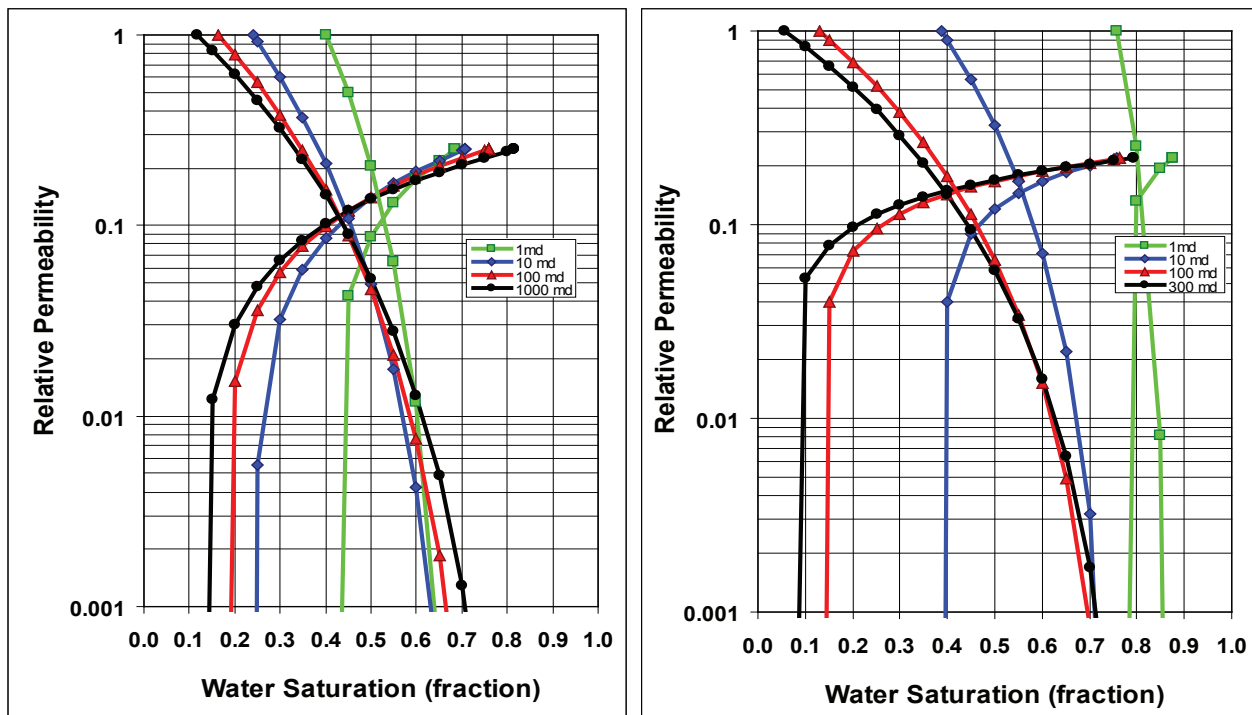


**Figure 2-12.** Imbibition oil and water relative permeability curves for Mississippi (top) and Lansing-Kansas City (bottom) calculated using equations 2-15 to 2-17,  $S_{wc}$  was calculated using equations 2-8 to 2-12, and  $S_{orwmax}$  was calculated using equations 2-1, 2-13, and 2-14 for oil.  $K_r$  curves shift to higher  $S_w$  with decreasing  $k$  in response to increasing  $S_{wirr}$  with decreasing  $k$ . For the L-KC, the imbibition curves terminate at progressively greater  $S_{orw}$  as  $k$  decreases and the trapping characteristic decreases. For the Mississippi rocks, the saturation at the  $k_r$  termination is more complex reflecting the countering influences of decreasing trapping characteristic and decreasing  $S_{oi}$  with decreasing  $k$ .

**Table 2-1.** Potential total oil recovery ( $S_{oi}-S_{orw}(S_{oi})$ ) from Mississippi reservoirs of various heights and permeabilities with 16% porosity, 40-acre drainage utilizing model with  $S_{orw}(S_{oi})$  through reservoir thickness. Incremental recovery is the additional recovery obtained using a model that employs  $S_{orw}(S_{oi})$  compared with a model that uses a single  $S_{orwmax}$  values for the entire reservoir.

Reservoir Height > Permeability (md)	40 ft			30 ft			20 ft		
	Cumulative Oil Recovery for Sorw(Soi) (BO)	Fraction Incremental Recovery to Cumulative (fraction)	Incremental Oil Recovery for Sorw(Soi)-Sorwmax (BO)	Cumulative Oil Recovery for Sorw(Soi) (BO)	Fraction Incremental Recovery to Cumulative (fraction)	Incremental Oil Recovery for Sorw(Soi)-Sorwmax (BO)	Cumulative Oil Recovery for Sorw(Soi) (BO)	Fraction Incremental Recovery to Cumulative (fraction)	Incremental Oil Recovery for Sorw(Soi)-Sorwmax (BO)
300	1,370,685	0.012	16,700	954,221	0.017	16,393	551,682	0.028	15,311
100	1,076,988	0.030	32,827	714,552	0.045	32,113	376,597	0.077	29,051
30	782,747	0.066	51,279	482,307	0.103	49,495	218,376	0.192	41,870
10	557,319	0.094	52,628	309,782	0.160	49,644	109,723	0.337	36,972
3	326,754	0.087	28,371	142,979	0.176	25,188	22,146	0.539	11,935
1	124,082	0.041	5,088	24,195	0.145	3,499	0	0.000	0

## 2.5 Relative Permeability

Frequently only a few relative permeability ( $k_r$ ) curves are utilized to simulate a field; however,  $k_r$  curves can change with pore architecture changes associated with lithologic variables, absolute permeability, starting saturations, and saturation hysteresis. For the rocks presented in this study a suite of relative permeability curves exist as a function of the absolute permeability and the associated increase in  $S_{wirr}$  and  $S_{wc}$  with decreasing  $k$ . In addition, changes in  $S_{orw}(S_{oi})$ , as indicated by the results presented above, result in changes in relative permeability curve end points for oil. For a reservoir of uniform properties and with  $S_{orw}(S_{oi})$  decreasing with depth in the transition zone, and  $S_{orw}$  being one of the end-points for  $k_r$  curves, proper modeling of  $k_r$  in the transition zone requires a suite of  $k_r$  curves for each  $S_{oi}$  and corresponding  $S_{orw}(S_{oi})$  through the transition zone as noted by Fanchi et al. (2002).

Generalized relative permeability curves can be used to illustrate comparative differences in relative permeability in response to changes in absolute permeability and  $S_{orw}(S_{oi})$  for the L-KC and Mississippian carbonates studied. Relative permeability curves for any given permeability were modeled using modified Corey (1954)-type equations where  $S_{wc}(=S_{wirr})$  was obtained from the  $P_c$ - $k$  relations presented in equations 8-12 and shown in Figure 2-5. The modified Corey relative permeability equations used were

$$k_{ro} = k_{romax} (1 - S_{wD})^n \quad (2-15)$$

$$k_{rw} = k_{rwmmax} S_{wD}^m \quad (2-16)$$

$$S_{wD} = (S_w - S_{wc}) / (1 - S_{wc} - S_{orw}) \quad (2-17)$$

where  $S_{wc}$  was defined as the saturation achieved at an oil column height of 40 ft using equation 2-12 and values for  $S_{orwmax}$  and  $S_{orw}(S_{oi})$  were determined based on porosity, the trapping characteristic, and the height in the transition zone. Average values for Mississippian relative permeability parameters used in the modeling exercise were:  $k_{romax} = 1$ ,  $k_{rwmmax} = 0.22$ ,  $n = 3.10$ ,  $m = 0.5$ . For L-KC rocks parameters used were:  $k_{romax} = 1$ ,  $k_{rwmmax} = 0.25$ ,  $n = 3.70$ ,  $m = 1.00$ . Height above free-water was determined from the capillary pressure relationships assuming a water density of 1.05 g/cc and an oil density of 0.82 g/cc.

For the basic model of  $S_{orw} = S_{orwmax}$ , Mississippian and L-KC carbonate imbibition relative permeability curves shift to higher water saturation with decreasing  $k$  in response to increasing  $S_{wirr}$  with decreasing  $k$  (**Fig. 2-12**). For the L-KC, the imbibition curves terminate at progressively greater  $S_{orw}$  as  $k$  decreases and the trapping characteristic decreases. For the Mississippian rocks, the saturation at the  $k_r$  termination is more complex.  $S_{orwmax}$  in a 40-ft reservoir begins to decrease for the range of  $k$  investigated due to significant increase in  $S_{wirr}$  and therefore decrease in  $S_{oi}$ . This reflects the countering influences of decreasing trapping characteristic and decreasing  $S_{oi}$  with decreasing  $k$ .

Other than decreasing  $k$ ,  $k_{ro}$  is also influenced by the endpoint  $S_{orw}$ .  $S_{oi}$  and  $S_{orw}(S_{oi})$  change vertically in the transition zone resulting in  $k_{ro}$  changes. **Figure 2-13** illustrates the  $k_{ro}$  curves for Mississippian

carbonates with different  $k$  values. In general, oil relative permeability increases with height in the transition zone due to decreasing  $S_w$ . However, at any given  $S_w$ ,  $k_{ro}$  decreases with increasing height relative to the  $k_{ro}$  of immediately underlying intervals due to increasing  $S_{orw}$  ( $S_{oi}$ ). Comparing  $k_{ro}$  curves for  $k_{ro}$  calculated using  $S_{orwmax}$  with  $k_{ro}$  calculated using  $S_{orw}$  ( $S_{oi}$ ) through the entire oil column (**Fig. 2-14**) indicates that the differences are small for high-permeability rocks because most of the oil column is near  $S_{wirr}$ . Differences are also small for low-permeability rocks because  $S_{oi}$  is not great. For the Mississippian carbonates maximum differences occur for rocks with  $k$  ranging between 3-30 md, which is the range of reservoir rock permeability for many Kansas Mississippian reservoirs.

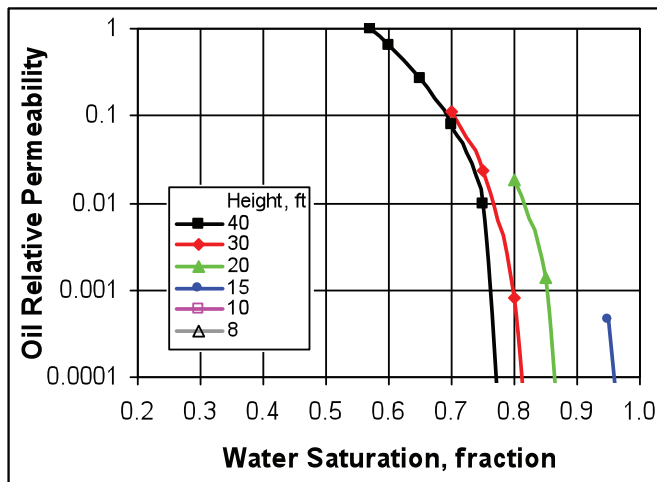
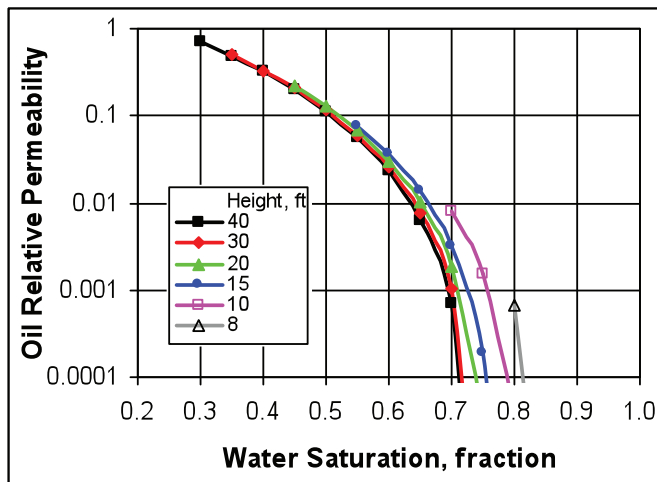
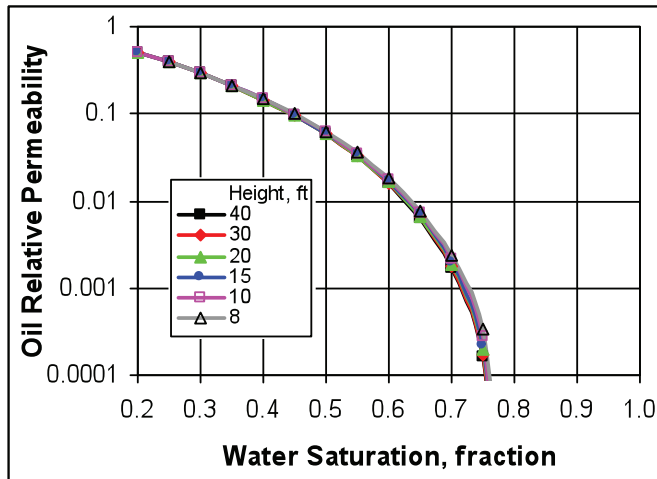


**Figure 2-13.**  $k_{ro}$  curves at different heights above free water level for Mississippian carbonates with  $k = 300$  md (top), 30 md (middle), and 3 md (bottom). Curves shift due to changing  $S_{orw}$  ( $S_{oi}$ ) through transition zone. Each curve starts at the water saturation appropriate for the height ( $S_{wh}$ ) as shown in Figure 5 and decreases to  $S_{orw}$  ( $S_{oi}$ ). At any given  $S_w$ ,  $k_{ro}$  decreases with increasing height relative to the  $k_{ro}$  of immediately underlying intervals due to increasing  $S_{orw}$  ( $S_{oi}$ ).

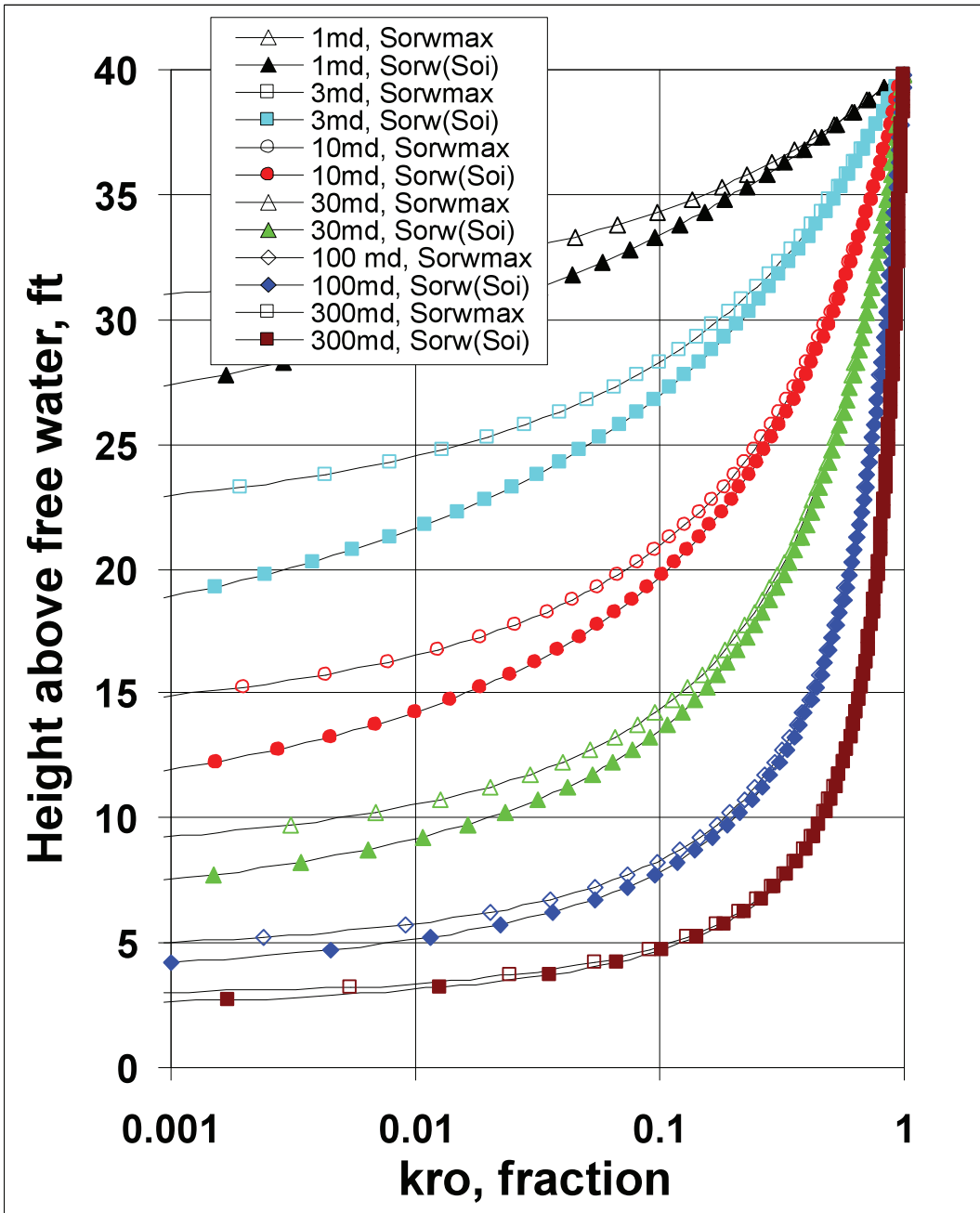


**Figure 2-14.** Comparing  $k_{ro}$  curves for  $k_{ro}$  calculated using  $S_{orwmax}$  and  $k_{ro}$  calculated using  $S_{orw}(S_{oi})$  through the entire oil column. Differences are small for high-permeability rocks because most of the oil column is near  $S_{wir}$ . Differences are also small for low-permeability rocks because  $S_{oi}$  is not great. For the Mississippian carbonates maximum differences occur for rocks with  $k$  ranging between 3-30 md.

Although it has been reported that changing  $S_{orw}$  does not significantly influence the water relative permeability curve (Land, 1968), it does exert influence relative to the new saturations in the reservoir. As  $S_{orw}(S_{oi})$  decreases with proximity to the free water level  $S_w$  increases. Even for the same  $k_{rw}$  curve this increase in  $S_w$ , compared to a  $S_{orwmax}$  model, leads to greater effective permeability to water since the interval is at a higher  $S_w$  and corresponding  $k_{rw}$ . This results in the slightly counter-intuitive conclusion that compared to models employing a simple  $S_{orwmax}$  a more accurate model that utilizes  $S_{orw}(S_{oi})$  results in both greater oil flow and greater water flow in the transition zone. This increase in the flow of both phases helps to understand and model high water production rates common to many thin shallow-shelf carbonate reservoirs. Frequently, since simpler models cannot model high water production rates with known properties, modeling of water production for these reservoirs simply invoke unexplained increases in  $k_{rw}$  or assume influence of water production from unidentified fractures. The influence of  $S_{orw}(S_{oi})$  may help resolve differences between actual and predicted production.

## 2.6 Conclusions

1. Thin carbonate reservoirs present complex petrophysical challenges to accurately simulate storage and flow.
2. Knowledge about lithofacies is important for effective prediction of permeability in many shallow-shelf carbonates. In the moldic and oomoldic carbonates of the Mississippian and Lansing-Kansas City formations in Kansas, permeability increases with increasing grain size and from mudstones to grainstones despite extensive diagenetic overprinting.
3. Capillary pressures for these carbonates can be modeled using modified Brooks-Corey equations where the threshold entry pressure and a measure of the pore size heterogeneity can be predicted using permeability.
4. In the transition zone of Mississippian and L-KC carbonates, accurate prediction of Pc is critical for correct prediction of water saturation and corresponding relative permeability.
5. In the carbonates studied here and in previous carbonate work the trapping characteristic,  $C$ , of residual oil saturation to waterflood increases with increasing permeability resulting in decreasing  $S_{orw}(S_{oi})$  with increasing permeability. However, the relationship between  $S_{orw}-\phi$  and  $S_{orw}-k$  exhibits a maximum due to the influence of both the  $C-\phi$  relationship and the decrease in  $S_{oi}$  with decreasing  $k$  resulting in decreasing  $S_{orw}(S_{oi})$ .
6. Oil relative permeability varies with  $k$  and  $S_{orw}(S_{oi})$ . Comparison of models utilizing  $S_{orw}(S_{oi})$  with models utilizing a single  $S_{orwmax}$  indicates that models using  $S_{orw}(S_{oi})$  predict more oil and more water production.
7. Given the interplay among permeability, capillary pressure character, fluid densities,  $S_{oi}$ ,  $S_{orw}(S_{oi})$  and  $k_{ro}$ , modeling of thin carbonate reservoirs in transition zones is complex and may need to account for all properties to provide accurate prediction.

## 3.0 Theoretical Geomodels

### 3.1 Overview

Fundamental to reservoir modeling is the assignment of petrophysical properties to geomodel cells. Imbibition oil-water relative permeability ( $k_r$ ) measurements performed on Pennsylvanian-age oomoldic limestones and Mississippian-age moldic-porosity mudstone to grainstone lime-dolomites show residual oil saturation after waterflood,  $S_{orw}$ , increases with increasing initial oil saturation,  $S_{oi}$ . This is due to increasing oil trapping in fine pores and is consistent with the Land-defined trapping characteristic. The trapping characteristic changes with lithofacies and porosity. As  $S_{oi}$  decreases with depth in the transition zone, proper modeling of  $k_r$  requires a family of  $k_r$  curves that reflect changes in  $k_r$  with changing  $S_{oi}$ . Utilizing a family of  $k_r$  curves in a vertically finely layered model shows that both oil and water recovery are greater than predicted from models utilizing  $k_r$  curves with a constant  $S_{oi}$  and  $S_{orw}$ . Oil recovery is higher because  $S_{orw}(S_{oi})$  is lower and water recovery is higher because  $S_w$  increases and  $S_{orw}(S_{oi})$  decreases with proximity to the oil-water contact. These systems further illustrate a larger issue with upscaling. Analysis indicates that systems comprising layers of different  $k_r$  cannot be rigorously upscaled using static  $k_r$  properties because  $k_r$  is a function of how the saturation was achieved. That is, relative permeability is not a state function, as it is widely applied in simulation, but is dependent on the saturation distribution which upscaled systems may not represent. Understanding  $S_{oi}$ ,  $S_{orw}$ , and  $k_r$  in transition-zone dominated reservoirs, and the limits on upscaling in systems with different  $k_r$  will improve planning and managing IOR and EOR operations.

### 3.2 Key Findings

1. Rather than being simpler to model, reservoirs in transition zones present complex petrophysical challenges to accurately simulate storage and flow.
2. In the transition zone (here shown for shallow-shelf Mississippian and L-KC carbonates), accurate prediction of capillary pressure is critical for correct prediction of water saturation and corresponding relative permeability.
3. For the carbonates studied here the trapping characteristic,  $C$ , of residual oil saturation to waterflood increases with increasing permeability resulting in decreasing  $S_{orw}(S_{oi})$  with increasing permeability. However, the relationship between  $S_{orw}-\phi$  and  $S_{orw}-k$  exhibits a maximum due to the influence of both the  $C-\phi$  relationship and the decrease in  $S_{oi}$  with decreasing  $k$  resulting in decreasing  $S_{orw}(S_{oi})$ .
4. To accurately model saturation in transition zones both for  $S_{oi}$  and  $k_r$  often requires  $> 10$  layers.
5. Oil relative permeability varies with  $k$  and  $S_{orw}(S_{oi})$ .
6. Comparison of models utilizing  $S_{orw}(S_{oi})$  with models utilizing a single  $S_{orwmax}$  indicates that models using  $S_{orw}(S_{oi})$  predict more oil and more water production.

7. In multilayer reservoirs, rigorously correct upscaling of relative permeability may not give correct results if changes in water saturation are not isotropic, i.e., upscaling of properties has to incorporate upscaling of saturation change tensor. If water is entering the gridcell predominantly from one direction, use of too few gridcells will give incorrect results even if all petrophysical properties have been “properly” upscaled.
8. Given the interplay among permeability, capillary pressure character, fluid densities,  $S_{oi}$ ,  $S_{orw}$  ( $S_{oi}$ ) and  $k_{ro}$ , modeling of thin carbonate reservoirs in transition zones is complex and may need to account for all properties to provide accurate prediction.

### 3.3 Geologic Setting

Properties of Kansas Mississippian and L-KC reservoirs are discussed in Byrnes et al. (2003). Multi-scale carbonate-dominated sequences were deposited in subtidal to supratidal environments on the broad shallow Kansas shelf throughout the Paleozoic. A repeating association of original depositional facies and early diagenesis for these rocks produced lithofacies ranging from mudstones to grainstones with abundant moldic porosity. The nature of the molds varied through time reflecting change in primary carbonate grain constituents: Upper Cambrian-Lower Ordovician Arbuckle peloid and ooid molds, Mississippian carbonate/siliceous sponge spicule and echinoderm/brachiopod molds, and Pennsylvanian ooid and bioclast molds.

For Mississippian strata, post-depositional regional uplift, subaerial exposure and differential erosion of the ramp strata at the pre-Pennsylvanian unconformity resulted in paleotopographic highs (buried hills) of low relief (generally <30-60 ft). The majority of production occurs at or near the top of the Mississippian section just below the sub-Pennsylvanian unconformity (**Fig. 3-1**). L-KC oolitic/oomoldic reservoirs exhibit geometries and architectures similar to modern oolites. Reservoirs usually comprise multiple stacked, or en echelon shoals that formed in response to sea-level fluctuations. Oomoldic reservoirs, ranging in thickness from several feet to several tens of feet, formed across the entire Kansas Pennsylvanian ramp; however, thicker, porous and permeable oolite deposits are commonly associated with the flanks or crests of paleostructural highs. These highs may have influenced the intensity of early diagenesis and may have been responsible for development of good reservoir properties. Grain-size variation, location on oolite buildups and interbedded carbonate mud (aquitards) influenced the nature and extent of diagenetic overprinting.

For Mississippian rocks, early dissolution of grains and dolomitization created moldic, intercrystalline and vuggy porosity important for favorable reservoir conditions (Fig. 3-1). Very finely crystalline (<10-50  $\mu\text{m}$ ) dolomite is characteristic of early reflux or mixing zone dolomitization. Despite overprinting by sub-Pennsylvanian subaerial exposure and burial processes, lithofacies and early diagenesis are the major controls on the nature and distribution of reservoir properties.

For L-KC rocks subaerial exposure and meteoric water percolation led to cementation around the aragonite ooids and often dissolution of the ooids and variable development of matrix and vuggy porosity. Resulting oomoldic grainstones, the principal reservoir lithofacies, underwent variable degrees of early or later fracturing and crushing, providing connection between otherwise isolated oomolds. Reservoir oomoldic rocks range from wackestones with isolated oomolds to grainstones with close-packed oomolds. Matrix properties range from dense crystalline to microporous micritic to sucrosic fine-medium crystalline.

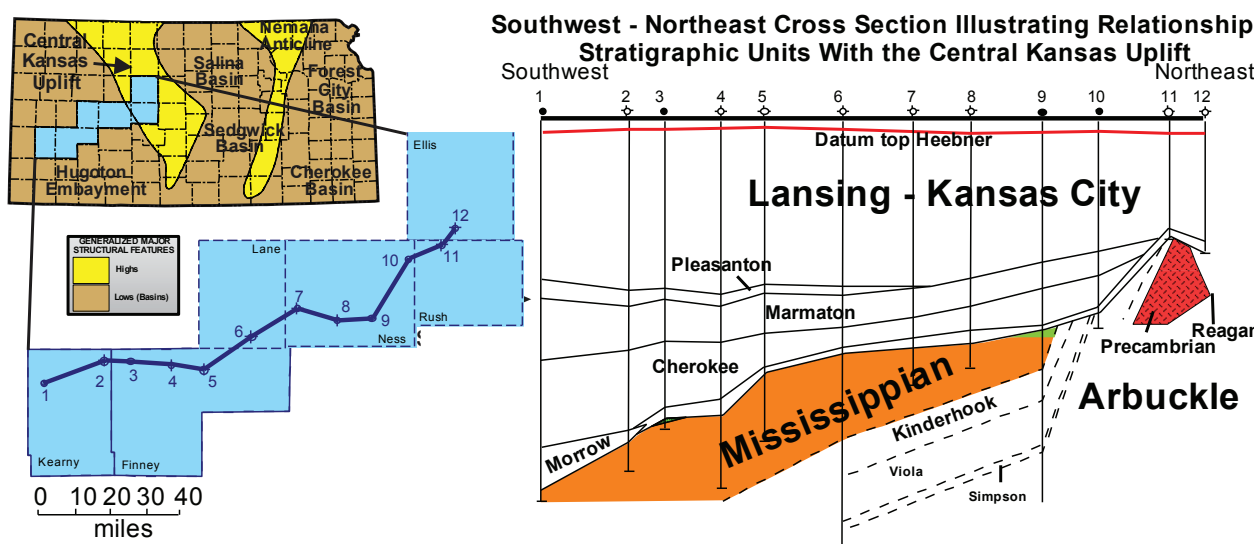


**Figure 3-1.** Cross section across western flank of Central Kansas Uplift showing subcrop and truncation of Mississippian on the CKU and the overlying Lansing-Kansas City Formation (after Byrnes et al, 2002).

### 3.4 Rock Properties for General Model

Many fundamental rock properties as they are applied in the reservoir system are discussed in the preceding section. This brief discussion reviews rock properties specifically assigned to the general flow models used to illustrate the role of variable relative permeability,  $S_{orw}$ , and number of layers on predicted oil recovery. The following discussion and example analysis focuses on Mississippian properties and a Mississippian reservoir model. The principals illustrated in this rock system apply also to the Arbuckle and Lansing-Kansas City reservoir systems though these can also have different drive energy systems including 1) no bottom-water drive but edge-water drive, 2) only solution-gas drive, and 3) fracturing with underlying aquifer supporting water production through the fracture system.

#### 3.4.1 Mississippian Lithofacies, Permeability, and Porosity

Lithofacies and early diagenesis are major controls on permeability ( $k$ ) and porosity ( $\phi$ ) despite complex diagenetic overprinting by sub-Pennsylvanian subaerial exposure and burial processes.  $k$  and  $\phi$  decrease significantly and continuously with decreasing grain/mold size from packstone to

mudstone and can range over 2 orders of magnitude for a given porosity. Lithofacies progression from mudstone through grainstone results in a greater change in permeability than increasing porosity. For a given facies, increasing mold content and porosity results in a k increase that is subparallel and at a lower slope to the general k- $\phi$  trend. Porosities range from 2% to 30% and permeabilities range from <0.001 md to 400 md. The k-trend for all Mississippian lithofacies is approximately bounded within two orders of magnitude by trendlines defined by

$$\log k = 0.25\phi - 2.5$$
$$\log k = 0.25\phi - 4.5.$$

Between these bounding trends (**Fig. 3-2**) each lithofacies exhibits a generally unique range of k and  $\phi$  which together define a continuous trend, with k decreasing with decreasing grain/mold size for any given porosity.

Each individual lithofacies exhibits a unique sub-parallel trend to the general trend where the relationship between k and  $\phi$  for each lithofacies can be represented by a power-law function of the form

$$k = A \phi^{-3.5}$$

where the coefficient, A, varies with lithofacies. Increasing moldic content, and associated increasing  $\phi$ , increase k at a lower rate than the overall k-trend indicating that matrix properties dominate control of flow in these rocks (**Fig. 3-3**).

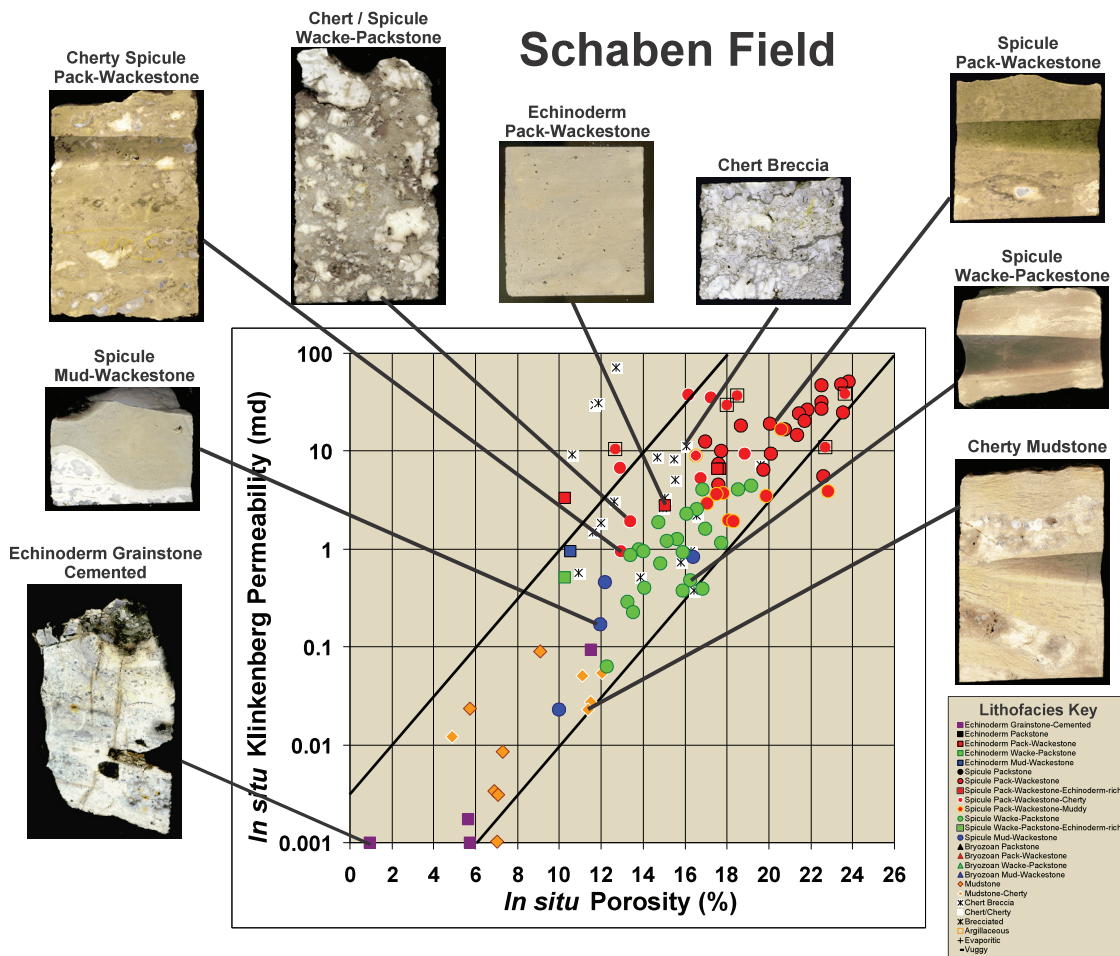


**Figure 3-2.** Example of Mississippian lithofacies-specific permeability-porosity trend showing general bounding trendlines.

The effect of variable relative permeability,  $S_{orw}$ , is discussed in Section 2. The question of how the number of layers influences estimated recovery is examined by comparing incremental recovery for a 40-layer and 10-layer model. Figure 2-10 in the section above illustrated the incremental recovery for a 40-layer model for Mississippian reservoirs of various permeability, the potentially recoverable saturation ( $S_{oi}-S_{orw}(S_{oi})$ ) for the condition where  $S_{orw}(S_{oi})$  varies vertically through the reservoir as a function of  $S_{oi}$  and the recoverable saturation  $S_{oi}-S_{orwmax}$  where  $S_{orw} = S_{orwmax} = S_{orw}$  at 40 ft. Variable  $S_{orw}(S_{oi})$  allows greater oil recovery in portions of the transition zone and approaches the fixed  $S_{orwmax}$  values at the maximum reservoir height. The difference between these two measures of recoverable oil represents the actual oil recovery versus that which is incorrectly estimated using a constant  $S_{orwmax}$ . Figure 3-4 illustrates the same reservoir properties but divided into a 10-layer model. Comparison of results for a 40-layer model and a 10-layer model show that the 10-layer model both under-predicts the amount of recoverable oil and shifts the vertical position of the interval of recovery to either a higher or lower position depending on the permeability.

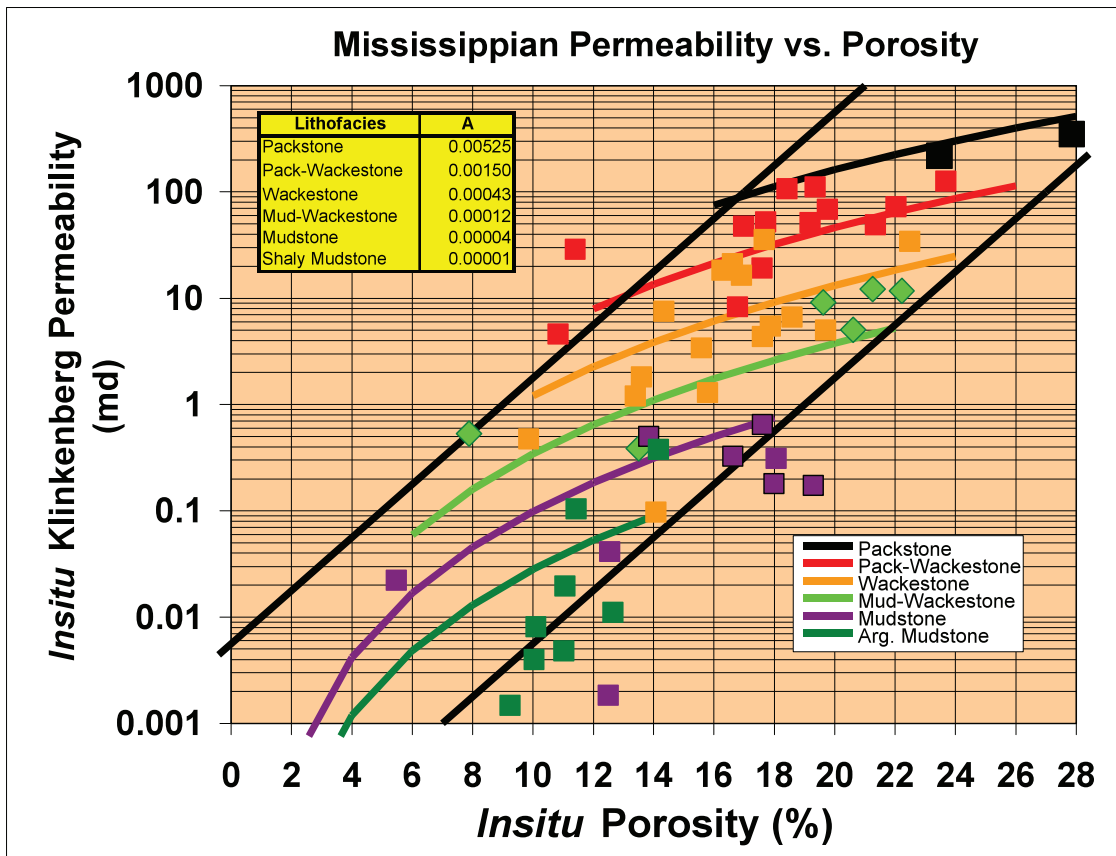


**Figure 3-3.** Lithofacies-specific generalized trends for Mississippian rocks of lithofacies ranging from mudstone through packstone. Individual lithofacies trends are defined by  $k = A \phi^{-3.5}$ .

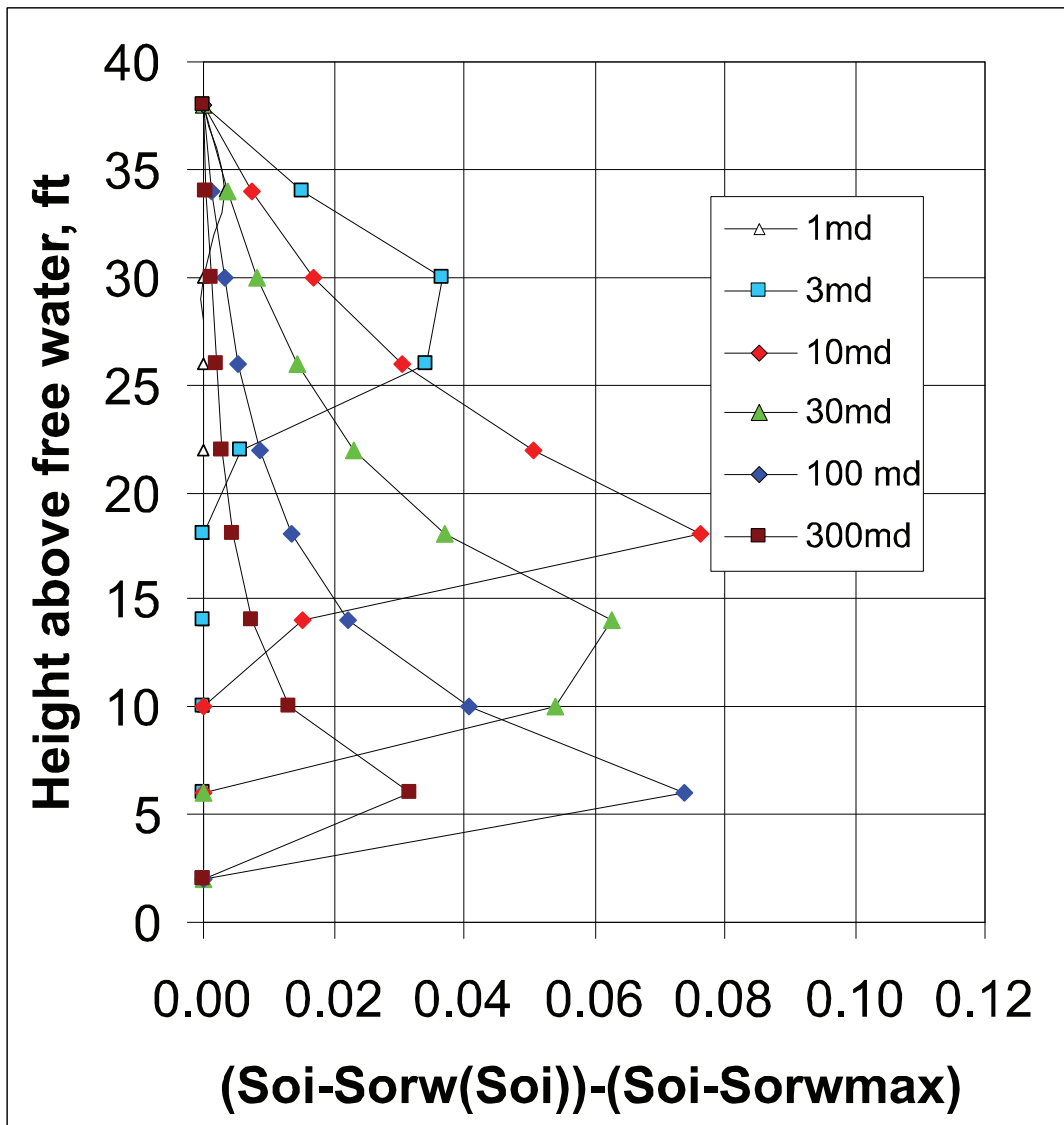


**Figure 3-4.** Utilizing data shown, difference in recoverable saturation for model with  $(S_{oi}-S_{orw}(S_{oi}))$ , for the condition where  $S_{orw}(S_{oi})$  varies vertically through the reservoir as a function of  $S_{oi}$ , and the recoverable saturation for a model with  $S_{oi}-S_{orwmax}$  where  $S_{orw} = S_{orwmax} = S_{orw}$  at 40 ft. Variable  $S_{orw}(S_{oi})$  allows greater oil recovery in portions of the transition zone and approaches the fixed  $S_{orwmax}$  values at the maximum reservoir height. Fluid densities assumed for capillary pressure relations were  $\rho_w = 1.05$  g/cc and  $\rho_o = 0.82$  g/cc. The recoveries shown are for one 10-layer model. Comparison of this figure with Fig. 2-10 illustrates the difference in predicted recovery for a 40-layer and 10-layer model.

## 3.5 Comparison Among Flow Simulation Models

### 3.5.1 Predicted Oil Recovery

Comparison among flow simulation models reveals that cumulative oil recovery increases with use of increasing number of layers in the model and with use of oil relative permeability curves that properly reflect  $S_{orw}(S_{oi})$  changes vertically in the transition zone resulting in kro changes. The lower  $S_{orw}$  in the lower portions of the transition zone result in greater oil recovery from this portion of the reservoir. Comparison of three different permeability models was performed. Models selected represented a “typical” permeability for a Kansas Mississippian reservoir rock (30 md) and reservoirs exhibiting four-times greater and four-times less permeability, approximately representing the upper- and lower-most reservoirs in the Mississippian system. **Figure 3-5** shows that for all permeabilities for a detailed 40-layer model (representing a layer for each foot), the cumulative oil recovery increases from 5% to 16% of the recovery predicted using a Sorwmax model for reservoirs with permeability decreasing from 120 md to 7.5 md. The changing differences between the  $S_{orw}(S_{oi})$  and Sorwmax models can be attributed to the increasing relative portion of the reservoir in the transition zone increases with decreasing permeability. This is illustrated by the increase in differences for the 40-layer models compared to the 40-20L models (**Fig. 3-6**). The 40-20L models represent the same 40-layer model but with removal of the upper 20 feet of reservoir interval. For many Mississippian reservoirs significant portions of the field are less than 20 feet above the free water and the 40-20L models represent these reservoir conditions. The greater difference between the  $S_{orw}(S_{oi})$  and Sorwmax models for these reservoirs is because a significant fraction of the total productive interval is in the lower transition zone. The 4-layer model is illustrated in **Figure 3-7**.

Upscaling also results in changes to predicted oil recovery. Comparison between the 40-layer and 4-layer models (**Fig. 3-8**) shows that the 40-layer model predicts higher oil recovery even for  $S_{orw}(S_{oi})$  models. Given that many basic Mississippian reservoir models utilize only 4-6 layers, **Figure 3-9** illustrates the difference between a full 40-layer  $S_{orw}(S_{oi})$  model and a more conventional 4-layer Sorwmax model. The difference between these models are 10.8%, 24.4%, and 38.6% for models with permeability of 120 md, 30 md, and 7.5 md, respectively. A difference of 24% for a typical reservoir could be interpreted to be significant. **Table 3-1** summarizes cumulative oil recoveries for the predicted production histories shown in **Figures 3-5** through **3-9**.

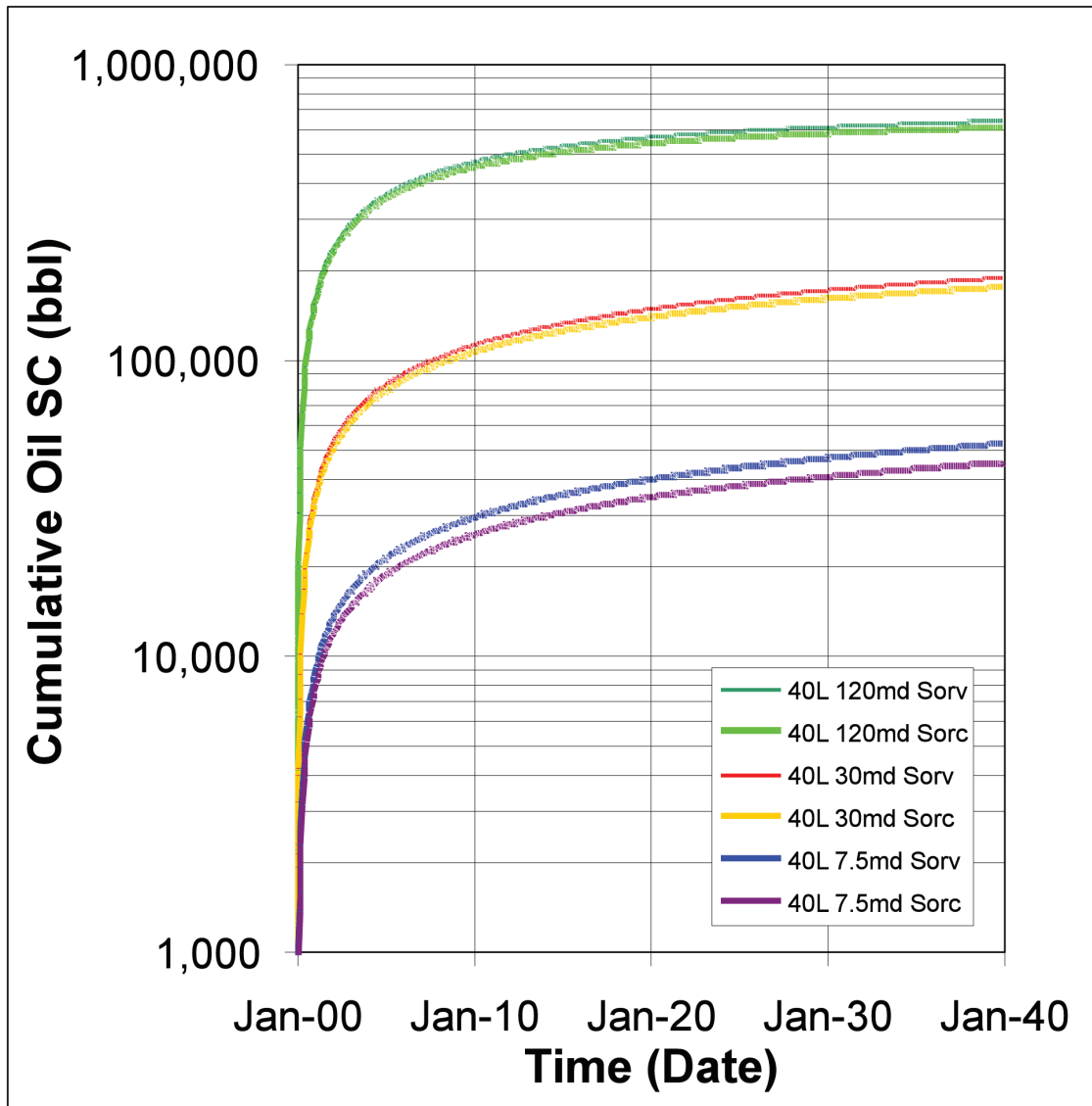


**Figure 3-5.** Estimated cumulative oil production with time for 40-ft thick, 40-layer model for both fixed  $S_{or}$  ( $S_{orc}$ ) and variable  $S_{or}$  ( $S_{orv}$ ).

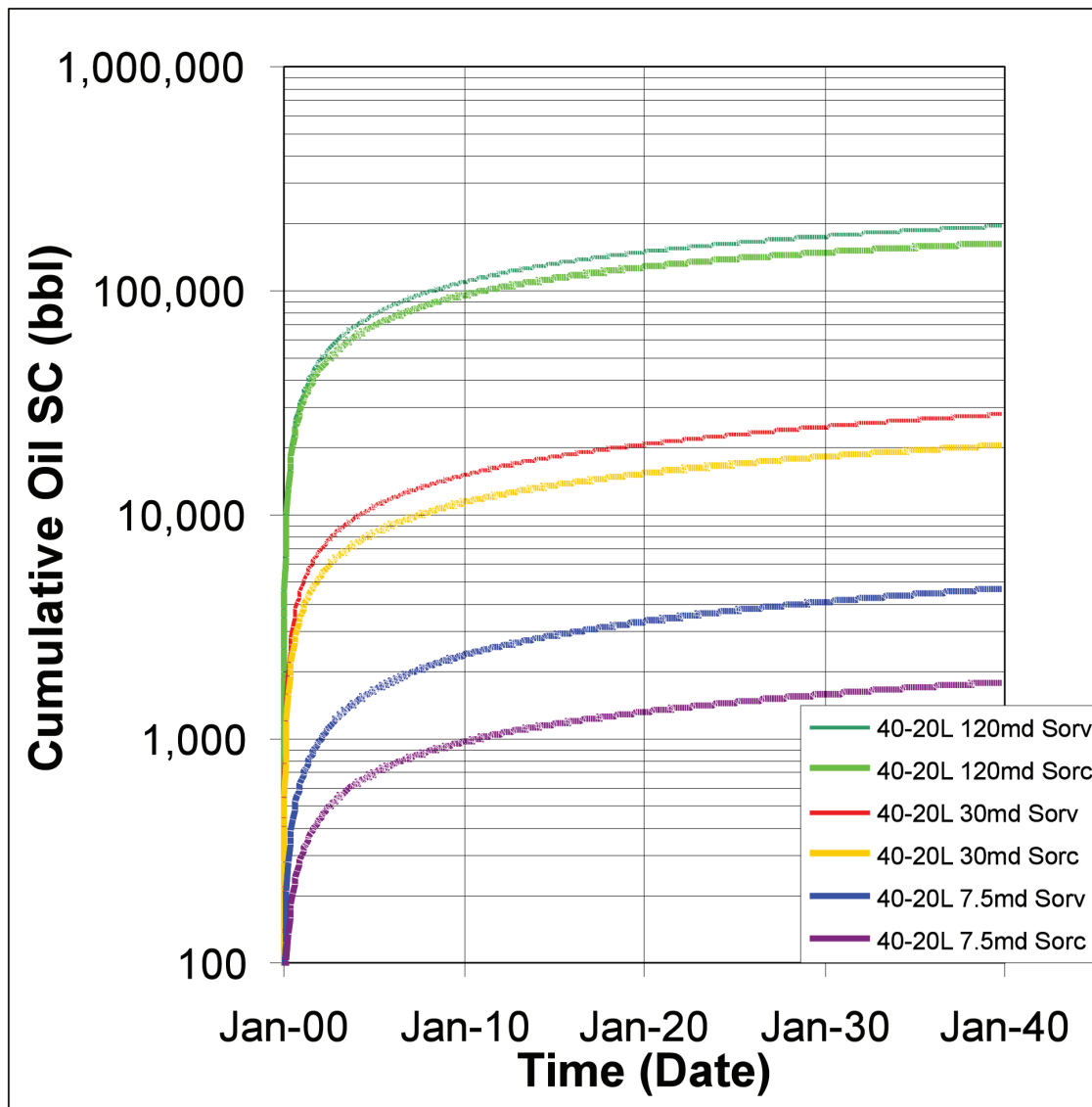


**Figure 3-6.** Estimated cumulative oil production with time for the bottom 20-ft of the model shown in Figure 3-5 for both fixed  $S_{or}$  ( $S_{orc}$ ) and variable  $S_{or}$  ( $S_{orv}$ ). This 40-20L models represents the same 40-layer model in Fig. 3-5 but with removal of the upper 20 ft of reservoir interval. For many Mississippian reservoirs significant portions of the field are less than 20 ft above the free water and the 40-20L models represent these reservoir conditions.

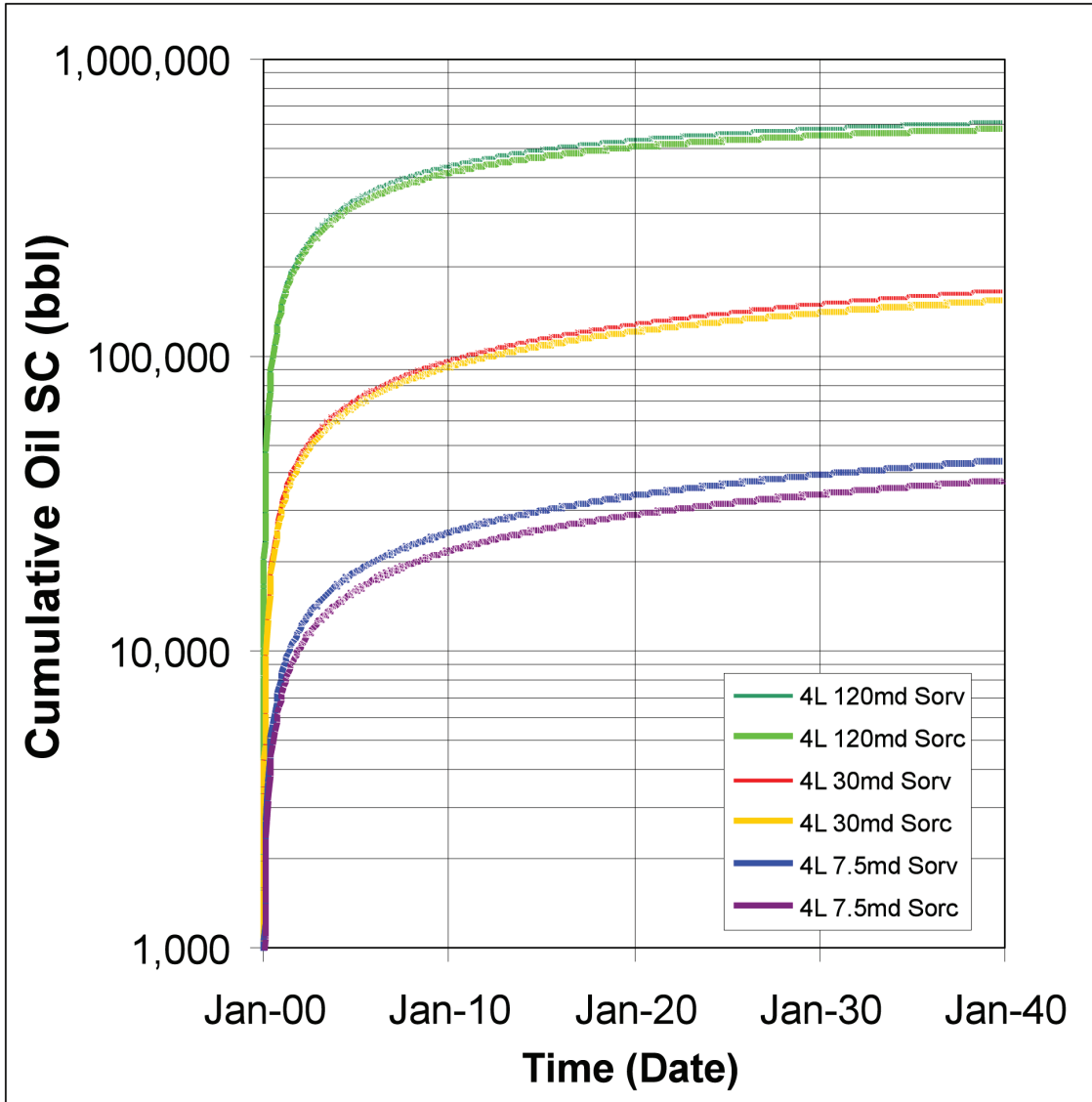


**Figure 3-7.** Estimated cumulative oil production with time for 40-ft thick, 4-layer model for both fixed  $S_{or}$  ( $S_{orc}$ ) and variable  $S_{or}$  ( $S_{orv}$ ).

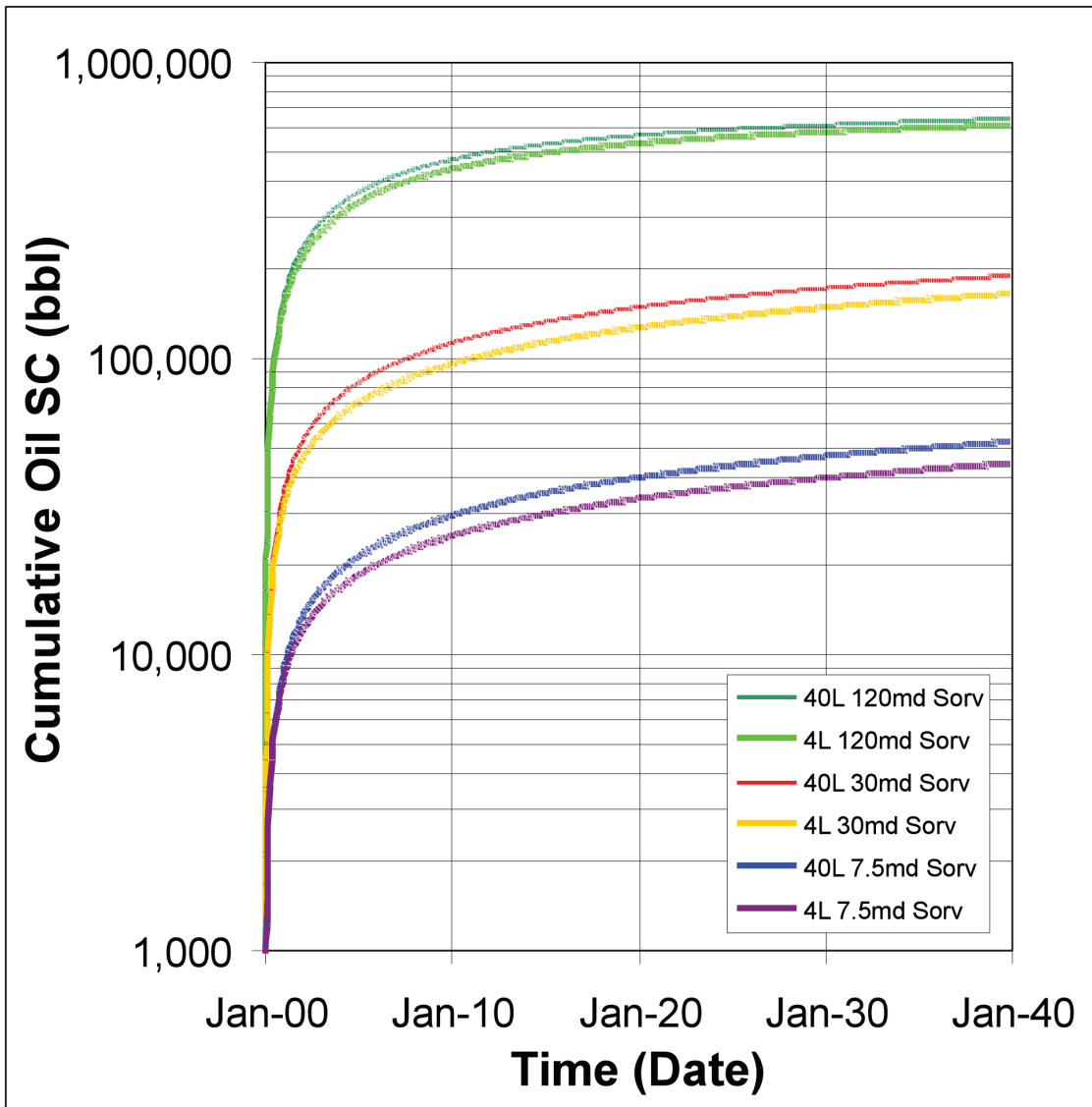


**Figure 3-8.** Estimated cumulative oil production with time for 40-ft thick, model comparing the 40-layer model results with a 4-layer model results for variable  $S_{or}$  ( $S_{orv}$ ).

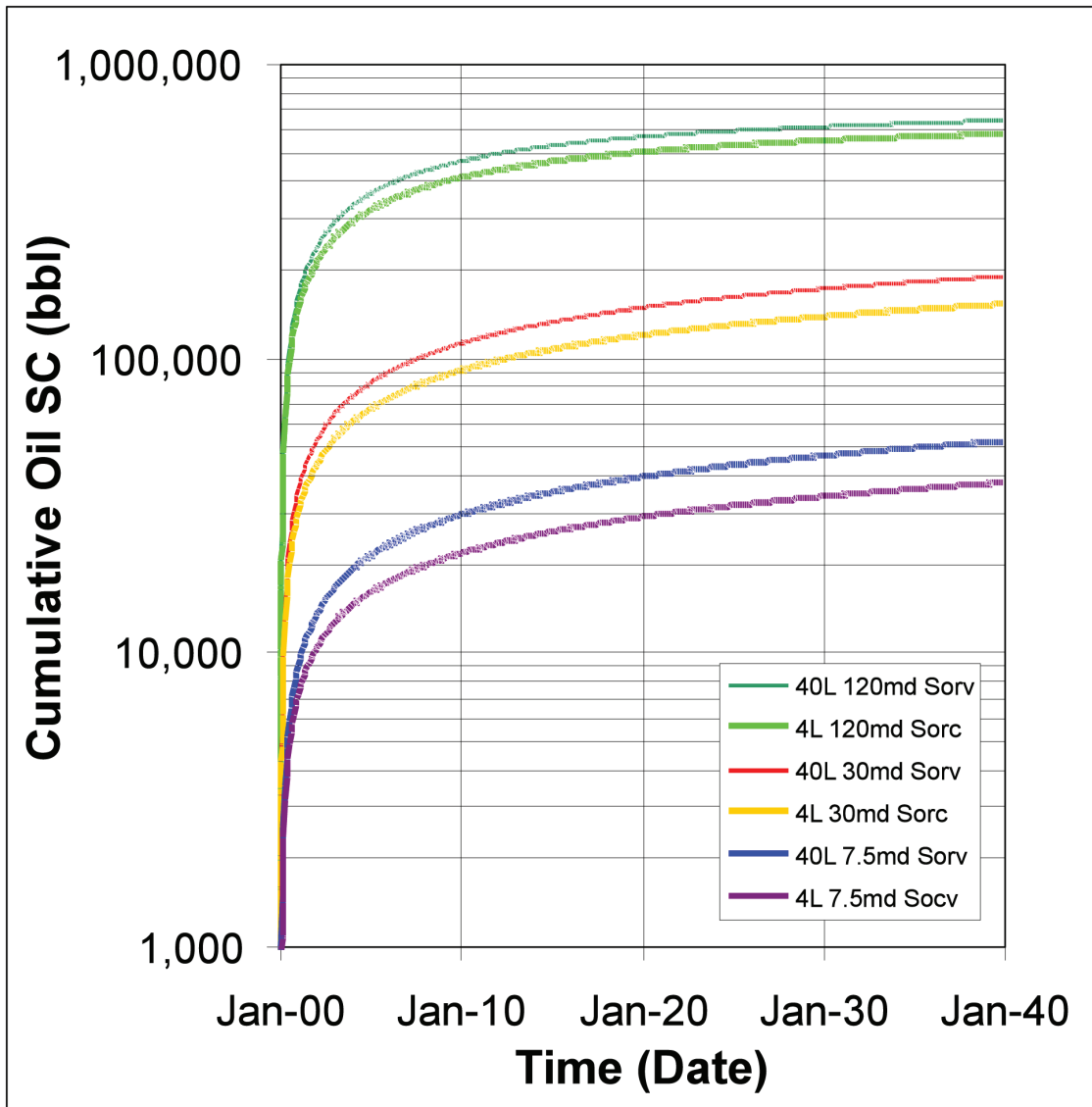


**Figure 3-9.** Estimated cumulative oil production with time for 40-ft thick, model comparing the 40-layer model results using variable  $S_{or}$  ( $S_{orv}$ ) compared with 4-layer model results using fixed  $S_{or}$  ( $S_{orc}$ ). This compares a more complex model with what might be representative of a more commonly used basic model.

**Table 3-1.** Summary of cumulative oil at 40 years for various models shown in Figures 3-5 through 3-9.

40L	7.5 md Cum MBO	30 md Cum MBO	120 md Cum MBO
Const	45	177	614
Var	52	191	646
% change	15.6	7.9	5.2

40-20L	7.5 md Cum MBO	30 md Cum MBO	120 md Cum MBO
Const	1.8	20.5	163.7
Var	4.7	28.1	194.4
% change	161.1	37.1	18.8

120 md	40 Layer Cum MBO	4 Layer Cum MBO	Diff, %
Const	61.4	58.3	5.3
Var	64.6	61.4	5.2
Diff (%) - 40L variable & 4 Layer constant			10.8

30 md	40 Layer Cum MBO	4 Layer Cum MBO	Diff, %
Const	177.5	153.4	15.7
Var	190.8	165.5	15.3
Diff (%) - 40L variable & 4 Layer constant			24.4

7.5 md	40 Layer Cum MBO	4 Layer Cum MBO	Diff, %
Const	45.2	37.8	19.6
Var	52.4	44.3	18.3
Diff (%) - 40L variable & 4 Layer constant			38.6

### 3.5.2 Predicted Water Recovery

Although it has been reported that changing  $S_{orw}$  does not significantly influence the water relative permeability curve, it does exert influence relative to the new saturations in the reservoir. As  $S_{orw}(S_{oi})$  decreases with proximity to the free water level,  $S_w$  increases. Even for the same  $krw$  curve this increase in  $S_w$ , compared to a  $S_{orwmax}$  model, leads to greater effective permeability to water since the interval is at a higher  $S_w$  and corresponding  $krw$ . **Figures 3-10** through **3-14** illustrate predicted cumulative water production for the 40-layer and 4-layer models presented above and for which cumulative oil is shown in **Figures 3-5** through **3-9**. **Table 3-2** summarizes cumulative water recovery at 40 years for the various models.

This results in the slightly counter-intuitive conclusion that compared to models employing a simple  $S_{orwmax}$  a more accurate model that utilizes  $S_{orw}(S_{oi})$  results in both greater oil flow and greater water flow in the transition zone. This increase in the flow of both phases helps to understand and model high water production rates common to many thin shallow-shelf carbonate reservoirs. Frequently, since simpler models cannot model high water production rates with known properties, modeling of water production for these reservoirs simply invoke unexplained increases in  $krw$  or assume influence of water production from unidentified fractures. The influence of  $S_{orw}(S_{oi})$  may help resolve differences between actual and predicted production.

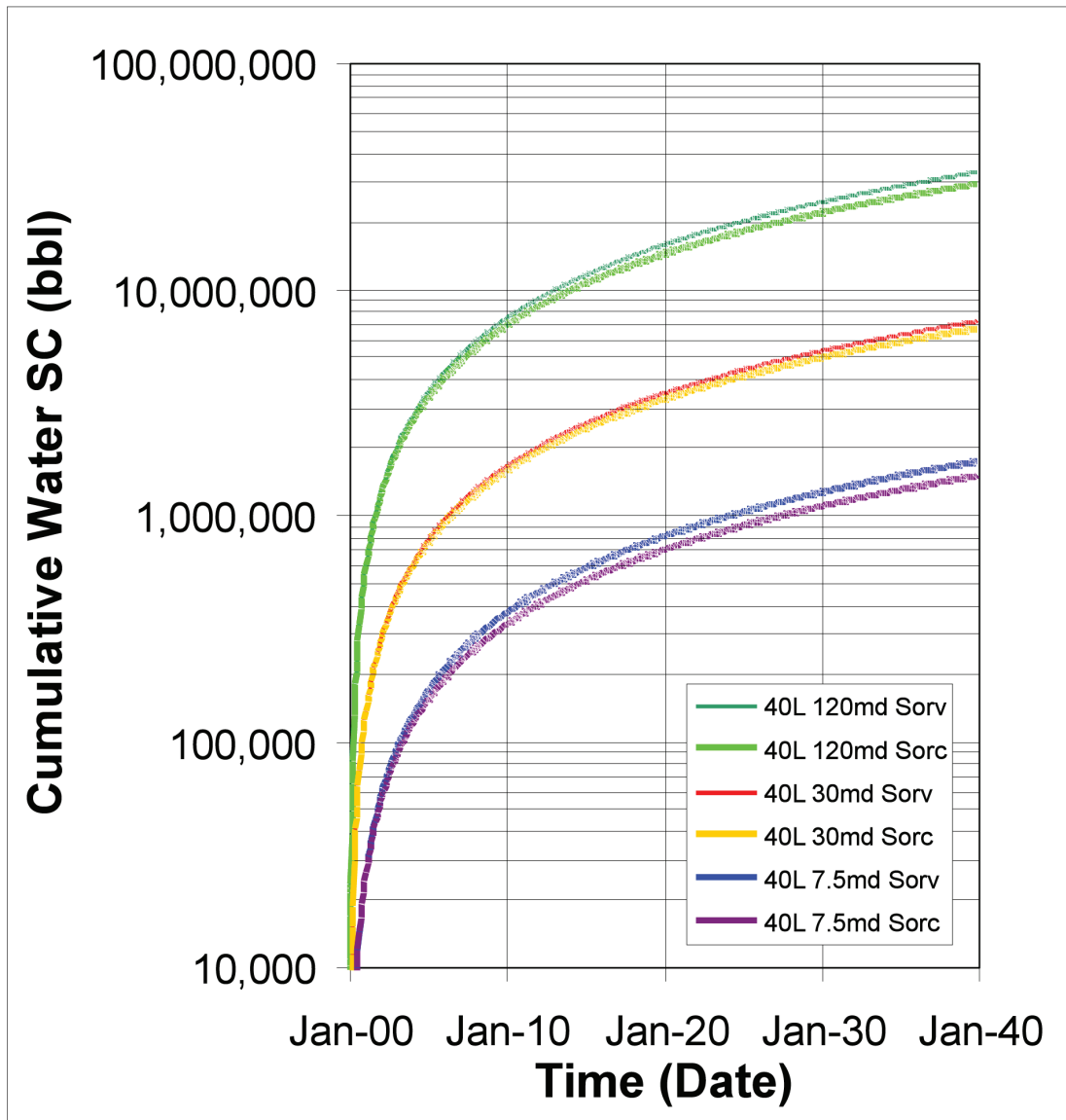


**Figure 3-10.** Estimated cumulative water production with time for 40-ft thick, 40-layer model for both fixed  $S_{or}$  ( $S_{orc}$ ) and variable  $S_{or}$  ( $S_{orv}$ ).

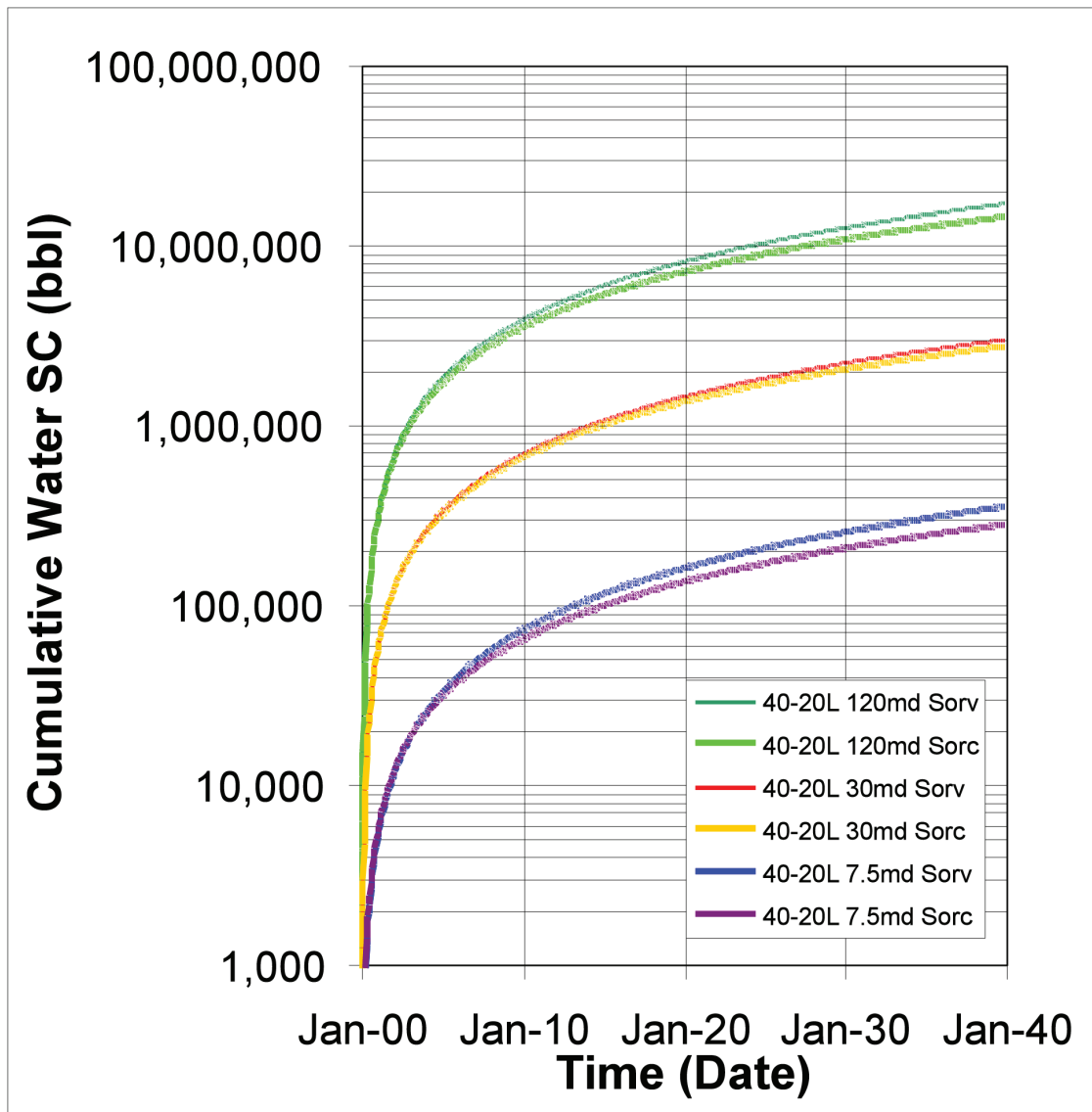


**Figure 3-11.** Estimated cumulative water production with time for the bottom 20-ft of the model shown in Figure 3-5 for both fixed  $S_{or}$  ( $S_{orc}$ ) and variable  $S_{or}$  ( $S_{orv}$ ). This 40-20L models represents the same 40-layer model in Fig. 3-5 but with removal of the upper 20 ft of reservoir interval. For many Mississippian reservoirs significant portions of the field are less than 20 ft above the free water and the 40-20L models represent these reservoir conditions.

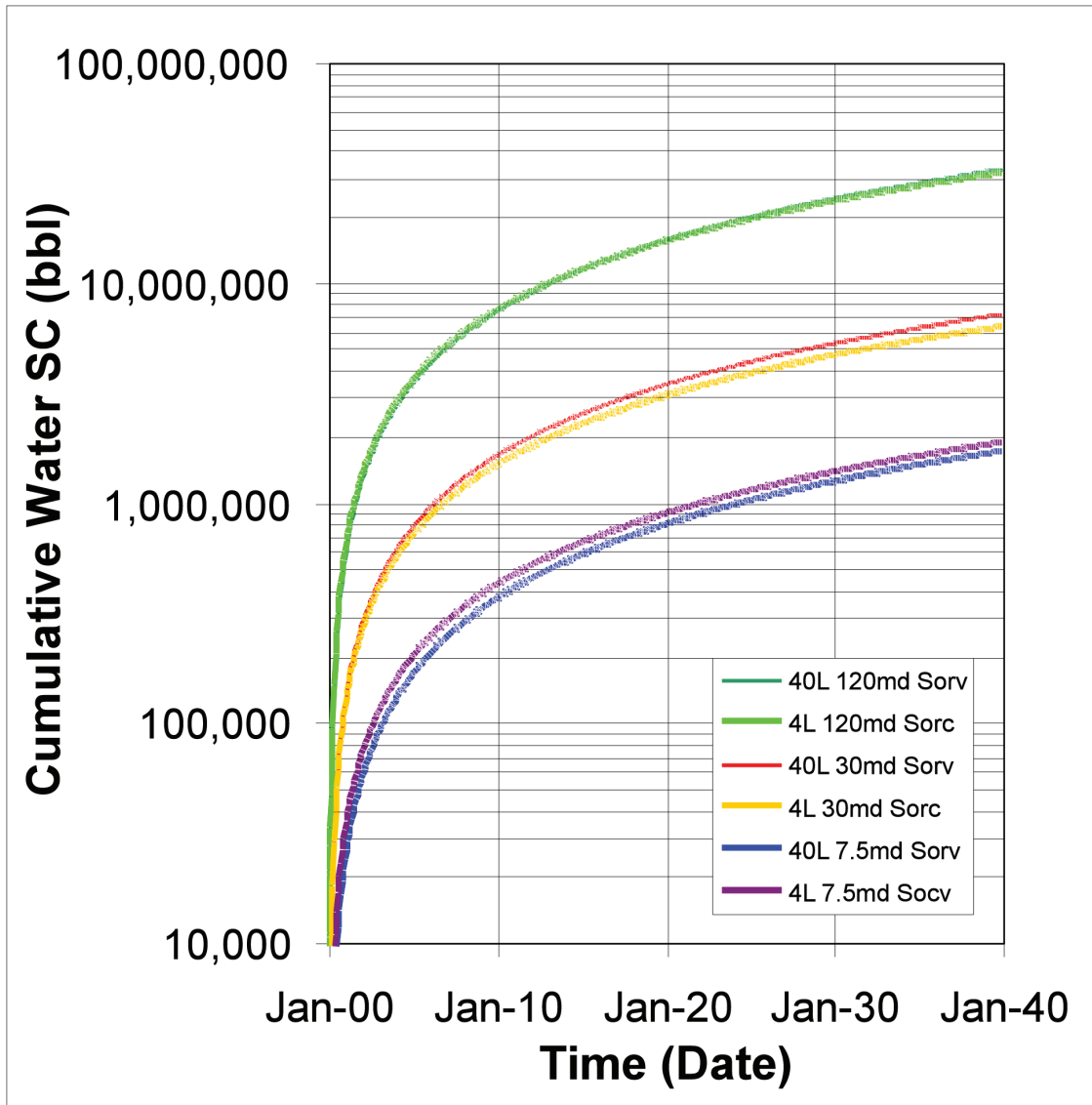


**Figure 3-12.** Estimated cumulative water production with time for 40-ft thick, 4-layer model for both fixed  $S_{or}$  ( $S_{orc}$ ) and variable  $S_{or}$  ( $S_{orv}$ ).

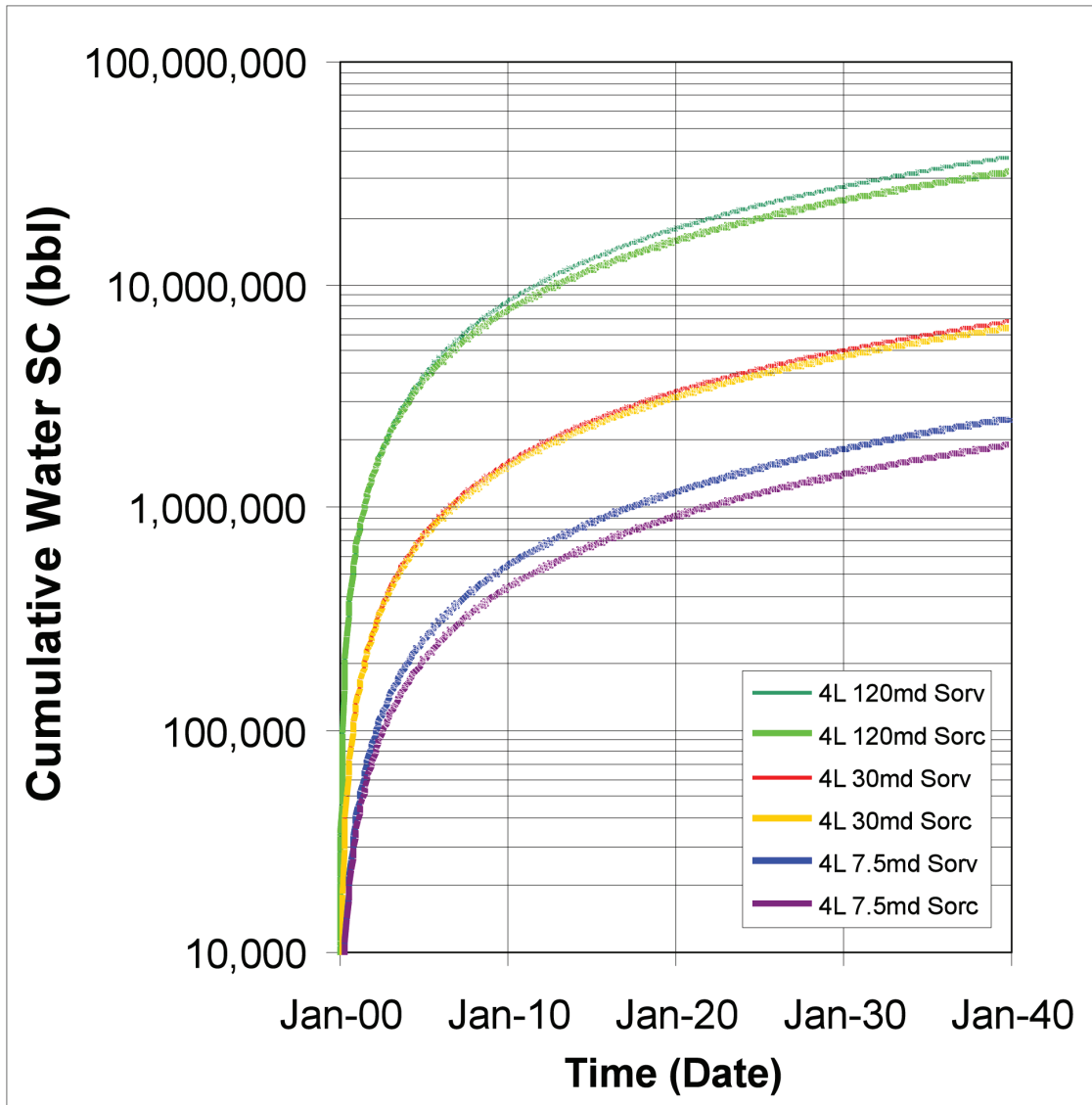


**Figure 3-13.** Estimated cumulative water production with time for 40-ft thick, model comparing the 40-layer model results with a 4-layer model results for variable  $S_{or}$  ( $S_{orv}$ ).

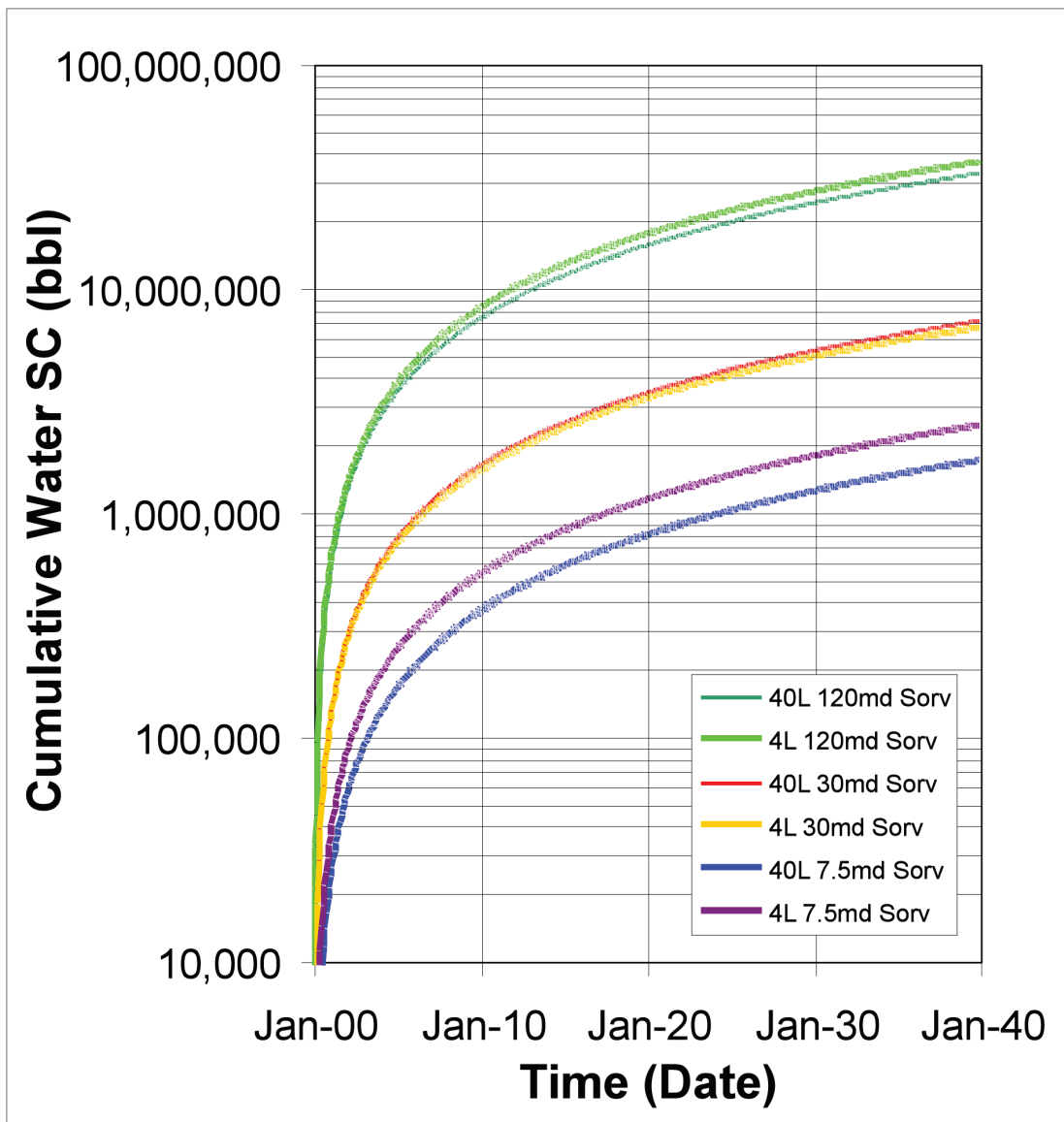


**Figure 3-14.** Estimated cumulative water production with time for 40-ft thick, model comparing the 40-layer model results using variable  $S_{or}$  ( $S_{orv}$ ) compared with 4-layer model results using fixed  $S_{or}$  ( $S_{orc}$ ). This compares a more complex model with what might be representative of a more commonly used basic model.

**Table 3-2.** Summary of cumulative water at 40 years for various models shown in Figures 3-10 through 3-14.

40L	7.5 md	30 md	120 md
	Cum MMBW	Cum MMBW	Cum MMBW
Const	1.5	6.7	29.4
Var	1.7	7.3	33.1
% change	13.3	9.0	12.6

40-20L	7.5 md	30 md	120 md
	Cum MMBW	Cum MMBW	Cum MMBW
Const	0.28	2.8	14.6
Var	0.36	3	17.2
% change	28.6	7.1	17.8

30 md	40 Layer	4 Layer	Diff, %
	Cum MMWO	Cum MMWO	
Const	6.7	6.4	4.7
Var	7.2	6.8	5.9
Diff (%) - 40L variable & 4 Layer constant			12.5

120 md	40 Layer	4 Layer	Diff, %
	Cum MMWO	Cum MMWO	
Const	29.4	32.1	-8.4
Var	33.1	37.3	-11.3
Diff (%) - 40L variable & 4 Layer constant			3.1

### 3.6 Vertical Scaling of Water Saturation

Reservoir flow simulation requires that water saturations be defined using either input  $S_w$  values or using capillary pressure curves and a defined free water level. Using either of these methods the upscaling of water saturation that is defined for a given upscaled porosity involves only an algebraic calculation. However, upscaling a capillary pressure to obtain accurate water saturations is dependent on 1) the number of layers and the capillary pressure curve, and 2) the height of the transition zone relative to the total pay interval. To avoid the complexity of upscaling capillary pressure simulations sometimes simply assign a water saturation that is calculated by whatever upscaling procedure was selected. This methodology, however, presents problems for numerical flow simulations where capillary pressure is included in the simulation. A flow simulation model that initiates with an assigned water saturation may be initiating with a conflict between the assigned water saturation and a capillary pressure calculated water saturation. Generally, this conflict is resolved during the initial start-up of the simulation by the numerical flow simulator working to re-establish capillary equilibrium in the initial phase of the simulation. This process can have two problems: 1) initiation times for computation can be very long, and 2) the initial saturations do not necessarily represent the equilibrium saturations in cases where assigned initial saturations were not equal to saturations that would have been estimated from capillary pressure equilibrium relationships. In effect, the decoupling of initial water saturation from capillary equilibrium saturation sets up a conflict in the initial stages of simulation if capillary pressure forces are also initially activated.

Models with fewer layers than 10 can exhibit significant error as a function of the capillary pressure curve. Differences in the oil interval ( $oi$ ) are different than the total section. Differences are greater as the transition zone represents a greater fraction of the total section modeled (and vice versa).

As noted, even when water saturations are calculated using capillary pressure relations and a defined free water level, there can be differences among models of differing numbers of layers. Figure 3-15 illustrates water saturations calculated for Mississippian reservoirs of various permeability that are all 40 feet in height. The capillary pressure relations that apply to each of these reservoirs are described in Section 2. To provide a common reference frame the average saturations calculated for each permeability-layer model were divided by the average saturation estimated using an 80-layer model where each layer represents 0.5 feet in thickness. The 80-layer model was considered to be sufficiently accurate to represent the true continuous profile average water saturation.

Comparison of average water saturations for the entire reservoir interval (solid symbols in **Fig. 3-15**) show that all models with greater than 8 layers estimate nearly the same average water saturation. However, the entire reservoir interval is, for some permeability reservoirs, dominated by either a large oil column or a large water column that dominate the comparison. Comparing just the intervals in which oil saturation is greater than zero (open symbols in Fig. 3-15) shows that models of different number of layers calculate different average water saturations and can exhibit average water satura-

tions that differ by up to 25% from a true continuous profile average saturation. The nature of the difference is not the same among different permeabilities and does not exhibit the same characteristics for differing layer numbers. These differences can be attributed to how splitting of layers happens to intersect different portions of the capillary pressure curve for each permeability, and consequently, each associated capillary pressure curve. When layer boundaries lie near or on significant capillary pressure transition regions, where saturation changes are significant over small height changes, differences from a continuous saturation profile can be large. This contributes to the progressive shift toward increasing error with increasing number of layers with increasing permeability. The lowest permeability reservoir exhibits the least error for many layers because the water saturation values approach  $S_w=1$ . **Figure 3-16** illustrates an example of the differences in water and oil saturations for models of various numbers of layers for a 30-mD reservoir.

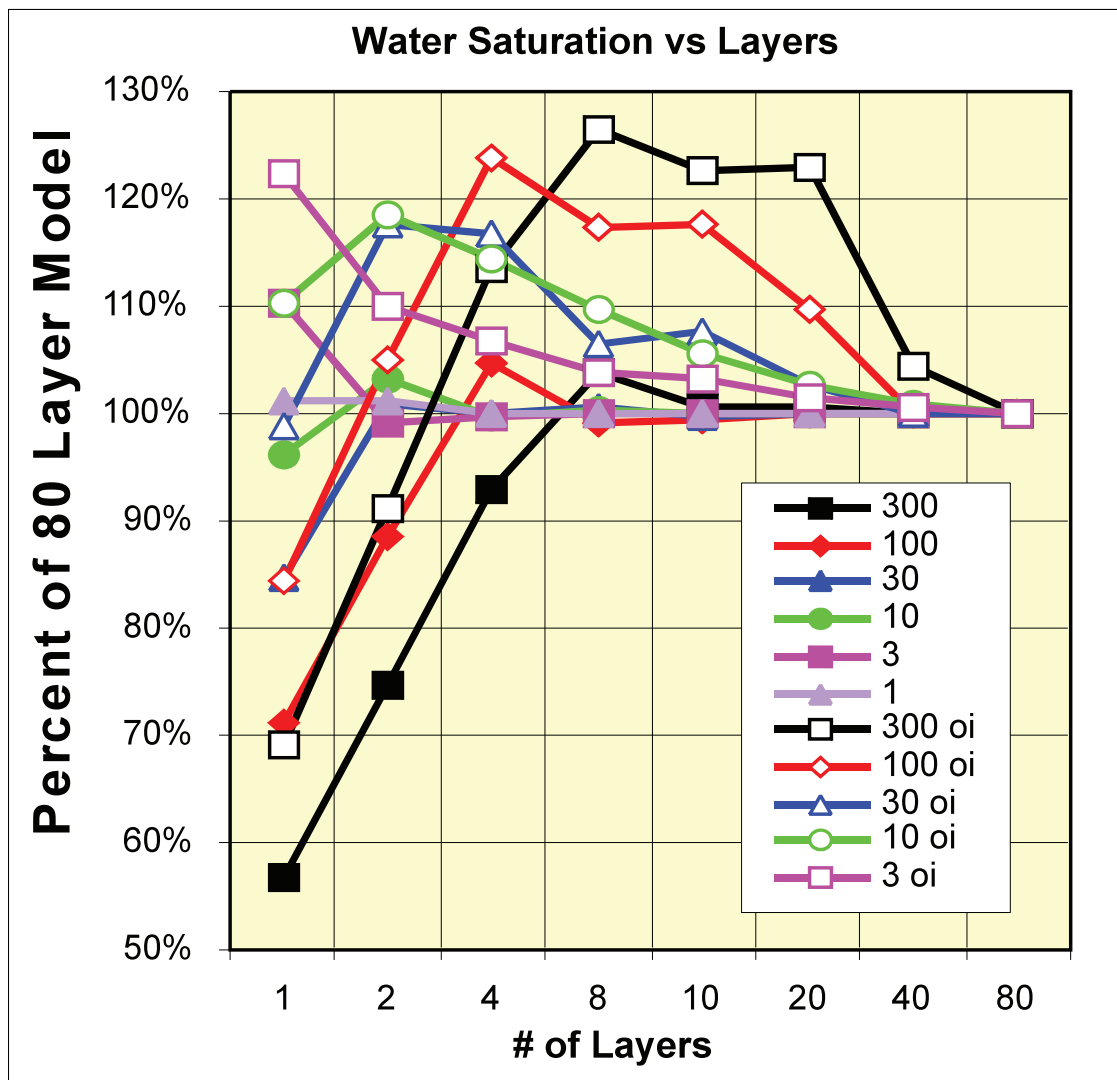


**Figure 3-15.** Comparison of the ratio of total average water saturation for the entire reservoir interval to average saturations calculated for a highly refined 80-layer model (i.e. each layer represents 0.5 ft). Average water saturations were estimated using capillary pressure curves for Mississippian rocks exhibiting various permeabilities described in Section 2. Solid symbols represent total reservoir interval average saturation and open symbols represent average saturations only for the interval above the threshold entry pressure which exhibits an oil saturation greater than zero.

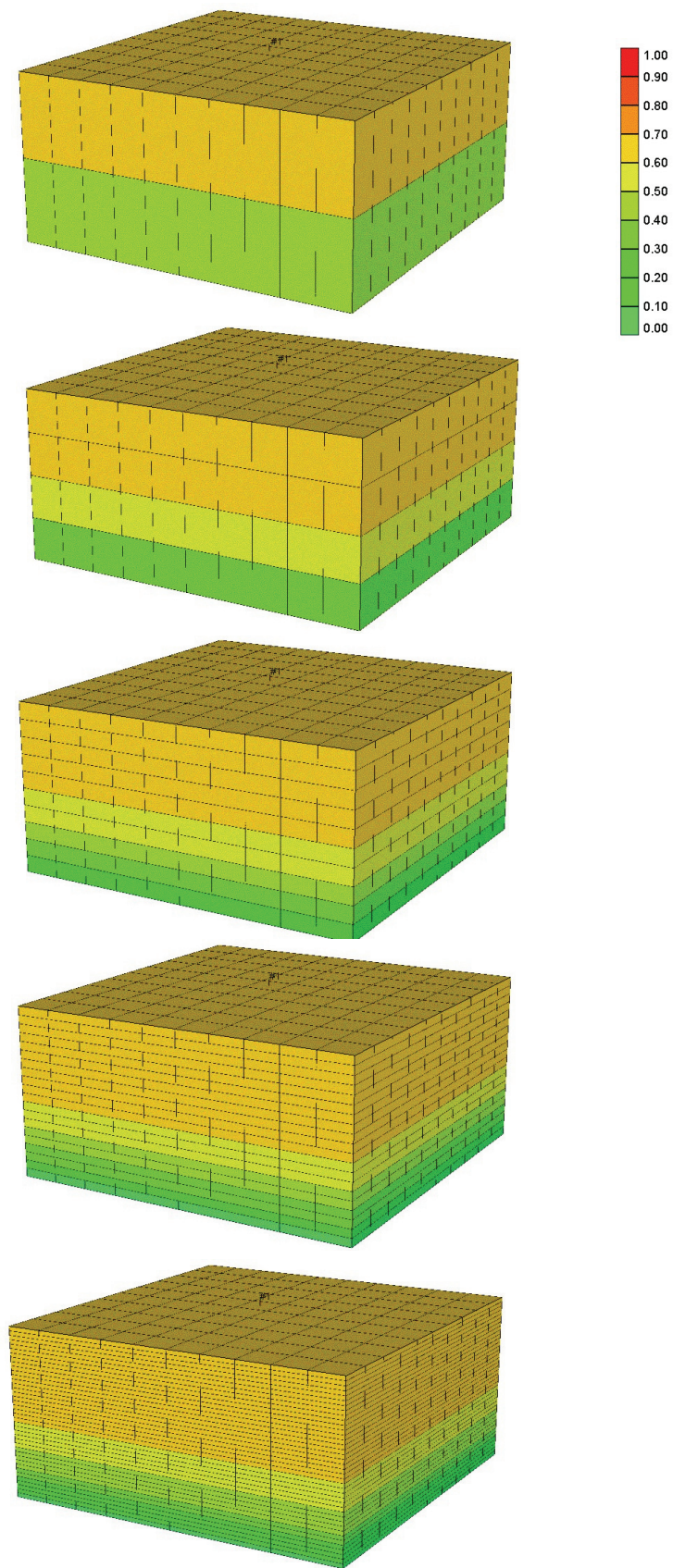


**Figure 3-16.** Comparison calculated oil saturations for a 30-mD reservoir for models with different numbers of layers representing 2 (top), 4, 10, 20, and 40. Color scale indicates calculated oil saturation.

### 3.7 Predicted Cumulative Water/Oil Ratio

Although both oil and water production are predicted to be greater with a  $S_{orw}(S_{oi})$  model compared to a  $S_{orwmax}$  model, the amount of increase of oil and water and the cumulative water/oil ratio (WORcum) does not exhibit a simple relationship with permeability or with the number of layers utilized in the model. The 40-layer model (Fig. 3-17) indicates that WORcum is predicted to be greater for a  $S_{orw}(S_{oi})$  model compared to a  $S_{orwmax}$  model for high-permeability reservoirs (e.g., 120 md) but is lower for a 30 md reservoir and is the same for a 7.5 md reservoir. However, comparison between a 40-layer  $S_{orw}(S_{oi})$  model and a basic 4-layer  $S_{orwmax}$  model (Fig. 3-18) shows that the  $S_{orw}(S_{oi})$  model always predicts lower WORcum.

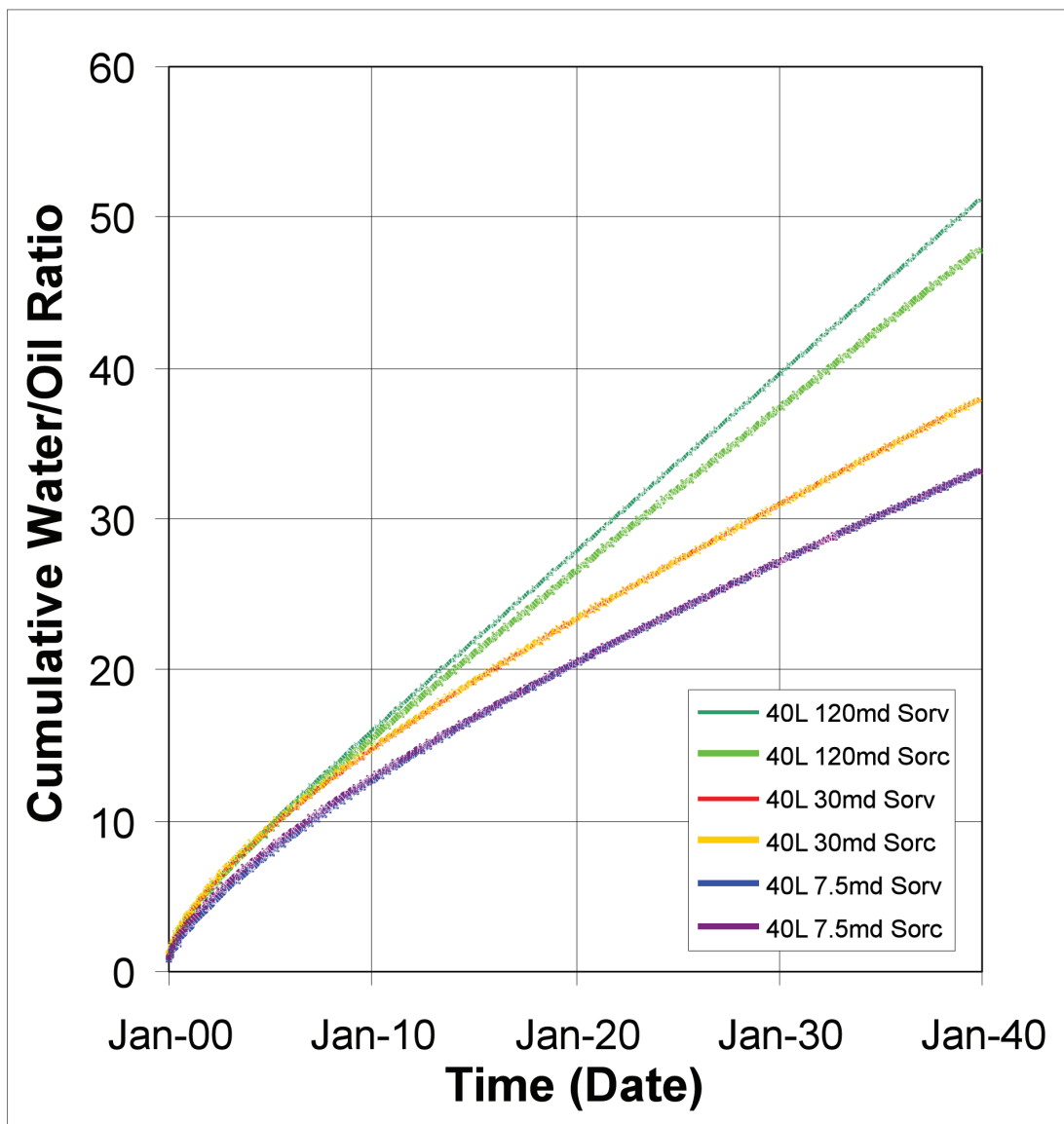
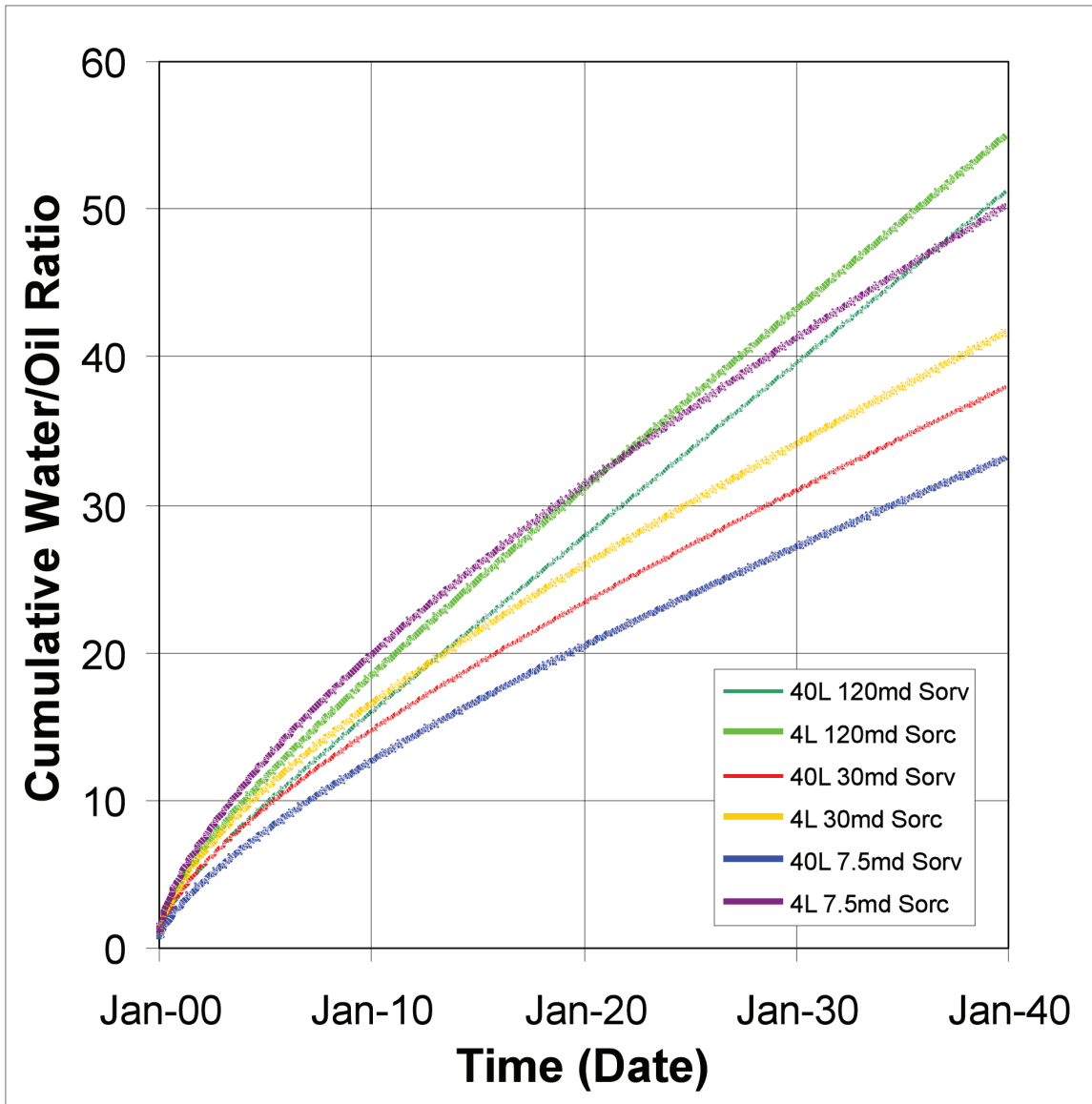


Figure 3-17. Estimated water/oil ratio with time for 40-ft thick, 40-layer model for both fixed  $S_{or}$  ( $S_{orc}$ ) and variable  $S_{orw}$  ( $S_{orv}$ ) for reservoir of different permeability.



**Figure 3-18.** Estimated water/oil ratio with time for 40-ft thick, model comparing the 40-layer model results using variable  $S_{or}$  ( $S_{orv}$ ) compared with 4-layer model results using fixed  $S_{or}$  ( $S_{orc}$ ). This compares a more complex model with what might be representative of a more commonly used basic model.

### 3.8 Perforation Criteria and Upscaled Models

Examination of the upscaled 4-layer models for various permeabilities (**Figures 3-19 to 3-21**) shows that criteria typically applied for the lowermost portion of a transition-zone reservoir can be somewhat problematic. For the 120-md model the small transition zone results in the bottom layer exhibiting  $S_w = 0.496$ . This water saturation is sufficiently low that the high  $k_{ro}$  warrants the layer be perforated. By perforating the layer, significantly greater water is produced. If the interval is not perforated oil production is diminished. In contrast, the 30-md model shows that the lower layer is primarily below the transition zone and the second layer appropriately defines the first transition zone oil productive interval. For the 7.5-md interval the bottom layer is below the transition zone but the second layer saturation of  $S_w = 0.619$  exhibits a  $k_{ro} = 0.095$ . As with the 120-md interval, the decision to perforate or not perforate becomes dependent on the predicted water production.

Finer-scale models (**Fig. 3-22**) more clearly indicate optimum perforation strategies and consequent accurate reservoir flow prediction. Comparison of Figures 3-19 through 3-21 with Figure 3-22 illustrates how decisions about perforation depth might change with differences in interpreted upscaled saturations and predicted final water saturations and associated water and oil cumulative recoveries.

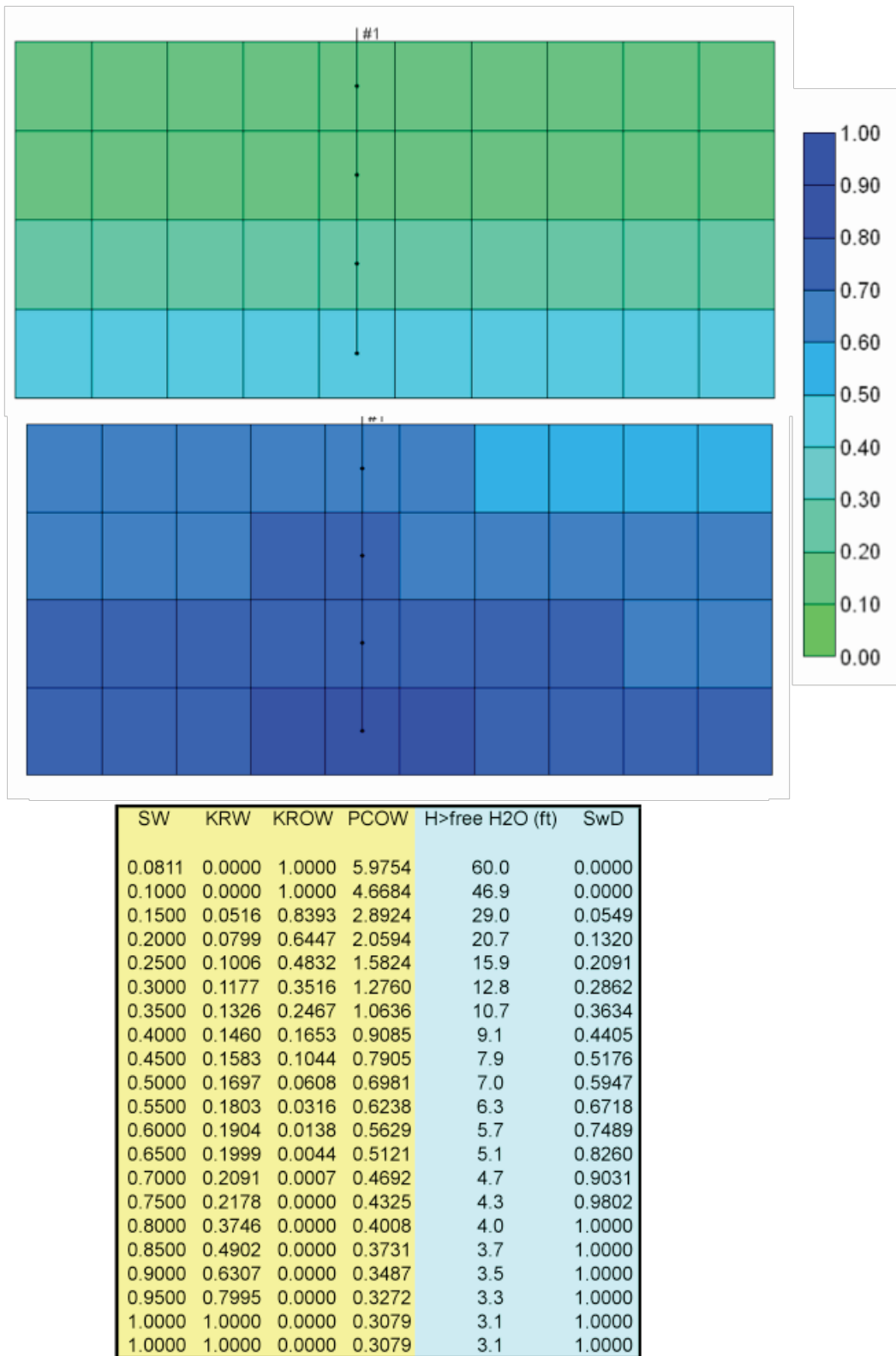
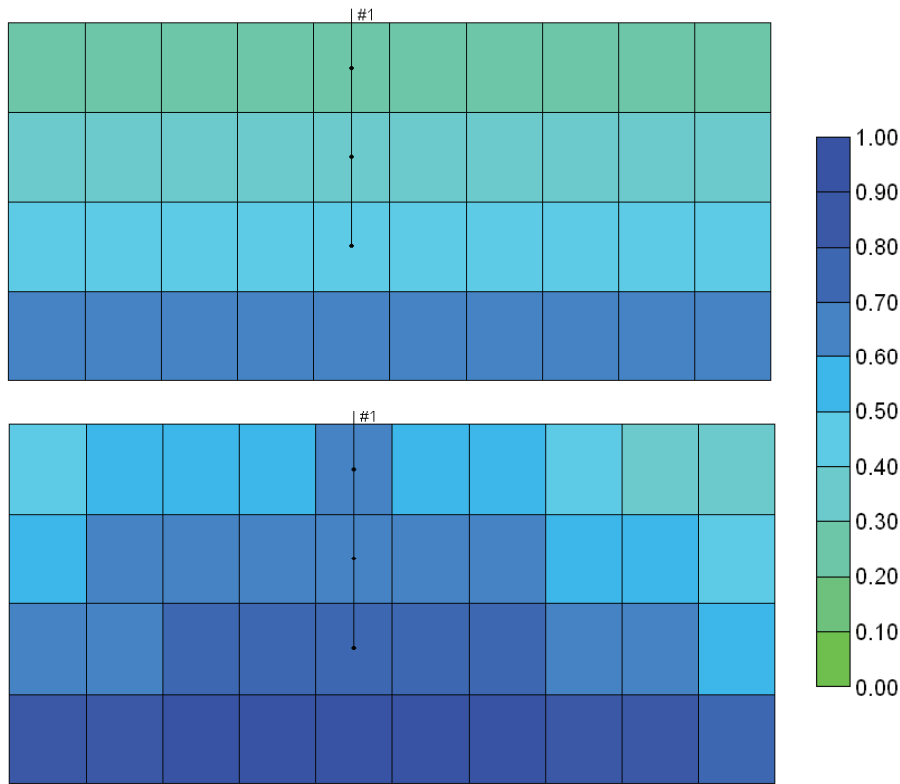
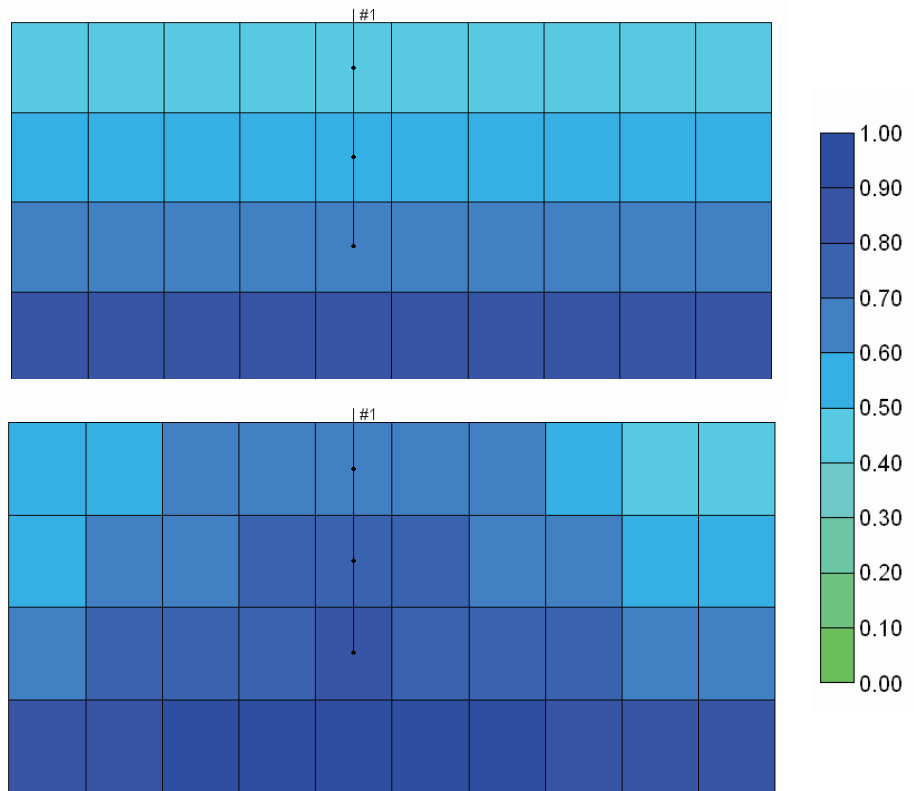


**Figure 3-19.** Water saturation distribution in 4-layer, 120-mD model showing initial saturations (top), final saturations at 40 years (bottom), and initial saturations as a function of height above free water level and associated oil and water relative permeabilities (bottom table).



SW	KRW	KROW	PCOW	H, ft	SwD
0.1853	0.0000	1.0000	5.9754	60.0	0.0
0.2000	0.0000	1.0000	5.3629	53.9	0.0
0.2500	0.0177	0.9800	3.9121	39.3	0.0
0.3000	0.0724	0.7009	3.0233	30.4	0.1
0.3500	0.1009	0.4812	2.4313	24.4	0.2
0.4000	0.1229	0.3137	2.0131	20.2	0.3
0.4500	0.1415	0.1909	1.7043	17.1	0.4
0.5000	0.1580	0.1057	1.4685	14.7	0.5
0.5500	0.1729	0.0508	1.2834	12.9	0.6
0.6000	0.1866	0.0195	1.1349	11.4	0.7
0.6500	0.1994	0.0048	1.0135	10.2	0.8
0.7000	0.2114	0.0004	0.9127	9.2	0.9
0.7500	0.2308	0.0000	0.8279	8.3	1.0
0.8000	0.3241	0.0000	0.7557	7.6	1.0
0.8500	0.4431	0.0000	0.6936	7.0	1.0
0.9000	0.5923	0.0000	0.6398	6.4	1.0
0.9500	0.7762	0.0000	0.5927	6.0	1.0
1.0000	1.0000	0.0000	0.5512	5.5	1.0
1.0000	1.0000	0.0000	0.5512	5.5	1.0
1.0000	1.0000	0.0000	0.5512	5.5	1.0
1.0000	1.0000	0.0000	0.5512	5.5	1.0

**Figure 3-20.** Water saturation distribution in 4-layer, 30-mD model showing initial saturations (top), final saturations at 40 years (bottom), and initial saturations as a function of height above free water level and associated oil and water relative permeabilities (bottom table).



SW	KRW	KROW	PCOW	H>free H2O (ft)	SwD
0.3349	0.0000	1.0000	5.9754	60.0	0.0000
0.3500	0.0000	1.0000	5.5577	55.8	0.0000
0.4000	0.0000	1.0000	4.4608	44.8	0.0000
0.4500	0.0569	0.8071	3.6744	36.9	0.0668
0.5000	0.1036	0.4596	3.0892	31.0	0.2218
0.5500	0.1351	0.2308	2.6406	26.5	0.3768
0.6000	0.1604	0.0951	2.2881	23.0	0.5318
0.6500	0.1823	0.0273	2.0056	20.1	0.6869
0.7000	0.2019	0.0033	1.7752	17.8	0.8419
0.7500	0.3077	0.0000	1.5846	15.9	0.9969
0.8000	0.4089	0.0000	1.4248	14.3	1.0000
0.8500	0.5278	0.0000	1.2895	12.9	1.0000
0.9000	0.6654	0.0000	1.1737	11.8	1.0000
0.9500	0.8225	0.0000	1.0737	10.8	1.0000
1.0000	1.0000	0.0000	0.9867	9.9	1.0000
1.0000	1.0000	0.0000	0.9867	9.9	1.0000
1.0000	1.0000	0.0000	0.9867	9.9	1.0000
1.0000	1.0000	0.0000	0.9867	9.9	1.0000
1.0000	1.0000	0.0000	0.9867	9.9	1.0000
1.0000	1.0000	0.0000	0.9867	9.9	1.0000
1.0000	1.0000	0.0000	0.9867	9.9	1.0000

**Figure 3-21.** Water saturation distribution in 4-layer, 7.5-mD model showing initial saturations (top), final saturations at 40 years (bottom), and initial saturations as a function of height above free water level and associated oil and water relative permeabilities (bottom table).

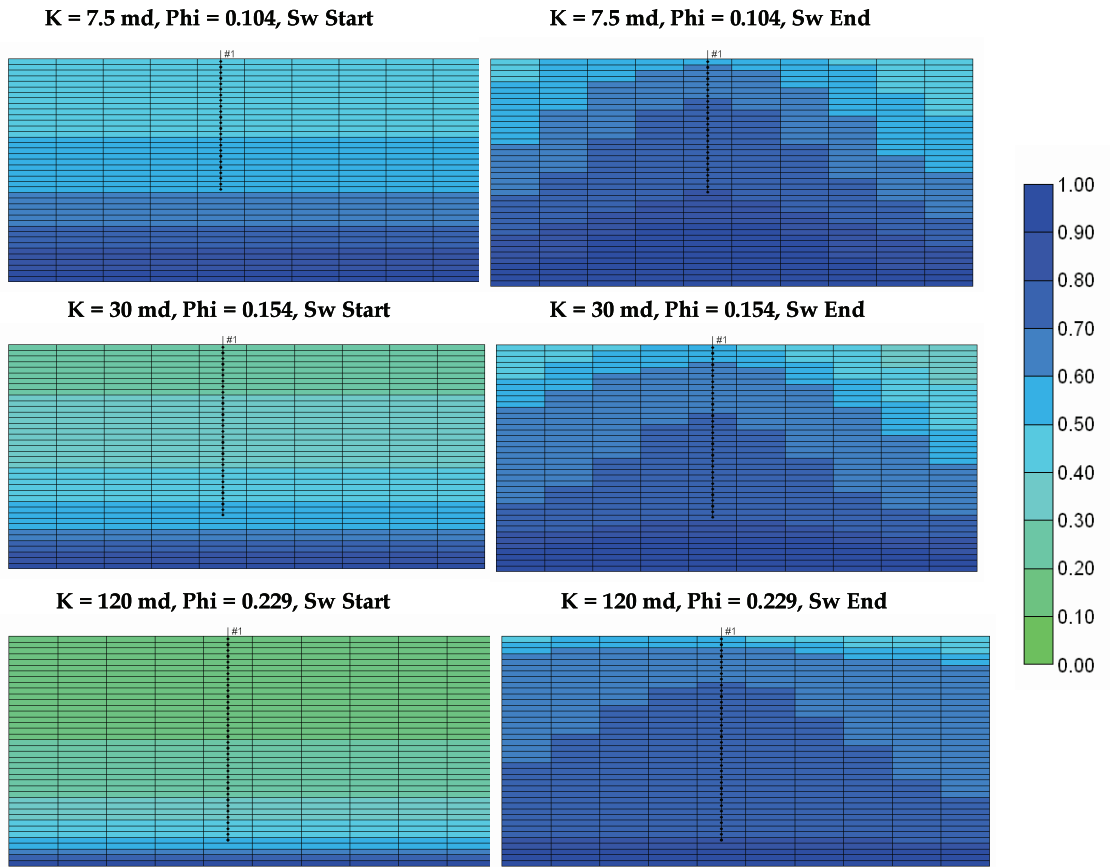


**Figure 3-22.** Water saturation distribution in 40-layer, 7.5-mD, 30-mD, and 120-mD models showing initial saturations (left), and final saturations at 40 years (right).

### 3.9 Upscaled System Response

Thin midcontinent shallow-shelf carbonates and transition-zone-dominated reservoirs often have natural or planned waterfloods that involve a strong bottom-water drive component but are dominated by horizontal flow. Typically upscaling from finer to coarser grid-cell size results in premature predicted water breakthrough because with each timestep the coarse grid cell is required to have a saturation change that allows water flow before water should be arriving. In transition-zone reservoirs bottom-water drive results in initial increase in water saturation in the bottom of the reservoir and with production resulting from horizontal flow. A simplified model (**Fig. 3-23**) illustrates how upscaling results in incorrect prediction even when all aspects of porosity, permeability, relative permeability, and capillary pressure have been correctly upscaled. Two cases are examined representing two different oil relative permeability curves ( $k_{roA}$  and  $k_{roB}$ ; **Fig. 3-24**) and similar water relative permeability. For simplicity flow can be pictured as dominantly horizontal but with water influx from the bottom. The paired sets of boxes illustrate the progressive depletion of a reservoir that is modeled using 10 vertical grid cells of identical properties and with a single grid cell with the same properties as the 10 grid cells and thus the upscaled properties are identical. This represents a perfectly homogeneous reservoir. Initial water saturation is assumed to equal zero ( $S_{wi} = 0$ ) and for simplicity  $S_{orw} = 0$ . Which oil relative permeability curve is used is immaterial for the 10-layer model since composite  $k_{ro}$  is simply the fraction of cells occupied times  $k_{ro} = 1$ . The two  $k_{ro}$  models only influence the upscaled model. It is implicitly assumed that the 10-layer model is correct.

With initial production the bottom of the reservoir changes saturation significantly ( $S_w 10 = 1$ ,  $S_w 1-9 = 0$ ) and the top is unchanged but for the upscaled model  $S_w 1-10 = 0.1$ . From the relative permeability curves actual  $k_{ro}$  (10 layer model; designated  $k_{ro1-9}$ ) is  $k_{ro1-9} = 0.9$  and with the upscaled model  $k_{roA} > k_{ro1-9}$  while  $k_{roB} < k_{ro1-9}$ . Water production has actually begun but the upscaled model indicates water is not producing.

With production increasing  $S_w$  to  $S_w = 0.3$  and  $S_w = 0.5$  actual water production increases significantly, reaching a WOR = 1 at  $S_w = 0.5$ , but both upscaled models indicate water production is negligible. The high  $k_{ro}$  model just approaches the actual  $k_{ro1-10}$  at  $S_w = 0.5$  ( $k_{roA} = k_{ro1-5}$ ) while the low  $k_{roB} < k_{ro1-5}$ .

By  $S_w = 0.8$ ,  $k_{roA} < k_{ro1-2}$  and  $k_{roB} \ll k_{ro1-2}$  and finally  $k_{rw}$  indicates water is productive even though  $k_{rwAB} < k_{rw1-8}$ .

It is evident that the upscaled model under-predicted water production for the entire history of the reservoir and either over-predicted or under-predicted oil production. It is interesting to note that for the upscaled model:

#### **During Early Production**

- Any  $k_{ro}$  curve would work - the model is insensitive to  $k_{ro}$  variation at low  $S_w$ .
- No measured  $k_{rw}$  curve would work because no measured  $k_{rw}$  curve is going to predict water mobility at low  $S_w$ .

### **During Late Production**

- Only a high kro curve will work
- krw curves could work but still predict low

### **During the Entire Process**

- A reservoir simulation model would be unable to model actual production using a single set of kro and krw curves and still successfully match production through the life of the reservoir
- Early oil production would be easily matched but water production would either require a major adjustment to the krw curve or the operator would assume there are fractures present
- Any single kro curve would become progressively more incorrect during the history match and to adjust would have to be adjusted, but could be adjusted to give a correct response. The adjustment could not be a simple multiplier but would have to require adjustment with saturation change

Any adjustment to kro or krw curves represents the creation of a pseudo-kr curve that is responding to a specific saturation change. Since the flow simulator is being used to predict how  $S_w$  changes the final kr curves represent the modeled vertical and horizontal contributions to  $S_w$  change but those contributions were based on a potentially incorrect average  $S_w$ .

One solution is to treat upscaling kr as a vector just as is done with permeability this would potentially require that the upscaled vector solution would have to be performed sequentially as the saturation change progressed (effectively representing the vector component in  $S_w$  space).

What is perhaps just as important is that all of the above discussion applies analogously to capillary pressure.

We are taught to test grid-cell size dependence of flow simulation models; these results indicate that may be very important in transition-zone reservoirs.

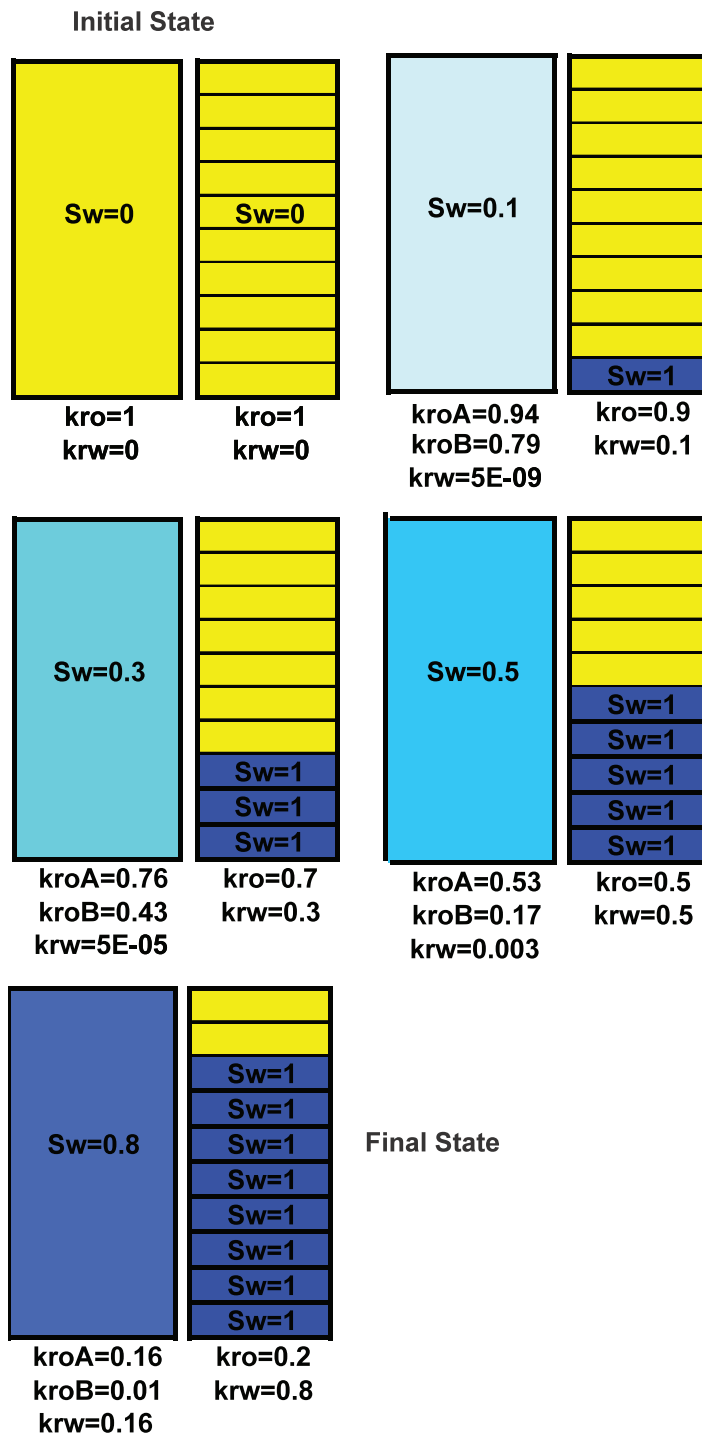


**Figure 3-23.** Sequence of saturation states for a reservoir modeled using a single layer and using 10 layers. Differences in interpreted kro and krw values for each state illustrates the significant differences that can be predicted using the two different models. The text discussed implications.

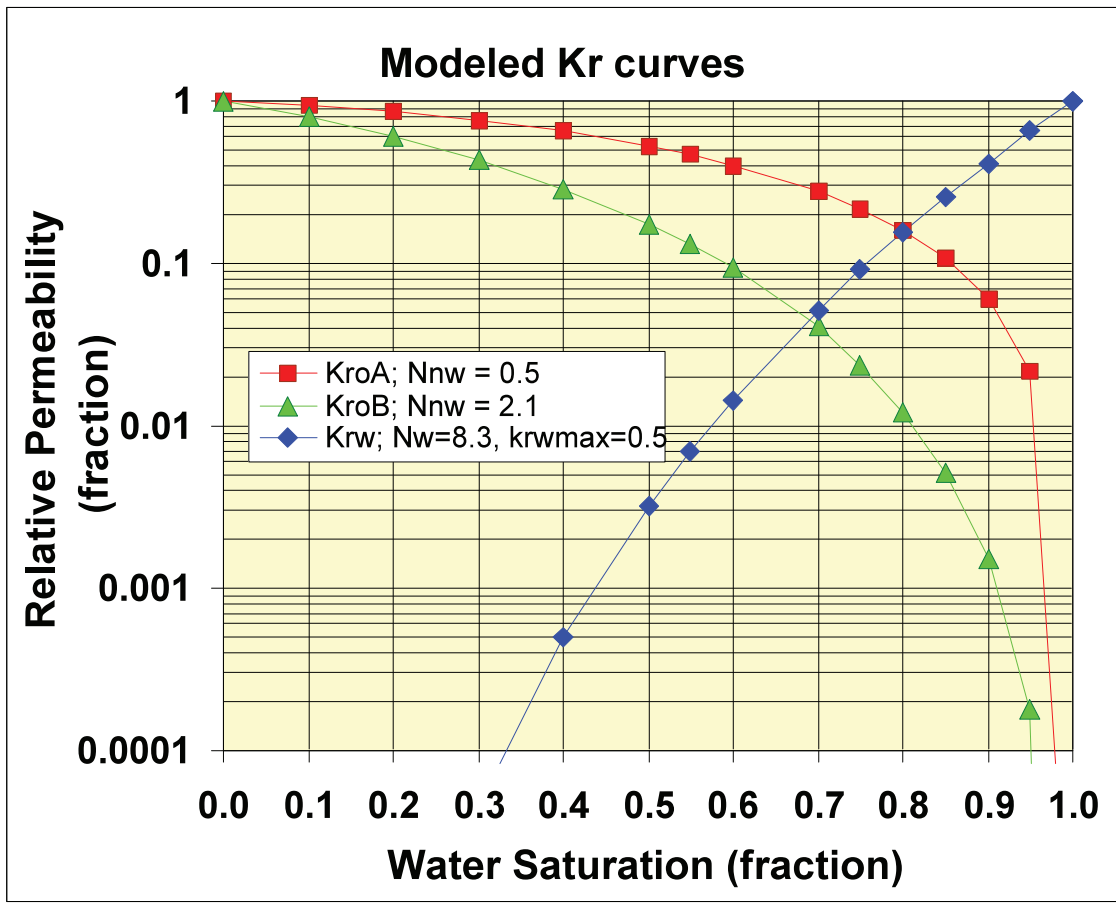


**Figure 3-24.** Two cases representing two different oil relative permeability curves (kroA and kroB) discussed in text.

### 3.10 Scaling of Transition Zone Effects with Permeability and Capillary Pressure

It is important to note that

- Issues with capillary pressure and relative permeability in the transition zone scale with permeability and capillary pressure.
- Capillary conditions in the Mississippian and L-KC that present issues at 40 ft of hydrocarbon column height present similar issues; for example, in Niobrara chinks, generally less than 3 md, at heights up to 1,000 ft (**Fig. 3-25**).

Figure 3-25 shows that the transition zone for the Niobrara chalk exhibits similar properties to the Mississippian described above but the capillary pressure curves are scaled over 1,000 feet instead of 40 feet, as they are in the Mississippian. The same issues with layer numbers and upscaling discussed above would apply to the Niobrara but would be scaled to the difference in scales presented in Figure 3-25.

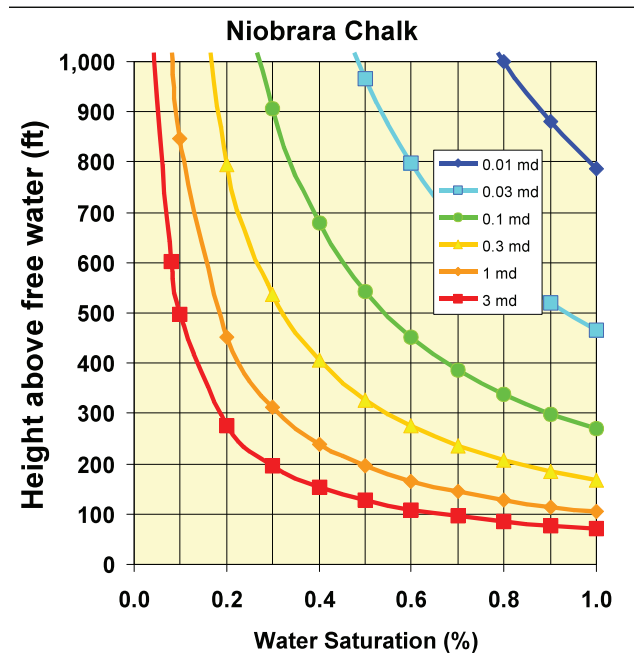
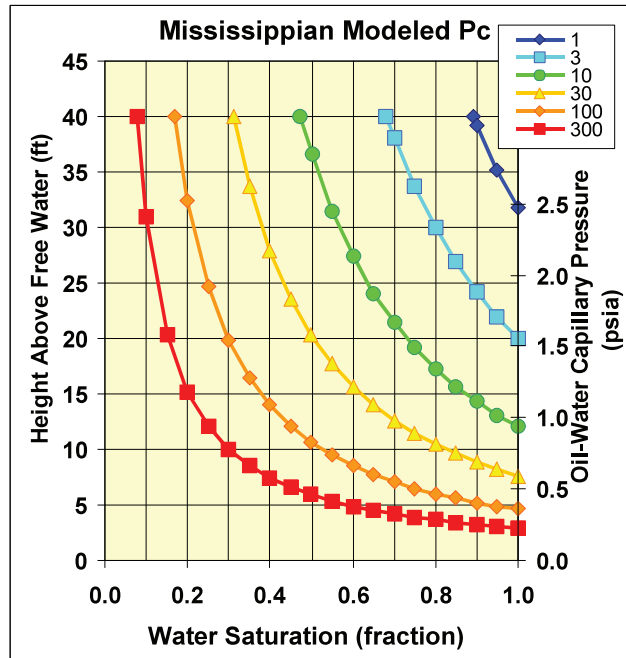


**Figure 3-25.** Comparison of generalized capillary pressure curves for the Mississippian and the Niobrara in Kansas illustrating how capillary pressure scales between the two systems.

Sections 2 and 3 present theoretical geomodels representing a range of rock properties and lithofacies architectures. These sections compare results between models that are designed to handle the vertical change in petrophysical properties through the transition zone and models that are fixed in their properties. The examples given above focused primarily on Mississippian reservoir with discussion of Lansing-Kansas City properties. During the time when this study was being performed, the optimum wells for participation in this program were in an Arbuckle and a Lansing-Kansas City field. Therefore numerical flow simulations were designed to investigate these formations. The fields were both small and relatively isolated. Therefore efforts were directed at models appropriate for an isolated well in a small field. These small fields represent an important contribution to the total productivity from both formations.

Four simple numerical flow simulations were performed to expand on the theoretical work discussed in Sections 2 and 3 above.

Two simulations were performed for Lansing-Kansas City reservoirs: 1) To examine performance of more isolated L-KC wells, a single-well flow simulation of the existing Terry Unit #7-32 in Raile field drilled in June 2003, and 2) a single well flow simulation of the region where the proposed Austin #2-27 was to be drilled. The Austin #2-27 simulation was performed both before the well was drilled and after core data were available.

Two simulations were performed for Arbuckle reservoirs: 1) The L Hadley #4 well (API #15-051-25131) was drilled in May 2002 and provided: 1) an opportunity to examine the Arbuckle within a region of the Bemis-Shutts field that has produced since 1947, and 2) a single well flow simulation of the region where the proposed Keja #1-3 was to be drilled. The Keja #1-3 simulation was performed both before the well was drilled and after core data were available.

## 4.1 Lansing-Kansas City

### 4.1.1 Terry Unit #7-32

The Terry Unit #7-32 is located in Raile field (**Fig. 4-1**). Wireline log analysis (**Fig. 4-2**) shows the L-KC in this location is a limestone, 28-ft thick, 9-15% porosity, with 23-30% water saturation. Pickett plot analysis using standard Archie parameters ( $a = 1$ ,  $m = 2$ ,  $n = 2$ ) and a formation brine resistivity of 0.05 ohm-m indicate similar water saturations in the high porosity portion of the reservoir (**Fig. 4-3**). Core analysis provides a permeability-porosity trend (**Fig. 4-4**) that can be characterized by a power-law relationship. Comparison of this permeability-porosity trend with more oomoldic Lansing-Kansas City limestones (**Fig. 1-15**) shows that these rocks, which have both interparticle and moldic porosity, exhibit higher permeability for a given porosity than oomoldic-porosity dominated rocks. Water saturations calculated using Archie  $m = 2$  provide the water saturation estimate near approximately 24% for the higher porosity interval from 4745 ft to 4752

ft. If the Archie cementation is changed to  $m = 2.3$  as indicated by core measurements, then the log-estimated water saturation increases to 36%. A thin interval at 4740 shows an increase in water saturation (where the Sw arrow points in Fig. 4-2). Comparison with the core analysis **Table 4-1** shows that this interval is a thin-bed low-porosity interval that the wireline logs did not resolve. This interval is likely to be completely water saturated.

For a Lansing-Kansas City reservoir with properties similar to the Terry #7-32 standard numerical simulation is effective. Upper and lower bounding low porosity and permeability beds limit reservoir production to primarily solution-gas drive. The relatively uniform saturation distribution over the reservoir interval indicates it is not in the transition zone. With reservoir KH = 750 md-ft (sum of permeability x thickness) this well is capable of draining over 640 acres. If the properties observed at this well extended laterally over even a full 160 acres, this well is capable of producing nearly 700 MBO in a field at virgin pressure. The Terry #7-32 has produced less than 50 MB since it was placed on production in 2003. The Raile 1-32 and Culwell Unit 4-32 wells were completed prior to 2001 and produced 220 MBO and 354 MBO, respectively. The performance of Terry #7-32 can be hypothesized to result from prior depletion and proximity to a reservoir boundary limiting the drainage area.

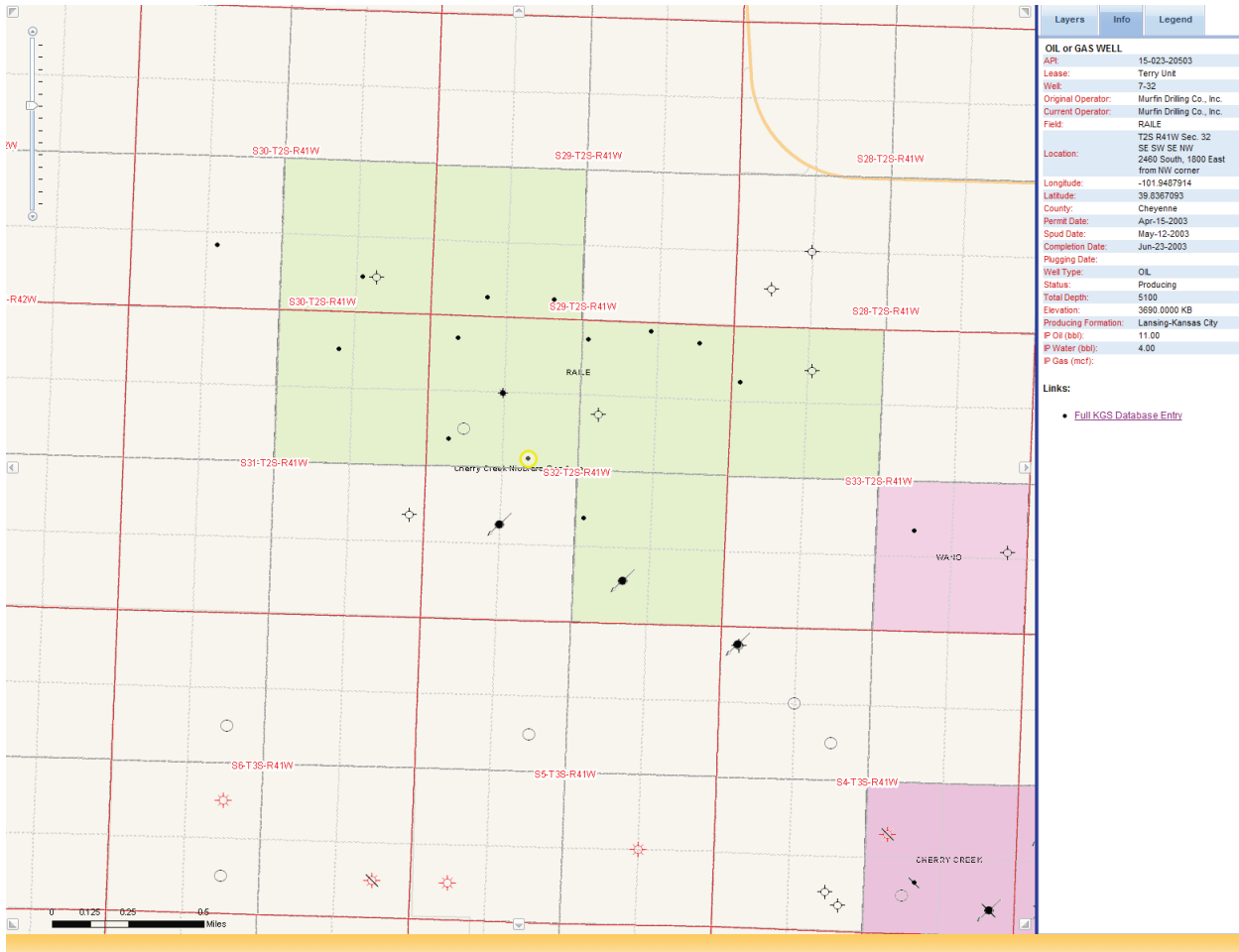


**Figure 4-1.** Map location of Terry Unit #7-32 well shown highlighted in yellow on the south boundary of Raile field.

20 CLF	1	0	Gamma Ray (GAPI)	50	1	SW	0	0.3	PHIE	0	0	VCL	1
2.6Dga	3.1	6	DCAL (in)	16	30	PAYFLAG	0	0.3	BYW	0	0	VSAND	1
		-150	SPC (mV)	0	1	SXO	0	0	PERM	30	0	VLIME	1
								0.3	BVWSXO	0	0	VDOLO	1
								-2	DST	28			

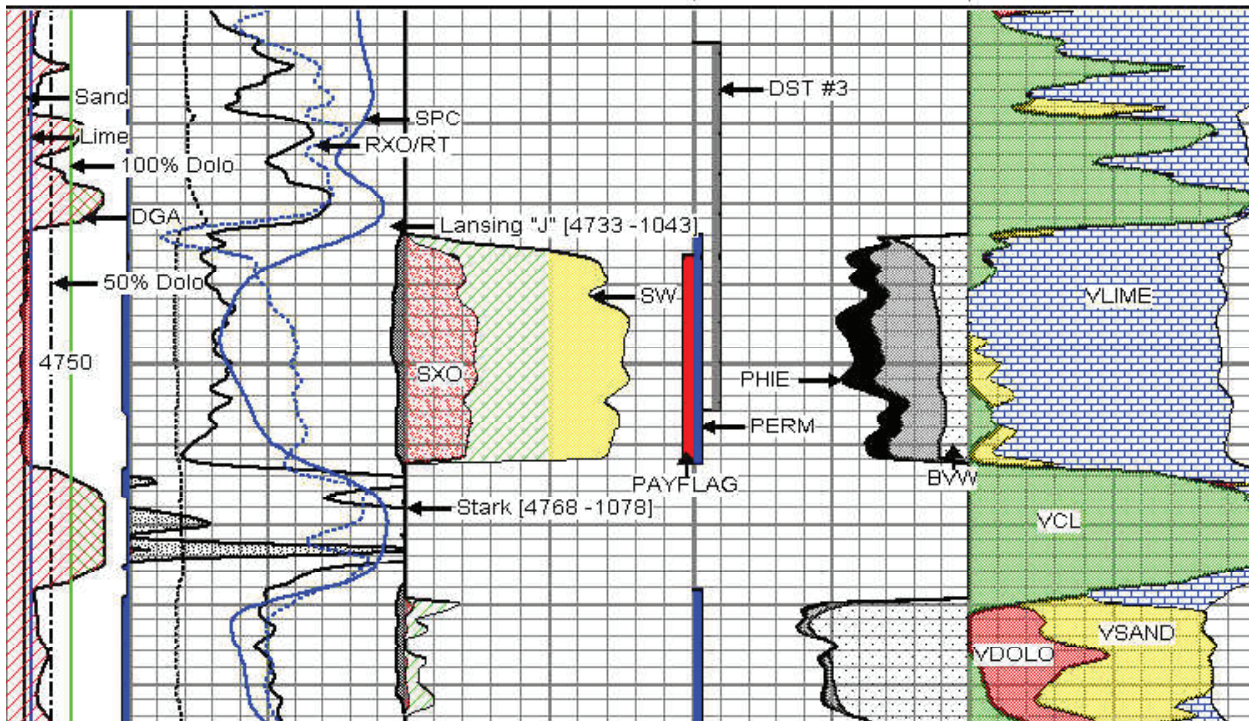


**Figure 4-2.** Standard wireline log analysis of Terry Unit #7-32 showing L-KC interval comprises a limestone section interval approximately 28 ft thick. Conventional log analysis estimates porosity ranges from 9 to 15% and water saturation ranges from 23 to 30%.

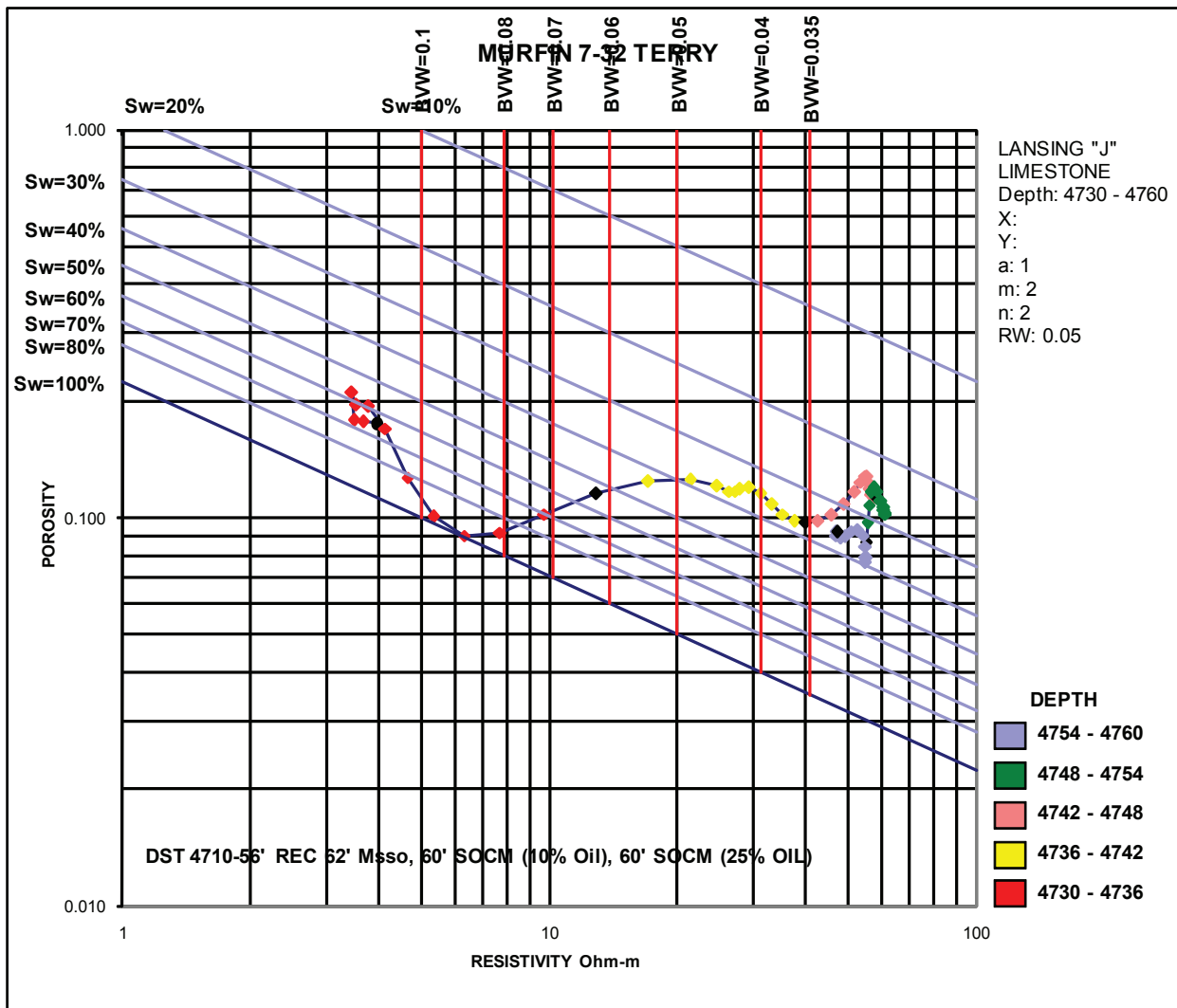


**Figure 4-3.** Pickett plot of Terry Unit #7-32 reservoir interval showing low Sw in higher porosity reservoir and saturations increasing through the interval 4736-4742 in response to facies change into overlying shale.

**Table 4-1.** Summary of core analysis for Murfin Terry Unit #7-32. Archie cementation exponent values reflect partial moldic porosity character of reservoir rock.

Murfin Drilling Company  
 Terry Unit #7-32 API # 15-023-20503-0001  
 Cheyenne County, Kansas  
 Sec 32-T2S-R41W 2460' FNL 1800' FWL  
 3685'GL 3690' KB

Driller Depth (ft)	Routine Helium Porosity (%)	In situ Klinkenberg Permeability (md)	Grain Density (g/cc)	Archie Cementation Exponent (m)	Description
4722.8	12.2	38.2	2.70	2.10	Ls; upper very fine-lower fine pelloidal packstone, well cemented, minor moldic porosity
4734.3	4.8	0.0001	2.63		Ls; upper very fine-lower fine pelloidal packstone, well cemented, minor moldic porosity
4735.8	19.9	174	2.71		Ls; upper very fine-lower fine pelloidal packstone, good interparticle and moldic porosity
4736.5	15.5	39.4	2.73		Ls; upper very fine-lower fine pelloidal packstone, good interparticle and moldic porosity
4737.3	7.8	0.92	2.73		Ls; upper very fine-lower fine pelloidal packstone, bedded, sparry cement, isolated moldic porosity
4737.9	15.3	54.0	2.73		Ls; upper very fine-lower fine pelloidal packstone, bedded, sparry cement, isolated moldic porosity
4738.5	13.0	7.29	2.72		Ls; upper very fine-lower fine pelloidal packstone, fair interparticle and moldic porosity
4738.9	7.5	0.0094	2.73		Ls; upper very fine-lower fine pelloidal packstone, minor interparticle and moldic porosity
4739.0	5.5	0.0082	2.71		Ls; upper very fine-lower fine pelloidal packstone, minor interparticle and moldic porosity
4739.5	15.2	61.6	2.73		Ls; upper very fine-lower fine pelloidal packstone, variable good & [poor moldic porosity
4740.2	11.0	0.918	2.63		Ls; upper very fine-lower fine pelloidal packstone, moderate moldic porosity poor connectivity
4740.5	4.7	0.0028	2.67		Ls; upper very fine-lower fine pelloidal packstone, moderate moldic porosity poor connectivity
4740.9	5.4	0.0406	2.70		Ls; upper very fine-lower fine pelloidal packstone, moderate moldic porosity poor connectivity
4742.0	15.1	44.0	2.71		Ls; upper very fine-lower fine pelloidal packstone, churned good & poor moldic porosity
4743.4	16.1	17.0	2.70	Ls; upper very fine-lower fine pelloidal packstone, good interparticle & moldic porosity	
4743.5	18.7	173	2.71	2.27	Ls; upper very fine-lower fine pelloidal packstone, good interparticle & moldic porosity
4744.3	17.1	47.3	2.72		Ls; upper very fine-lower fine pelloidal packstone, good interparticle & moldic porosity, foram & brach clasts
4744.6	15.5	35.3	2.72	2.13	Ls; upper very fine-lower fine pelloidal packstone, moderate interparticle, minor moldic porosity
4745.5	16.5	37.6	2.71		Ls; upper very fine-lower fine pelloidal packstone, churned good & poor moldic porosity
4746.5	14.9	26.6	2.71	2.43	Ls; upper very fine-lower fine pelloidal packstone, churned good & poor moldic porosity
4747.5	13.9	7.18	2.70		Ls; upper very fine-lower fine pelloidal packstone, churned good & poor moldic porosity
4748.6	13.9	26.6	2.70		Ls; upper very fine-lower fine pelloidal packstone, churned good & poor moldic porosity
4749.5	16.1	75.8	2.71		Ls; upper very fine-lower fine pelloidal packstone, churned good & poor moldic porosity
4750.8	15.9	80.6	2.70		Ls; upper very fine-lower fine pelloidal packstone, churned good & poor moldic porosity
4751.6	14.0	69.2	2.70		Ls; upper very fine-lower fine pelloidal packstone, churned good & poor moldic porosity
4752.7	8.5	1.10	2.68		Ls; upper very fine-lower fine pelloidal packstone, minor interparticle & moldic porosity
4753.5	9.1	5.01	2.67		Ls; upper very fine-lower fine pelloidal packstone, minor interparticle & moldic porosity, bedded
4754.5	10.9	18.5	2.68		Ls; upper very fine-lower fine pelloidal packstone, churned good & poor moldic porosity, bedded

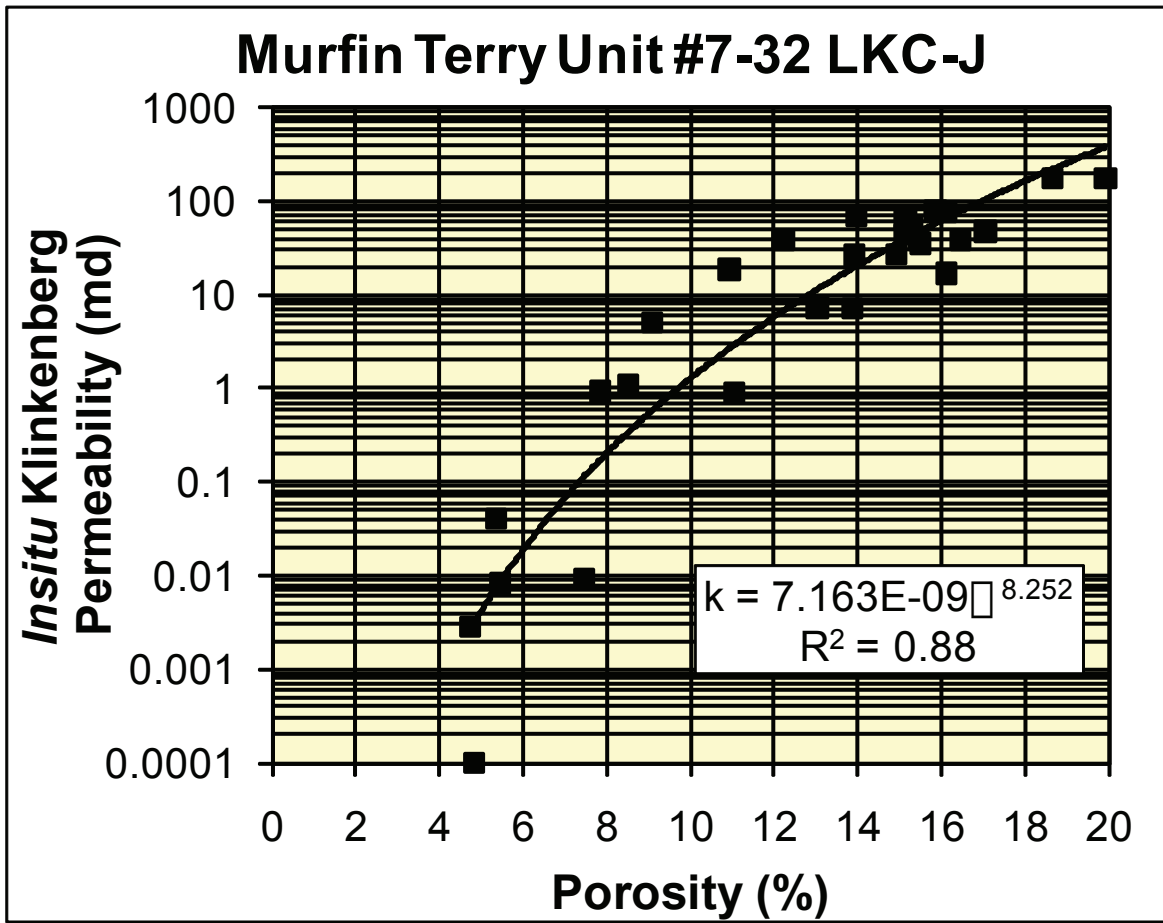


**Figure 4-4.** Permeability-porosity trend for pelloidal packstone with moderate moldic porosity development in the Lansing-Kansas City J interval.

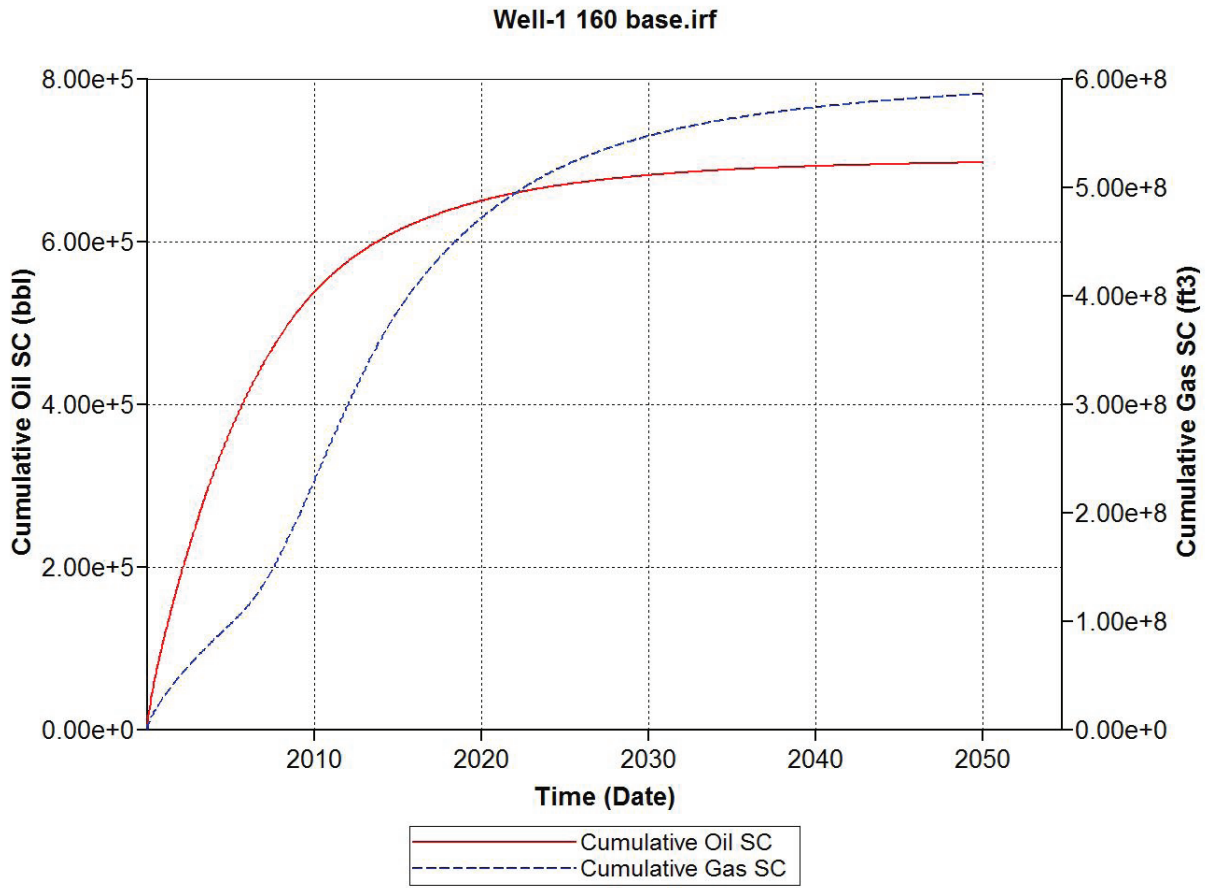


**Figure 4-5.** Estimated cumulative production for the Terry #7-32 assuming the reservoir properties shown in Table 4-1 extend over a 160-acre region.

### 4.1.2 Austin #2-27

The proposed potential L-KC well (Austin #2-27) was located in the Claussen Northeast field. A detailed production history for the Claussen Northeast field did not exist. The Austin #1-27 was completed in Sept. 2005 and the Austin #2-27 was completed in March 2006. Cumulative production from the Austin #1-27 in 2005 was 2,095 BO and through the three months prior to drill of the Austin #2-27, the Austin #1-27 produced at a rate of approximately 300 BO/month. A Tech Log Dual-Compensated Porosity log (**Fig. 4-6**) showed approximately 18 feet of potentially porous limestone from 2900 ft to 2918 ft but significant borehole washout precluded quantitative analysis. The Borehole-Compensated Sonic log also was affected by borehole rugosity (**Fig. 4-7**). If it was assumed that the porosity equaled the values shown on logs, then the L-KC interval could be assigned a porosity of 22% for approximately 10 ft centered on 2910-ft log depth. Based on the average permeability-porosity trend for oomoldic limestones (Fig. 1-15) the interval might have approximately 10 feet of 22% porosity with a permeability of 1 md but could equally have oomoldic limestone that could be as permeable as 20 md or impermeable as 0.1 md. Deep resistivity over the interval averaged 24 ohm-m. A standard Archie solution ( $a = 1$ ,  $m = 2$ ,  $n = 2$ ) would calculate a water saturation of 22%. However, Archie parameters appropriate for oomoldic rocks in published work (Doveton, 2003, from Byrnes, 2001;  $a = 10$ ,  $m = 1.4$ ,  $n = 2$ ) estimate water saturation near 46%.

Simple flow simulation of a 10-ft-thick interval with this range in properties (**Fig. 4-8**) show that cumulative oil production could range widely for the permeability range. Oil rates of approximately 300 BO/month were consistent with the higher permeability model. Based on the well production this analysis supported the potential for a second well.

Well and core properties for the subsequent Austin #2-27 are discussed in Section 5. The core confirmed that porosities averaged near 24% for a 10-ft-thick interval. Permeability measurements show that the permeability in the porous interval was less than the generalized L-KC permeability-porosity trend except for a 2-ft-thick interval in the uppermost, less porous portion of the reservoir. The electrical properties were consistent with the model discussed in Section 1.4. Use of the Archie parameters appropriate for these rocks estimates water saturation of approximately 64% over the most porous interval.

Numerical flow simulation confirmed the obvious conclusion that this well would be nonproductive (**Fig. 4-9**). Well test performance confirmed this conclusion.

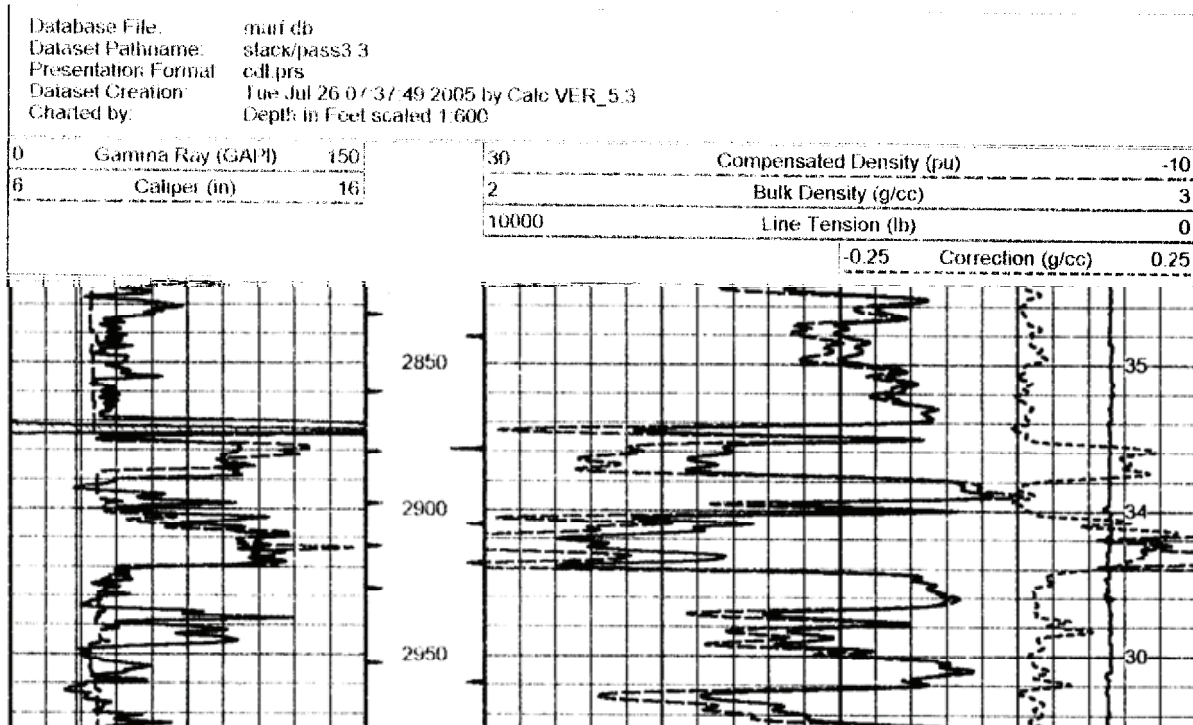


**Figure 4-6.** Tech Log Dual-Compensated Porosity log for the Austin #1-27 in Claussen Northeast field. Significant washout precluded quantitative analysis.

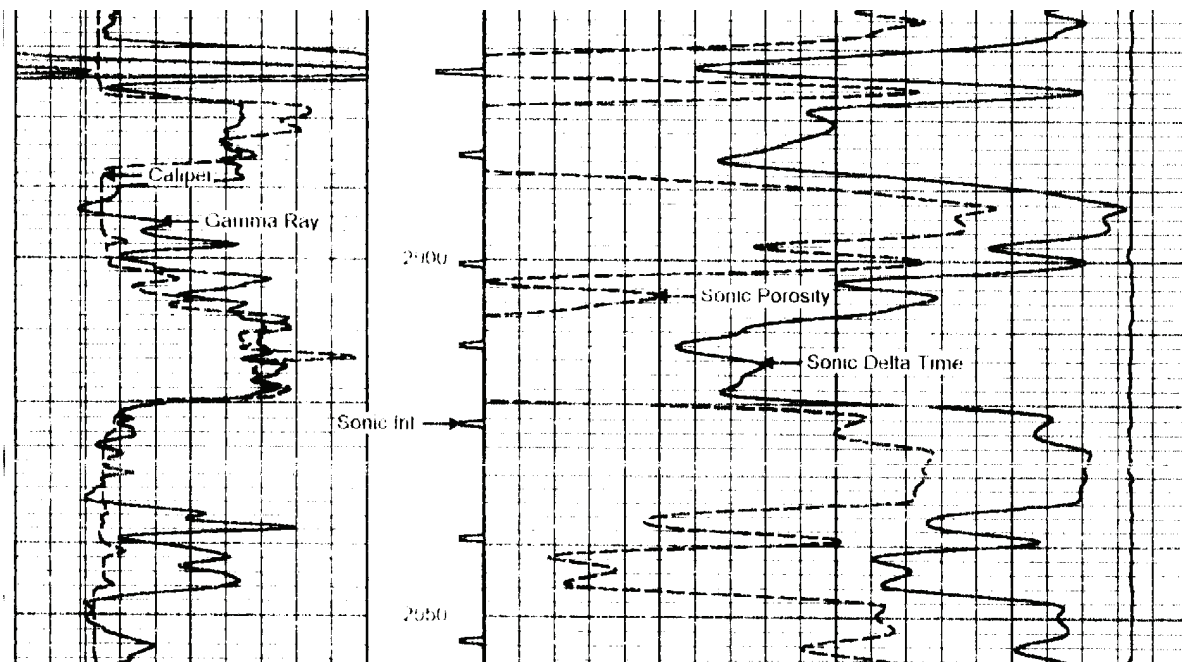


**Figure 4-7.** Tech Log Borehole-Compensated Sonic log for the Austin #1-27 in Claussen Northeast field (scaled from -10 to 30, right to left).

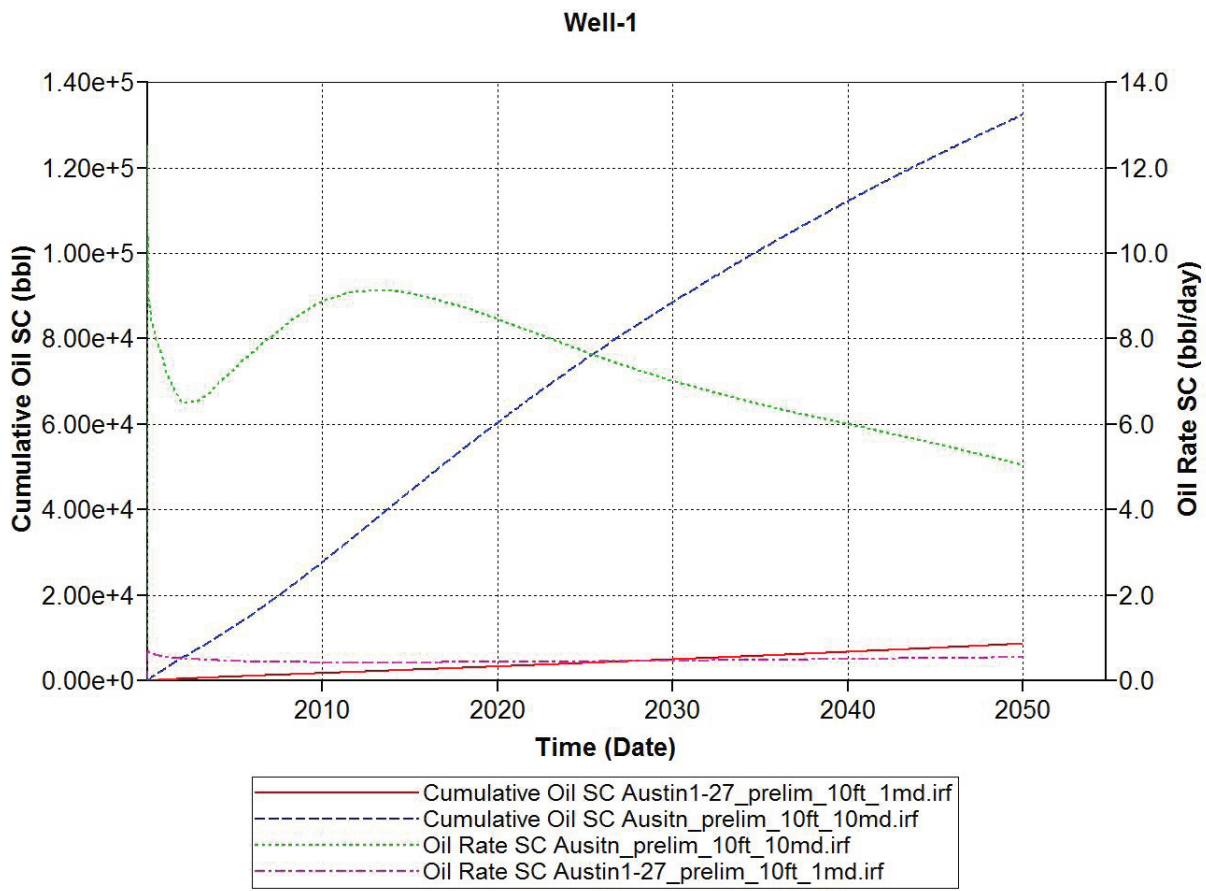


**Figure 4-8.** Numerical flow simulation prediction of Austin #1-27 production assuming reservoir properties estimated from wireline logs as discussed in text.

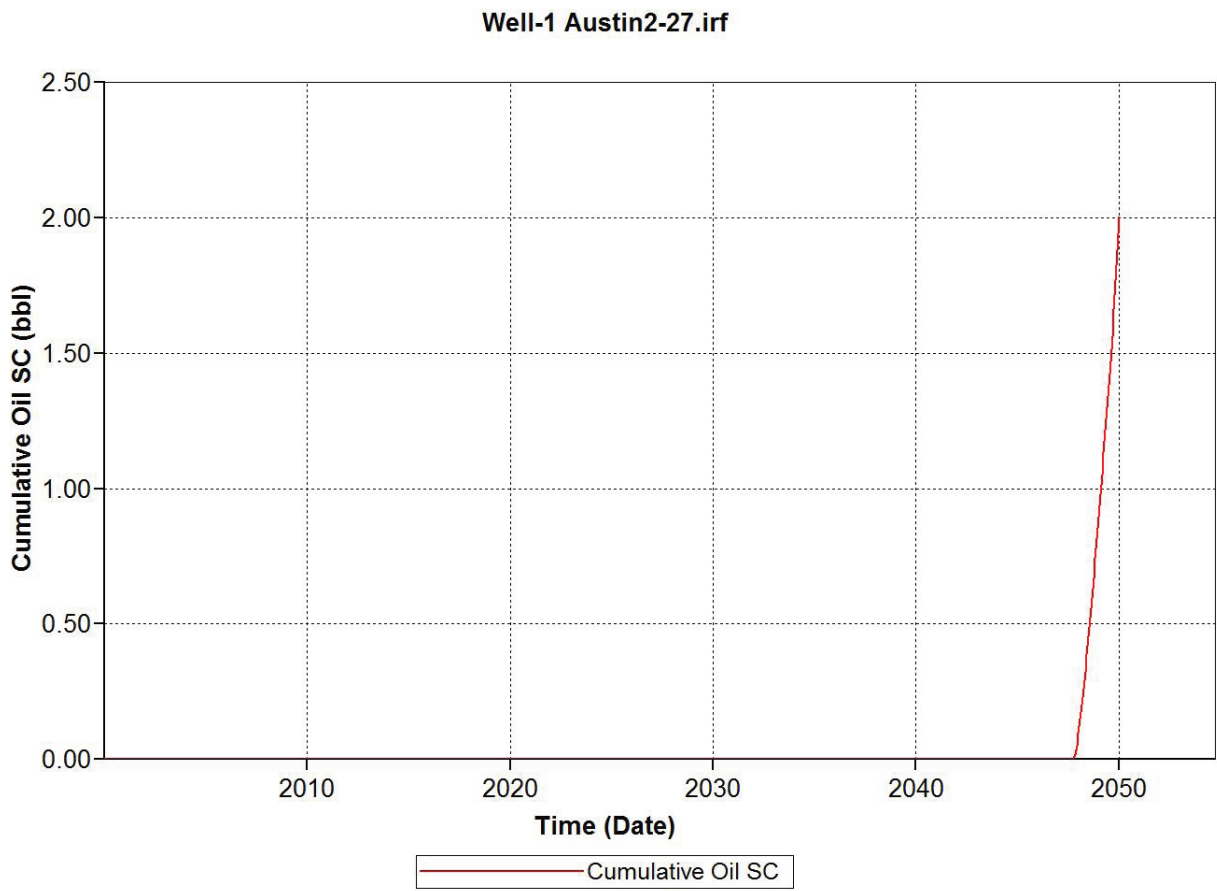


**Figure 4-9.** Flow simulation estimation of potential performance of Austin #2-27 well showing that the well would be nonproductive. Well testing confirmed this conclusion.

## 4.2 Arbuckle

### 4.2.1 Hadley L#4

The Hadley L#4 (API 15-051-25131; W/2 SE sec. 30, T. 11 S., R. 17 W.) is located in Bemis-Shutts field. Bemis-Shutts field has produced over 260 MMBO oil in a history dating back to the earliest discovery well in 1928. The Hadley Lease in this field has been active since 1938 and the Hadley L#4 infill well (**Fig. 4-10**) was testing an area that had been shut-in for many years.

Wireline log analysis showed the two intervals with potential; 3559 ft-3572 ft (with porosity exceeding 24%) and 3620 ft-3640 ft (with porosity ranging from 8% to 16% with associated water saturation ranging from 70% to 40%, respectively; **Fig. 4-11**). Pickett-plot analysis indicated the intervals from 3623 ft to 3630 ft exhibited potential (**Fig. 4-12**). Core was obtained in this area and both full-diameter and plug analysis were performed. In addition, electrical properties were measured on 14 select samples. These analyses confirmed that the Archie cementation exponents were approximately equal to  $m = 2 \pm 0.1$  although it is interesting to note that the population may be bimodal (**Fig. 4-13**). Core analysis and description showed the highly vertically heterolithic nature of the Arbuckle. Of particular note is the high-frequency cyclicity of porosity and permeability values, reflecting the rock properties associated with each thin peritidal sequence (**Fig. 4-14**). This same vertical cyclicity is represented in numerical simulation (**Fig. 4-15**).

At the Hadley L#4 location, and by analogy much of the Arbuckle reservoir system, well productivity is controlled by a combination of factors. The transition zone issues discussed in previous sections apply to this location, but additional important factors in the Arbuckle include 1) frequency and horizontal permeability of very high permeability beds, 2) frequency and vertical permeability of very low permeability beds, 3) time period in reservoir history when new well is completed and extent of prior depletion, and 4) underlying aquifer permeability and consequent pressure support. For reservoirs with the very high permeability beds, like the Hadley L#4, the initial reservoir conditions are strongly influenced by the transition zone properties; however, very early in the productive life of the reservoir, the permeability architecture of the system and the aquifer support become the dominant influences on performance.

Cumulative oil for this system when it begins at virgin pressures reach up to 400 MBO at 50 years with associated gas of 360 MMscf (**Fig. 4-16**). Water is produced from the connate reservoir water only in the first several years of well production. Following this period water production is principally associated with bottom-water drive influx from the underlying aquifer and reaches an equilibrium rate that for this well is approximately 850 BWPD.

In an area of prior pressure depletion, but where a well is introduced into an area that was inactive for an extended period of time, cumulative recovery is less than in a virgin area but can still be economic (**Fig. 4-17 and Fig. 4-18**).

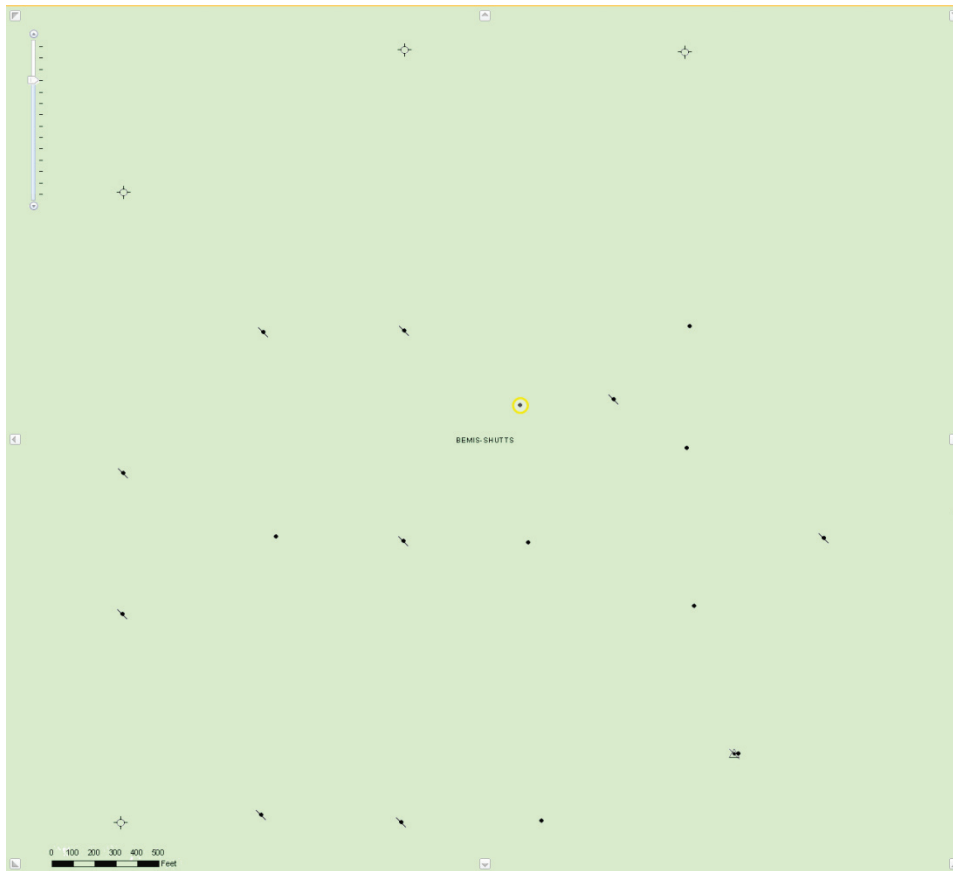


**Figure 4-10.** Location of Hadley L#4 in Bemis-Shutts field. The Hadley L#4 is an infill well within a mature part of the field that had been shut-in for many years.

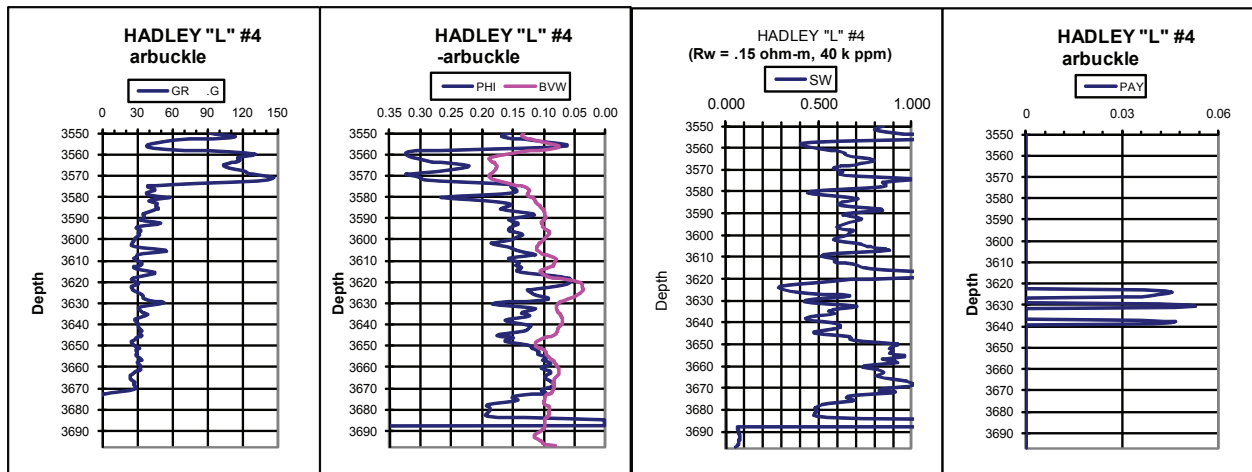


**Figure 4-11.** Log analysis of the Hadley L#4 well showing interval at 3620 ft-3640 ft in which pay potential was identified.

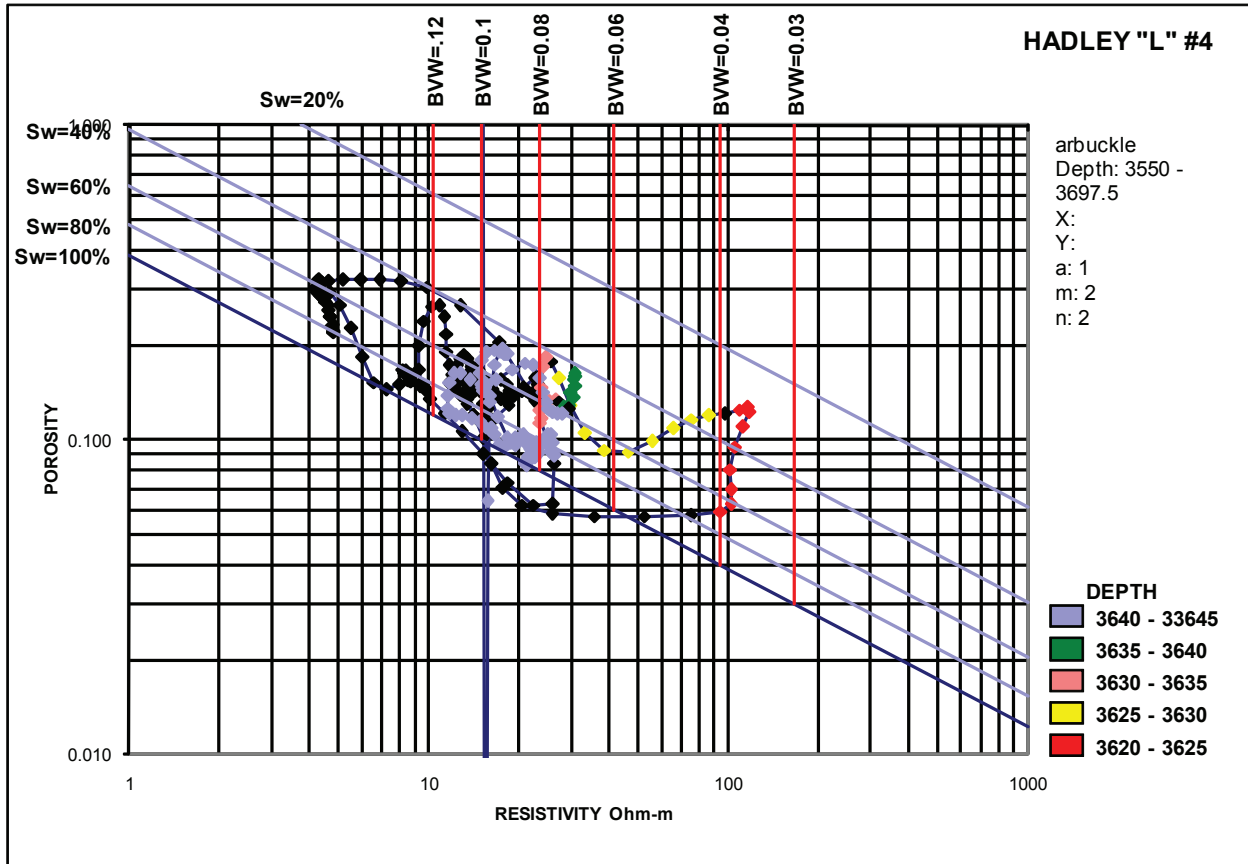


**Figure 4-12.** Pickett-plot analysis of the Arbuckle interval in Hadley L#4 showing interval with potential from 3623 to 3630 ft.

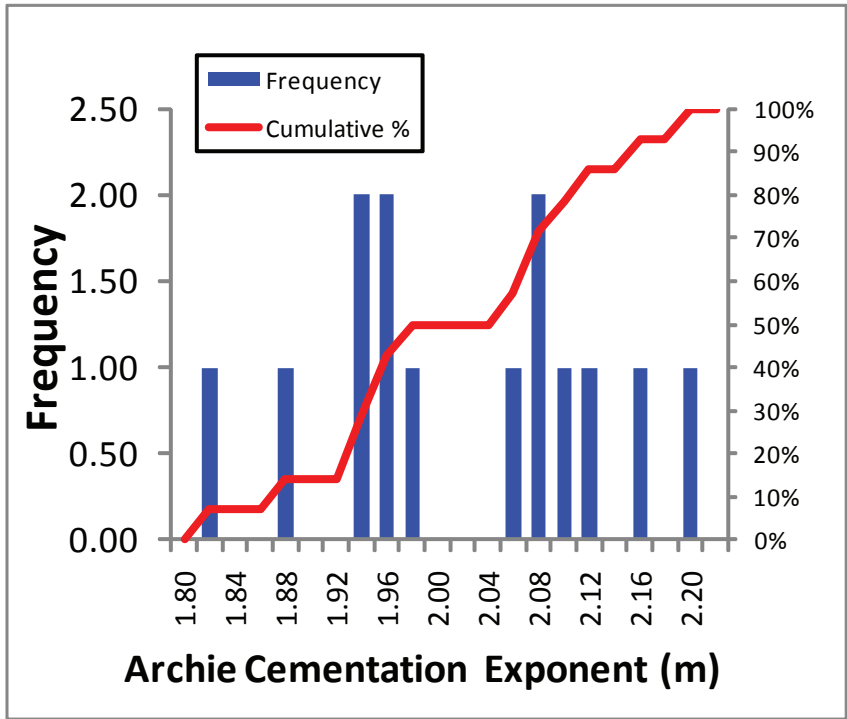


**Figure 4-13.** Histogram of Arbuckle Archie cementation exponents. Values average  $2 \pm 0.1$  though it is interesting to note possible bimodal distribution.

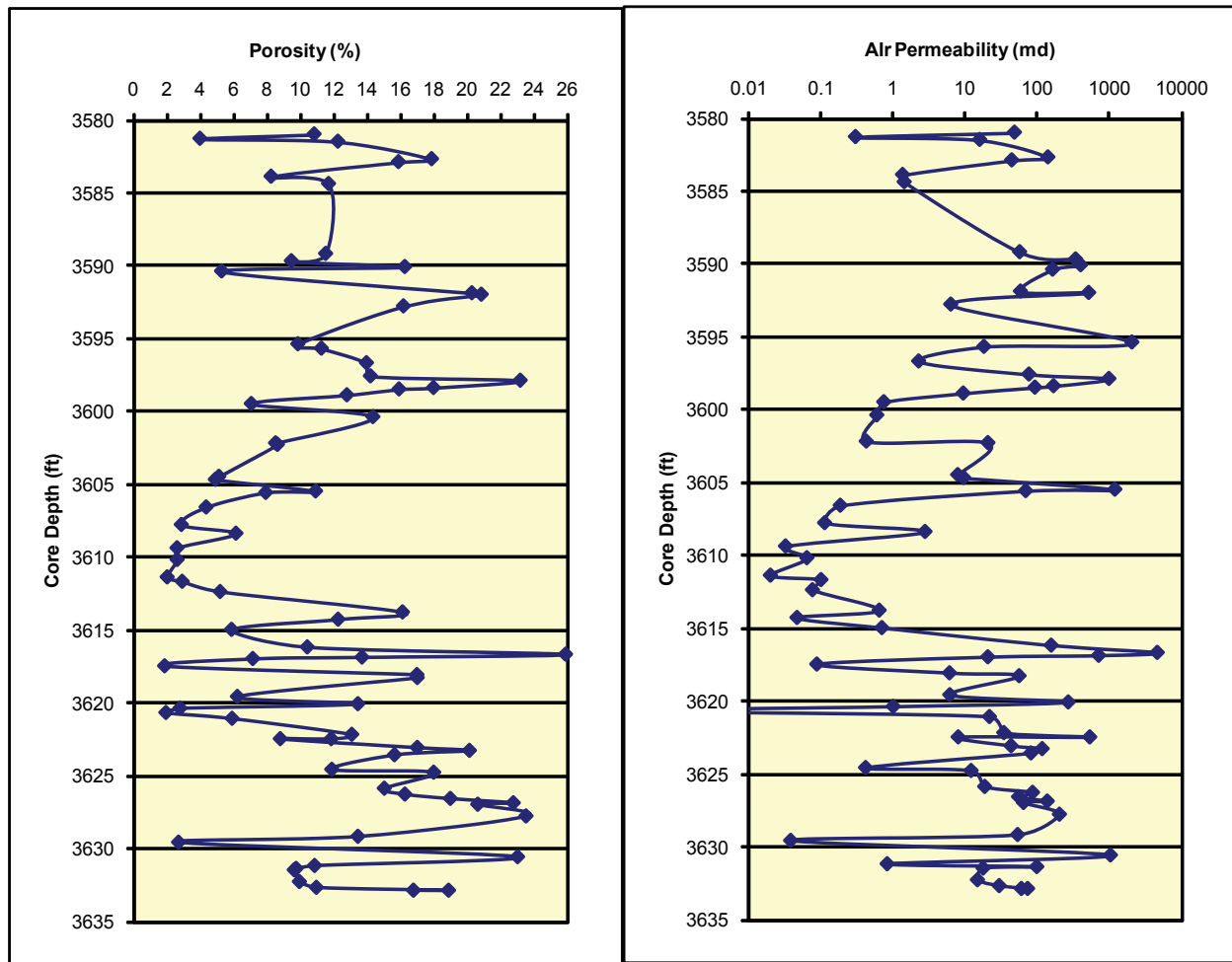


**Figure 4-14.** Porosity and permeability profiles showing high-frequency cyclicality associated with changing rock properties in each thin peritidal sequence.

Permeability I (md) 2050-01-01

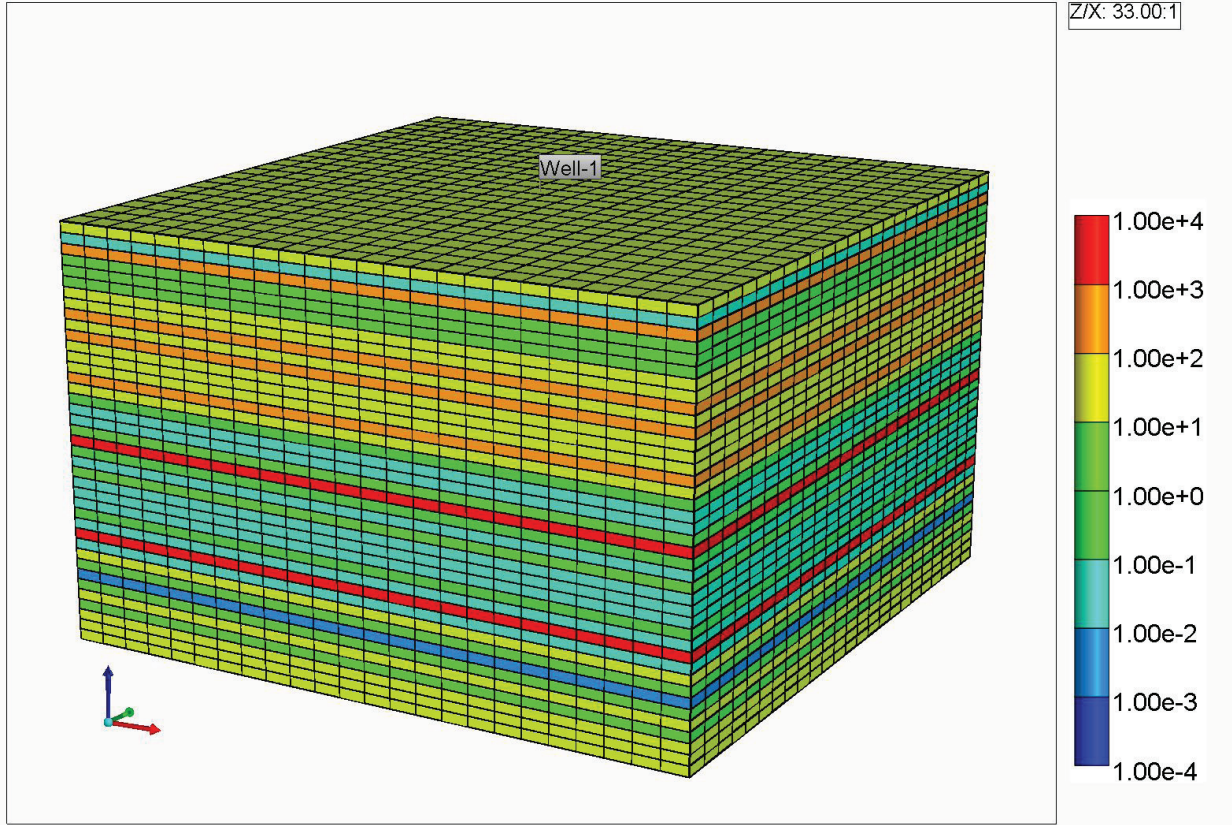


**Figure 4-15.** Horizontal-permeability distribution for Hadley L #4 location showing high-frequency cyclicality associated with changing rock properties in each thin peritidal sequence.

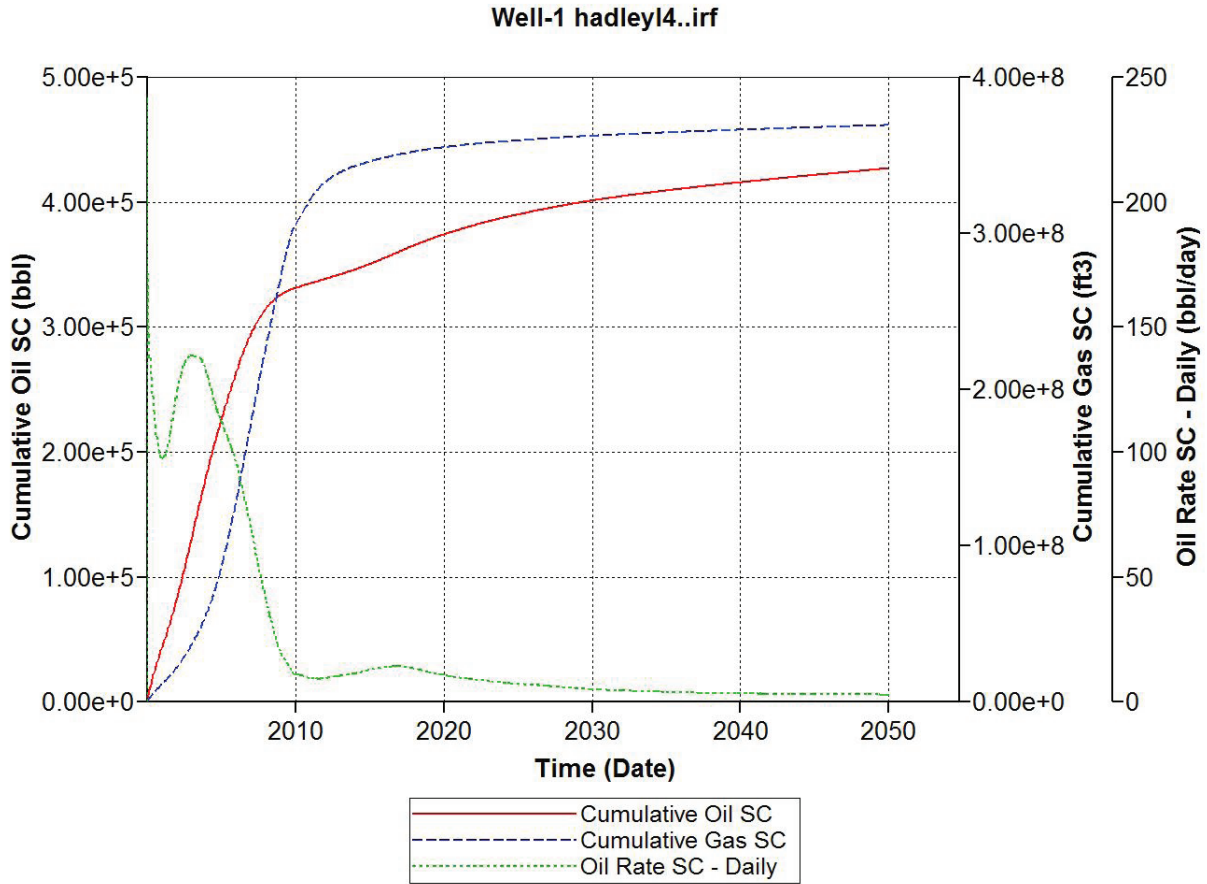
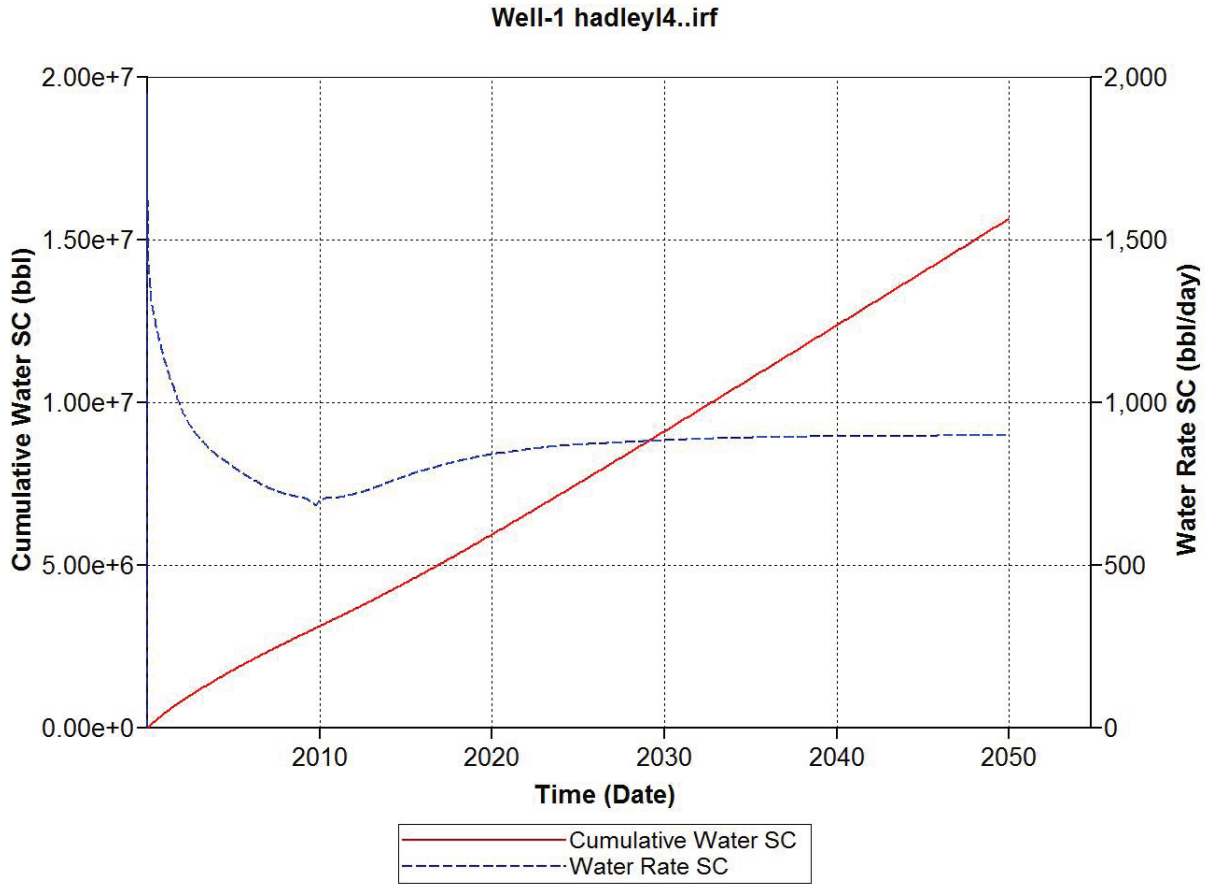
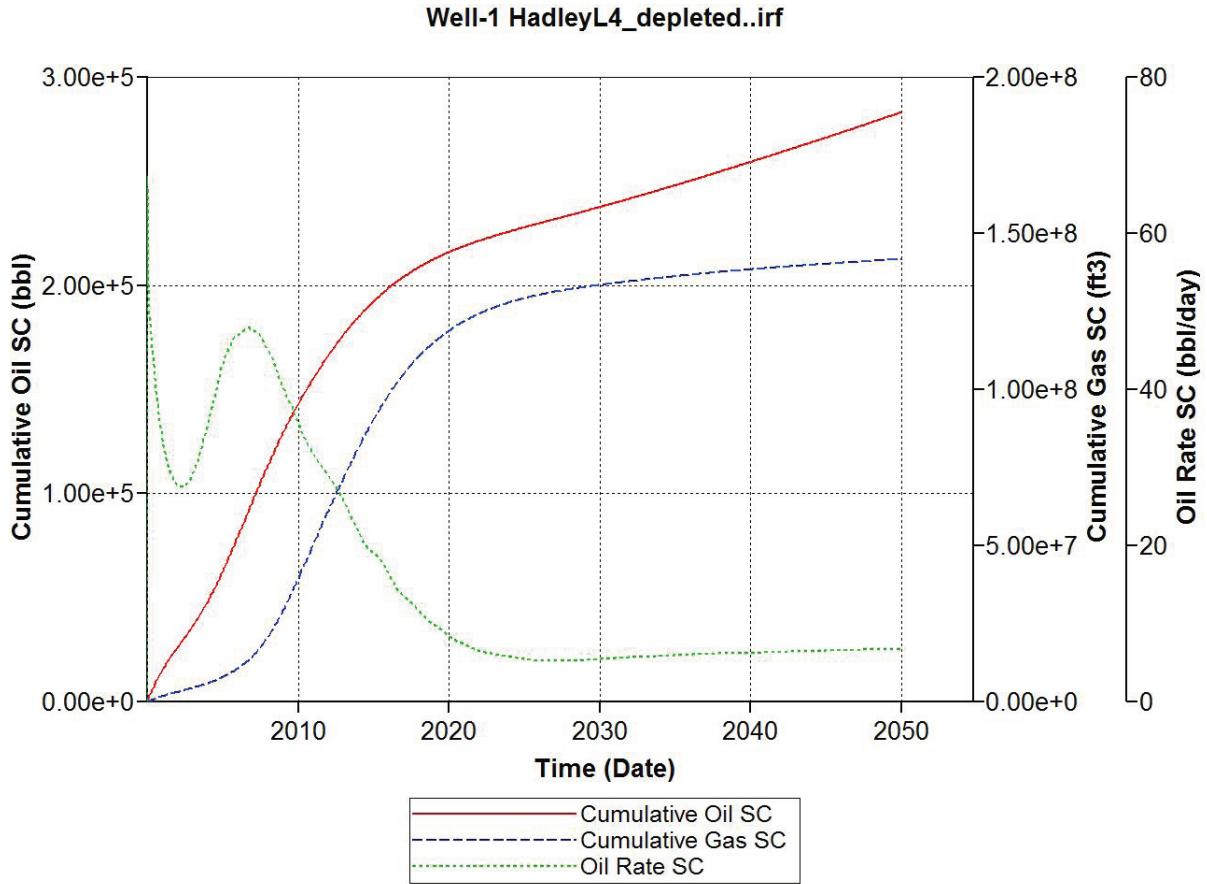


Figure 4-16. Simulation estimate of cumulative gas and oil and oil rate for Hadley L#4 using model shown in Figure 4-15 and for assumed initial pressure condition of  $P_i = 1,500$  psi.



**Figure 4-17.** Simulation estimate of cumulative water and water rate for Hadley L#4 using model shown in Figure 4-15 and for assumed initial pressure condition of  $P_i = 1,500$  psi.



**Figure 4-18.** Simulation estimate of cumulative gas and oil and oil rate for Hadley L#4 using model shown in Figure 4-15 and for assumed initial depleted pressure condition of  $P_i = 700$  psi.

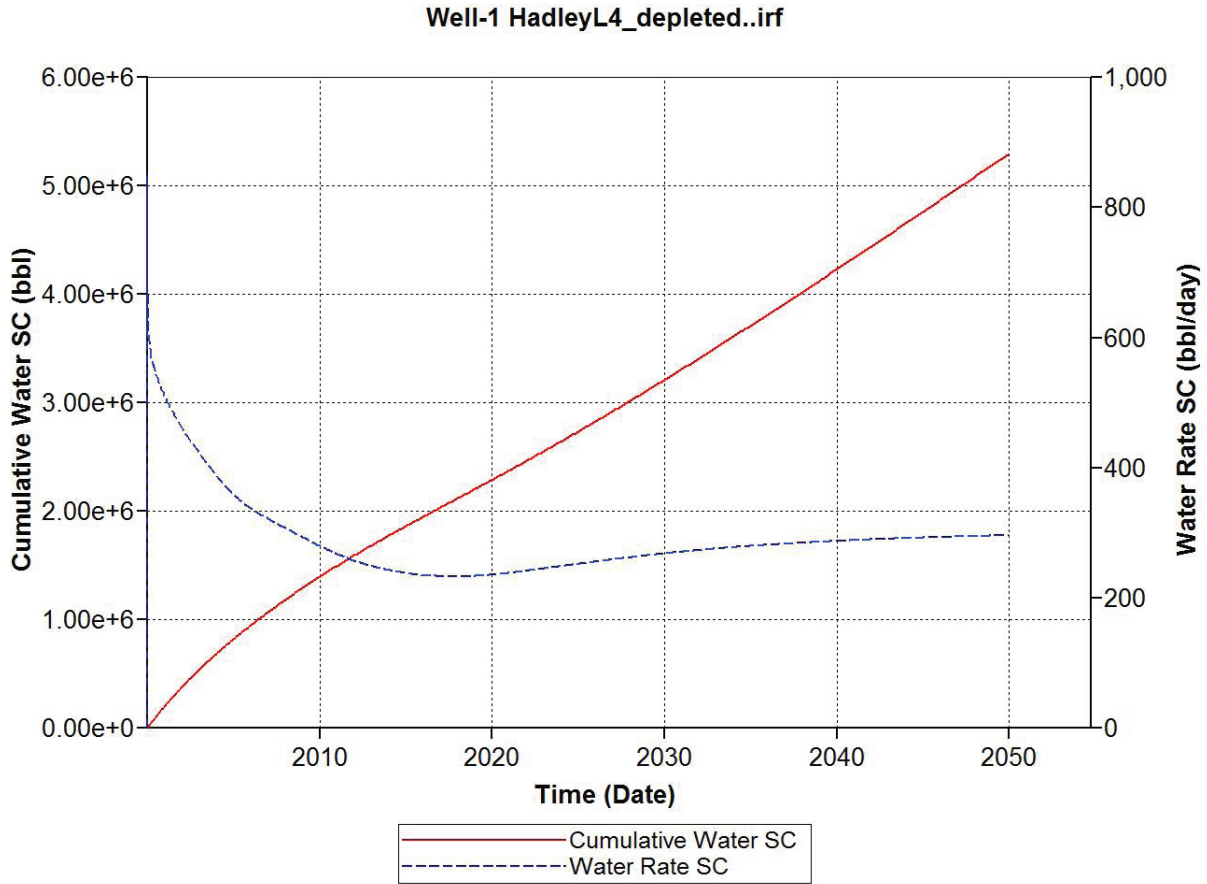


**Figure 4-19.** Simulation estimate of cumulative water and water rate for Hadley L#4 using model shown in Figure 4-15 and for assumed initial depleted pressure condition of  $P_i = 700$  psi.

### 4.2.2 Keja #1-3

The proposed potential Arbuckle well (Keja #1-3) is located in Hadlew field on the southwest boundary of Trico field (Sec 5.2, Fig. 5-13 and 5-14). A detailed production history for the Hadlew field did not exist. This well location was selected to penetrate the Arbuckle in an area already verified to have Arbuckle production in the Trico field and in the Hadlew Unit #1-3 (API #15-195-22320) completed 02/21/2006 at location 2600 ft FSL 660 ft FWL sec.3, T. 11 S., R. 12 W. The Keja #1-3 (API# 15-195-22357-0001) spud on 04/25/2006 at location 1815 ft FSL 850 ft FWL E/2 NW SW sec. 3, T. 11 S., R. 12 W. (Fig. 5.13 and Fig. 5.14) and cored the Arbuckle on 05/02/2006. Core was obtained for the interval 3695-3718 ft when core barrel jammed. Core #2 from 3719-3776 ft was obtained on 05/03/2006. Figure 5-15 shows that the Arbuckle interval was located at the depth anticipated from the spotting well.

General properties in the proposed location represented an extrapolation of wireline log-predicted properties from Hadlew Unit #1-3 well to the north. A Tech Log Dual-Compensated Porosity log (Fig. 4-20) showed approximately 40 feet of potentially porous dolomite from 3706 ft to 3746 ft. This interval exhibited an average porosity of 10%. Based on the average permeability-porosity trend for the Arbuckle (Fig. 1-30), the interval might have approximately 40 feet of 10% porosity with a permeability of 1 md and with a possible range in permeability from 10 md to 0.1 md. Deep resistivity over the interval ranged from 40 to 80 ohm-m (Fig. 4-21). A standard Archie solution ( $a = 1$ ,  $m = 2$ ,  $n = 2$ ) for this would calculate a water saturation of 50% for an assumed formation brine resistivity of 0.1 ohm-m.

Simple flow simulation of a 40-ft-thick interval with this range in properties indicated that cumulative oil production could range widely for the permeability range. Initial oil rates of approximately 300 BO/month were consistent with the regional Arbuckle wells (Fig. 4-22). As with the Hadley L#4 strong bottom water drive resulted in significant water production (Fig. 4-23). Based on the well production this analysis supported the potential for drilling the Keja #1-3.

Well and core properties for the subsequent Keja #1-3 are discussed in Section 5.2. Core porosities average 8% over the 40-ft interval cored. Permeability measurements show that the log-normal average permeability for the cored interval is 0.6 md, generally consistent with the average Arbuckle trend.

Core analysis for the Keja #1-3 revealed that the Arbuckle in this location exhibits the characteristic high-frequency changes in lithologic and petrophysical properties associated with these thin peritidal sequence deposits (Fig. 5-15 and Fig. 5-16). Porosities in these cycles range from 0% to 20% and associated permeabilities change from values as low as 0.0002 md to as high as 300 md.

As with the Hadley L#4 location, and by analogy much of the Arbuckle reservoir system, well productivity is controlled by the combination of factors including 1) frequency and horizontal permeability of very high permeability beds, 2) frequency and vertical permeability of very low permeability beds, 3) time period in reservoir history when new well is completed and extent of

prior depletion, and 4) underlying aquifer permeability and consequent pressure support. Unlike the Hadley L#4, the Arbuckle in this location only has a few feet of high permeability (e.g.  $K_{ik} > 100\text{md}$ ) and KH ( permeability-feet) for the interval is 700 md-ft. For reservoirs with the very high permeability beds, like the Hadley L#4, the initial reservoir conditions are strongly influenced by the transition zone properties but very early in the productive life of the reservoir the permeability architecture of the system and the aquifer support become the dominant influences on performance. In the Keja #1-3 location the lower permeabilities change the influences on production to be less influenced by the few highest permeability beds and more influenced by transition zone properties and vertical permeability.

The numerical flow model for the Keja #1-3 shows the highly variable nature of porosity (**Fig. 4-24**) and permeability (**Fig. 4-25**) vertically in the reservoir. Cumulative oil for this system when it begins at virgin pressures reaches up to 165 MBO at 50 years with associated gas of 160 MMscf (**Figure 4-26**). Water is produced from the connate reservoir water only in the first several years of well production. Following this period water production is principally associated with bottom-water drive influx from the underlying aquifer and reaches a pseudo-equilibrium rate that for this well of 40-60 BWPD (**Fig. 4-27**).

In an area of prior pressure depletion, but where a well is introduced into an area that was inactive for an extended period of time, cumulative recovery is less than in a virgin area but can still be economic (**Fig. 4-17 and Fig. 4-18**).

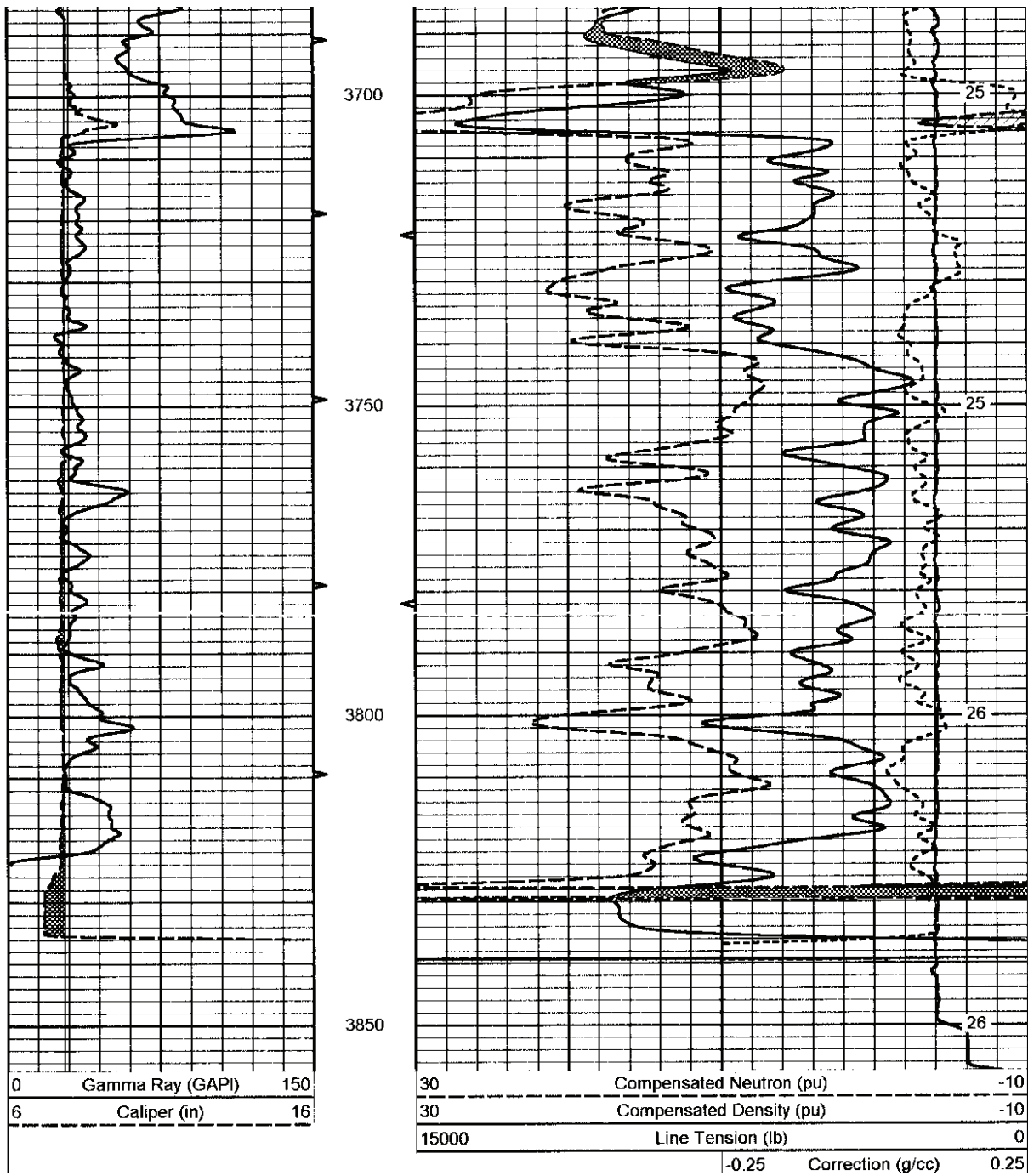
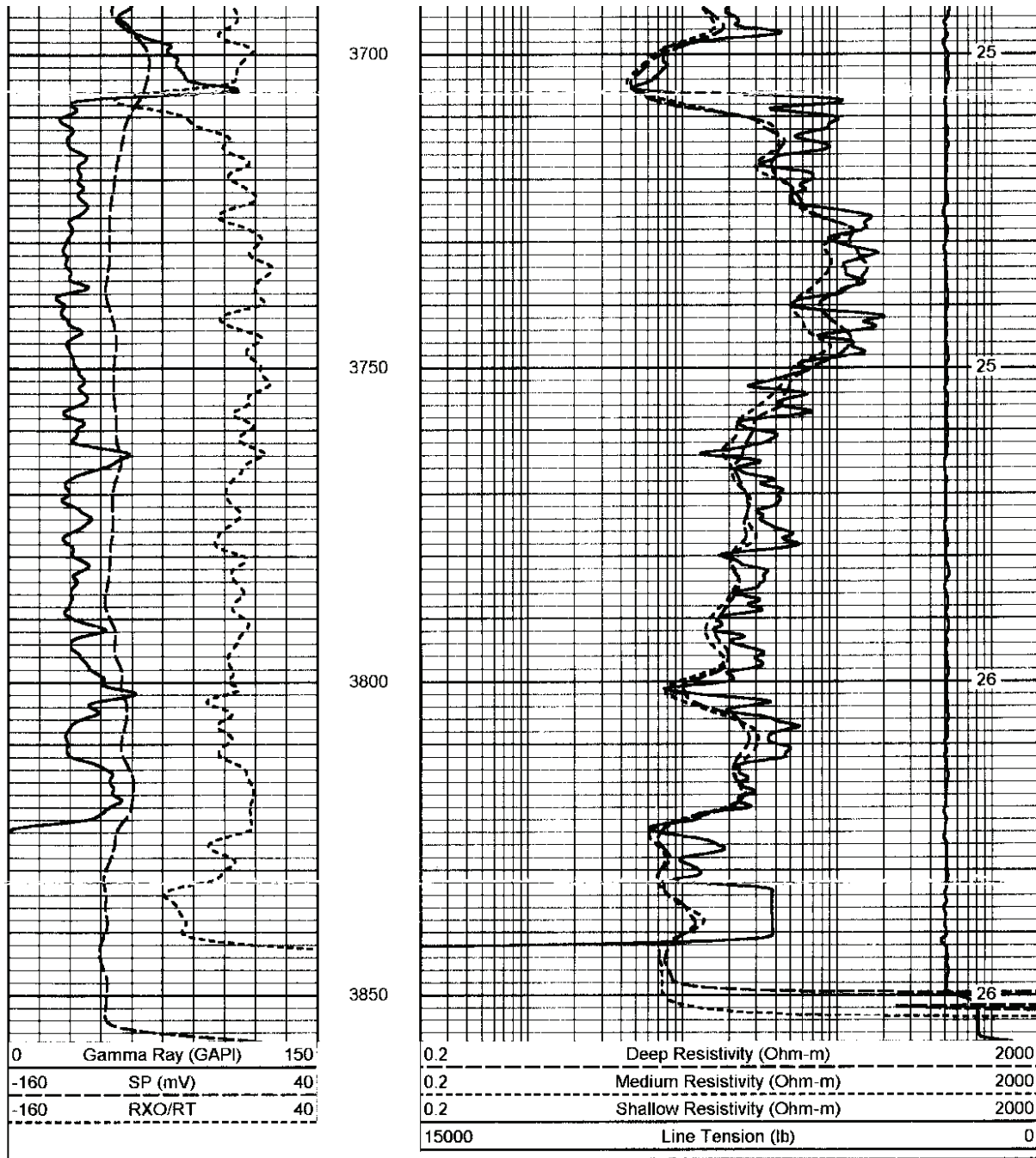
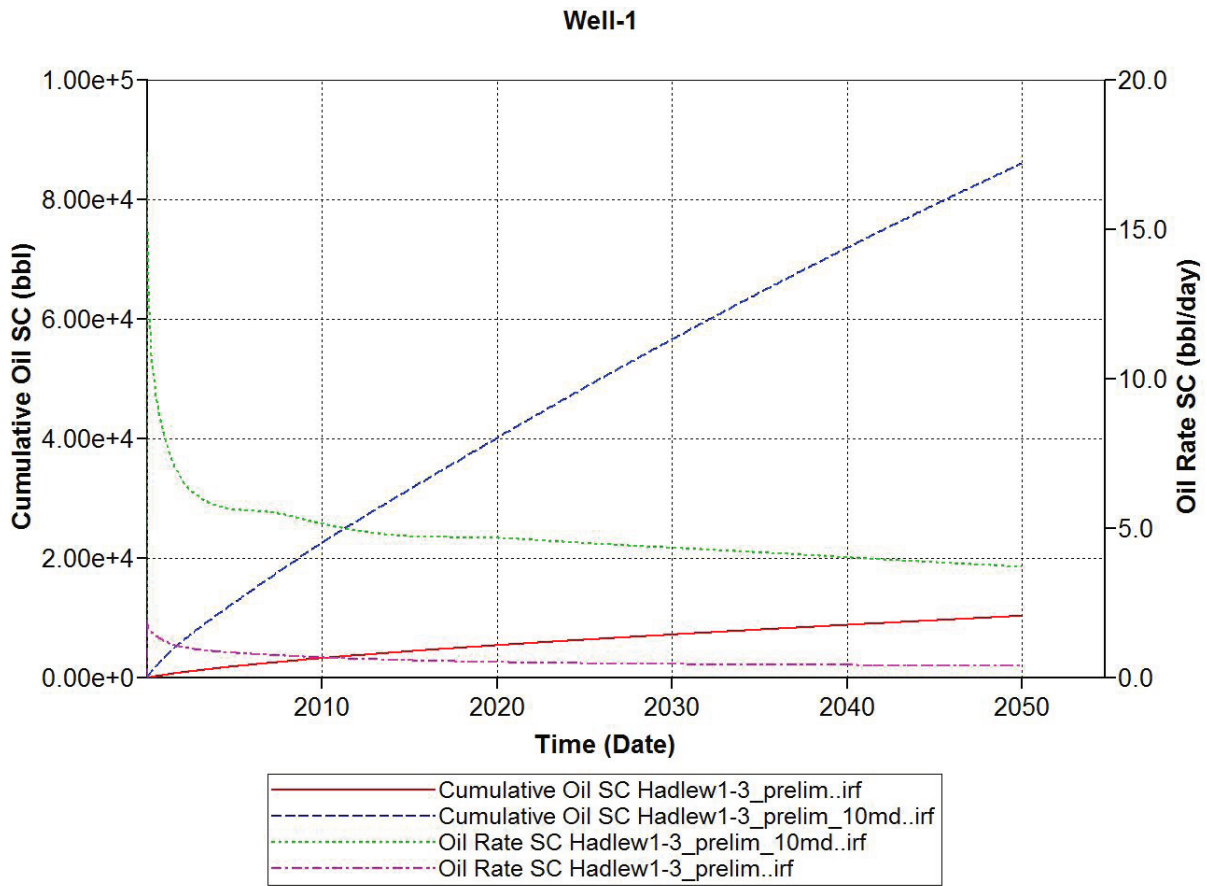


Figure 4-20. Dual-compensated porosity log for the Hadlew Unit #1-3 well drilled prior to the Keja #1-3. Top of Arbuckle is at 3706 feet. Upper Arbuckle exhibits average porosity near 10%.



**Figure 4-21.** Dual-induction log for the Hadlew Unit #1-3 well drilled prior to the Keja #1-3. Top of Arbuckle is at 3706 feet. Upper Arbuckle exhibits deep resistivity ranging from 40 to 80 ohm-m.



**Figure 4-22.** Flow simulation estimate of cumulative gas and oil and oil rates for Hadlew #1-3 using basic properties modeled for wireline log analysis and for and assumed initial pressure condition of  $P_i = 1,500$  psi.

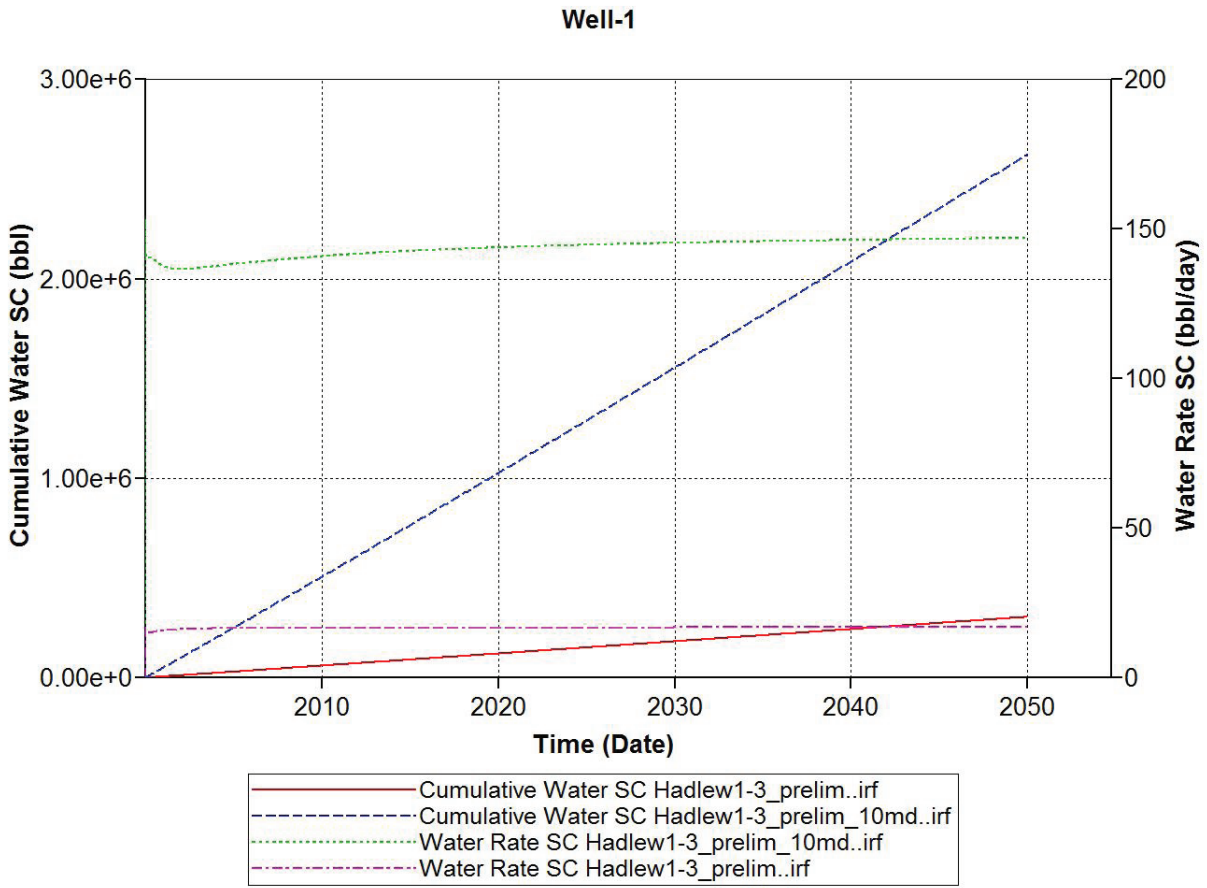


**Figure 4-23.** Flow simulation estimate of cumulative water oil and oil rates for Hadlew #1-3 using basic properties modeled for wireline log analysis and for and assumed initial pressure condition of  $P_i = 1,500$  psi.

Porosity 2000-01-01

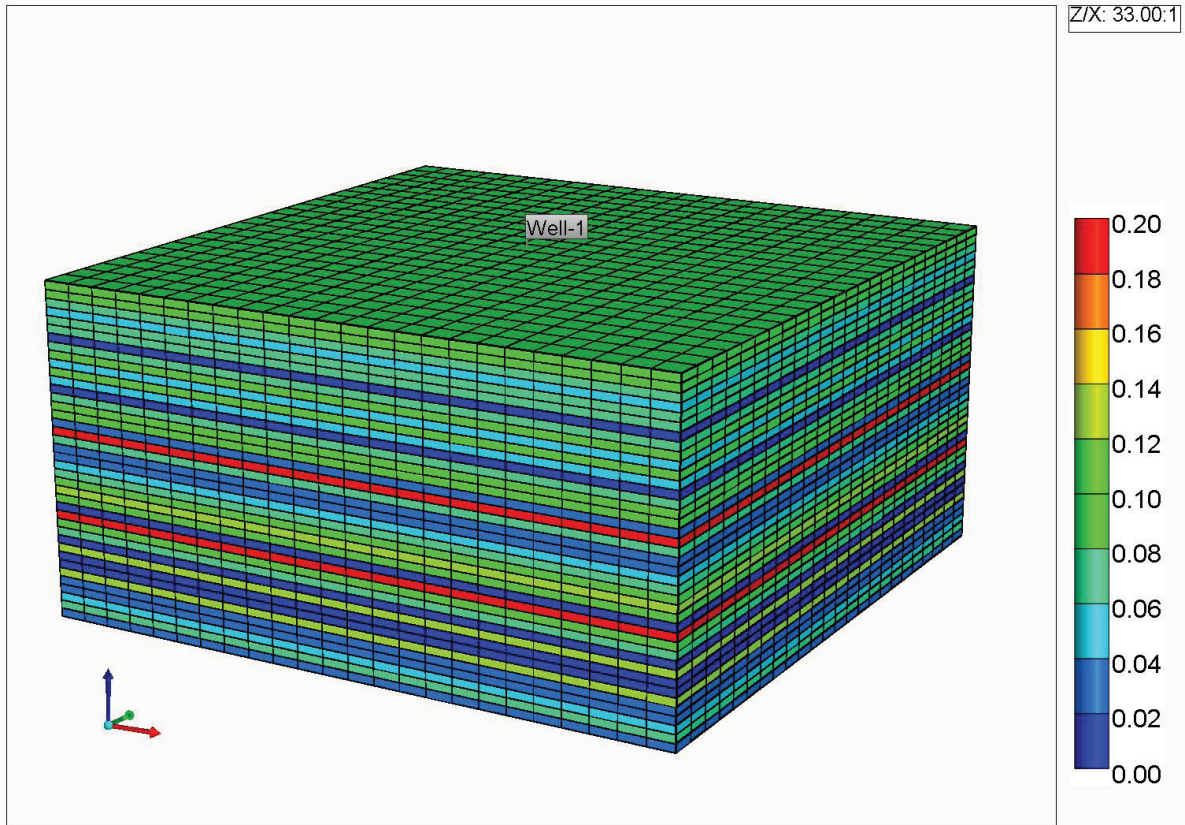


**Figure 4-24.** Porosity distribution for Keja #1-3 location showing high-frequency cyclicality associated with changing rock properties in each thin peritidal sequence.

Permeability I (md) 2000-01-01

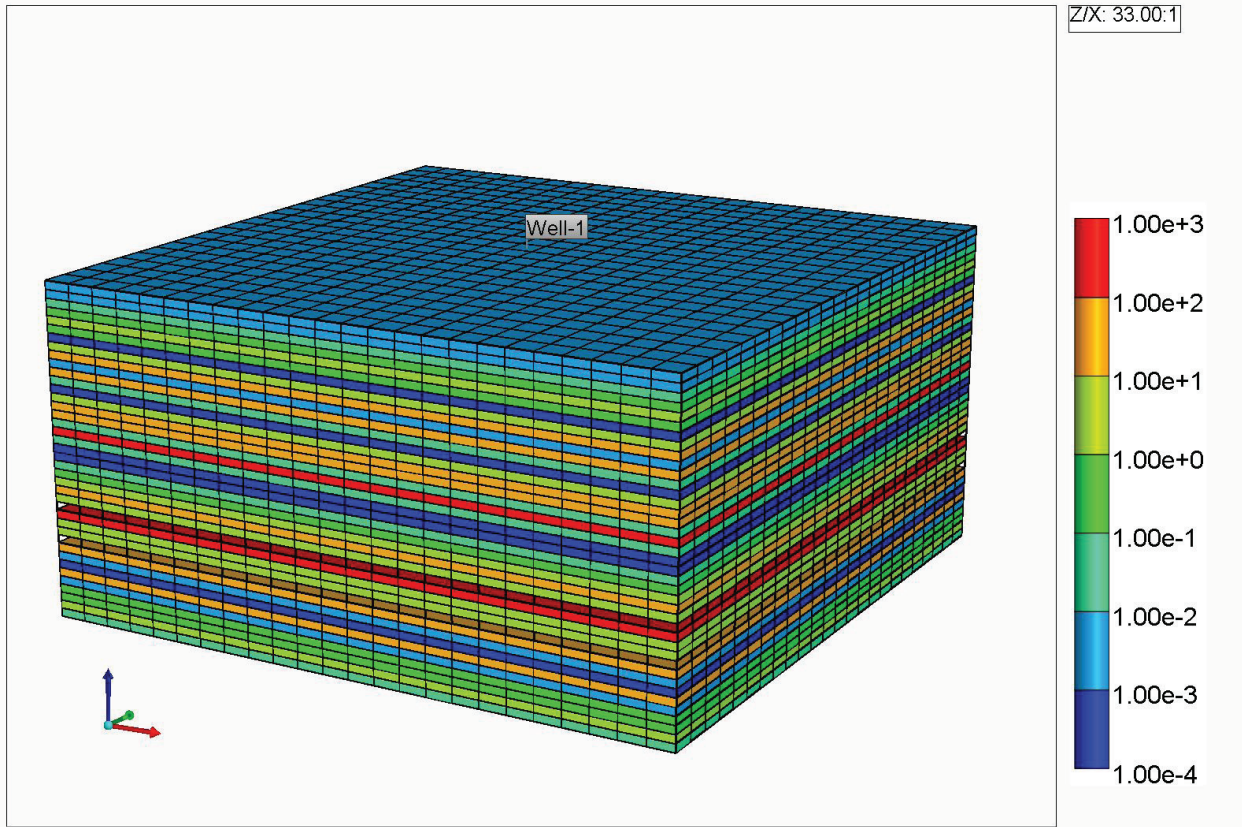


**Figure 4-25.** Horizontal-permeability distribution for Keja #1-3 location showing high-frequency cyclicality associated with changing rock properties in each thin peritidal sequence.

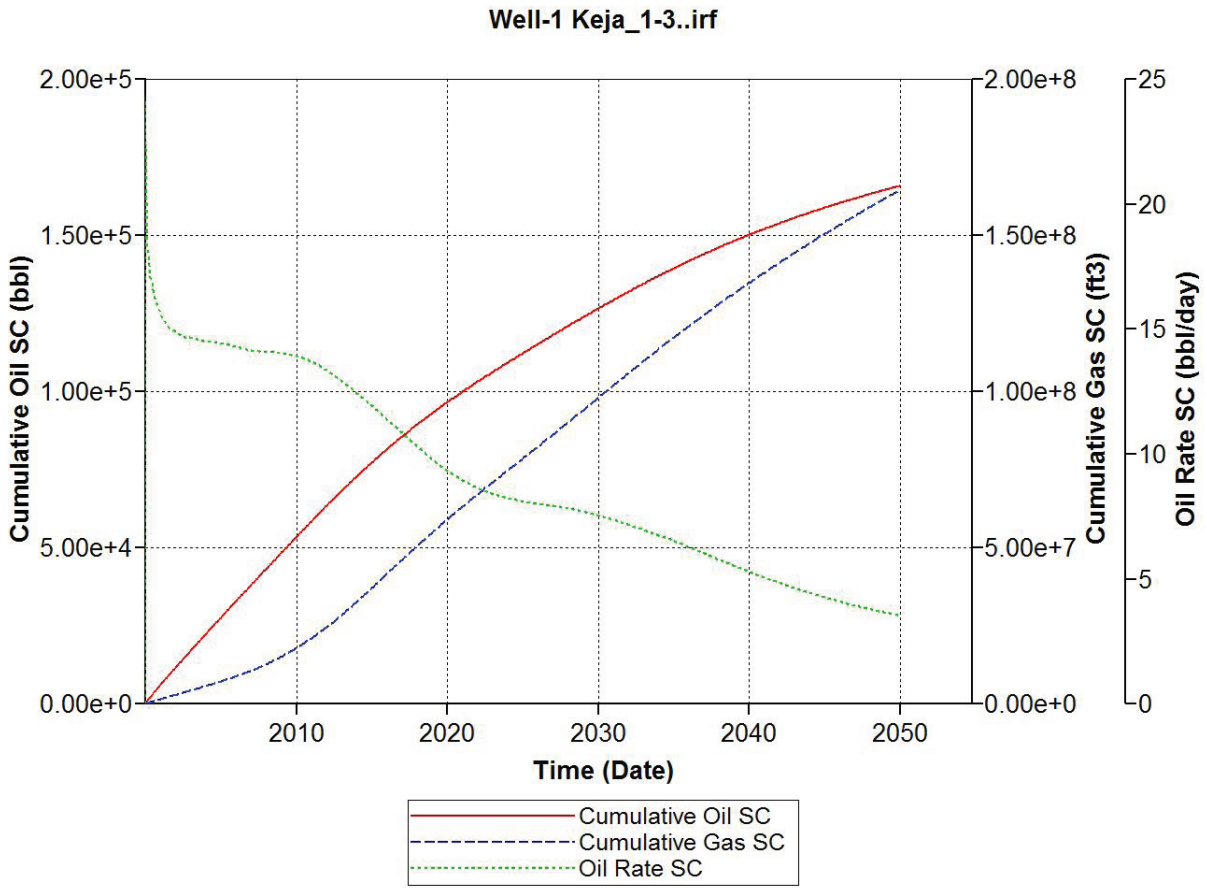


**Figure 4-26.** Flow-simulation estimate of cumulative gas and oil and oil rates for Keja #1-3 using basic properties modeled from wireline log and core analysis and for assumed initial pressure condition of  $P_i = 1,500$  psi.

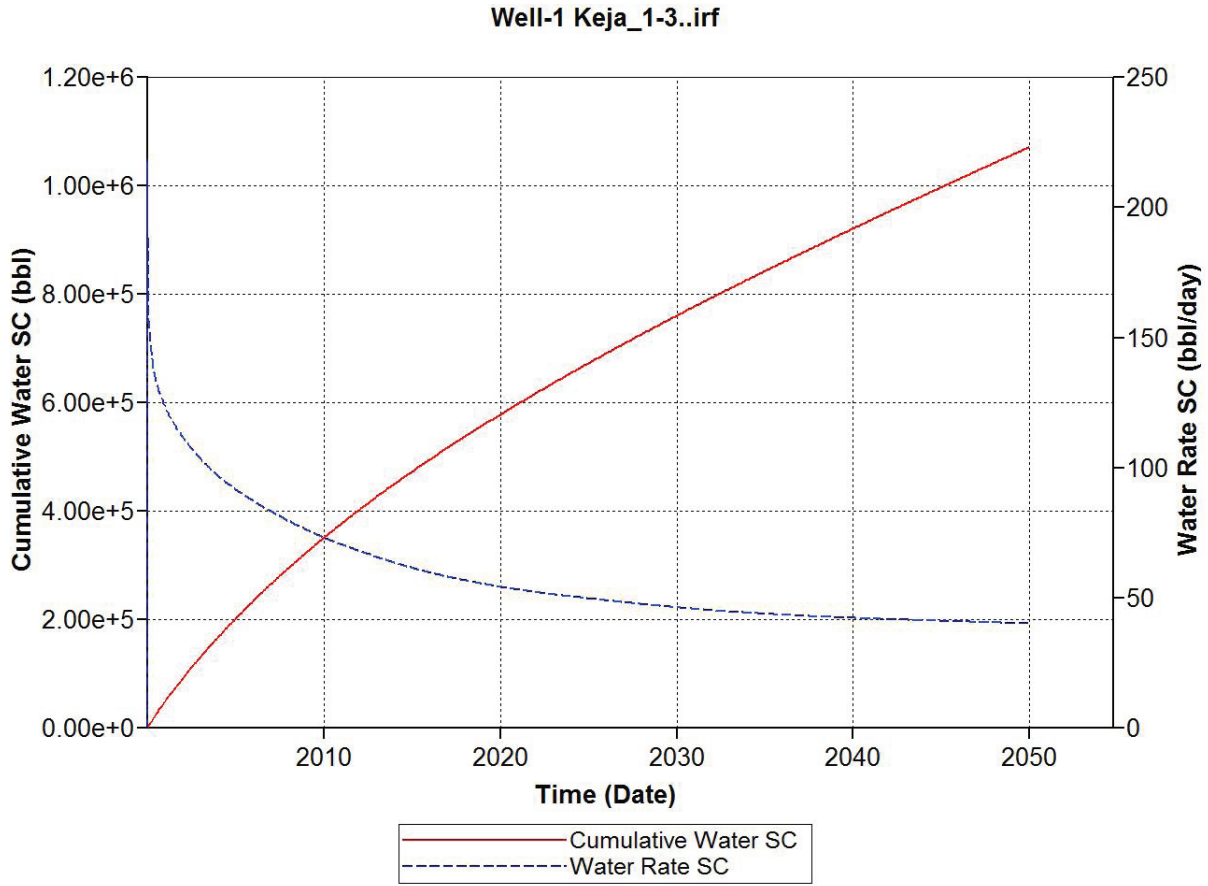


**Figure 4-27.** Flow-simulation estimate of cumulative water oil and oil rates for Keja #1-3 using basic properties modeled from wireline log and core analysis and for and assumed initial pressure condition of  $P_i = 1,500$  psi.

## 5.0 Coring the Lansing-Kansas City and Arbuckle

### 5.1 Lansing-Kansas City Core: Austin 2-27

#### 5.1.1 Well Location, Drilling, and Testing

To obtain a native-state core of the Lansing-Kansas City Formation the industry partner in the project, Murfin Drilling Company, selected a location in SE SW NE sec. 27, T. 12 S., R. 14 W., Russell County, KS. This location is within Claussen Northeast field. This well was selected to penetrate the Lansing-Kansas City in an area already verified to have L-KC production. The Austin #2-27 (API# 15-195-23336) spud on 03/21/2006 at location 231 ft FNL 1450 ft FEL SE SW NE sec. 27, T. 12 S., R. 14 W. (**Fig. 5-1 and Fig. 5-2**) and cored the L-KC on 03/25/2006 as noted in the drilling log below.

Open-hole logs were run using the vendor LOG TECH. Open-hole wireline logs obtained on 03/27/2006 included Dual Induction, Gamma Ray, Compensated Neutron, Density, Borehole Compensated Sonic, Microresistivity, and a Cement Bond Sonic log. Logs are available from the KGS website at

[http://chasm.kgs.ku.edu/pls/abyss/qualified.well\\_page.DisplayWell?f\\_kid=1033974024](http://chasm.kgs.ku.edu/pls/abyss/qualified.well_page.DisplayWell?f_kid=1033974024)

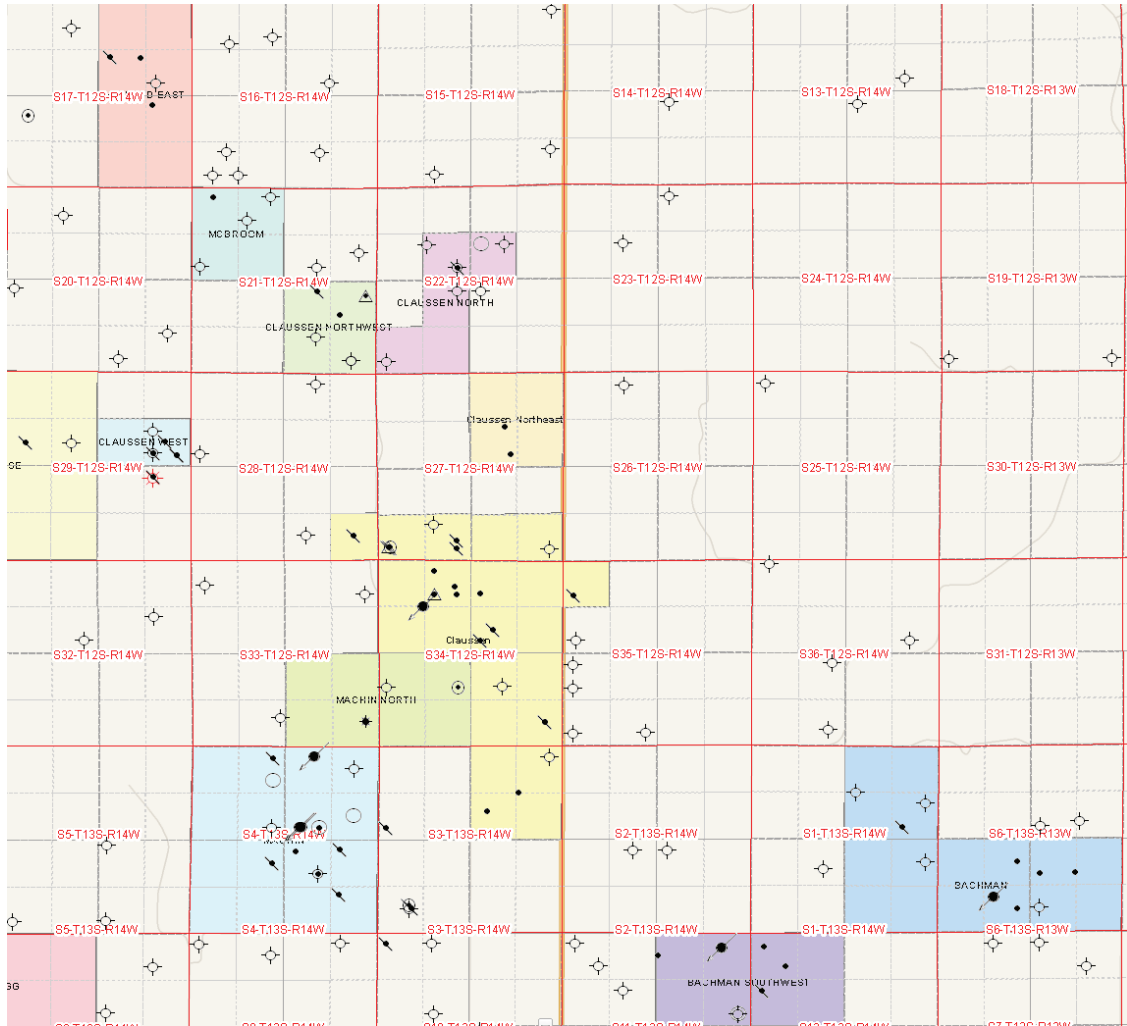


**Figure 5-1.** Location of Murfin Drilling Co. Austin #2-27. Claussen Northeast field is located in center of figure and shown in tan. The Austin #2-27 is located at SE SW NE sec. 27, T. 12 S., R. 14 W.

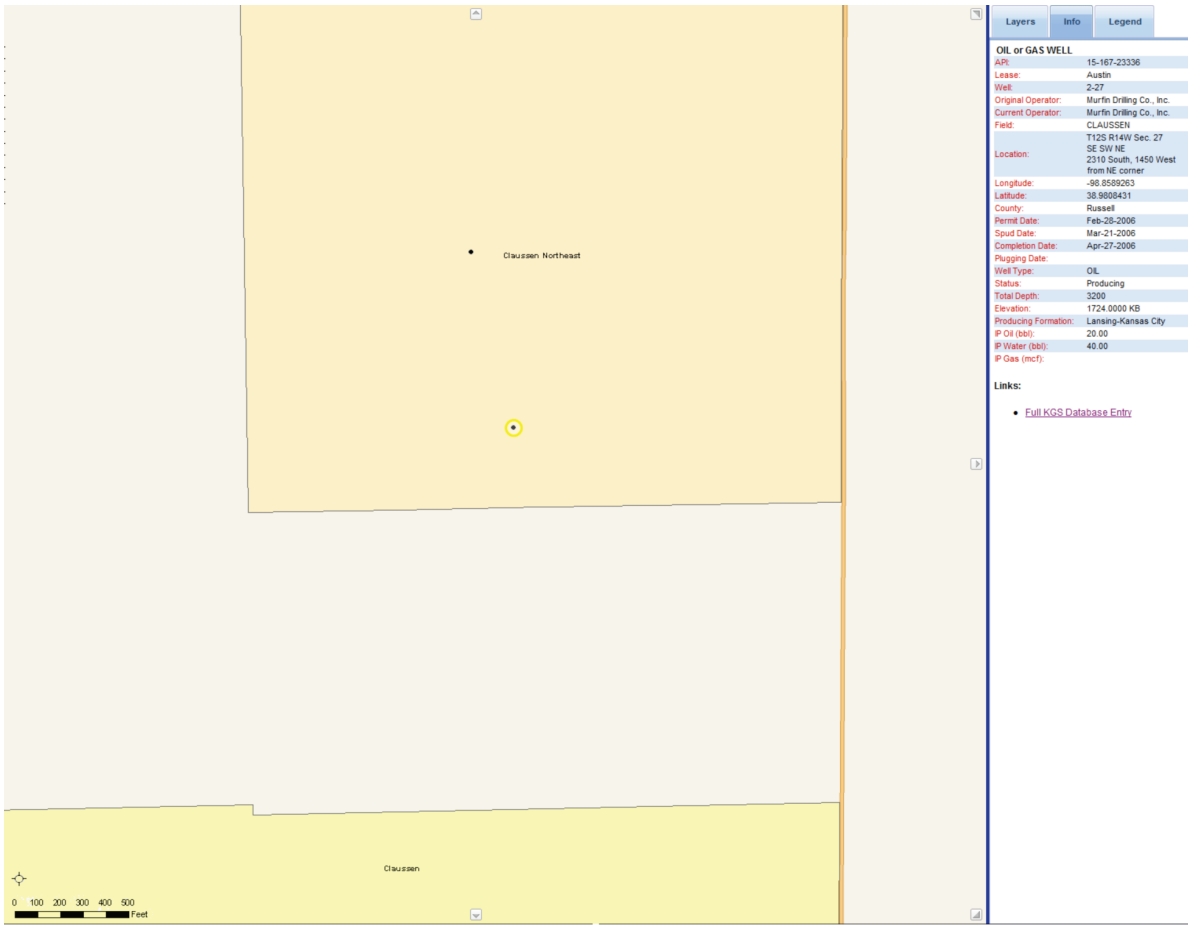


**Figure 5-2.** Location of Murfin Drilling Co. Austin #2-27. Claussen Northeast field is located to north of Claussen field. The Austin #2-27 is shown highlighted in yellow located at SE SW NE sec. 27, T. 12 S., R. 14 W.

KANSAS CORPORATION COMMISSION  
OIL & GAS CONSERVATION DIVISION  
**WELL COMPLETION FORM**  
WELL HISTORY - DESCRIPTION OF WELL & LEASE

RECEIVED  
MAY 24 2006  
Form ACO-1  
September 1999  
Form Must Be Typed  
KCC WICHITA

Operator: License # 30606  
Name: Murfin Drilling Company, Inc.  
Address: 250 N. Water, Suite 300  
City/State/Zip: Wichita, Kansas 67202  
Purchaser: Eagling  
Operator Contact Person: Tom W. Nichols  
Phone: ( 316 ) 267-3241  
Contractor: Name: Murfin Drilling Company, Inc.  
License: 30606  
Wellsite Geologist: Brad Rine  
Designate Type of Completion:  
 New Well  Re-Entry  Workover  
 Oil  SWD  SLOW  Temp. Abd.  
 Gas  ENHR  SIGW  
 Dry  Other (Core, WSW, Expl., Cathodic, etc)  
If Workover/Re-entry: Old Well Info as follows:  
Operator: \_\_\_\_\_  
Well Name: \_\_\_\_\_  
Original Comp. Date: \_\_\_\_\_ Original Total Depth: \_\_\_\_\_  
 Deepening  Re-perf.  Conv. to Enhr./SWD  
 Plug Back \_\_\_\_\_ Plug Back Total Depth \_\_\_\_\_  
 Commingled \_\_\_\_\_ Docket No. \_\_\_\_\_  
 Dual Completion \_\_\_\_\_ Docket No. \_\_\_\_\_  
 Other (SWD or Enhr.?) \_\_\_\_\_ Docket No. \_\_\_\_\_  
3/21/06                      3/29/06                      4/27/06  
Spud Date or                      Date Reached TD                      Completion Date or  
Recompletion Date                                           Recompletion Date

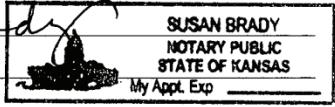
KCC  
MAY 23 2006

API No. 15 - 167-23336-0000  
County: Russell  
SE SW NE \_\_\_\_\_ Sec. 27 Twp. 12 S. R. 14  East  West  
2310 N \_\_\_\_\_ feet from S / N (circle one) Line of Section  
1450 E \_\_\_\_\_ feet from E / W (circle one) Line of Section  
Footages Calculated from Nearest Outside Section Corner:  
(circle one) NE SE NW SW  
Lease Name: Austin Well #: 2-27  
Field Name: Claussen  
Producing Formation: LKC  
Elevation: Ground: 1719' Kelly Bushing: 1724'  
Total Depth: 3200' Plug Back Total Depth: 3138'  
Amount of Surface Pipe Set and Cemented at 220 Feet  
Multiple Stage Cementing Collar Used?  Yes  No  
If yes, show depth set 804 Feet  
If Alternate II completion, cement circulated from 804  
feet depth to surface w/ 100 sx cmt.  
Drilling Fluid Management Plan Alt II NW @ 6-08  
(Data must be collected from the Reserve Pit)  
Chloride content \_\_\_\_\_ ppm Fluid volume \_\_\_\_\_ bbls  
Dewatering method used \_\_\_\_\_  
Location of fluid disposal if hauled offsite: \_\_\_\_\_  
Operator Name: \_\_\_\_\_  
Lease Name: \_\_\_\_\_ License No.: \_\_\_\_\_  
Quarter \_\_\_\_\_ Sec. \_\_\_\_\_ Twp. \_\_\_\_\_ S. R. \_\_\_\_\_  East  West  
County: \_\_\_\_\_ Docket No.: \_\_\_\_\_

**INSTRUCTIONS:** An original and two copies of this form shall be filed with the Kansas Corporation Commission, 130 S. Market - Room 2078, Wichita, Kansas 67202, within 120 days of the spud date, recompletion, workover or conversion of a well. Rule 82-3-130, 82-3-106 and 82-3-107 apply. Information of side two of this form will be held confidential for a period of 12 months if requested in writing and submitted with the form (see rule 82-3-107 for confidentiality in excess of 12 months). One copy of all wireline logs and geologist well report shall be attached with this form. ALL CEMENTING TICKETS MUST BE ATTACHED. Submit CP-4 form with all plugged wells. Submit CP-111 form with all temporarily abandoned wells.

All requirements of the statutes, rules and regulations promulgated to regulate the oil and gas industry have been fully complied with and the statements herein are complete and correct to the best of my knowledge.

Signature: [Signature]  
Title: Tom Nichols, Production Manager Date: 5/19/06  
Subscribed and sworn to before me this 19th day of May, 2006.  
Notary Public: Susan Brady  
Date Commission Expires: 11-4-07



**KCC Office Use ONLY**  
 Letter of Confidentiality Received  
If Denied, Yes  Date: \_\_\_\_\_  
 Wireline Log Received  
 Geologist Report Received  
 UIC Distribution

KCC

MAY 23 2006

Side Two

Operator Name: Murfin Drilling Company, Inc. Lease Name: Austin #: 2-27
Sec. 27 Twp. 12 S. R. 14 [ ] East [x] West County: Russell

INSTRUCTIONS: Show important tops and base of formations penetrated. Detail all cores. Report all final copies of drill stems tests giving interval tested, time tool open and closed, flowing and shut-in pressures, whether shut-in pressure reached static level, hydrostatic pressures, bottom hole temperature, fluid recovery, and flow rates if gas to surface test, along with final chart(s). Attach extra sheet if more space is needed. Attach copy of all Electric Wireline Logs surveyed. Attach final geological well site report.

Drill Stem Tests Taken [x] Yes [ ] No (Attach Additional Sheets)
Samples Sent to Geological Survey [x] Yes [ ] No
Cores Taken [ ] Yes [x] No
Electric Log Run [x] Yes [ ] No (Submit Copy)
List All E. Logs Run:
Dual Induction, Compensated Porosity, Microresistivity
[ ] Log Formation (Top), Depth and Datum [ ] Sample
Name Top Datum
SEE ATTACHED LIST
RECEIVED MAY 24 2006 KCC WICHITA

CASING RECORD [ ] New [ ] Used
Report all strings set-conductor, surface, intermediate, production, etc.
Table with columns: Purpose of String, Size Hole Drilled, Size Casing Set (In O.D.), Weight Lbs. / Ft., Setting Depth, Type of Cement, # Sacks Used, Type and Percent Additives.
Rows: Surface, Production

ADDITIONAL CEMENTING / SQUEEZE RECORD
Table with columns: Purpose, Depth Top Bottom, Type of Cement, #Sacks Used, Type and Percent Additives.
Row: Protect Casing, 0-804, A-con, 100, 3% cc, 1/4# cellflake

PERFORATION RECORD - Bridge Plugs Set/Type
Specify Footage of Each Interval Perforated
Table with columns: Shots Per Foot, PERFORATION RECORD, Acid, Fracture, Shot, Cement Squeeze Record, Depth.
Row: 4, 2919-2926, 1500 gal NeFe w/5% misc solvent, 20 ball sealers

TUBING RECORD
Size 2 3/8 Set At 2942 Packer At
Liner Run [ ] Yes [x] No
Date of First, Resumerd Production, SWD or Enhr. 4/28/06
Producing Method [ ] Flowing [x] Pumping [ ] Gas Lift [ ] Other (Explain)
Estimated Production Per 24 Hours: Oil 20 Bbls., Gas ---- Mcf, Water 40 Bbls., Gas-Oil Ratio ----, Gravity

Disposition of Gas METHOD OF COMPLETION Production Interval
[ ] Vented [ ] Sold [ ] Used on Lease [ ] Open Hole [x] Perf. [ ] Dually Comp. [ ] Commingled
(If vented, Submit ACO-18.) [ ] Other (Specify)

**Austin #2-27**

Operator: Murfin Drilling Company, Inc.  
Contractor: Murfin Drilling Company, Inc.  
Rig #8

Stuttgart #3133

2310 FNL 1450 FEL  
Sec. 27-T12S-R14W  
Russell County, Kansas

Contact Person: Scott Robinson  
Phone number: 316-267-3241  
Well site Geologist: Brad Rine

Call Depth: 2200'  
Spud: 11:00 am 3/21/06

API #: 15-167-23336  
Casing: 8 5/8" @ 220'  
5 1/2" @ 3185'

TD: 3200'

Elevation: 1719' GL  
1724' KB

**DAILY INFORMATION:**

- 3/17/06 MIRT. Will shut down for the weekend and spud on Monday.  
3/20/06 Heavy snow. Will wait until storm passes to spud.  
3/21/06 Start up this morning.  
3/22/06 Depth 750'. Cut 750'. DT: 8 hrs (WOC). CT: none. Dev.: 1/2° @ 220'.  
Spud 11:00 am 3/21/06. Ran 5 jts = 212.07' of 8 5/8" surf csg, set @ 220'.  
Cmt w/150 sxs comm 3% cc, 2% gel. Plug down @ 5:15 pm 3/21/06.  
Drilled out @ 1:15 am 3/22/06. Circ 6 bbls by Allied.  
3/23/06 Depth 2040'. Cut 1290'. DT: none. CT: none. Dev.: 3/4° @ 1574'.  
3/24/06 Depth 2870'. Cut 830'. DT: none. CT: 3 3/4 hrs. Dev.: none. Running  
**DST #1 2821-2905' (Tor – Lan A)**. Should have test on bottom this  
afternoon.  
3/25/06 Depth 2935'. Cut 65'. DT: none. CT: 23 1/4 hrs. Dev.: 1° @ 2905'.  
**DST #1 2821-2905' (Tor – Lan A)**: 30-30-30-30 IF: wk blow died in 2  
min. FF: no blow. Rec. 25' M. HP: 1383-1337; FP: 16/21, 25/27; SIP:  
227-70. **CORE #1 2905-2935' (Lan B, C, D)**, cut 30', Rec. 30'; 12' Lan B  
@ 2910' 6-8 of bleeding core drk brn FO; 2' shale; 10' Lan C 2920-2930',  
bleeding core drk brn FO sl odor fluor fr show brn FO; 1' shale; 5' Lan D  
@ 2932' 4' of bleeding core brn FO. **DST #2 2892-2935 (Lan B, C, D)**:  
30-60-60-90; IF: wk blow slowly building to 8". FF: wk blow slowly  
building to 4". Rec. 2' CO, 69' O & WCM, (20% O, 10% W, 70% M), 145'  
SLO & MCW, (1% O, 20% M, 79% W), 10' M, 226' TF. HP: 1408-1388;  
FP: 18/69, 75/111; SIP: 509-462. Chl 27,600 ppm, pit 9300 ppm chl.  
3/26/06 Depth 2973'. Cut 38'. DT: none. CT: 22 3/4 hrs. Dev.: none. **DST #3**  
**2937-2973' (Lan D, E/F)**: 30-60-45-60. IF: wk surface blow. FF: wk  
surface blow, died in 15 min. Rec. 10' O sptd M (1% O, 99% M). HP:  
1423-1361' FP: 14/16, 17/18; SIP: 31-25.

**RECEIVED**

Austin #2-27  
 Daily drilling report  
 Page two

- 3/27/06 Depth 3160'. Cut 187'. DT: ¼ hr. (tight conn @ 3040'). CT: 16 hrs. **DST #4 3025-3160' (Lan H, I, J, K, L):** IF: wk surface blow.
- 3/28/06 RTD 3200'. Cut 40'. DT: none. CT: 22 ¾ hrs. Dev.: 1° @ 3200'. **DST #4 3025-3160' (Lan H, I, J, K, L):** IF: wk surface blow. FF: no blow. Rec. 10' M. HP: 1477-1406; FP: 10/20, 22/24; SIP: 560-462. HC @ 1:45 P.M. 3/27/06 Log Tech logged from 5:30 p.m. to 10:00 p.m. 3/27/06, LTD @ 3200'. Ran 75 jts. of 5 1/2" prod. csg. set @ 3185', cmt. w/155 sx. AA-2 by Acid Services, port collar set @ 807', 15 sx. in RH, 10 sx. in MH.
- 3/29/06 RTD 3200'. CT: 6 ½ hrs. plug down @ 9:30 a.m. 3/28/06 by Jet Star. FINAL REPORT.

Formations	MDCI Austin #2-27 2310 FNL 1450 FEL Sec. 27-12-14W 1724' KB						MDCI Austin #1-27 1530 FNL 1640 FEL Sec. 27-12-14W 1762' KB	
	Sample Tops	Datum	Ref	Log tops	Datum	Ref	Log Tops	Datum
Anhydrite	752	+972	+8				798	+964
B/Anhydrite	785	+939	+9				832	+930
Topeka	2569	845	+4	2568	-844	+5	2611	-849
Oread Por	2796	-1072	+2	2792	-1068	+6	2836	-1074
Heebner	2830	-1106	+2	2827	-1103	+5	2870	-1108
Toronto	2850	-1126	+1	2845	-1121	+6	2889	-1127
Lansing	2882	-1158	FLAT	2878	-1154	+4	2920	-1158
Lansing B	2906	-1182	+3	2903	-1179	+6	2947	-1185
Lansing C	2920	-1196	+2	2918	-1194	+4	2960	-1198
BKC	3152	-1428	-1	3149	-1425	+2	3189	-1427
Arbuckle	NR						3260	-1498
RTD	3200							
LTD				3200				



KCC  
MAY 23 2006  
CONFIDENTIAL

Austin #2-27  
Completion Report  
Section 27-12S-14W  
Russell County, KS

03/28/06 MDC Rig #8 ran 76 joints new Maverick 5 1/2" MAV 50 LT&C 15.5# 8rd range 3 casing = 3224.96'. Francis Casing crew drifted casing prior to running casing in hole. Stacked out with casing 20' above 3200'RTD. Hooked-up rig mud pump to casing. Circulated guide shoe down to 3200' and tagged bottom. Top of 76<sup>th</sup> joint was 7' above KB. Acid Services cementer refused to hook-up casing rotating head to casing due to his company's safety policy of not using rotator if top joint is more than 6' above KB. Pulled 76<sup>th</sup> joint (20.00') back out of hole and laid joint down. Landed guide shoe @ 3182'. Shoe joint = 43.51'. Insert @ 3138.49'. Centralizers on 1<sup>st</sup>, 3<sup>rd</sup>, 5<sup>th</sup>, 7<sup>th</sup>, 9<sup>th</sup>, 11<sup>th</sup>, 13<sup>th</sup>, 15<sup>th</sup>, 55<sup>th</sup>, and 57<sup>th</sup> joints. Cement basket on bottom of 56<sup>th</sup> joint. Port collar @ 804.38'. Scratched from (2893-2923'). Circulated and rotated casing 1 hour prior to cementing casing. RU Acid Services. Pumped 500 gallon mud-flush and 12 water spacer ahead of cement. SI casing and mixed 25 sacks 60/40 Poz and plugged rathole. Mixed 155 sacks AA-2 cement. Displaced cement with 73.5BFW @ 6bpm with 500psi. Lost circulation @ start of displacement then regained it with approximately 35 barrels out. Stopped rotation. Plug landed with 1500psi @ 9:33am. Released back, held. Landed casing in slips.

ed  
sg

Centralizers: 1<sup>st</sup> joint @ 3179', 3138'; 3<sup>rd</sup> joint @ 3053'; 5<sup>th</sup> joint @ 2967'; 7<sup>th</sup> joint @ 2882'; 9<sup>th</sup> joint @ 2797'; 11<sup>th</sup> joint @ 2712'; 13<sup>th</sup> joint @ 2628'; 15<sup>th</sup> joint @ 2543'; 55<sup>th</sup> joint @ 848'; 57<sup>th</sup> joint @ 761'.

- Port collar @ 804.38'.
- Cement basket @ 847'.
- Scratchers (30.00') on 7<sup>th</sup> joint from 2893' to 2923'.
- Guide shoe @ 3182'; shoe joint = 43.51'. Insert @ 3138.49'.

04/06/06 Mai Excavating RO's plumbed bradenhead to GL. Back-filled cellar. RU Log-Tech with portable mast. Ran CCL-CBL from (2150-3133'). Port-collar @ 806'.

04/13/06 MIRU MDC #750. Honas Tank Service MI swab tank. Mai Excavating MI 103 joints new 2 3/8" 4.7# 8rd EUE tubing. TIH with X-pert Service Tools 5 1/2" port-collar positioning tool and 25 joints 2 3/8" tubing. Found port-collar @ 806'. RU Acid Services. Pressured casing to 750psi., held. Opened port-collar. Took injection rate. 2 1/4 bpm @ 300psi. Gained circulation with 2 bbls. pumped. Mixed 100sx A-con cement with 3%CC, 1/4# C.F. Cement circulated to surface. Closed port-collar. Pressured casing to 750psi., held. Ran 5 joints tubing. Positioning tool @ 970'. Circulated cement out of tubing and casing with 10BFW. TOH with 30 joints 2 3/8" tubing and 5 1/2" port-collar positioning tool. SDON. Job witnessed and approved by Rich Williams with K.C.C. District #4 Hays, Ks.

C

Daily estimated cost: \$ 2450 Day 1 cumulative cost: \$ 4800

04/14/06 Ran 5 1/2" casing swab. Swabbed casing down to 2700'. 438FIH. RU Perf-Tech. Perforated L-KC "C" (2919-26') with 7' 4spf EHSC gun. TIH with X-pert Service Tools 5 1/2" Model R packer, SN, 2 3/8" X 6.00' tubing sub, and 91 joints 2 3/8" tubing. Packer hanging @ 2953'. SN @ 2947'. Ran swab. Tagged FL @ 2575' 372FIH. Had a trace of heavy gassy oil on sample bucket on 1<sup>st</sup> pull. Swabbed down to 2900' 47FIH. Recovered 10.86 bbls. Very slight sheen of oil on sample bucket. RU Allied Cementing & Acidizing to treat perms with 250 gallons 15% MCA acid with 10% surfactant. Spotted 1 bbl. acid @ 2920'. Pulled one joint and set packer @ 2888'. SN @ 2882'. Tubing loaded and pressured to 250psi. Staged to 300psi. Broke to 250psi then started feeding. 1/4bpm @ 275psi. Rate increased to 1/2bpm @ 30psi. 1bpm @ 30psi. 1.1bpm @ 30psi. with all acid out. Displaced with 18.5BLW. 5.5 bbls. over displacement. ISIP vacuum. Total load 24.5 bbls. Ran swab. Tagged FL @ 300' 2582FIH. Swabbed down to 2500' 382FIH. Recovered 25.89 bbls. Started 1 hour 4pphr swab test @ 3:00pm. FL staying steady @ 2500' 382FIH. Average G.O. 15% oil 84.95%W .5%fines. Recovered 5.84 bbls. Released packer. Packer hanging @ 2888'. SN @ 2882'. Ran swab and tagged FL @ 2725' 157FIH. SIW. SDOWE. 4/15 SDOWE. 4/16 SDOWE.

Daily estimated cost: \$ 4670 Day 2 cumulative cost \$ 9470

04/17/06 Ran swab. Tagged FL @ 1825' 1057FIH. Pkr. hanging @ 2888'. 900' of tubing & casing fill-up in 64 hours. Pulled 950' on 1<sup>st</sup> pull. Recovered 3.68 bbls. with a trace of oil. Set pkr. @ 2888'. Swabbed tubing down to 2500' 382FIH. Recovered 24.22 bbls. Started swab-testing @ 9:30am.

- 1<sup>st</sup> hr. 4pphr. FL @ 2500' 382FIH Rec. 5.01 bbls. G.O. 25% oil 74%W 1% fines (mud).
- 2<sup>nd</sup> hr. 4pphr FL @ 2450' 432FIH Rec. 6.68 bbls. G.O. 60% oil 38.8%W 1.2% fines (mud).
- 3<sup>rd</sup> hr. 4pphr FL @ 2450' 432FIH Rec. 7.52 bbls. G.O. 60% oil 39%W 1% fines (mud).
- SD 30 minutes. Ran swab. Tagged FL @ 2450' 432FIH. Resumed swab testing @ 1:00pm.
- 4th hr. 4pphr. FL @ 2450' 432FIH. Rec. 6.26 bbls. G.O. 50% oil 49.7%W .3% fines (mud).
- 5th hr. 4pphr FL @ 2450' 432FIH. Rec. 6.26 bbls. G.O. 52% oil 47.7%W .2% fines (mud).

RECEIVED



**Austin #2-27  
Completion Report  
Section 27-12S-14W  
Russell County, KS**

RU Allied Cementing & Acidizing Inc. to treat L-KC "C" ( 2919-26') with 1500 gallons 15% NEFE containing acid containing 5% miscible solvent and 20-ball sealers. 4bpm @ 450psi with acid on perfs. 3.5bpm @ 550psi. with 1<sup>st</sup> perf balls on perfs. Had slight increase in pressure. 4bpm @ 550psi with 2<sup>nd</sup> set of perf balls on perfs. 4bpm @ 600psi with 3<sup>rd</sup> set of perf balls on perfs. Started flush. 4<sup>th</sup> set of perf balls on perfs with 4bpm @ 650psi. 4bpm @ 700psi with 5<sup>th</sup> set of perf balls on perfs. Displaced with 14BLW. 1bpm on vacuum @ end of flush. ISIP vacuum. Total load 50 bbls. Ran swab. FL @ 500' FS 3382FIH. Swabbed down to 2250' 632FIH. Recovered 50 bbls. of 50 bbl. load. Had a good show of oil last two pulls. Ran swab and tagged FL @ 2400' 482FIH. SIWON. SDON.

Estimated daily cost: \$4700                      Day 3 cumulative cost: \$14,170

Austin #2-27

4/18/06    Ran swab. Tagged FL @ 1800' 1082FIH. 600' overnight fill-up. Pulled 1080' on 1<sup>st</sup> pull. 630' oil and 450' water. Swabbed down to 2350' 532FIH. Recovered 11.32 bbls. Started swab-testing @ 8:45am.  
1<sup>st</sup> hour 4 pphr FL @ 2400' 482FIH. Recovered 6.67 bbls. G.O. 50% oil 49.7%W .3% fines (mud).  
2<sup>nd</sup> hour 4 pphr FL @ 2400' 482FIH. Recovered 8.12 bbls. G.O. 65% oil 34.4%W .6% fines (mud).  
3<sup>rd</sup> hour 4 pphr FL @ 2450' 432FIH. Recovered 5.22 bbls. G.O. 75% oil 24%W 1% fines (mud).  
SD 1 hour. Ran swab. Tagged FL @ 2200' 682FIH. Swabbed down to 2300' 582FIH. Recovered 3.48 bbls. Resumed swab-testing @ 12:45pm.  
4<sup>th</sup> hour 4 pphr FL @ 2300' 582FIH. Recovered 9.57 bbls. G.O. 60% oil 39.4%W .6% fines (mud).  
5<sup>th</sup> hour 4 pphr FL @ 2400' 482FIH. Recovered 5.51 bbls. G.O. 60% oil 39%W 1% fines (mud).  
6<sup>th</sup> hour 4 pphr FL @ 2400' 482FIH. Recovered 4.35 bbls. G.O. 60% oil 39%W 1% fines (mud).  
7<sup>th</sup> hour 4 pphr FL @ 2500' 382FIH. Recovered 4.64 bbls. G.O. 65% oil 34%W 1% fines (mud).  
SIWON. SDON. Swabbed a total of 58.88 bbls.

Daily estimated cost: \$ 2632                      Day 4 cumulative cost: \$ 16,802

Austin #2-27

04/19/06    Ran swab. Tagged FL @ 1950' 932FIH. Pulled 932' on 1<sup>st</sup> pull. 832' oil and 100' water. Swabbed down to 2450' 432FIH. Started swab-testing @ 8:45am.  
  
1<sup>st</sup> hour 4 pphr FL @ 2450' 432FIH. Recovered 6.67 bbls. G.O. 52% oil 47%W 1% fines (mud).  
2<sup>nd</sup> hour 4 pphr FL @ 2450' 432FIH. Recovered 8.12 bbls. G.O. 65% oil 34%W 1% fines (mud).  
SD 20 minutes to allow watertruck to haul 80BSW out of swab tank. Resumed swab-testing.  
3<sup>rd</sup> hour 4 pphr FL @ 2450' 432FIH. Recovered 5.80 bbls. G.O. 65% oil 34%W 1% fines (mud).  
4<sup>th</sup> hour 4 pphr FL @ 2450' 432FIH. Recovered 5.80 bbls. G.O. 60% oil 39.2%W .8% fines (mud).  
5<sup>th</sup> hour 4 pphr FL @ 2450' 432FIH. Recovered 5.80 bbls. G.O. 60% oil 39.4%W .6% fines (mud).

Released packer. TOH with 89 joints 2 3/8" tubing , 2 3/8" X 6.00' sub, SN, and model "R" packer. SDON.

Daily estimated cost: \$ 2850                      Day 5 cumulative cost: \$ 19,652

04/20/06    Installed new 5 1/2" X 2 3/8" tubing head. TIH with new 2 3/8" X 3.00' perforated sub (bull-plugged) = 3.74', new 2" X 1.10' SN, and 91 joints 2 3/8" 8rd 4.7# EUE tubing. Landed bottom of string @ 2946.22'. SN @ 2942.48'. RU for rods. TIH with 2" X 1 1/2" X 12' RWTC ( 20-ring P-A plunger) with 10" strainer, 2' X 3/4" rod sub, 10 X 7/8" grade "D" 7/8" rods, 106 X 3/4" rods, 4' X 3/4" rod sub, new 1 1/4" X 16' P-rod with new 6' liner. Clamped off rods. RDMOL.

Daily estimated cost: \$ 2200                      Day 6 cumulative cost: \$ 21852

04/21/06    Mai Excavating built unit grade. Spread sand on grade. Back-filled rotary working pits. Will set p.u. 4/25/06.

04/24/06    Mai Excavating loaded and hauled Sentry CH114D-173-64" pumping unit from Dick's Oilfield Supply to location. Assembled unit. Placed in 44" SL. Set unit on pad, aligned over hole and sanded in. Will ditch LL and electrical lines 4/25/06.

04/26/06    Hammersmith Electric ditched and laid 1300' of 2" SCH40 PVC LL from well to a point 600' NE of #1-27. Dug out LL. Installed new 2" PVC Y-branch. Used backhoe to dig most of ditch near loc. Large limestone boulders slowed digging. Will install electric line and finish hook-up 4/27.

**RECEIVED**  
MAY 2 1 2006



**Austin #2-27  
Completion Report  
Section 27-12S-14W  
Russell County, KS**

---

04/27/06 Hammersmith Electric ditched and laid 1100' of underground from well to a point 600' east of #1-27. Tied underground into #1-27 existing underground. Set new TECO 15HP motor and size 2 panel. Installed new 3C6" sheave and (3)C-225 belts. Shane's Tk. Service emptied swab tk. Pumped 27 bbl. swab oil through GB. Loaded tbg. Balanced p.u. POP @ 5:30pm. Running 10.61 X 44" X 1 1/2". Amps: wts. 15 – rods 14.

04/28/06 10.61 X 44" X 1 1/2" 24 hrs. on. 86.4BTF 100%W NPF 71%PE. 32.56BOIS

04/29/06 33.83BO 78.95BW 70%W 112.78BTF NPF 93%PE. 38.41BOIS

04/30/06 10.61 X 44" X 1 1/2" 24 hrs. on. 34.65BO 56.55BW 62%W 91.20BTF NPF 75%PE 45.92BOIS w/ 2-wells.

05/01/06 19.96BO 42.44BW 68%W 62.40BTF PF 51%PE 40.08BOIS w/ 2-wells.

05/02/06 19.58BO 38.02BW 66%W 57.60BTF PF 47%PE 30.06BOIS.

05/03/06 19.00BO 33.79BW 64%W 52.79BTF PF 43%PE 28.39BOIS w/ 2-wells.

05/04/06 14.59BO 31.01BW 68%W 45.60BTF PF 37%PE 23.38BOIS.

05/05/06 10.61 X 44" X 1 1/2" 24 hrs. on. 15.35BO 32.64BW 68%W 47.97BTF PF 39%PE. 28.38BOIS.

05/06/06 14.68BO 28.52BW 66%W 43.20BTF PF 35%PE 21.71BOIS.

05/07/06 14.68BO 26.11BW 64%W 40.79BTF PF 33%PE 21.71BOIS.

05/08/06 13.82BO 24.57BW 64%W 38.89BTF PF 31%PE 21.71BOIS.

05/09/06 10.61 X 44" X 1 1/2" 24 hrs. on. 13.05BO 25.34BW 66%W 38.39BTF PF 32%PE 20.08BOIS.

05/10/06 10.61 X 44" X 1 1/2" 24 hrs. on. 12.24BO 23.76BW 66%W 36.00BTF PF 29%PE. 18.37BOIS

05/11/06 10.61 X 44" X 1 1/2" 24 hrs. on. 11.42BO 22.17BW 66%W 33.59BTF PF 27%PE 18.37BOIS.

05/17/06 10.07BO 23.52BW 70%W 33.59BTF PF 27%PE. 17.54BOIS w/ 2-wells.

15-167-23336



## DRILL STEM TEST REPORT

Prepared For: **Murfin Drilling Co**

250 N Water Ste 300  
Wichita KS 67202

ATTN: Brad Rine

**27-12s-14w-Russell**

**Austin 2-27**

Start Date: 2006.03.24 @ 13:41:02

End Date: 2006.03.24 @ 20:20:02

Job Ticket #: 24737      DST #: 1

Trilobite Testing, Inc  
PO Box 362 Hays, KS 67601  
ph: 785-625-4778 fax: 785-625-5620

**RECEIVED**  
**MAY 24 2006**  
**KCC WICHITA**

Printed: 2006.03.28 @ 15:01:58 Page 1



**TRILOBITE  
TESTING, INC**

## DRILL STEM TEST REPORT

Murfin Drilling Co  
250 N Water Ste 300  
Wichita KS 67202  
ATTN: Brad Rine

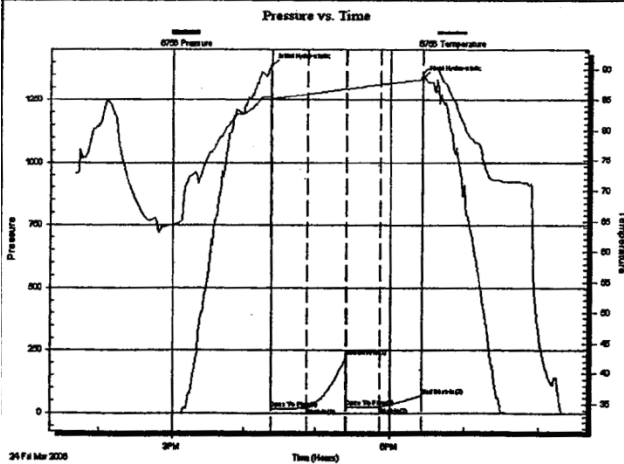
**Austin 2-27**  
**27-12s-14w-Russell**  
Job Ticket: 24737      DST#: 1  
Test Start: 2006.03.24 @ 13:41:02

### GENERAL INFORMATION:

Formation: **Toronto, L, Kc " A "**  
Deviated: **No Whipstock**      ft (KB)  
Time Tool Opened: 16:22:32  
Time Test Ended: 20:20:02  
Test Type: **Conventional Bottom Hole**  
Tester: **Joe**  
Unit No: **22**  
Interval: **2821.00 ft (KB) To 2905.00 ft (KB) (TVD)**  
Reference Elevations: **1726.00 ft (KB)**  
Total Depth: **2905.00 ft (KB) (TVD)**      **1721.00 ft (CF)**  
Hole Diameter: **7.80 inches** Hole Condition: **Good**      KB to GR/CF: **5.00 ft**

**Serial #: 6756**      Inside  
Press@RunDepth: **26.85 psig @ 2822.00 ft (KB)**      Capacity: **7000.00 psig**  
Start Date: **2006.03.24**      End Date: **2006.03.24**      Last Calib.: **2006.03.24**  
Start Time: **13:41:04**      End Time: **20:20:02**      Time On Btm: **2006.03.24 @ 16:22:17**  
Time Off Btm: **2006.03.24 @ 18:26:02**

TEST COMMENT: **F-Weak Surface Blow Died after 2 min**  
**ISI-Dead**  
**FF-Dead**  
**FSI-Dead**



### PRESSURE SUMMARY

Time (Min.)	Pressure (psig)	Temp (deg F)	Annotation
0	1383.47	85.46	Initial Hydro-static
1	16.23	85.19	Open To Flow (1)
31	20.69	85.91	Shut-In(1)
62	226.60	86.84	End Shut-In(1)
63	24.51	86.78	Open To Flow (2)
90	26.85	87.54	Shut-In(2)
124	69.92	88.33	End Shut-In(2)
124	1336.55	88.81	Final Hydro-static

### Recovery

Length (ft)	Description	Volume (bbl)
25.00	DM	0.12

### Gas Rates

	Choke (inches)	Pressure (psig)	Gas Rate (Mcf/d)



**TRILOBITE  
TESTING, INC.**

**DRILL STEM TEST REPORT**

**TOOL DIAGRAM**

Murfin Drilling Co  
250 N Water Ste 300  
Wichita KS 67202  
ATTN: Brad Rine

**Austin 2-27**  
**27-12s-14w-Russell**  
Job Ticket: 24737      **DST#: 1**  
Test Start: 2006.03.24 @ 13:41:02

**Tool Information**

Drill Pipe:	Length: 2644.00 ft	Diameter: 3.80 inches	Volume: 37.09 bbl	Tool Weight: 2000.00 lb
Heavy Wt. Pipe:	Length: 0.00 ft	Diameter: 2.25 inches	Volume: 0.00 bbl	Weight set on Packer: 25000.00 lb
Drill Collar:	Length: 186.00 ft	Diameter: 2.25 inches	Volume: 0.91 bbl	Weight to Pull Loose: 31000.00 lb
			<b>Total Volume: 38.00 bbl</b>	Tool Chased 0.00 ft
Drill Pipe Above KB:	31.00 ft			String Weight: <b>Initial 30000.00 lb</b>
Depth to Top Packer:	2821.00 ft			<b>Final 31000.00 lb</b>
Depth to Bottom Packer:	ft			
Interval between Packers:	84.00 ft			
Tool Length:	106.00 ft			
Number of Packers:	2	Diameter: 6.75 inches		

Tool Comments:

Tool Description	Length (ft)	Serial No.	Position	Depth (ft)	Accum. Lengths
Shut In Tool	5.00			2804.00	
Hydraulic tool	5.00			2809.00	
Safety Joint	2.00			2811.00	
Packer	5.00			2816.00	22.00      Bottom Of Top Packer
Packer	5.00			2821.00	
Stubb	1.00			2822.00	
Recorder	0.00	6756	Inside	2822.00	
Perforations	3.00			2825.00	
Change Over Sub	1.00			2826.00	
Blank Spacing	61.00			2887.00	
Change Over Sub	1.00			2888.00	
Perforations	14.00			2902.00	
Recorder	0.00	10991	Inside	2902.00	
Bullnose	3.00			2905.00	84.00      Bottom Packers & Anchor

**Total Tool Length: 106.00**



**TRILOBITE  
TESTING, INC**

### DRILL STEM TEST REPORT

FLUID SUMMARY

Murfin Drilling Co

Austin 2-27

250 N Water Ste 300  
Wichita KS 67202

27-12s-14w-Russell

Job Ticket: 24737

DST#: 1

ATTN: Brad Rine

Test Start: 2006.03.24 @ 13:41:02

#### Mud and Cushion Information

Mud Type: Gel Chem

Cushion Type:

Oil Apt:

deg API

Mud Weight: 9.00 lb/gal

Cushion Length:

ft

Water Salinity:

ppm

Viscosity: 64.00 sec/qt

Cushion Volume:

bbl

Water Loss: 5.58 in<sup>3</sup>

Gas Cushion Type:

Resistivity: ohm.m

Gas Cushion Pressure:

psig

Salinity: ppm

Filter Cake: inches

#### Recovery Information

Recovery Table

Length ft	Description	Volume bbl
25.00	DM	0.123

Total Length: 25.00 ft

Total Volume: 0.123 bbl

Num Fluid Samples: 0

Num Gas Bombs: 0

Serial #:

Laboratory Name:

Laboratory Location:

Recovery Comments:

DST Test Number: 1

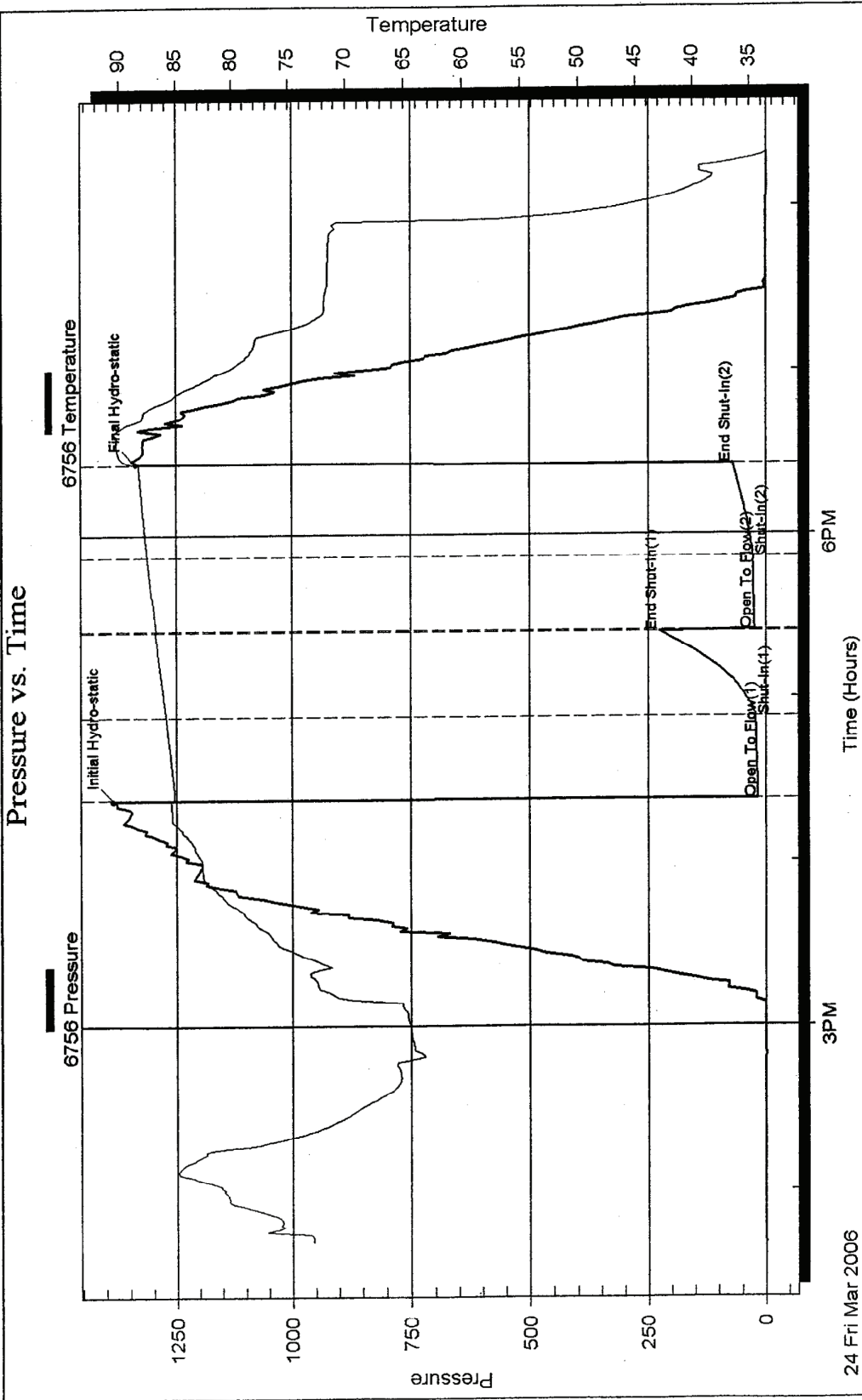
27-12s-14w-Russell

Murfin Drilling Co

Inside

Serial #: 6756

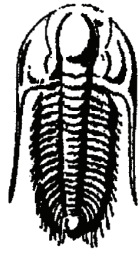
### Pressure vs. Time



Printed: 2006.03.28 @ 15:02:00 Page 5

Ref. No: 24737

Trilobite Testing, Inc



**TRILOBITE  
TESTING, INC.**

## DRILL STEM TEST REPORT

Prepared For: **Murfin Drilling Co**

250 N Water Ste 300  
Wichita KS 67202

ATTN: Brad Rine

**27-12s-14w-Russell**

**Austin 2-27**

Start Date: 2006.03.25 @ 10:43:22

End Date: 2006.03.25 @ 18:35:37

Job Ticket #: 24738          DST #: 2

Murfin Drilling Co

Austin 2-27

27-12s-14w-Russell

DST # 2

L,Kc B-D

2006.03.25

Trilobite Testing, Inc  
PO Box 362 Hays, KS 67601  
ph: 785-625-4778 fax: 785-625-5620

Printed: 2006.03.28 @ 15:03:48 Page 1



**TRILOBITE TESTING, INC**

## DRILL STEM TEST REPORT

Murfin Drilling Co  
 250 N Water Ste 300  
 Wichita KS 67202  
 ATTN: Brad Rine

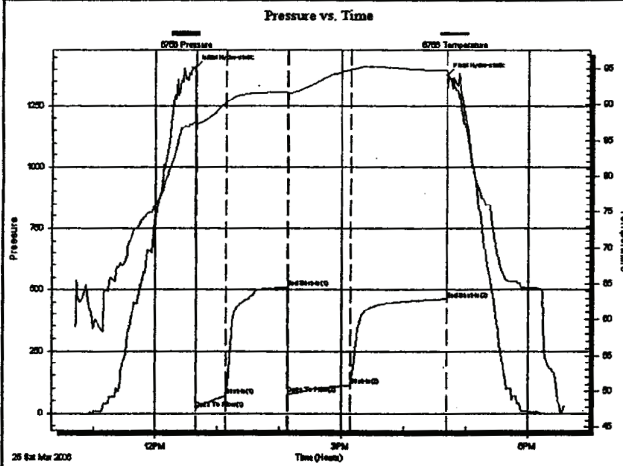
**Austin 2-27**  
**27-12s-14w-Russell**  
 Job Ticket: 24738      DST#: 2  
 Test Start: 2006.03.25 @ 10:43:22

### GENERAL INFORMATION:

Formation: **L,Kc B-D**  
 Deviated: **No Whipstock**      ft (KB)  
 Test Type: **Conventional Bottom Hole**  
 Time Tool Opened: 12:39:07      Tester: **Joe**  
 Time Test Ended: 18:35:37      Unit No: **22**  
 Interval: **2892.00 ft (KB) To 2935.00 ft (KB) (TVD)**      Reference Elevations: **1726.00 ft (KB)**  
 Total Depth: **2905.00 ft (KB) (TVD)**      **1721.00 ft (CF)**  
 Hole Diameter: **7.80 inches** Hole Condition: **Good**      KB to GR/CF: **5.00 ft**

**Serial #: 6756**      **Inside**  
 Press@RunDepth: **110.93 psig @ 2893.00 ft (KB)**      Capacity: **7000.00 psig**  
 Start Date: **2006.03.25**      End Date: **2006.03.25**      Last Calib.: **2006.03.25**  
 Start Time: **10:43:24**      End Time: **18:35:37**      Time On Btm: **2006.03.25 @ 12:38:52**  
 Time Off Btm: **2006.03.25 @ 16:41:37**

**TEST COMMENT:** Fair Blow built to 8" in  
 ISI-Weak Surface Blow back  
 FF-Weak Blow built to 4" in  
 FSI-Weak Surface Blow back



### PRESSURE SUMMARY

Time (Min.)	Pressure (psig)	Temp (deg F)	Annotation
0	1407.57	87.51	Initial Hydro-static
1	18.25	87.22	Open To Flow (1)
30	69.29	90.22	Shut-in(1)
90	509.49	91.77	End Shut-in(1)
90	74.81	91.65	Open To Flow (2)
150	110.93	94.82	Shut-in(2)
243	462.12	94.73	End Shut-in(2)
243	1373.51	94.73	Final Hydro-static

### Recovery

Length (ft)	Description	Volume (bbl)
2.00	Free Oil	0.01
69.00	OCM10%W20%O70%M	0.34
145.00	OCMW1%O20%M79%W	0.99
10.00	DM	0.14

### Gas Rates

	Choke (inches)	Pressure (psig)	Gas Rate (Mcf/d)



**TRILOBITE  
TESTING, INC.**

**DRILL STEM TEST REPORT**

**TOOL DIAGRAM**

Murfin Drilling Co  
250 N Water Ste 300  
Wichita KS 67202  
ATTN: Brad Rine

**Austin 2-27**  
**27-12s-14w-Russell**  
Job Ticket: 24738      **DST#: 2**  
Test Start: 2006.03.25 @ 10:43:22

**Tool Information**

Drill Pipe:	Length: 2704.00 ft	Diameter: 3.80 inches	Volume: 37.93 bbl	Tool Weight: 2000.00 lb
Heavy Wt. Pipe:	Length: 0.00 ft	Diameter: 2.25 inches	Volume: 0.00 bbl	Weight set on Packer: 25000.00 lb
Drill Collar:	Length: 186.00 ft	Diameter: 2.25 inches	Volume: 0.91 bbl	Weight to Pull Loose: 32000.00 lb
		Total Volume: 38.84 bbl		Tool Chased 0.00 ft
Drill Pipe Above KB:	20.00 ft			String Weight: Initial 31000.00 lb
Depth to Top Packer:	2892.00 ft			Final 32000.00 lb
Depth to Bottom Packer:	ft			
Interval between Packers:	43.00 ft			
Tool Length:	65.00 ft			
Number of Packers:	2	Diameter: 6.75 inches		

Tool Comments:

Tool Description	Length (ft)	Serial No.	Position	Depth (ft)	Accum. Lengths
Shut In Tool	5.00			2875.00	
Hydraulic tool	5.00			2880.00	
Safety Joint	2.00			2882.00	
Packer	5.00			2887.00	22.00      Bottom Of Top Packer
Packer	5.00			2892.00	
Stubb	1.00			2893.00	
Recorder	0.00	6756	inside	2893.00	
Perforations	39.00			2932.00	
Recorder	0.00	10991	inside	2932.00	
Bullnose	3.00			2935.00	43.00      Bottom Packers & Anchor
<b>Total Tool Length:</b>	<b>65.00</b>				



**TRILOBITE  
TESTING, INC.**

## DRILL STEM TEST REPORT

FLUID SUMMARY

Murfin Drilling Co

Austin 2-27

250 N Water Ste 300  
Wichita KS 67202

27-12s-14w-Russell

Job Ticket: 24738

DST#: 2

ATTN: Brad Rine

Test Start: 2006.03.25 @ 10:43:22

### Mud and Cushion Information

Mud Type: Gel Chem

Cushion Type:

Oil API:

deg API

Mud Weight: 9.00 lb/gal

Cushion Length:

ft

Water Salinity:

ppm

Viscosity: 64.00 sec/qt

Cushion Volume:

bbbl

Water Loss: 5.59 in<sup>3</sup>

Gas Cushion Type:

Resistivity: ohm.m

Gas Cushion Pressure:

psig

Salinity: ppm

Filter Cake: inches

### Recovery Information

Recovery Table

Length ft	Description	Volume bbl
2.00	Free Oil	0.010
69.00	OCM10%W20%O70%M	0.339
145.00	OCMW1%O20%M79%W	0.986
10.00	DM	0.140

Total Length: 226.00 ft      Total Volume: 1.475 bbl

Num Fluid Samples: 0

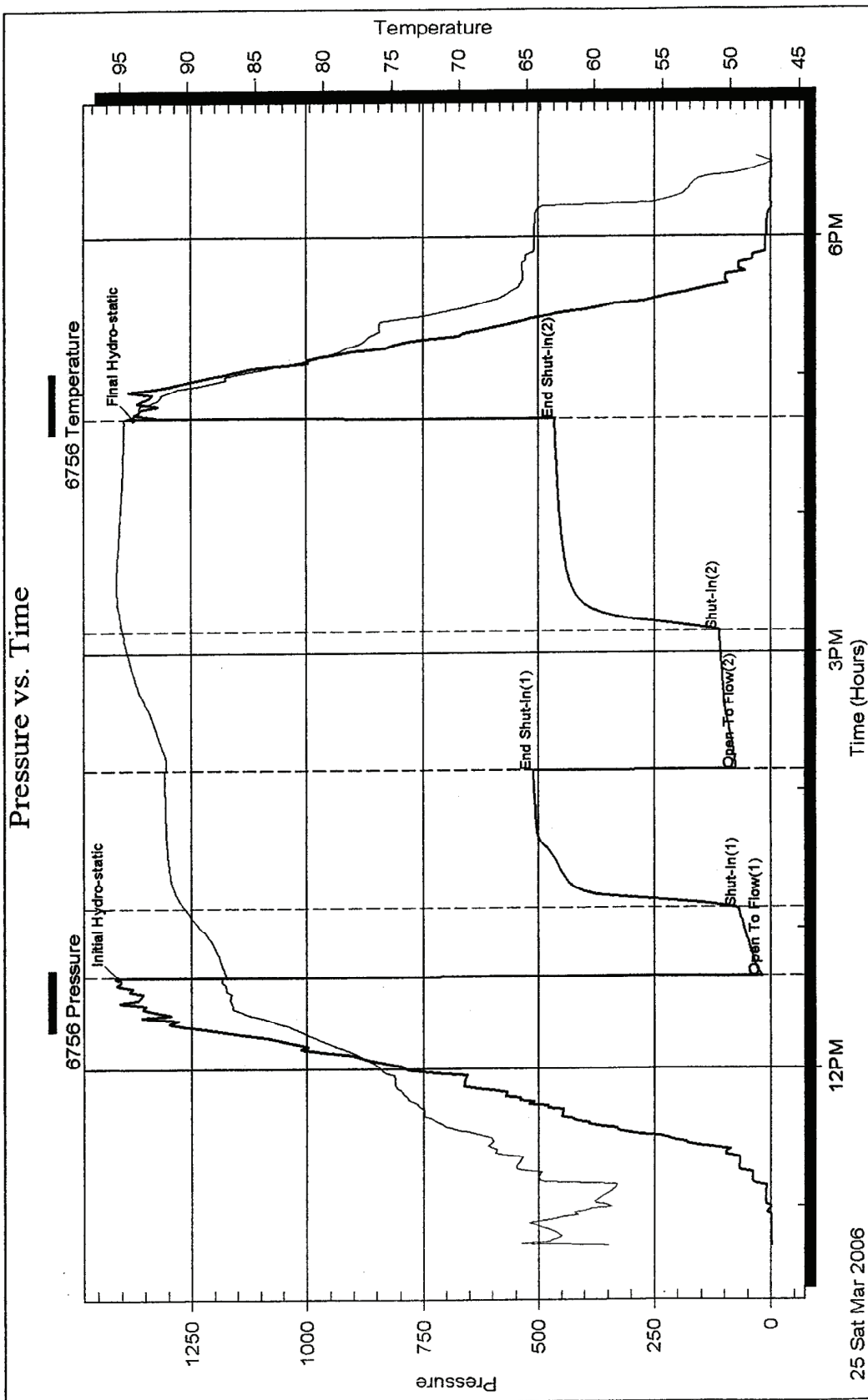
Num Gas Bombs: 0

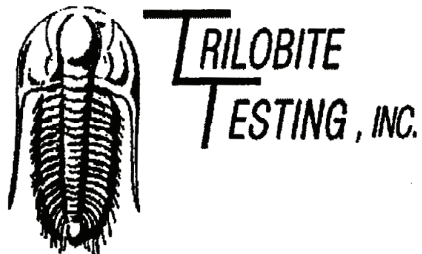
Serial #:

Laboratory Name:

Laboratory Location:

Recovery Comments:





## DRILL STEM TEST REPORT

Prepared For: **Murfin Drilling Co**

250 N Water Ste 300  
Wichita KS 67202

ATTN: Brad Rine

**27-12s-14w-Russell**

**Austin 2-27**

Start Date: 2006.03.26 @ 02:20:04

End Date: 2006.03.26 @ 09:23:34

Job Ticket #: 24739      DST #: 3

Trilobite Testing, Inc

PO Box 362 Hays, KS 67601

ph: 785-625-4778 fax: 785-625-5620

Printed: 2006.03.28 @ 15:04:45 Page 1

Murfin Drilling Co

Austin 2-27

27-12s-14w-Russell

DST # 3

L,Kc D-F

2006.03.26



**TRILOBITE  
TESTING, INC.**

## DRILL STEM TEST REPORT

Murfin Drilling Co  
250 N Water Ste 300  
Wichita KS 67202  
ATTN: Brad Fine

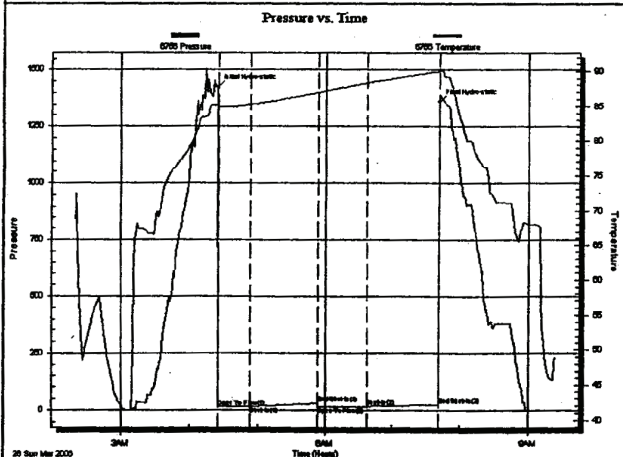
**Austin 2-27**  
**27-12s-14w-Russell**  
Job Ticket: 24739      **DST#: 3**  
Test Start: 2006.03.26 @ 02:20:04

### GENERAL INFORMATION:

Formation: **L,Kc D-F**  
Deviated: **No Whipstock**      ft (KB)  
Time Tool Opened: 04:24:49      Test Type: **Conventional Bottom Hole**  
Time Test Ended: 09:23:34      Tester: **Joe**  
Unit No: **22**  
Interval: **2937.00 ft (KB) To 2973.00 ft (KB) (TVD)**      Reference Elevations: **1726.00 ft (KB)**  
Total Depth: **2973.00 ft (KB) (TVD)**      **1721.00 ft (CF)**  
Hole Diameter: **7.80 inches** Hole Condition: **Good**      KB to GR/CF: **5.00 ft**

**Serial #: 6756**      **Inside**  
Press@RunDepth: **17.59 psig @ 2938.00 ft (KB)**      Capacity: **7000.00 psig**  
Start Date: **2006.03.26**      End Date: **2006.03.26**      Last Calib.: **2006.03.26**  
Start Time: **02:20:06**      End Time: **09:23:34**      Time On Btrnt: **2006.03.26 @ 04:24:34**  
Time Off Btrnt: **2006.03.26 @ 07:41:34**

TEST COMMENT: **F-Weak Surface Blow**  
**IS-Dead**  
**FF-Weak Surface Blow back Died after 15 min**  
**FSI-Dead**



### PRESSURE SUMMARY

Time (Min.)	Pressure (psig)	Temp (deg F)	Annotation
0	1423.23	85.32	Initial Hydro-static
1	13.93	84.74	Open To Flow (1)
29	15.90	85.28	Shut-in(1)
89	31.43	86.97	End Shut-in(1)
89	17.27	86.97	Open To Flow (2)
134	17.59	88.32	Shut-in(2)
197	24.81	89.94	End Shut-in(2)
197	1361.02	90.37	Final Hydro-static

### Recovery

Length (ft)	Description	Volume (bbl)
10.00	OSpkdM1%O99%M	0.05

### Gas Rates

Choke (inches)	Pressure (psig)	Gas Rate (Mcf/d)



**TRILOBITE  
TESTING, INC.**

**DRILL STEM TEST REPORT**

**TOOL DIAGRAM**

Murfin Drilling Co  
250 N Water Ste 300  
Wichita KS 67202  
ATTN: Brad Rine

**Austin 2-27**  
**27-12s-14w-Russell**  
Job Ticket: 24739      DST#: 3  
Test Start: 2006.03.26 @ 02:20:04

**Tool Information**

Drill Pipe:	Length: 2740.00 ft	Diameter: 3.80 inches	Volume: 38.43 bbl	Tool Weight: 2000.00 lb
Heavy Wt. Pipe:	Length: 0.00 ft	Diameter: 2.25 inches	Volume: 0.00 bbl	Weight set on Packer: 25000.00 lb
Drill Collar:	Length: 186.00 ft	Diameter: 2.25 inches	Volume: 0.91 bbl	Weight to Pull Loose: 40000.00 lb
		<u>Total Volume: 39.34 bbl</u>		Tool Chased 0.00 ft
Drill Pipe Above KB:	10.00 ft			String Weight: Initial 32000.00 lb
Depth to Top Packer:	2937.00 ft			Final 32000.00 lb
Depth to Bottom Packer:	ft			
Interval between Packers:	36.00 ft			
Tool Length:	57.00 ft			
Number of Packers:	2	Diameter: 6.75 inches		

Tool Comments:

Tool Description	Length (ft)	Serial No.	Position	Depth (ft)	Accum. Lengths
Shut In Tool	5.00			2921.00	
Hydraulic tool	5.00			2926.00	
Safety Joint	2.00			2928.00	
Packer	5.00			2933.00	21.00      Bottom Of Top Packer
Packer	4.00			2937.00	
Stubb	1.00			2938.00	
Recorder	0.00	6756	Inside	2938.00	
Perforations	32.00			2970.00	
Recorder	0.00	10991	Inside	2970.00	
Bullnose	3.00			2973.00	36.00      Bottom Packers & Anchor
<b>Total Tool Length:</b>	<b>57.00</b>				



**TRILOBITE  
TESTING, INC**

### DRILL STEM TEST REPORT

### FLUID SUMMARY

Murfin Drilling Co  
250 N Water Ste 300  
Wichita KS 67202  
ATTN: Brad Rine

Austin 2-27  
27-12s-14w-Russell  
Job Ticket: 24739      DST#: 3  
Test Start: 2006.03.26 @ 02:20:04

#### Mud and Cushion Information

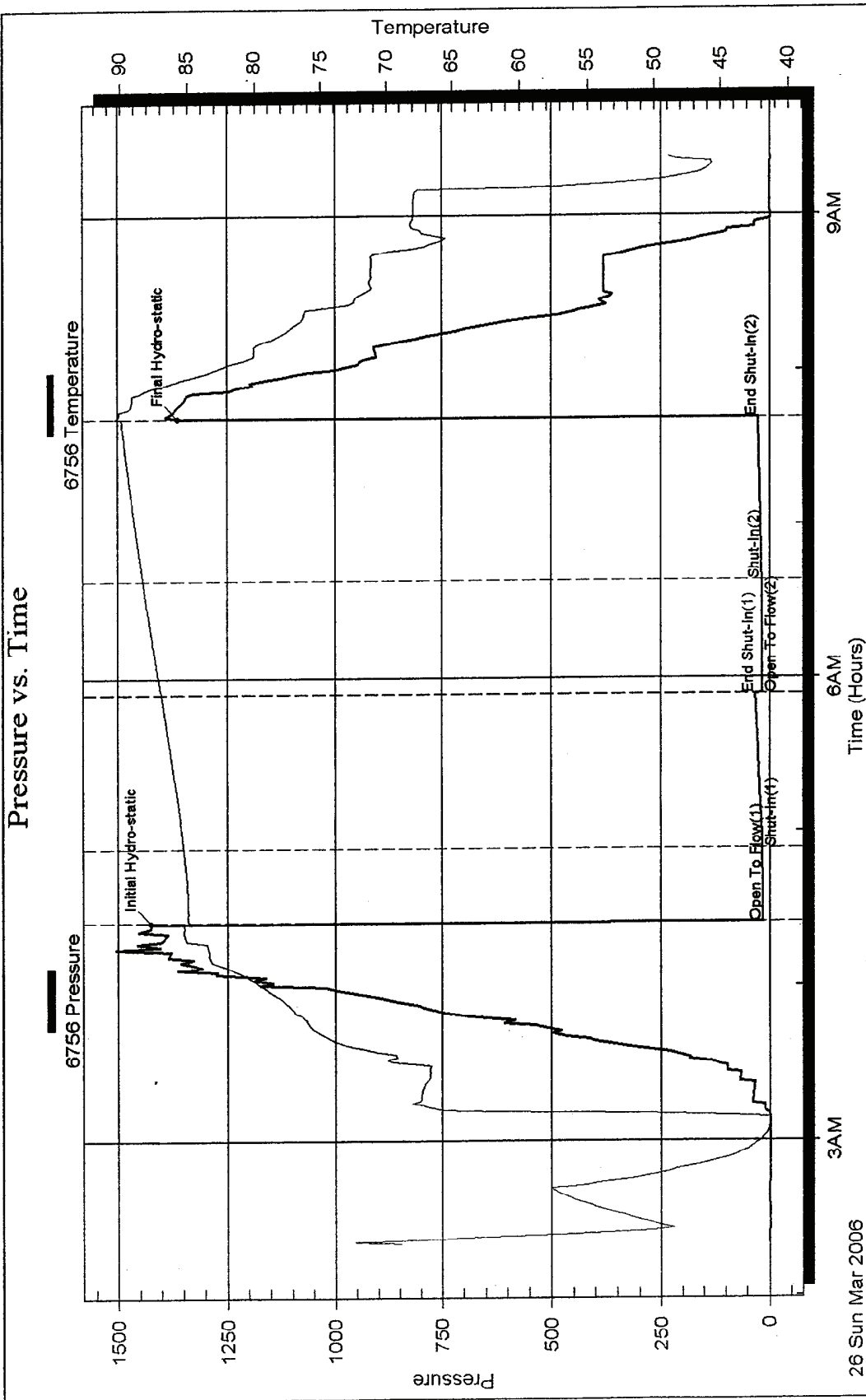
Mud Type:	Gel Chem	Cushion Type:		Oil API:	deg API
Mud Weight:	9.00 lb/gal	Cushion Length:	ft	Water Salinity:	ppm
Viscosity:	55.00 sec/qt	Cushion Volume:	bbl		
Water Loss:	5.99 in <sup>3</sup>	Gas Cushion Type:			
Resistivity:	ohm.m	Gas Cushion Pressure:	psig		
Salinity:	ppm				
Filter Cake:	inches				

#### Recovery Information

Recovery Table

Length ft	Description	Volume bbl
10.00	OSpkdM1%O99%M	0.049

Total Length: 10.00 ft      Total Volume: 0.049 bbl  
 Num Fluid Samples: 0      Num Gas Bombs: 0      Serial #:  
 Laboratory Name:      Laboratory Location:  
 Recovery Comments:



### 5.1.2 Core Description

The core description in the drilling report is as follows: **AUSTIN #2-27 CORE #1 2905-2935 ft (Lan B, C, D)**, cut 30 ft, Rec. 30 ft; 12 ft Lan B @ 2910 ft 6-8 of bleeding core drk brn FO; 2 ft shale; 10 ft Lan C 2920-2930 ft, bleeding core drk brn FO sl odor fluor fr show brn FO; 1 ft shale; 5 ft Lan D @ 2932 ft, 4 ft of bleeding core brn FO.

**Figure 5-3** shows a plain light photograph of the core. Examination of the core photo shows that the L-KC B comprises a low-porosity limestone. The L-KC C zone contains porous oomoldic limestone, and the L-KC D zone contains a 1-ft interval of fractured low porosity, but oil-stained and bleeding, oomoldic limestone.



**Figure 5-3.** Austin #2-27 core photo for Lansing-Kansas City core. Plain light.

### 5.1.3 Routine Core Analysis

Subsequent to photographing the core, horizontal core plugs measuring 1 inch in diameter by 2-3 inches long were obtained from the core using a diamond core drill bit and using tap water as a coolant. Core plug ends were cut off to make regular right cylinders using a diamond saw with tap water as a coolant. The core plugs were cleaned using a sohxlet extractor using a methyl alcohol-toluene azeotrope to remove fluids and salts. Plugs were dried at 80°C to a constant weight within  $\pm 0.003$  g. Boyle's Law helium porosity was measured and the *in situ* Klinkenberg permeability measured at a net confining stress of 1,500 psi. **Table 5-1** presents the results of the core analysis.

**Table 5-1.** Summary of core analysis porosity, permeability, and grain density for the Austin #2-27 Lansing-Kansas City core.

Log Depth (ft)	Core Depth (ft)	In situ Klinkenberg Permeability (md)	Routine Helium Porosity (%)	Approx In situ Porosity (%)	Grain Density (g/cc)
2918.3	2919.6	0.0002	0.4	0.4	2.71
2918.8	2920.1	0.19	7.4	7.2	2.71
2919.3	2920.6	1.1	13.8	13.4	2.71
2919.8	2921.1	0.97	17.5	17.0	2.71
<b>2920.4</b>	<b>2921.7</b>	18.4	21.8	21.1	2.71
2921.0	2922.3	39.7	21.6	21.0	2.70
2921.4	2922.7	0.08	23.3	22.6	2.71
2921.6	2922.9	0.065	26.4	25.6	2.71
2922.0	2923.3	0.104	32.9	31.9	2.70
<b>2923.0</b>	<b>2924.3</b>	0.049	31.5	30.6	2.69
2923.1	2924.4	1.294	27.5	26.6	2.71
2923.4	2924.7		25.2	24.4	2.71
<b>2923.8</b>	<b>2925.1</b>	0.044	23.5	22.8	2.71
2924.4	2925.7	0.027	23.7	22.9	2.70
2924.7	2926.0	0.042	25.0	24.3	2.71
<b>2924.8</b>	<b>2926.1</b>	0.036	25.8	25.0	2.72
<b>2925.1</b>	<b>2926.4</b>	0.134	21.9	21.2	2.71
<b>2925.4</b>	<b>2926.7</b>	0.372	17.9	17.3	2.71
2925.8	2927.1	0.056	19.8	19.2	2.71
<b>2926.1</b>	<b>2927.4</b>	0.022	16.0	15.6	2.71
2926.2	2927.5	0.021	22.0	21.3	2.71
<b>2926.5</b>	<b>2927.8</b>	0.016	19.6	19.0	2.70
<b>2928.2</b>	<b>2929.5</b>	0.073	9.9	9.6	2.70
<b>2928.6</b>	<b>2929.9</b>	0.034	3.7	3.6	2.71
<b>2929.0</b>	<b>2930.3</b>	0.081	7.3	7.1	2.71

Grain density measurements confirm that the interval is limestone.

Vertical distribution of porosity in the Austin #2-27 (**Fig. 5-4**) is similar to porosity profiles exhibited by many L-KC wells. Comparison of core-measured and wireline-log-compensated neutron- and density-measured porosity values (run on a limestone matrix) are generally consistent though the core analysis reveals that the interval from 292 to 2923 ft exhibits higher porosity than measured by logs. This difference can be attributed to the larger scale of investigation of the wireline tools.

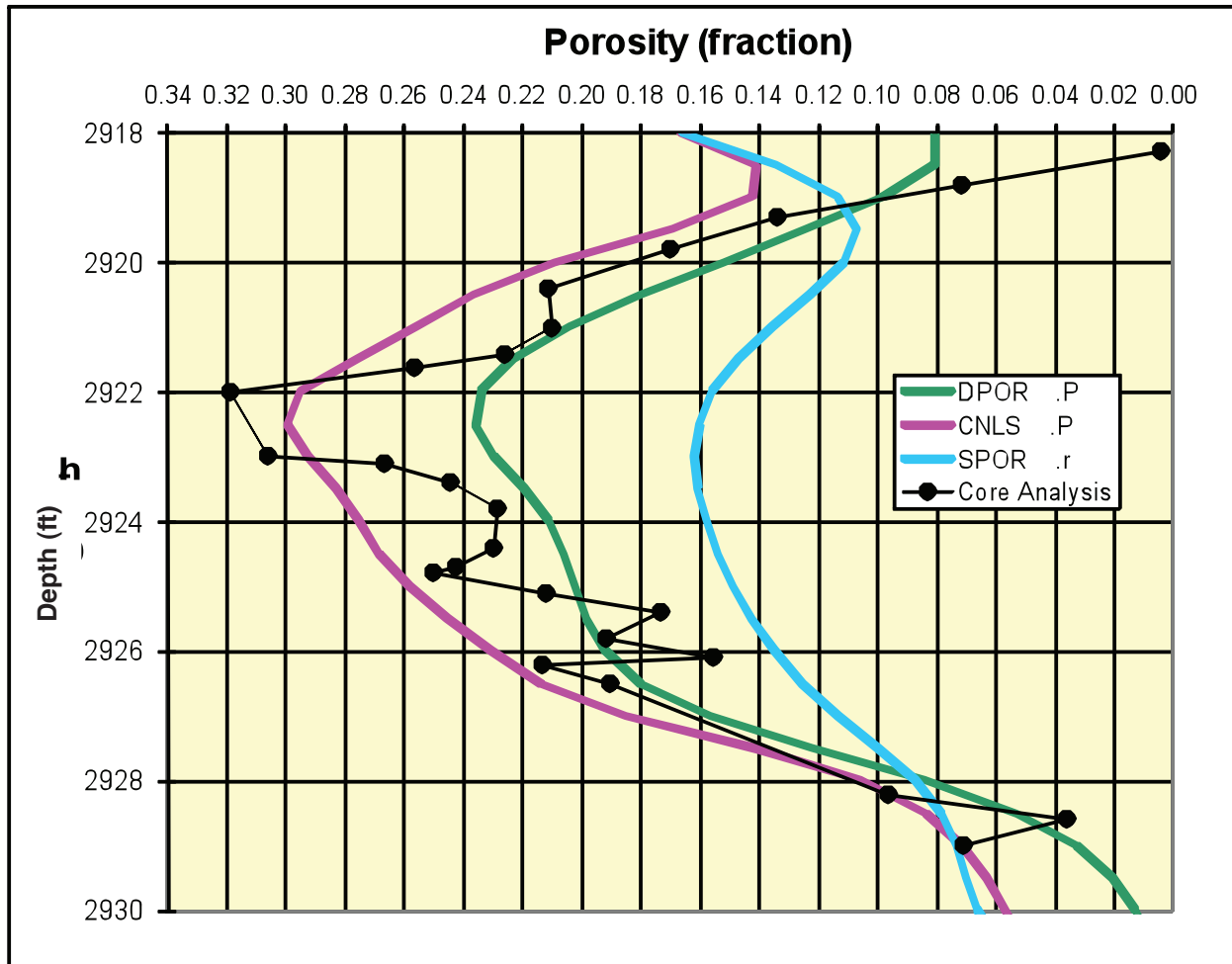


**Figure 5-4.** Porosity profile for the Austin #2-27 through the cored interval of the L-KC BCD zones.

Vertical permeability distribution in the Austin #2-27 shows the upper 2 feet of the L-KC C zone exhibits high permeability but that most of the L-KC interval cored exhibits permeabilities less than 0.1 mD (**Fig. 5-5**). Comparison of the permeability-porosity relationship exhibited by the Austin #2-27 with other L-KC wells (**Fig. 5-6**) shows that the high permeability upper 2 feet of the interval exhibit permeabilities consistent with the maximum permeability-porosity trend for L-KC oomoldic limestones. In contrast, the lower portion of the interval exhibit a permeability-porosity relationship that is below the standard lower limit trend for the L-KC.

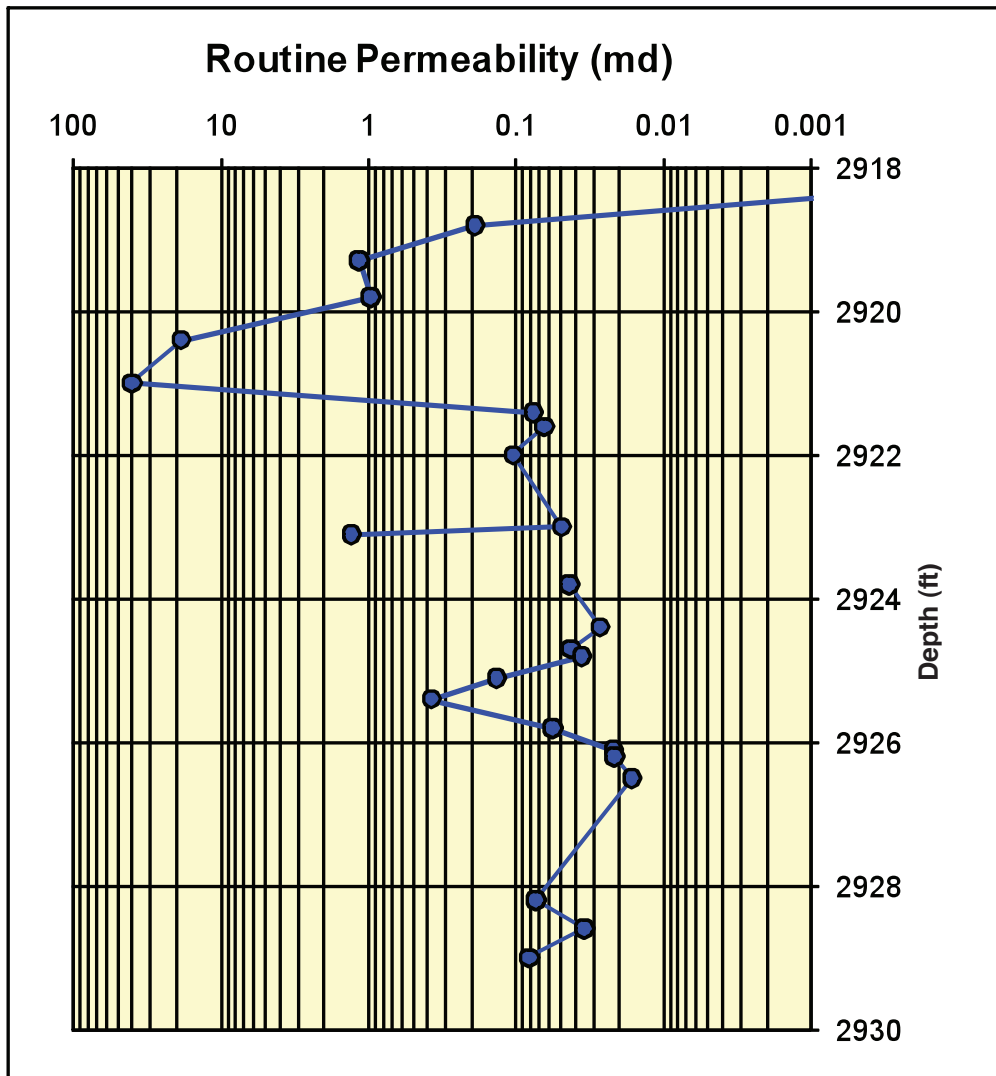


**Figure 5-5.** Permeability profile for the Austin #2-27 through the cored interval of the L-KC BCD zones.

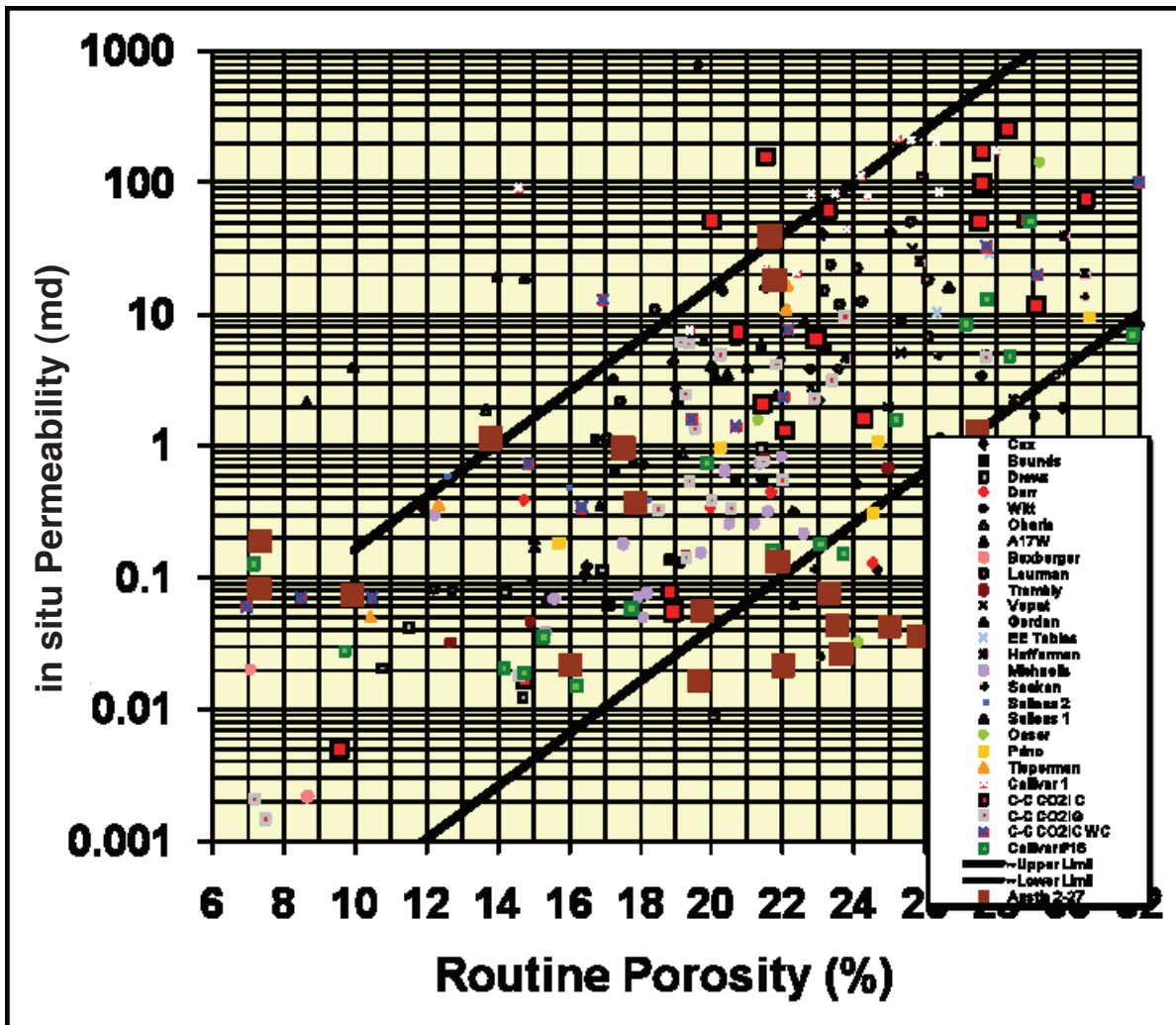
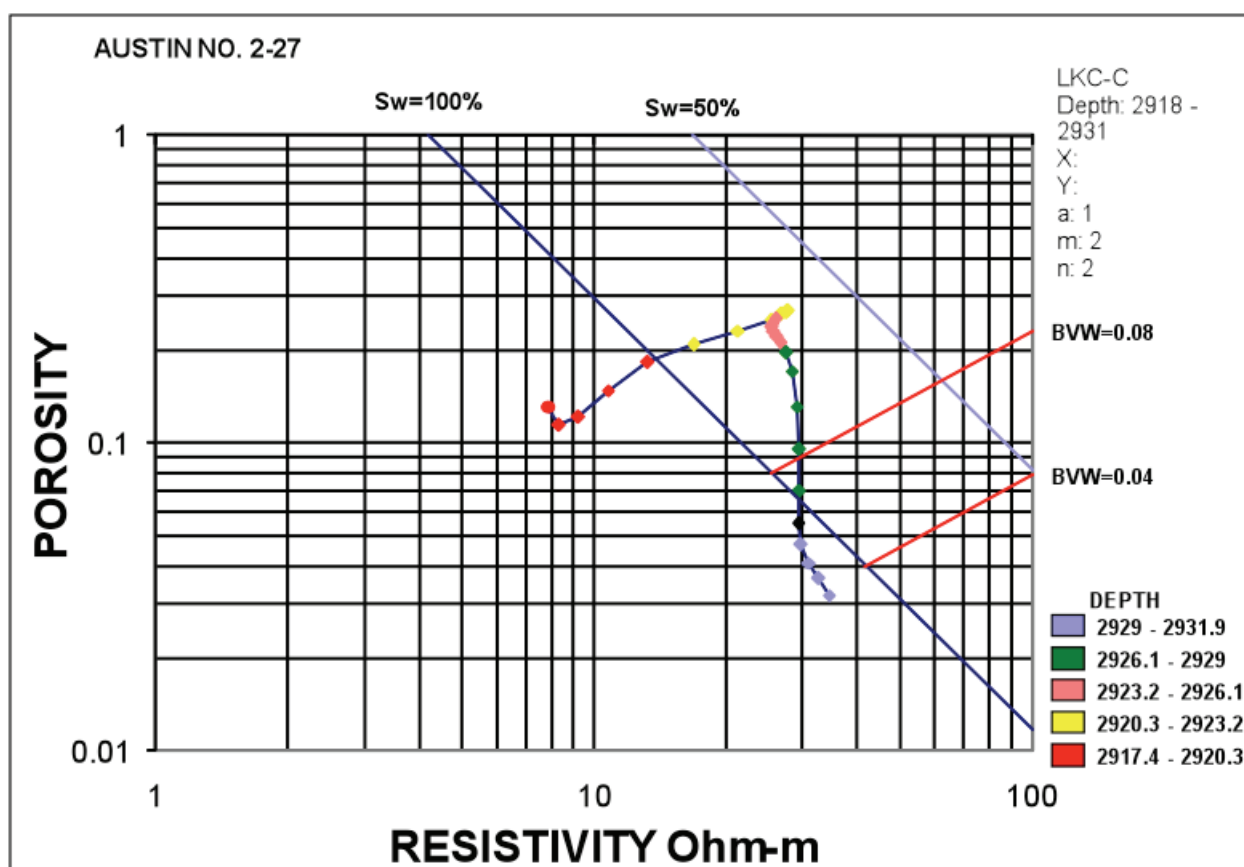


Figure 5-6. Comparison of Austin #2-27 permeability-porosity relationship (brown solid squares) with other Lansing-Kansas City oomoldic limestones across Kansas.

### 5.1.4 Electrical Properties

Previous work (Byrnes et al., 2000; Doveton, 2001; Byrnes et al., 2003) has shown that the moldic porosity in L-KC oomoldic limestones can significantly affect electrical properties and the Archie porosity and saturation exponents. This is also discussed in Section 1. Archie porosity exponent measurements were performed on the core from Murfin Austin #2-27. Standard resistivity log analysis using the Archie parameters of a porosity intercept of  $A = 1$ , porosity exponent of  $m = 2$ , and saturation exponent of  $n = 2$ , indicate the L-KC interval in the Austin #2-27 has low water saturations (Fig. 5-7), averaging  $S_w = 0.25$  between 2,920-2,928 feet. Measurements of the formation resistivity factor and the resulting Archie porosity exponent are shown in Table 5-2. The porosity exponent values measured are significantly different than  $m = 2$  and are consistent with high porosity exponent values exhibited by L-KC oomoldic rocks.



**Figure 5-7.** Pickett plot for Austin #2-27 using standard Archie electrical property parameters of  $a = 1$ ,  $m = 2$ , and  $n = 2$ . Using these parameters the L-KC interval exhibits low water saturation ( $S_{w_{avg}} = 0.24$ ) over the L-KC B interval.

**Table 5-2.** Summary of Archie porosity exponent measurements for the Austin #2-27.

Core Plug I.D.	Core Depth ft	Ambient Porosity %	Approx Ins itu Porosity %	Grain Density g/cc	Formation Resitivity Factor FRF (Ro/Rw)	Archie Cementation Exponent, m at insitu psi	Porosity (%)	log FRF	log In situ Porosity
2	2920.1	7.4	7.2	2.71	375.9	2.25	7.2	2.58	0.85
3	2920.6	13.8	13.4	2.71	293.5	2.83	13.4	2.47	1.13
12	2923.3	32.9	31.9	2.70	141.0	4.33	31.9	2.15	1.50
18	2924.4	27.5	26.6	2.71	163.3	3.85	26.6	2.21	1.43
20	2925.7	23.7	22.9	2.70	151.5	3.41	22.9	2.18	1.36
27	2927.5	22.0	21.3	2.71	166.9	3.31	21.3	2.22	1.33

The Archie porosity exponent and intercept,  $a$ , can either be expressed as a constant porosity exponent with an intercept  $a \neq 1$  or can be expressed as a variable porosity exponent with porosity with an intercept  $a = 1$ . **Figure 5-8** shows the log-log crossplot of formation resistivity factor versus porosity. For this crossplot the Archie  $m$  is the slope of the trendline and the intercept is where the trendline intersects the Y-axis at porosity = 100%. Linear regression analysis for the measured data provides values of  $m = 0.714$  and, solving the linear equation for the intercept at  $\phi = 100\%$ ,  $a = 59.9$ .

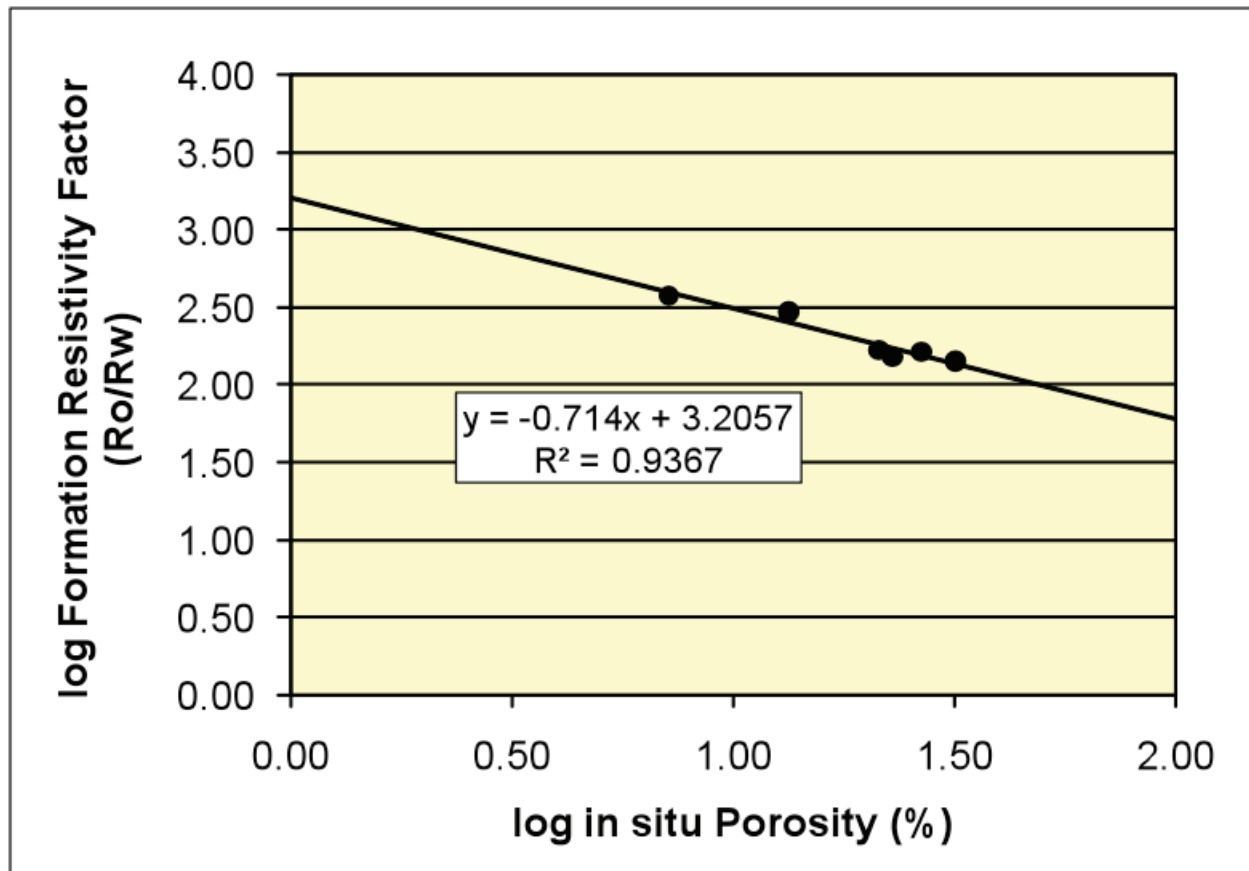


**Figure 5-8.** Crossplot of formation resistivity factor versus porosity for Austin #2-27 shown in Table 5.2. Linear regression analysis provides values for Archie  $m = 0.714$  and  $a = 59.9$ .

Using the alternate method, the Archie intercept can be assigned a value of  $a = 1$  and the slope to each individual value determined to assign the Archie porosity exponent (**Fig. 5-9**). Linear regression analysis between Archie  $m$  and  $\phi$  provides a predictive relationship for estimating Archie  $m$  from measured porosity.

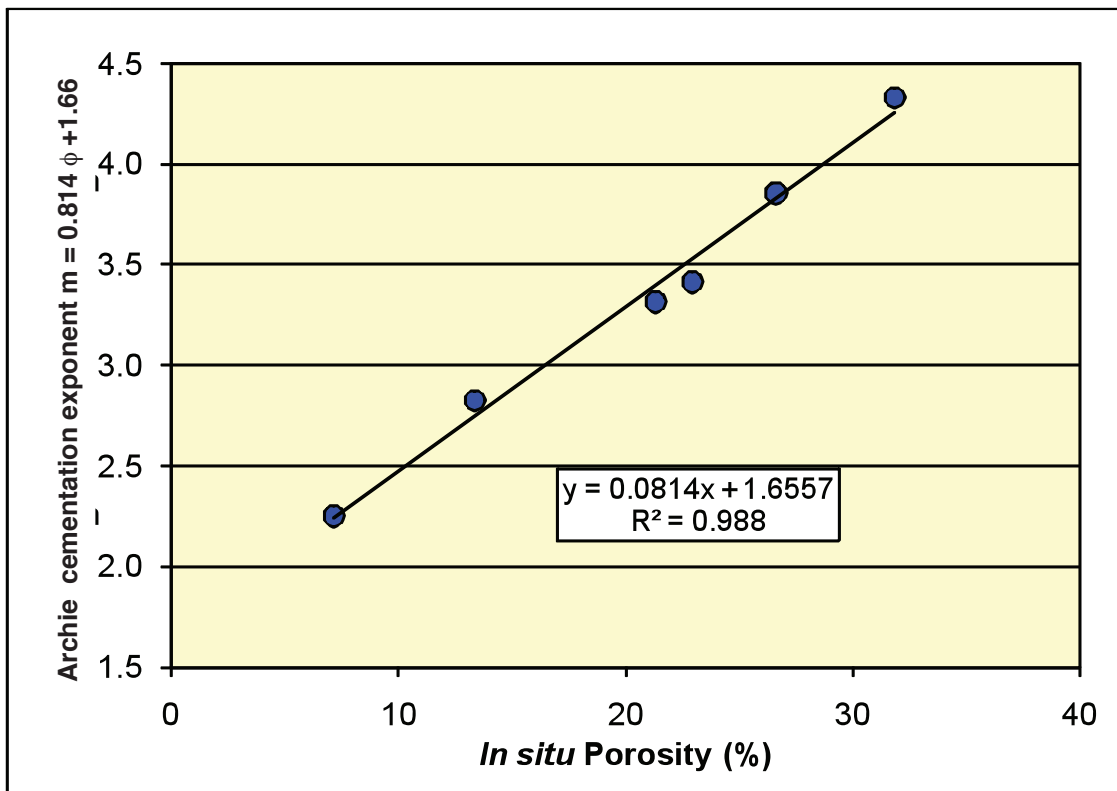


**Figure 5-9.** Crossplot of Archie porosity exponent,  $m$ , versus porosity for Austin #2-27 shown in Table 5.2. Linear regression analysis provides values for Archie  $m = 0.814 \phi + 1.66$ .

Utilizing the Archie parameters in Figure 5.8 to re-analyze the Austin #2-27 L-KC interval, water saturations in the L-KC interval average  $S_w = 0.72$  compared to  $S_w = 0.25$  obtained using standard Archie parameters (**Fig. 5-10**).

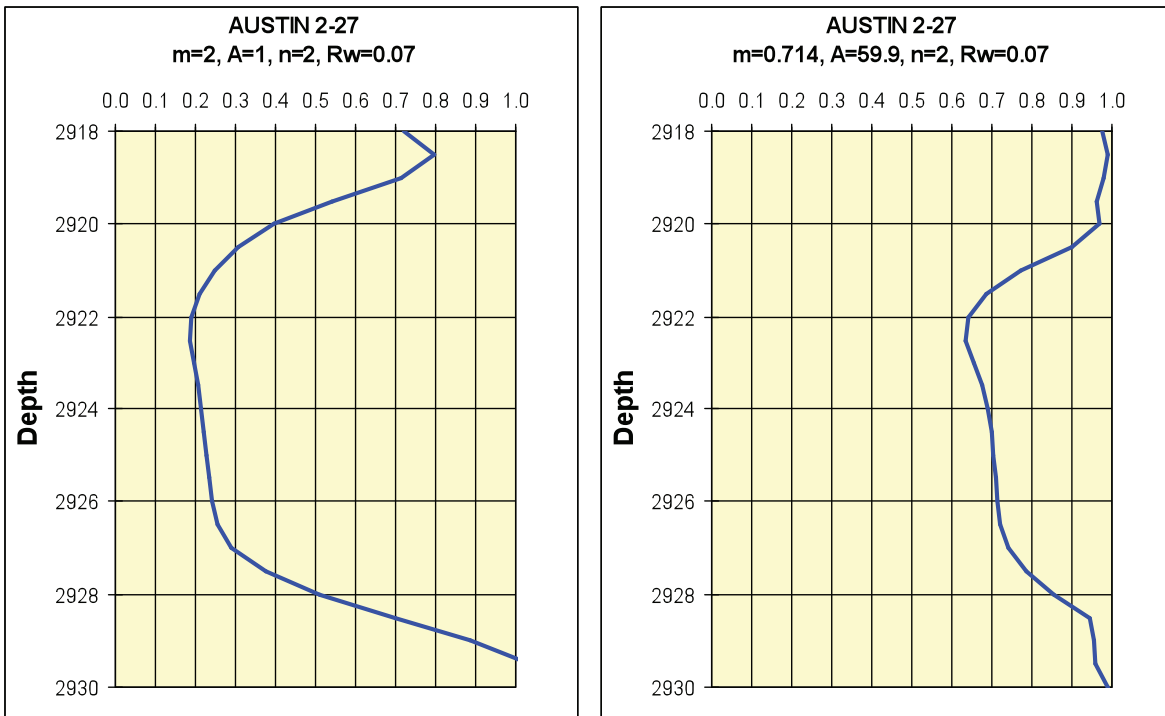


**Figure 5-10.** Comparison of water saturation profiles obtained using the standard Archie parameters and using the Archie parameters measured on the Austin #2-27 core. Average water saturations through the reservoir interval average  $S_w = 0.25$  using standard analysis and  $S_w = 0.72$  using the measured properties.

### 5.1.5 Capillary Pressure Properties

To understand the high and low permeabilities evident in the L-KC C interval, mercury intrusion capillary pressure analysis was performed on two samples. Sample 2921.7 ft exhibits high porosity ( $\phi = 21.1\%$ ) and high permeability ( $K = 18.4$  mD). Sample 2926.1 ft exhibits high porosity ( $\phi = 25.0\%$ ) but low permeability ( $K = 0.036$  mD). **Tables 5-3 and 5-4** summarize mercury intrusion results and **Figures 5-11 and 5-12** illustrate the capillary pressure curves, pore-throat size distribution curves, saturation versus height above free water level, and estimated oil and water relative permeability using Honapour et al. (1995) and Corey (1954) capillary pressure-relative permeability models.

**Table 5-3. Mercury injection capillary pressure analysis for Austin #2-27 2921.7 ft.**

**Mercury Injection Capillary Pressure Analysis  
Austin 2-27 2921.7 ft**

*In situ* Klinkenberg Permeability = 18.4 md  
*In situ* Porosity = 21.1 %

Mercury Injection Capillary Pressure (psia)	Approx. Pore Entry Diameter (um)	Cumulative Wetting Phase Saturation (% pore vol)	Pore Size Distribution Frequency	Cumulative Surface Area (m2/g)	Approx. Gas-Water Height Above Free Water Level (ft)	Approx. Oil-Water Height Above Free Water Level (ft)	Honarpour <i>et al.</i> Imbibition Carbonate		Corey Calculated		
							Oil Relative Permeability (%)	Water Relative Permeability (%)	Oil or Gas Relative Permeability (%)	Water Relative Permeability (%)	Log Oil/Brine Kro/Krw Ratio
2.0	107	100.0	0.0	0.000	0.1	0.1	0.0	100.0	0.0	100.0	-5.0
2.5	86	81.7	18.3	0.001	0.9	0.9	4.2	20.0	0.1	44.6	-2.6
3.3	65	80.2	1.6	0.001	1.1	1.1	5.0	19.2	0.2	41.2	-2.4
4.3	50	77.2	3.0	0.001	1.5	1.5	6.6	17.8	0.3	35.4	-2.1
5.5	39	74.2	2.9	0.001	1.9	2.0	8.4	16.5	0.4	30.3	-1.8
7.2	30	70.6	3.7	0.002	2.4	2.5	10.9	14.9	0.8	24.7	-1.5
9.3	23	64.9	5.6	0.002	3.2	3.3	15.5	12.6	1.5	17.7	-1.1
12.0	18	58.9	6.1	0.003	4.1	4.2	21.4	10.3	2.9	12.0	-0.6
15.5	14	51.4	7.5	0.005	5.3	5.5	29.9	7.9	5.6	6.9	-0.1
20	11	39.6	11.7	0.009	6.9	7.1	46.0	4.7	13.3	2.5	0.7
25	8.6	31.5	8.1	0.012	8.9	9.1	59.2	3.0	22.0	1.0	1.4
35	6.1	25.1	6.5	0.015	11.1	11.4	70.9	1.9	31.7	0.4	1.9
45	4.8	18.3	6.7	0.019	16	16	84.2	1.0	44.7	0.1	2.6
55	3.9	15.4	3.0	0.022	20	21	90.5	0.7	51.5	0.1	3.0
75	2.9	13.7	1.7	0.023	24	25	94.1	0.6	55.7	0.0	3.2
95	2.3	12.3	1.4	0.025	33	34	97.1	0.4	59.4	0.0	3.4
120	1.8	11.6	0.7	0.027	42	43	98.7	0.4	61.3	0.0	3.5
150	1.4	10.8	0.7	0.028	53	55	100.4	0.3	63.4	0.0	3.7
200	1.1	10.6	0.2	0.027	66	69	100.8	0.3	64.0	0.0	3.7
260	0.82	10.2	0.4	0.029	89	91	101.8	0.3	65.2	0.0	3.8
350	0.61	9.9	0.3	0.031	115	119	102.5	0.3	66.2	0.0	3.9
430	0.50	9.5	0.4	0.033	155	160	103.5	0.3	67.4	0.0	3.9
550	0.39	9.0	0.4	0.037	190	196	104.5	0.2	68.7	0.0	4.0
725	0.30	8.5	0.5	0.042	244	251	105.6	0.2	70.2	0.0	4.1
925	0.23	7.9	0.7	0.051	321	331	107.1	0.2	72.2	0.0	4.1
1200	0.18	7.2	0.7	0.063	410	422	108.8	0.2	74.5	0.0	4.1
1550	0.14	6.6	0.6	0.077	531	548	110.2	0.1	76.5	0.0	4.1
2000	0.11	5.9	0.7	0.097	687	708	111.8	0.1	78.7	0.0	4.1
2600	0.08	5.3	0.6	0.119	886	913	113.2	0.1	80.6	0.0	4.1
3350	0.06	4.7	0.7	0.151	1152	1188	114.7	0.1	82.9	0.0	4.1
4300	0.05	3.5	1.2	0.226	1484	1530	117.6	0.0	87.0	0.0	4.1
5550	0.04	2.6	0.9	0.298	1904	1964	119.7	0.0	90.3	0.0	4.1
7200	0.03	1.9	0.7	0.375	2458	2535	121.5	0.0	93.0	0.0	4.1
9300	0.02	1.2	0.7	0.465	3189	3289	123.2	0.0	95.5	0.0	4.1
		1.0	0.3	0.509	4119	4248	123.8	0.0	96.5	0.0	4.1

All Hg calculations assume air-mercury T=484 dyne/cm, contact angle=140deg.

Oil/Gas-Brine Pc assumes insitu o/g-brine Tcos0=	64.0000	22.0000	dynes/cm		
Oil/gas-Brine height assumes o/g density gradient =	0.0866	0.3464	psi/ft	0.01	0.031623
Oil/gas-Brine height assumes brine density gradient =	0.4763	0.4763	psi/ft	0.1	0.316228
Swi assumed for relative permeability =	0.1	0.1	%	1	3.162278
Sorw assumed for relative permeability =	0	0	%	10	31.62278
<i>In situ</i> Gas/Oil & Brine Density (g/cc)=	0.200/0.80	1.1	g/cc	100	316.2278

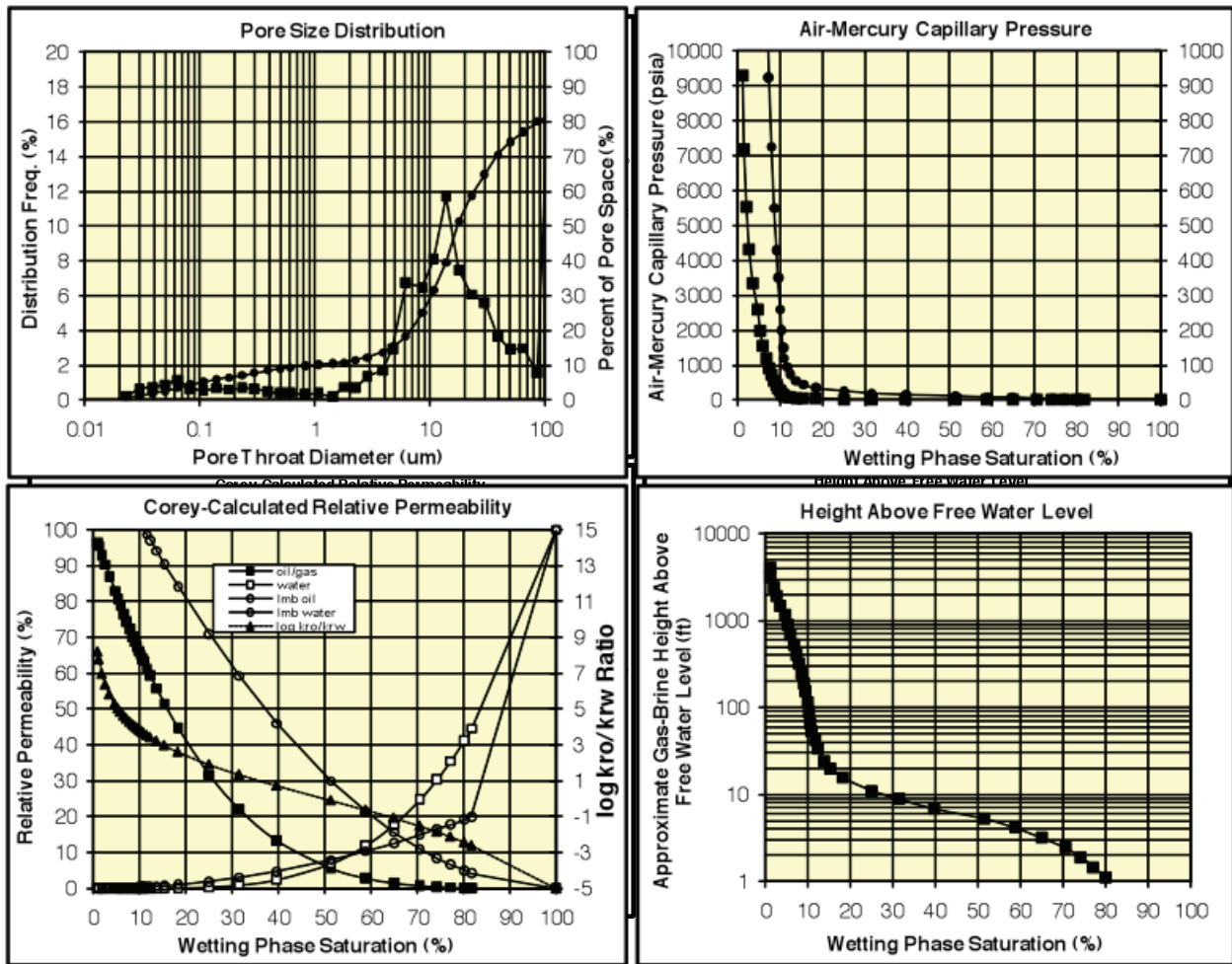


Figure 5-11. Mercury injection derived properties for the Austin #2-27 2921.7 ft oomoldic limestone sample.

**Table 5-4. Mercury injection capillary pressure analysis for Austin #2-27 2926.1 ft.**

**Mercury Injection Capillary Pressure Analysis  
Austin 2-27 2926.1**

*In situ* Klinkenberg Permeability = 0.036 md  
*In situ* Porosity = 25.0 %

Mercury Injection Capillary Pressure (psia)	Approx. Pore Entry Diameter (um)	Cumulative Wetting Phase Saturation (% pore vol)	Pore Size Distribution Frequency	Cumulative Surface Area (m2/g)	Approx. Gas-Water Height Above Free Water Level (ft)	Approx. Oil-Water Height Above Free Water Level (ft)	Honarpour <i>et al.</i> Imbibition Carbonate		Corey Calculated		
							Oil Relative Permeability (%)	Water Relative Permeability (%)	Oil or Gas Relative Permeability (%)	Water Relative Permeability (%)	Log Oil/Brine Kro/Krw Ratio
2.0	107	100.0	0.0	0.000	0.1	0.1	0.0	100.0	0.0	100.0	-5.0
2.5	86	100.0	0.0	0.000	0.9	0.9	0.0	100.0	0.0	100.0	-5.0
3.3	65	100.0	0.0	0.000	1.1	1.1	0.0	100.0	0.0	100.0	-5.0
4.3	50	99.8	0.2	0.000	1.5	1.5	0.0	100.0	0.0	100.0	-5.0
5.5	39	99.6	0.2	0.000	1.9	2.0	0.0	29.9	0.0	99.2	-5.0
7.2	30	99.6	0.0	0.000	2.4	2.5	0.0	29.8	0.0	98.5	-5.0
9.3	23	99.4	0.3	0.000	3.2	3.3	0.0	29.8	0.0	98.5	-5.0
12.0	18	99.4	0.0	0.000	4.1	4.2	0.0	29.7	0.0	97.5	-5.0
15.5	14	99.0	0.4	0.000	5.3	5.5	0.0	29.7	0.0	97.5	-5.0
20	11	98.5	0.5	0.000	6.9	7.1	0.0	29.4	0.0	96.0	-5.0
25	8.6	97.9	0.5	0.001	8.9	9.1	0.0	29.1	0.0	94.0	-5.0
35	6.1	96.2	1.7	0.002	11.1	11.4	0.1	28.8	0.0	92.0	-6.7
45	4.8	94.8	1.4	0.003	16	16	0.2	27.8	0.0	85.7	-5.6
55	3.9	93.0	1.8	0.006	20	21	0.3	27.0	0.0	80.8	-5.0
75	2.9	88.9	4.1	0.012	24	25	0.6	25.9	0.0	74.7	-4.5
95	2.3	80.4	8.5	0.029	33	34	1.6	23.7	0.0	62.4	-3.6
120	1.8	74.1	6.3	0.045	42	43	4.8	19.4	0.1	41.8	-2.5
150	1.4	69.4	4.7	0.045	53	55	8.4	16.4	0.4	30.2	-1.8
200	1.1	64.8	4.6	0.064	66	69	11.8	14.4	0.9	23.2	-1.4
260	0.82	58.6	6.1	0.099	89	91	15.7	12.5	1.5	17.6	-1.1
350	0.61	50.3	8.3	0.161	115	119	21.6	10.3	2.9	11.8	-0.6
430	0.50	42.8	7.5	0.230	155	160	31.2	7.6	6.1	6.4	0.0
550	0.39	30.3	12.5	0.378	190	196	41.2	5.5	10.7	3.4	0.5
725	0.30	21.3	9.0	0.518	244	251	61.3	2.7	23.7	0.8	1.5
925	0.23	15.0	6.3	0.643	321	331	78.2	1.3	38.5	0.2	2.3
1200	0.18	10.3	4.6	0.762	410	422	91.3	0.7	52.4	0.0	3.0
1550	0.14	5.2	5.1	0.932	531	548	101.5	0.3	64.9	0.0	3.8
2000	0.11	2.3	3.0	1.059	687	708	113.4	0.1	81.0	0.0	5.1
2600	0.08	0.9	1.3	1.134	886	913	120.6	0.0	91.6	0.0	6.6
3350	0.06	0.6	0.3	1.159	1152	1188	124.0	0.0	96.8	0.0	8.3
4300	0.05	0.3	0.3	1.183	1484	1530	124.8	0.0	98.1	0.0	9.3
5550	0.04	0.2	0.1	1.192	1904	1964	125.5	0.0	99.1	0.0	10.7
7200	0.03	0.1	0.1	1.210	2458	2535	125.7	0.0	99.4	0.0	11.3
9300	0.02	0.1	0.0	1.213	3189	3289	126.0	0.0	99.9	0.0	14.1
					4119	4248	126.0	0.0	100.0	0.0	15.7

All Hg calculations assume air-mercury T=484 dyne/cm, contact angle=140deg.  
 Oil/Gas-Brine Pc assumes insitu o/g-brine Tcos0= 64.0000 22.0000 dynes/cm  
 Oil/gas-Brine height assumes o/g density gradient = 0.0866 0.3464 psi/ft  
 Oil/gas-Brine height assumes brine density gradient = 0.4763 0.4763 psi/ft  
 Swi assumed for relative permeability = 0.1 0.1 %  
 Sorw assumed for relative permeability = 0 0 %  
*In situ* Gas/Oil & Brine Density (g/cc)= 0.200/0.80 1.1 g/cc

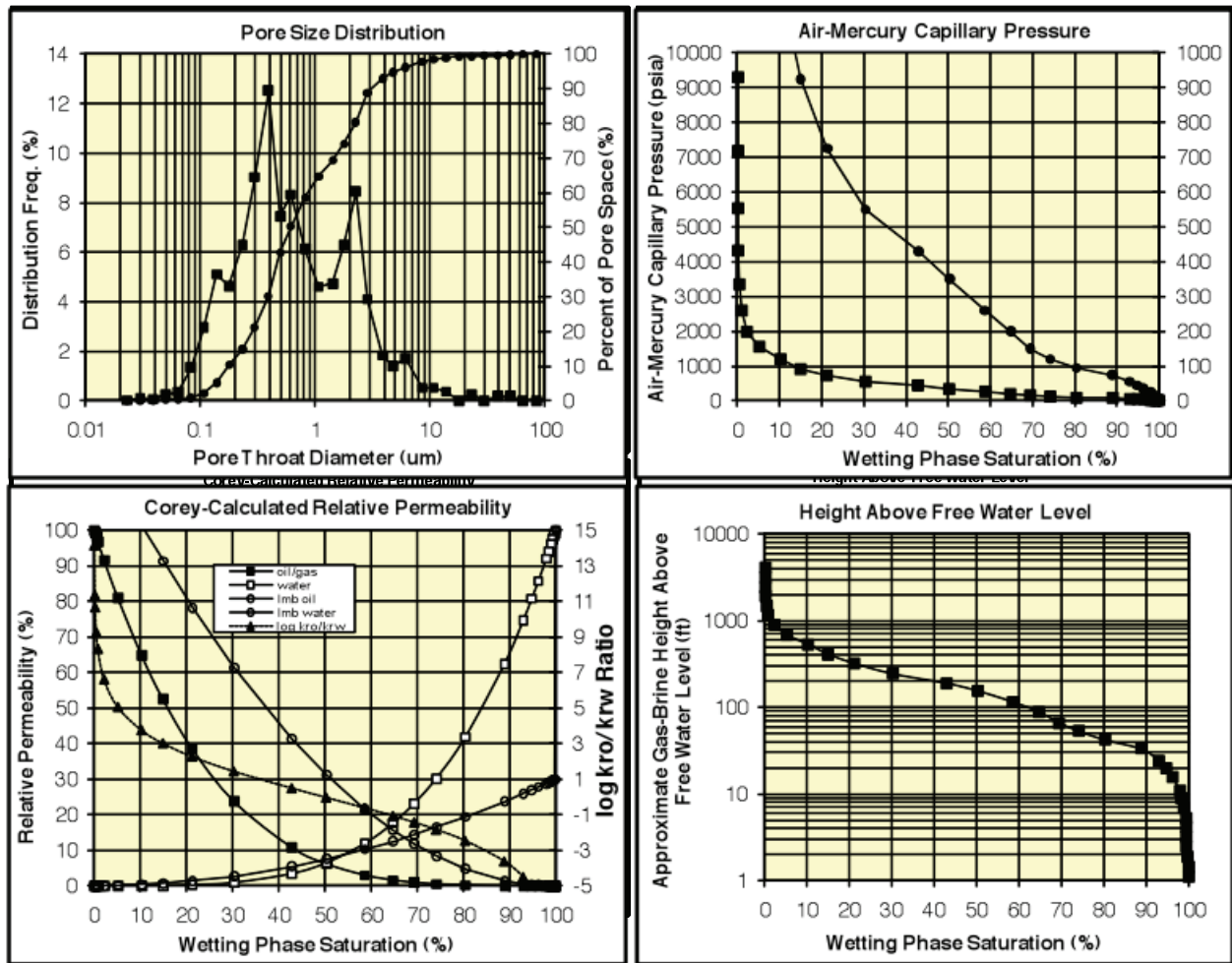


**Figure 5-12.** Mercury injection derived properties for the Austin #2-27 2926. 1-ft oomoldic limestone sample.

The large principal pore throat diameter exhibited by sample 2921.7 ( $D_{ppt} = 14 \text{ mm}$ ) is generally consistent with the higher measured permeability. The smaller principal pore-throat diameter exhibited by sample 2926.1 ft ( $D_{ppt} = 0.39 \text{ mm}$ ) is generally consistent with the low measured permeability.

The log-measured water saturation near  $S_w = 0.72$  are consistent with saturations for 2926.1 ft at approximately 30-50 feet above free water level. This value is consistent with estimated height above free water level for the area. Assuming this height above free water, the capillary pressure data for sample 2921.7 ft indicate this rock should be at a water saturation of  $S_w < 15\%$ . The wireline logs do not show this low a saturation. This difference can be attributed to thin-bed effect and the lack of resolution of the resistivity log to properly resolve saturations at this vertical scale. This is discussed in Section 1.

## 5.2 Arbuckle Core: Keja #1-3, Hadlew Field

### 5.2.1 Well Location, Drilling, and Testing

To obtain a native-state core of the Arbuckle the industry partner in the project, Murfin Drilling Company, selected a location in sec. 3, T. 11 S., R. 21 W., Trego County, KS. This location is within the Hadlew field on the southwestern boundary of Trico field. This well was selected to penetrate the Arbuckle in an area already verified to have Arbuckle production in the Trico field and in the Hadlew Unit #1-3 (API #15-195-22320) drilled 22-Jan-2006 at location 2600'FSL 660'FWL sec.3, T. 11 S., R. 12 W. The Keja #1-3 (API# 15-195-22357-0001) spud on 04/25/2006 at location 1815 ft FSL 850 ft FWL E/2 NW SW sec. 3, T. 11 S., R. 12 W. (**Fig. 5-13 and 5-14**) and cored the Arbuckle on 05/02/2006. Core was obtained for the interval 3,695-3,718 feet when core barrel jammed. Core #2 from 3,719 to 3,776 feet was obtained on 05/03/2006. Figure 5-15 shows that the Arbuckle interval was located at the depth anticipated from the spotting well.

DST#4: 3714-3736 (Arbuckle): 30-60-60-90. IF: wk blow building to 4.5". FF: wk blow building to 3". Rec 150 ft TF, 30 ft O (97%O, 3% M), 30 ft MO (20%M, 80% O), 90 ft SLOCM (90% M, 10%O). HP 1797-1735; FP: 20/55, 58/77; SIP: 576-583. BHT 114°.

DST #5: 3740-3750 (Arbuckle): 30-60-60-90. IF: strong blow BOB in 22 min. FF: strong blow BOB in 25 min. Rec. 60 ft GIP, 405 ft TF, 45 ft WM w/SO (30% W, 70%M) 350 ft MW (80% W, 20% M). 10 ft M. Chl 32,000 ppm, pit 5300 ppm. HP: 1804-1768; FP19/94, 97/208; SIP: 1153-1128. BHT 119°.

Following coring open hole logs were run using the vendor LOG TECH. Open-hole wireline logs obtained on 05/04/2006 included Dual Induction, Gamma Ray, Compensated Neutron, Density, Sonic, and Micro resistivity. Well logs are public domain on the KGS website and can be obtained at [http://chasm.kgs.ku.edu/pls/abyss/qualified.well\\_page.DisplayWell?f\\_kid=1034572508](http://chasm.kgs.ku.edu/pls/abyss/qualified.well_page.DisplayWell?f_kid=1034572508)

Following a period of testing, the well was completed as a gas well 08/17/2006 and later converted to a saltwater-disposal (SWD) well.

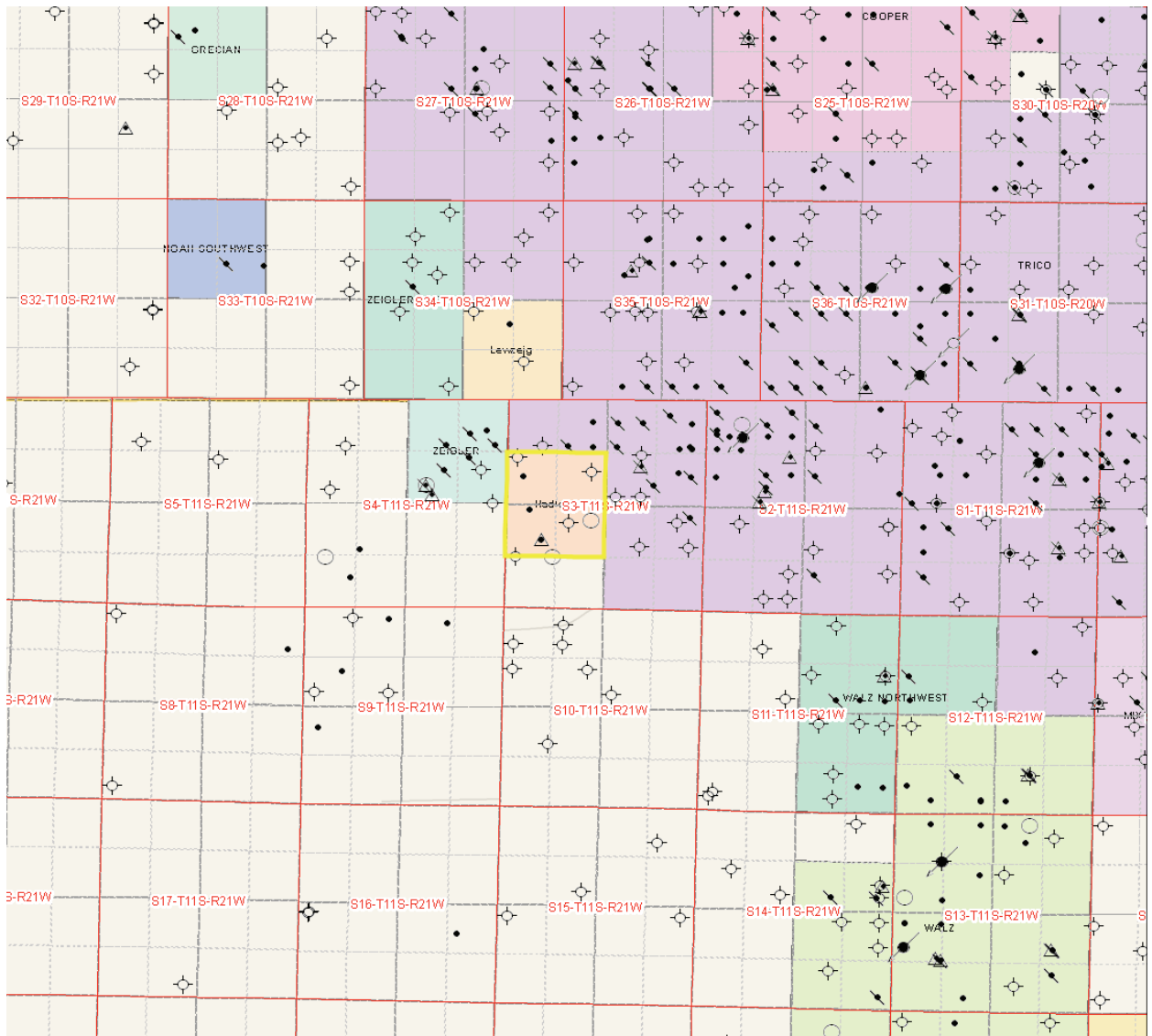


**Figure 5-13.** Location of Murfin Drilling Co. Keja #1-3. Hadlew field is located in center of figure and shown in tan and outlined in yellow. The Keja #1-3 is located at E/2 NW SW sec. 3, T. 11 S., R. 12 W.

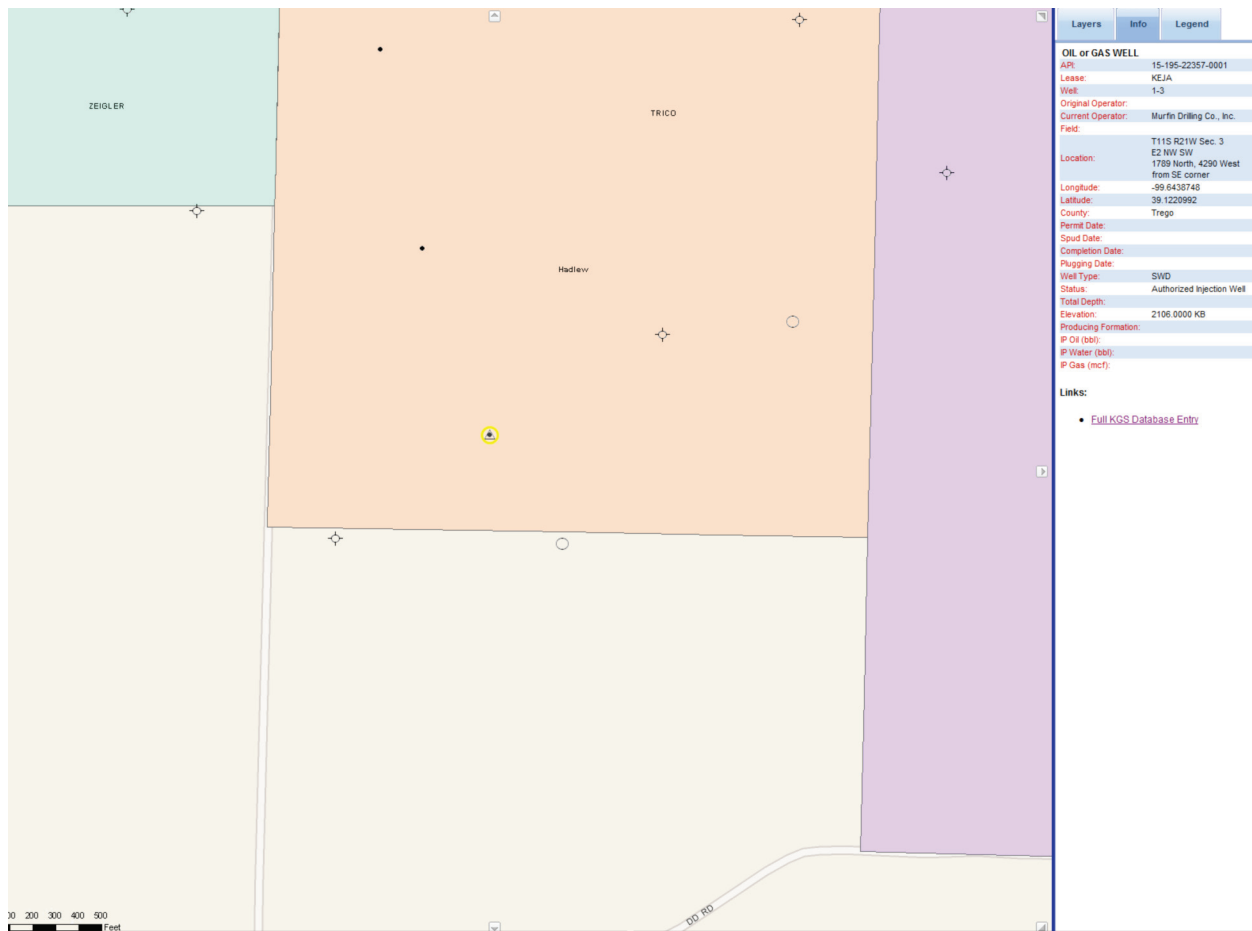


**Figure 5-14.** Location of Murfin Drilling Co. Keja #1-3. Hadlew field is located in center of figure and shown in tan and outlined in yellow. The Keja #1-3 is located at E/2 NW SW sec. 3, T. 11 S., R. 12 W., and is highlighted in yellow.

KEJA #1-3  
 Daily drilling report  
 Page two

- 5/3/06 RTD 3840'. Cut 122'. DT: none. CT: 21 hrs. Dev.: 1° @ 3840'. HC @ 1:00 a.m. **Core #2 3718-3776:** Cut 58' Rec. 58' dolomite, oil shows down to 3750'. Log Tech began logging @ 5:30 a.m., LTD @ 3839'. Will run **DST #4 3714-3736 (Arbuckle):**
- 5/4/06 RTD 3840'. Cut 0'. DT: none. CT: 24 hrs. Log Tech finished logging @ 10:00 a.m. 5/3/06. **DST #4 3714-3736 (Arbuckle):** 30-60-60-90. IF: wk blow building to 4 ½". FF: wk blow building to 3". Rec. 150' TF, 30' O (97% O, 3% M), 30' MO (20% M, 80% O), 90' SLOCM (90% M, 10% O). HP: 1797-1735; FP: 20/55, 58/77; SIP: 576-583. BHT 114°. **DST #5 3740-3750 (Arbuckle):** 30-60-60-90. IF: strong blow BOB in 22 min. FF: strong blow BOB in 25 min. Rec. 60' GIP, 405' TF, 45' WM w/SO (30% W, 70% M) 350' MW (80% W, 20% M). 10' M. Chl. 32,000 ppm, pit 5300 ppm. HP: 1804-1768; FP: 19/94, 97/208; SIP: 1153-1128. BHT 119°. Preparing to run 5 ½" prod. csg.
- 5/5/06 RTD 3840'. CT: 14 hrs. Ran 91 jts. = 3823' of 5 ½' prod. csg. set @ 3826', cmt. w/155 sx. AA-2, plug down @ 5:00 p.m. 5/4/06, port collar @ 1599', 15 sx in RH, 10 MH. Rig released @ 9:00 p.m 5/4/06. FINAL REPORT.

Formation	KEJA #1-3 1815 FSL 850 FWL 2106' KB						Hadlew Unit #1-3 2600' FSL 660' FWL 2111' KB	
	Sample tops	Datum	Ref	Log Tops	Datum	Ref	Log Tops	Datum
Anhydrite	1565	+541	-2	1562	+544	+1	1568	+543
B/Anhydrite	1611	+495	flat	1609	+497	+2	1616	+495
Topeka	3139	-1033	+1	3138	-1032	+2	3145	-1034
Heebner	3347	-1241	-1	3346	-1240	flat	3351	-1240
Toronto	3372	-1266	-3	3366	-1260	+3	3374	-1263
Lansing	3389	-1283	-2	3385	-1279	+2	3392	-1281
BKC	3621	-1515	-2	3620	-1514	-1	3624	-1513
Arbuckle	3700	-1594	+2	3707	-1601	-5	3707	-1596
Total Depth	3840			3839			3850	

**KEJA #1-3**

Operator: Murfin Drilling Company, Inc.  
Contractor: Murfin Drilling Company, Inc.  
Rig #24

Enilas #3196  
1815 FSL 850 FWL  
Sec. 3-T11S-R21W  
Trego County, Kansas

Contact Person: Scott Robinson  
Phone number: 316-267-3241  
Well site Geologist: Terry McLeod

Call Depth: 2700'  
Spud: 4/25/06 @ 4:15 p.m.

API # 15-195-22357  
Casing: 8 5/8" @ 220'  
5 1/2" @ 3826

TD: 3840'

Elevation: 2101' GL  
2106' KB

DAILY INFORMATION:

4/24/06 Move rained out ¾". Will try tomorrow.

4/25/06 MIRT.

4/26/06 Depth 350'. Cut 350'. DT: 8 hrs. (WOC). CT: none. Dev.: ¾" @ 220'. Spud @ 4:15 p.m. 4/25/06. Ran 5 jts. = 211.15' of 8 5/8" surf. csg. set @ 220', cmt. w/160 sx. comm., 2% gel, 3% cc. Plug down @ 8:30 p.m. 4/25/06, drilled out @ 4:30 a.m. 4/26/06, circ. 3 bbls by Allied.

4/27/06 Depth 2200'. Cut 1850'. DT: ¼ hr. (totco). CT: none. Dev.: none.

4/28/06 Depth 2990'. Cut 790'. DT: none. CT: none. Dev.: ½" @ 2246'. **DST #1 3155-3175 (Topeka 30' zone).**

4/29/06 Depth 3210. Cut 220'. DT: 1 ½ hrs. pump. CT: 14 hrs. Dev.: ½" @ 3170'. **DST #1 3155-3175 (Topeka 30' zone):** 30-45-60-60. IF: weak blow ¼" building to 2". FF weak 1" blow. Rec 5' M, 60' WM w/ SO (25%M, 75%M). HP: 1444-1426; FP: 12-32/33-61; SIP 978-948. BHT: 104°. Pipe strap 1.19' long to the board.

4/30/06 Depth 3482. Cut 272'. DT: none. CT: 11 ¼ hrs. **DST #2 3411-3482 (Lansing B,D,E,F):** 30-45-60-60. IF: weak ¼" blow building to 5 ½". FF: weak blow building to bob in 35 min. Rec. 60' GIP, 152' TF, 2' FO, 30' HVOCM (5% G 40% O 55% M), 85' HVOCM w/ tr W (5% G 5% W 25% O 65% M), 30" MW w/ SO (1% O 40% M 59% W), 5' M. HP: 1606-1595; FP: 22-81/75-97; SIP: 590-589. BHT 110°. 70,000 ppm Chl, pit 2,400 ppm Chl. **DST #3 3510-3622 (Lansing H,I,J,K,L)**

5/01/06 Depth 3630. Cut 148'. DT: none. CT: 15 ¾ hrs. Dev.: none. **DST #3 3510-3622 (Lansing H,I,J,K,L):** 30-45-30-60. IF: weak 1" blow throughout. FF: no blow. Rec. 30'M w/ SO. HP: 1666-1650; FP 20-31/33-39; SIP: 793-752. BHT: 107°.

5/02/06 Depth 3718. Cut 88'. DT: none. CT: 18 ¾ hrs. **Core #1 3695-3718:** Cut 23', Rec. 5' sh ,18' dolomite. Core barrel jammed. Good show of oil 3705-3718. Going in the hole for Core #2

RECEIVED  
AUG 18 2016  
KCC WICHITA

KEJA #1-3  
 Daily drilling report  
 Page two

- 5/3/06 RTD 3840'. Cut 122'. DT: none. CT: 21 hrs. Dev.: 1° @ 3840'. HC @ 1:00 a.m. **Core #2 3718-3776:** Cut 58' Rec. 58' dolomite, oil shows down to 3750'. Log Tech began logging @ 5:30 a.m., LTD @ 3839'. Will run **DST #4 3714-3736 (Arbuckle):**
- 5/4/06 RTD 3840'. Cut 0'. DT: none. CT: 24 hrs. Log Tech finished logging @ 10:00 a.m. 5/3/06. **DST #4 3714-3736 (Arbuckle):** 30-60-60-90. IF: wk blow building to 4 ½". FF: wk blow building to 3". Rec. 150' TF, 30' O (97% O, 3% M), 30' MO (20% M, 80% O), 90' SLOCM (90% M, 10% O). HP: 1797-1735; FP: 20/55, 58/77; SIP: 576-583. BHT 114°. **DST #5 3740-3750 (Arbuckle):** 30-60-60-90. IF: strong blow BOB in 22 min. FF: strong blow BOB in 25 min. Rec. 60' GIP, 405' TF, 45' WM w/SO (30% W, 70% M) 350' MW (80% W, 20% M). 10' M. Chl. 32,000 ppm, pit 5300 ppm. HP: 1804-1768; FP: 19/94, 97/208; SIP: 1153-1128. BHT 119°. Preparing to run 5 ½" prod. csg.
- 5/5/06 RTD 3840'. CT: 14 hrs. Ran 91 jts. = 3823' of 5 ½' prod. csg. set @ 3826', cmt. w/155 sx. AA-2, plug down @ 5:00 p.m. 5/4/06, port collar @ 1599', 15 sx in RH, 10 MH. Rig released @ 9:00 p.m 5/4/06. FINAL REPORT.

Formation	KEJA #1-3 1815 FSL 850 FWL 2106' KB						Hadlew Unit #1-3 2600' FSL 660' FWL 2111' KE	
	Sample tops	Datum	Ref	Log Tops	Datum	Ref	Log Tops	Datum
Anhydrite	1565	+541	-2	1562	+544	+1	1568	+543
B/Anhydrite	1611	+495	flat	1609	+497	+2	1616	+495
Topeka	3139	-1033	+1	3138	-1032	+2	3145	-1034
Heebner	3347	-1241	-1	3346	-1240	flat	3351	-1240
Toronto	3372	-1266	-3	3366	-1260	+3	3374	-1263
Lansing	3389	-1283	-2	3385	-1279	+2	3392	-1281
BKC	3621	-1515	-2	3620	-1514	-1	3624	-1513
Arbuckle	3700	-1594	+2	3707	-1601	-5	3707	-1596
Total Depth	3840			3839			3850	

RECEIVED  
 AUG 18 2006  
 KCC WICHITA



**KEJA #1-3  
Completion Report  
Section 3-11S-21W  
Trego County, KS**

Keja #1-3 – Pipe Job

5/04/06 MDC Rig #24 rotated & circ drill pipe f/2 hrs. LDDP. Murray Csg crews drifted 94 jts 5 1/2", 15.5 PPF new L.S. Midwestern Pipeworks range 3 csg. 1 jt would not drift on collar end. RIH w/5 1/2" float shoe, 18.14 shoe jt w/latch dwn insert & 91 jts 5 1/2", 15.5 PPF csg. Tagged btm 3835'. Set btm float shoe 3829.37', insert 3808.23', port collar 1599.62' w/1 basket below port collar. Circulated & rotated 1 hr prior to cementing. RU Jet Star. Pumped 3 BFW, 12 bbl mud flush, 3 BFW, 155 sacks AA2 cmt, 10% salt, 5# sack gilsonite, 8/10% FLA322, 2/10% defoamer, .35% CFR. Displaced cmt w/90 BWF. Rotated to within 10 bbl of landing plug. Plug dwn @ 1500#, held @ 5:00 P.M. Released pressurc, float held. Good circulation when cementing. Cellar stayed full. Landed csg in slips.

Scratchers – 3419-29, 3441-51, 3701-26, 3738—53  
Centralizers – 3808, 3766, 3682, 3554, 3427, 3256, 3129, 2959, 1685, 1221

5/08/06 Backfilled cellar. Brought 8 5/8" connections to surface. Leveled location.

5/11/06 RU Log Tech & portable mast. Ran Sonic Cement Bond Log. TD 3804', T.O.C. 2948', P.C. 1597'

RECEIVED  
AUG 1 8 2006  
KCC WICHITA

Keja #1-3 – Completion Day 1

5/17/06 MIRU #396. MI swab tank. MI 2 7/8" tbg f/Midwestern Pipe Works. Est Cost \$1,500.00.

5/18/06 RIH w/PC tool & 2 7/8" tbg. Found port collar @ 1597'. RU Jet Star. Press test tbg & csg to 1200#, held. Opened port collar. Pumped 180 sx A-con to circ cement to surface. Witnessed by Roger Moses w/KCC. Closed PC. Press test to 1200#, held. Ran tbg to 1730'. Circ clean w/20 BW. TOH w/tbg & PC tool. Est Cost \$11,188.00.

5/19/06 S/D csg to 3400'. RU Log-Tech. Perf 5 1/2" csg @ 3732-34'. 4 SPE\_EHSC. Didn't feel fl going in hole. No show on gun. RIH w/model "R" pkr, SN & 2 7/8" tbg. Set pkr @ 3701' isolating 3732-34'. RIH w/swab. Tag fl 3300' f/surface, 401' FIT, all wtr. Swab dry. Let set 45 min, dry. SDOWE. Est Cost \$14,988.

Keja #1-3 – Completion Day 4

5/22/06 Pkr set @ 3701' isolating 3732-34. Tagged fluid 3450' = 250' FIH, all oil. 2<sup>nd</sup> pull dry. Released pkr & ran dwn to 3738', left hang. RIH w/swab, 75' FIH. RU Kansas Acid. Dumped 1 bbl 15% MCA dwn tbg to spot acid across perf. Set pkr 3701'. Treated w/250 gal 15%. Loaded tbg w/21 1/2 bbls. Pressured to 200#, 5 min 100#. W/2/10 out pressured to 700#, 2 min 600#, 1/2 bbl out feeding 1/4 BPM 500#, 2 bbls out 1/4 BPM 250#. Increased rate to 1.4 BPM 400#. Displaced acid w/24 BW, 1.4 BPM 400#, ISIP 200#, 2 min vac. Let set 45 min. Tagged fluid 800' f/surface, 30 BTL. S/D to 3100' = 600' FIT, rec 43.29 BTF, 1% oil. 1 hr test 6 PPH, FL 3100' = 600' FIT, rec 22.23 BTF, 1% oil. 2<sup>nd</sup> hr 6 PPH FL 3100' = 600' FIT, rec 25.74 BTF, 1% oil. Released pkr. Swabbed acid off backside. Reset pkr. SDON. To cut off 300' of sand line. Est cost \$14,894.

Keja #1-3 – Completion Day 5

5/23/06 Pkr set @ 3701', isolating 3732-34. Tagged fl 1150' f/surface, 1950' overnight fillup, 2251' FIT, trace of oil on top. S/D to 3100' = 600' FIT, rec 38.61 BTF, trace of oil.  
1 hr test 6 PPH, FL 3100' = 600' FIT, rec 25.74 BTF, 1/2% oil.  
2<sup>nd</sup> hr 6 PPH, FL 3100' = 600' FIT, rec 26.91 BTF, 1/2% oil.  
3<sup>rd</sup> hr 6 PPH, FL 3100' = 600' FIT, rec 24.57 BTF, 1/2% oil.  
Released pkr, ran dwn to 3766' & set. RU Swift Services. Loaded tbg, pressured test tbg & pkr to 2000#, held. Pulled pkr to 3636' & set. Loaded backside, pressured to 450#, held & SI. Injection rate on perforation 2 BPM 150#. Mixed & pumped 100 sacks common w/1/2% Halad. In 1<sup>st</sup> 50 sacks displaced w/22 1/4 BSW, max pressure 1900#, ISIP 1800#. SI, washed up pump. Opened tbg, 0# pressured on tbg. Let set 45 min. Loaded w/1/4 bbl. Pressured to 500#, held. Released pressure, dead. Released pkr. Circ 23 BW around pkr. Pulled pkr to 3603' & set. Pressured to 500#, held & SI. SDON. Est cost \$19,912.00

Keja #1-3 – Completion Day 6

5/24/06 Released pressure on tbg. TOH w/tbg & pkr. 2 hrs dwn time to repair spiders. RIH w/new 4 7/8" rock bit (Ser. #C199206) & 2 7/8" tbg. MI & RU mud pump. Tagged cmt 3666'. Pressure test to 500#, held. Drilled to 3751', fell through. Rotated to 3787', circ clean. Pressured to 500#, held. TOH w/tbg & bit. SDON. Est cost \$23112.00



**KEJA #1-3**  
**Completion Report**  
**Section 3-11S-21W**  
**Trego County, KS**

Keja #1-3 – Completion Day 7

5/25/06 Ran csg swab. S/D csg to 3400', 408 FIH. RU Log-Tech. Tag fl 3400', tag btm 3788.5'. Perf Arbuckle (3719-23') w/4 SPF EHSC gun, no show oil on gun. TIH w/pkr, SN, 2 7/8" x 6' sub & 113 jts 2 7/8" tbg. Set pkr 3701', SN 3695'. Ran swab, tag fl 3400', 295 FIH. Made 2 pulls & swabbed dry, rec 2.34 BW. Let set 45 mins. Ran swab, dry, no fl entry. SDON. Set up to acidize 5/26/06. Est Cost 27,416.

Keja #1-3 – Completion Day 8

5/26/06 Ran swab. Dry, no fld entry overnight. RU Kansas Acid to treat perfs: (3719-23') w/ 250 gal. 15% MCA acid containing 3% misc. solv. & 3% surfactant. Released pkr. Spotted 1 1/2 bbls. acid @ 3721'. Set pkr @ 3701'. Tbg. loaded & press. to 200#. Staged to 400# w/ very slow bleed-off. Acid spot was off due to approx. 300' of fluid above pkr. M.D.C wtr. truck loaded annulus w/ 54BW. Released pkr. Pumped 1BW down tbg. Set pkr. @3701'. Staged from 500# to 1000# in 3 hrs. w/ very slow bleed-off. Press. to 1200#. Started feeding w/ .25 BPM rate @ 1000#. .25 BPM @800#. .25 BPM @ 600#. .25 BPM @ 400#. .25 BPM @ 200#. Displaced w/ 21.5 BW. ISIP vac. Total load 27.5 bbls. Released pkr. Pkr. hanging @ 3734'. SN @ 3728'. Ran swab. Tagged FL @ 270' FS. S/D to 2250', 1478 FIH, rec. 80.73BW. Took 1 hr. swab test w/ 6 PPH, FL @ 2300', 1428 FIH. Rec. 33.93 BW w/ a trace of oil. Left pkr. hanging @ 3734'. SIWOE. SDOWE.

Keja #1-3 – Completion Day 9

5/30/06 Pkr hanging @ 3734'. Tagged fluid 1050' f/surface, 2684' FIH, 1250' weekend fillup, all wtr. S/D to 1800', rec 32.76 BTF, 100% wtr. Ran pkr to 3727' & set. Between 3719-23 & 3732-34 perforations. Tagged fluid 1300'. S/D to 2150', rec 51 BTF, no vac on backside. Shot FL on backside. 51 JTF, 1670 FTF. SD f/2 hrs due to thunderstorm & lightning. TOH w/tbg & pkr. TIH w/plug & pkr. Set plug 3727'. Set pkr 3700'. Isolating 3719-23. Tagged fluid 1000' f/surface. S/D to 3500' = 200' FIT. SDON. Est cost \$36,040.

Keja #1-3 – Completion Day 10

5/31/06 Plug 3727', pkr 3700' isolating 3719-23. RIH w/swab. Tagged 1250' f/surface, 2450' FIT, 2250' overnight fillup, all wtr. S/D to 3550' = 150' FIT, rec 19.82 BTF, 100% wtr. TOH w/tbg & tools. RU Log Tech. Perforated 5 1/2" csg @ 3708-12, 4 SPF EHSC. With 170' line left in hole one strand on line broke & balled up on sheave. Took 1 1/2 hrs to cut off broken line. TIH w/plug & pkr. Set plug 3715 & pkr @ 3698', isolating 3708-12. Tagged fluid 950' f/surface. Swabbed dry. Released pkr & left hang. S/D to 2950'. Reset pkr, swabbed dry. SDON. Est cost \$40,740.

Keja #1-3 – Completion Day 11

6/01/06 - Plug 3715', pkr set @ 3698' isolating 3708-12. Tagged fluid 3450' = 248' FIT, 248' overnight fillup, 25' oil on top = 10% oil. 2<sup>nd</sup> pull dry. Released pkr & ran dwn to 3713', left hang. Tagged fluid 3550' = 163' FIH. RU Kansas Acid. To treat w/250 gals 15% MCA w/3% surfactant & 3% solvent. Dumped 2 1/4 bbl 15% MCA to spot acid across perf. Set pkr 3694' isolating 3708-12. Loaded tbg w/21.80 bbl, acid is on btm by 2/10 (over spotted acid by 1 bbl) Pressured to 200# breaking back to 100# in 2 min w/1.10 acid out 200#, 2 min 100#. With 4.00 acid out 200#, 1 min 100#. With all acid out 200#, 1 min 0#, vac in 1 min. Displaced acid w/22 BW, 28 BTL. Let set 15 min. Tagged fluid 250' f/surface. S/D to 3644' = 50' FIT. Rec 25.74 BTF. 1 hr test, 6 PPH, FL 3644' = 50' FIT, rec 1.17 BTF, 20% oil, 1% fines. 2<sup>nd</sup> hr, 6 PPH, FL 3644' = 50' FIT, rec 2.34 BTF, 20% oil, 1% fines, 1 bbl over ld. Released pkr. Swabbed acid off backside & reset pkr. SDON. Est cost \$44,560.

Keja #1-3 – Completion Day 12

6/02/06 Plug 3715', pkr 3694' isolating 3708-12'. Tag fl 1950' f/surface, 1744' FIT, 1690' overnight fillup, 550' oil on top, 31% oil. S/D to 3619' = 75' FIT, rec 14.04 BTF, 22% oil, 8/10% fines. Called f/acid. 1 hr test, 6 PPH, FL 3619' = 75' FIT, rec 3.51 BTF, 25% oil, 1% fines. Released pkr & ran dwn to 3713' & left hang. Tag fl 3550' = 163' FIH. To treat w/500 gal 15% MCA w/3% solvent & 3% surfactant. Dumped 2 1/4 bbl acid to spot across perf. Set pkr 3694'. Took 23.40 to load tbg. Start 4 GPM w/4 bbl acid in, 4 GPM, 75#, 7 bbl acid in, 4 GPM, 100# all acid in, 4 GPM, 125#. Displaced acid w/22 BW, 34 BTL, ISIP 75#, 30 sec vac. Let set 30 min, tag 750' f/surface. S/D to 3300' = 394' FIT, rec 29.25 BTF. 1 hr test, 6 PPH, FL 3375' = 319' FIT, rec 11.70 BTF, 10% oil, 6/10% fines. 2<sup>nd</sup> hr, 6 PPH, FL 3375' = 319' FIT, rec 11.70 BTF, 10% oil, 4/10% fines. 3<sup>rd</sup> hr, 6 PPH, FL 3375' = 319' FIT, rec 10.42 BTF, 10% oil, 4/10% fines. Released pkr & ran dwn to 3713'. Swabbed acid off backside. Reset pkr @ 3694'. Made 1 pull off btm. SDOWE. Est Cost \$49,160.

RECEIVED

## 5.2.2 Core Description

The core description in the drilling report is as follows: **CORE #1 3695-3718:** Cut 23 ft Rec 5 ft sh, 18 ft dolomite. Core barrel jammed. Good show of oil 3705-3718 ft. Going in hole for Core #2. Core#2 3718-3776 ft: Cut 58 ft rec. 58 ft dolomite, oil shows down to 3750 ft. LogTech began logging @ 5:30 a.m.

**Figure 5.14** shows a plain light photograph of the core Examination of the core photo shows that the Arbuckle in the cored interval consists of a vertically heterolithic assemblage stacking of higher- and lower-porosity dolomites generally alternating between mudstones and packstones to pack-grainstones.



Figure 5-15. Murfin Keja #1-3 core photo for Arbuckle interval. Plain light.

### 5.2.3 Routine Core Analysis

Subsequent to photographing the core, horizontal core plugs measuring 1 inch in diameter by 2-3 inches long were obtained from the core using a diamond core drill bit and using tap water as a coolant. Core plug ends were cut off to make regular right cylinders using a diamond saw with tap water as a coolant. The core plugs were cleaned using a sohxlet extractor using a methyl alcohol-toluene azeotrope to remove fluids and salts. Plugs were dried at 80°C to a constant weight within +0.003 g. Boyle's Law helium porosity was measured and the *in situ* Klinkenberg permeability measured at a net confining stress of 1,800 psi. **Table 5-5** presents the results of the core analysis.

**Table 5-5.** Summary of core analysis porosity, permeability and grain density for the Keja #1-3 Arbuckle interval core. Permeability values are color coded for K>10 mD (orange), K < 0.1 mD (blue) and 0.1<K<10 mD (white).

Core Depth (ft)	Routine Helium	<i>In situ</i> Klinkenberg	Grain Density (g/cc)
	Porosity (%)	Permeability (md)	
3705.6	10.9	0.0041	2.76
3708.2	5.3	0.140	2.83
3708.3	7.3	0.702	2.84
3708.5	8.5	3.12	2.85
3709.5	6.5	4.82	3.18
3710.6	8.2	0.243	2.84
3710.7	9.0	0.116	2.84
3711.2	2.0	0.00048	2.83
3711.9	7.2	3.05	2.83
3712.5	10.9	26.4	2.82
3713.4	5.1	0.0035	2.71
3714.4	9.1	38.2	2.71
3714.7	10.6	0.571	2.80
3715.8	5.4	1.25	2.85
3716.7	7.3	0.0688	2.77
3717.5	0.2	0.00017	2.77
3718.3	6.7	3.45	2.80
3720.8	12.4	15.6	2.90
3721.3	3.2	0.0937	2.79
3721.4	7.1	14.9	2.80
3721.6	9.0	1.87	2.89
3722.3	7.7	4.87	2.80
3722.4	18.7	260	2.79
3723.6	8.2	58.2	2.79
3724.3	3.6	0.0016	2.81
3724.4	2.3	0.00020	2.81
3727.8	8.7	0.963	2.80
3727.9	10.0	4.88	2.81
3729.0	7.9	3.60	2.81
3729.6	13.1	29.6	2.82
3730.7	1.7	0.00010	2.83
3732.1	18.7	10.4	2.80
3732.15	7.7	6.39	2.81
3732.2	21.1	297	2.85
3732.4	12.6	124	2.82
3732.5	16.1	248	2.82
3733.4	10.4	2.53	2.81
3733.9	7.4	1.83	2.81
3734.5	7.0	0.278	2.80
3734.8	1.7	0.00010	2.80
3735.4	13.4	110	2.80
3735.6	5.0	0.0519	2.80
3735.9	6.3	0.179	2.78
3736.6	2.4	0.0138	2.81
3738.3	0.9	0.00042	2.80
3739.3	13.1	10.6	2.82
3739.5	13.7	20.6	2.82
3740.5	3.4	0.0103	2.81
3741.5	3.4	0.194	2.78

Grain density measurements confirm that the interval is a limy dolomite to dolomite.

Vertical distribution of porosity in the Keja #1-3 (Fig. 5-15) is similar to porosity profiles exhibited by many Arbuckle wells. The Arbuckle in this well can be characterized as comprising stacked thin peritidal sequences. Each sequence is generally characterized by a low-porosity and low-permeability basal mudstone capped by a coarser-grained more porous and permeable lithofacies.

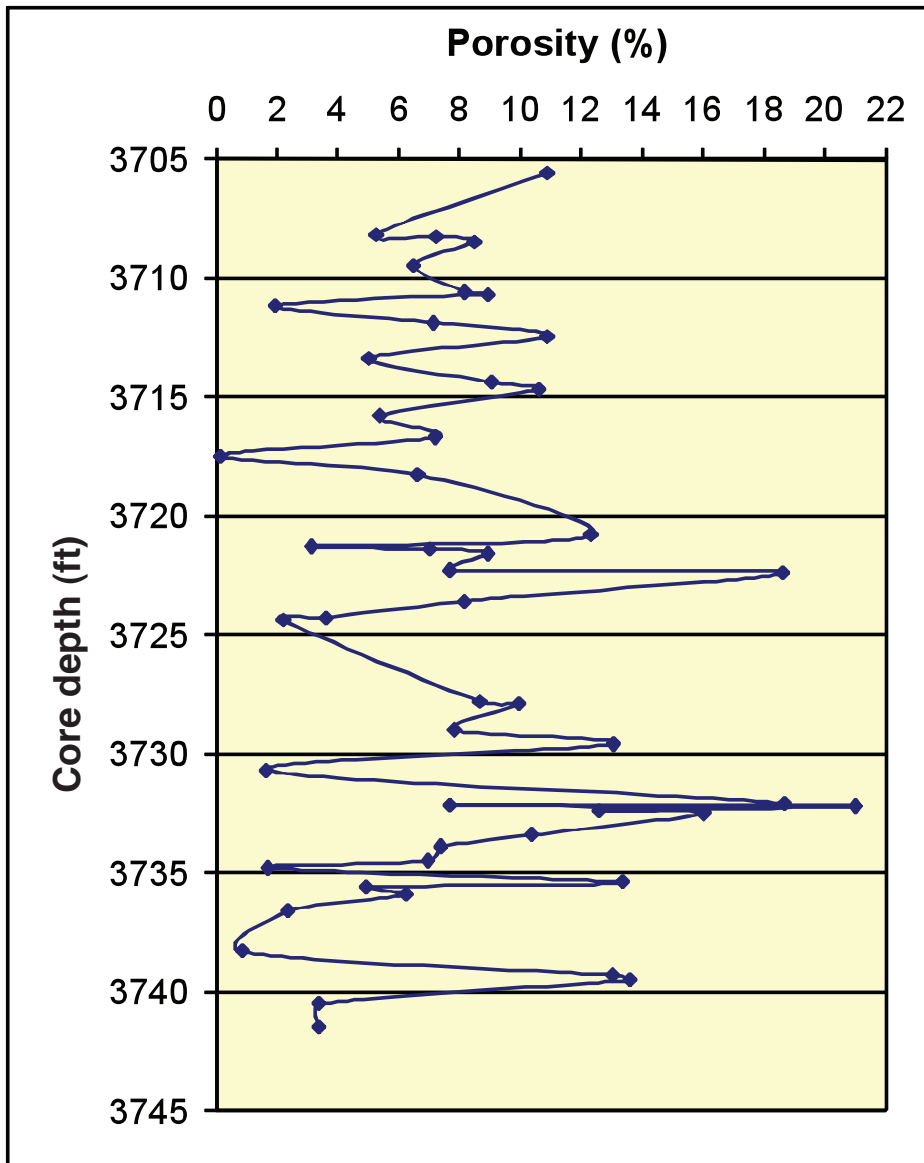


**Figure 5-16.** Porosity profile for the Keja #1-3 through the cored Arbuckle interval.

Vertical-permeability distribution in the Keja #1-3 exhibits thin stacked cycles ranging from 2 to 6 feet thick comprising a basal very low permeability interval ( $K < 0.01$  mD) with permeability increasing upward to a capping high-permeability interval ( $K > 5$  mD) that either is immediately overlain by a very low permeability interval or exhibits an abrupt decrease in permeability with shallowing depths (Fig. 5.16). Comparison of the permeability-porosity relationship exhibited by the Keja #1-3 with other Arbuckle wells (Fig. 5.17) shows that the Keja #1-3 exhibits similar properties to many other Arbuckle wells. Previous work (Franseen et al., 1998; Byrnes et al., 1999) showed that other Arbuckle wells also exhibit the stacked cycles evident in the Keja #1-3.

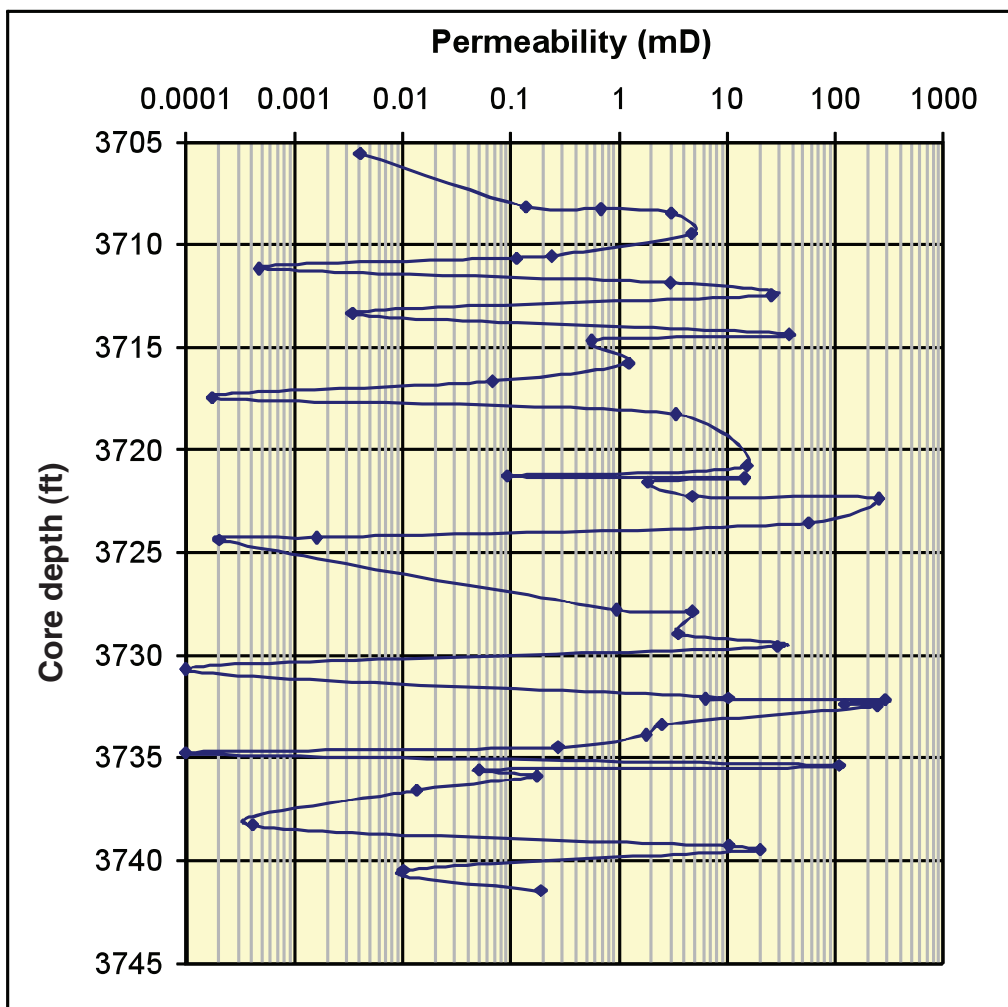


**Figure 5-17.** Permeability profile for the Keja #1-3 through the cored Arbuckle interval showing stacked cycles generally exhibiting upward permeability increase from very low ( $K < 0.01$  mD) to high ( $K > 5$  mD).

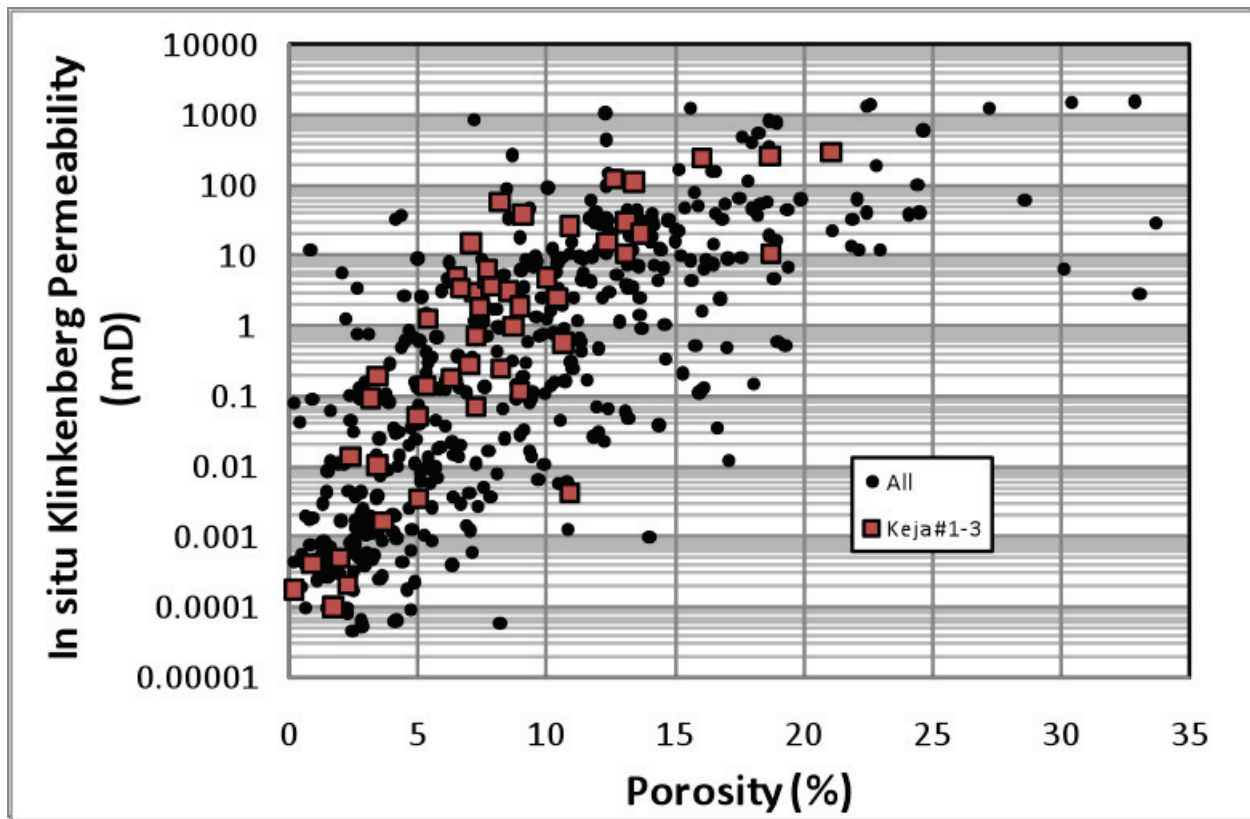


**Figure 5-18.** Comparison of Keja #1-3 permeability-porosity relationship (brown solid squares) with other Arbuckle dolomites across Kansas (black circles).

## REFERENCES

- Anderson, W. G., 1986, Wettability literature survey – Part 1: Rock/oil/brine interactions and the effects of core handling on wettability: *Journal of Petroleum Technology*, Oct. 1986, p. 1125-1144.
- Anderson, W. G., 1986, Wettability literature survey – Part 2: Wettability measurement: *Journal of Petroleum Technology*, Nov. 1986, p. 1246-1262.
- Anderson, W. G., 1986, Wettability literature survey – Part 3: The effects of wettability on the electrical properties of porous media: *Journal of Petroleum Technology*, Dec. 1986, p. 1371-1378.
- Anderson, W. G., 1987, Wettability literature survey – Part 4: The effects of wettability on capillary pressure: *Journal of Petroleum Technology*, Oct. 1987, p. 1283-1300.
- Anderson, W. G., 1987, Wettability literature survey – Part 5: The effects of wettability on relative permeability: *Journal of Petroleum Technology*, Nov. 1987, p. 1453-1468.
- Anderson, W. G., 1987, Wettability literature survey – Part 6: The effects of wettability on waterflooding: *Journal of Petroleum Technology*, Dec. 1987, p. 1605-1622.
- Angulo, R. F., Alvarado, V., and Gonzalez, “Fractal dimensions from mercury intrusion capillary tests,” Paper SPE 23695 (1992): Proc. Second Latin American Petroleum Engineering Conference, II LAPEC, Caracas, Venezuela, March 8-11, 1992, p. 255-263.
- Bear, J., 1968, *Dynamics of fluids in porous media*: Elsevier, New York.
- Bear, J., and Braester, C., 1972, On the flow of two immiscible fluids in fractured porous media: Proc. First Symposium on Fundamentals of Transport Phenomena in Porous Media, Elsevier, New York, p. 177-202.
- Brooks, R. H., and Corey, A. T., 1964, *Hydraulic properties of porous media*: Colorado State University, Hydro Paper No. 5.
- Brooks, R. H., and Corey, A. T., 1966, “Properties of porous media affecting fluid flow”: *Journal of the Irrigation and Drainage Division*, Proc. of the American Soc. of Civil Engineers June 1966, p. 61-88.
- Byrnes, A. P., Franseen, E. K., Watney, W. L., and Dubois, M. K., 2003, The role of moldic porosity in Paleozoic Kansas reservoirs and the association of original depositional facies and early diagenesis with reservoir properties: Kansas Geological Survey, Open-file Report 2003-32, <http://www.kgs.ku.edu/PRS/publication/2003/ofr2003-32/index.html>
- Byrnes, A. P., Watney, W. L., Guy, W. J., and Gerlach, P. G., 2000, Oomoldic reservoirs of central Kansas—Controls on porosity, permeability, capillary pressure and architecture: Kansas Geological Survey, Open-file Report 2000-88, 3 panels.
- Christiansen, R.L., and Heymans, M.J., “Estimating Oil Reserves in Oil-Water Transition Zones,” Paper SPE 59403, presented at the 2000 Asia Pacific Conference on Integrated Modelling for Asset Management, Yokohama, Japan, April 25-26, 2000, 10 p.
- Christiansen, R., Heymans, M. J., Kumar, A., 1999, Transition zone characterization with appropriate rock-fluid property measurements: Proceedings of the Society of Core Analysts Annual Meeting, Aug 1-4, 1999, Golden Colorado, SCA 1999-32.
- Corey, A. T., 1954, “The interrelations between gas and oil relative permeabilities”: *Producers Monthly* (Nov. 1954), v. 19, p. 38-41.
- Corey, A. T., and Rathjens, C. H., 1956, Effect of stratification on relative permeability: *Journal. Pet. Tech. Trans AIME*, v. 69, p 207.
- Craft, B. C., and Hawkins, M., 1991, *Applied Petroleum Reservoir Engineering*, revised by R. E. Terry: Prentice Hall, Englewood Cliffs, NJ.

- Crowell, D. C., Dean, G. W., and Loomis, A. G., 1966, Efficiency of gas displacement from a water-drive reservoir: U.S. Bureau of Mines, Report of Investigations #6735.
- Desbarats, A. J., 1987, Numerical simulation of effective permeability in sand-shale formation: *Water Resources Research*, v. 23, no. 2, p. 273-286.
- DiCarlo, D. A., 1998, The effect of wettability on three-phase relative permeability: Society of Petroleum Engineers, SPE 49137, 8 p.
- Dyes, A. B., 1954, Production of water-driven reservoirs below their bubble point: *Trans. AIME*, v. 201, p. 240-244.
- Doveton, J. H., 2001, Development of an Archie Equation model for log analysis of Pennsylvanian oomoldic zones in Kansas: Kansas Geological Survey, Open-file Report 2001-67, 13 pgs.
- Fanchi, J. R., Christiansen, R. L., and Heymans, M. J., 2002, Estimating oil reserves of fields with oil/water transition zones: *SPE RE&E* (Aug. 2002), p. 311-316.
- Franseen, E. K., 2006, Mississippian (Osagean) shallow-water, mid-latitude siliceous sponge spicule and heterozoan carbonate facies—an example from Kansas with implications for regional controls and distribution of potential reservoir facies; *in*, *Current Research in Earth Sciences: Kansas Geological Survey, Bulletin 252, part 1* (<http://www.kgs.ku.edu/Current/2006/franseen/index.html>)
- Gerlach, P. M., 1998, Maps of pre-Pennsylvanian subcrop, Lansing-Kansas City oil production, and Arbuckle oil production; *in*, *Digital Petroleum Atlas: Kansas Geological Survey, Digital Petroleum Atlas*, <http://www.kgs.ku.edu/DPA/dpaHome.html>
- Heymans, M. J., 1997, A method for developing 3-D hydrocarbon saturation distributions in old and new reservoirs; *in*, *Innovative Applications of Petroleum Technology in the Rocky Mountains Area*, E. B. Coalson, J. C. Osmond, and E. T. Williams, eds.: RMAG, p. 171-182.
- Holmgren, C. R., and Morse, R. A., 1951, Effect of flow gas saturation on oil recovery by waterflooding: *Trans. AIME*, v. 192, p. 135-140.
- Honarpour, M. M., Cullick, A. S., Saad, N., and Humphreys, N. V., 1995, Effect of rock heterogeneity on relative permeability—implications for scaleup: *Journal of Pet. Tech.*, Nov., p. 980-986.
- Keelan, D. K., and Pugh, V. J., 1975, Trapped-gas saturations in carbonate formations: *SPE Journal* (Apr. 1975), p. 149-160.
- King, P. R., 1989, The use of renormalization for calculating effective permeability: *Transport in Porous Media*, v. 4, p. 37-58.
- Kortekaas, T. F. M., 1985, Water/oil displacement characteristics in crossbedded reservoir zones: *Soc. Pet. Eng. Journ.*, Dec., p. 917-926.
- Kyle, J. R., Stanclift, R. J., Jr., Stephan, S. C., Jr., and Rapoport, L. A., 1956, Mechanism of waterflooding in the presence of free gas: *Trans. AIME*, v. 207, p. 215-221.
- Land, C. S., 1968, Calculation of imbibition relative permeability for two- and three-phase flow from rock properties: *SPE Journal*, (June 1968), p. 149-156.
- Land, C. S., 1971, Comparison of calculated with experimental imbibition relative permeability: *SPE Journal*, (Dec. 1971), p. 419-425.
- Lenormand, R., and Thiele, M. R., 1997, Calculation of large scale relative permeabilities from stochastic properties of the permeability field and fluid properties: *Proceedings Fourth International Reservoir Characterization Technical Conference*, Houston, TX, March 2-4, p. 137-139.
- Ma, S. M., Morrow, N. R., Zhang, X., and Zhou, X. 1999, Characterization of wettability from spontaneous imbibitions measurements: *Journal of Canadian Petroleum Technology*, v. 38, no. 13, 8 p.
- Masalmeh, S, and Oedai, S., 2000, Oil mobility in transition zones, SCA 2000-02: *Proceedings of the International Symposium of the Society of Core Analysts*, October 18-20, Abu Dhabi, UAE.
- McCaffery, F. G., and Bennion, D. W., 1974, The effect of wettability on two-phase relative permeabilities: *Journal of Canadian Petroleum Geology*, v. 13, no. 4, p. 42-53.

- Morrow, N. R., 1987, A review of the effects of initial saturation, pore structure, and wettability on oil recovery by waterflooding: North Sea Oil and Gas Reservoirs, Graham and Trotman (eds.), p. 179-191.
- Morrow, N. R., Cram, P. J., and McCaffery, F. G., 1973, Displacement studies in dolomite with wettability control by octanoic acid: Soc. Pet. Eng. Journal, Aug. 1973, p. 221-232.
- Naylor, P., and Puckett, D. A., 1994, In situ saturation distributions—the key to understanding core analysis, SCA1994-05: Proceedings of the International Symposium of the Society of Core Analysts, Sept. 12-14, Stavanger, Norway.
- Owens, W. W., and Archer, D. L., 1971, The effect of wettability on oil-water relative permeability relationships, Journal of Petroleum Technology, July 1971, p. 873-878
- Pickell, J. J., Swanson, B. F., and Hickman, W. B., 1966, Application of air-mercury and oil-air capillary pressure data in the study of pore structure and fluid distribution: SPE Journal, (Mar. 1966), p. 55-61.
- Rasmus, J. C., 1986, A summary of the effects of various geometries and their wettabilities on measured and in situ values of cementation and saturation exponents: Society of Professional Well Log Analysts, 27th Annual Logging Symposium, June 9-13, 1986, Paper PP, 25 p.
- Ringrose, P. S., Jensen, J. L., and Sorbie, K. S., 1996, Use of geology in the interpretation of core-scale relative permeability data: Soc. Pet. Eng. Formation Evaluation, Sept., p. 171-176.
- Stegemeier, G. L., 1974, Relationship of trapped oil saturation to petrophysical properties of porous media: Paper SPE 4754 (1974) presented at Improved Oil Recovery Symposium, Tulsa, Oklahoma, April 22-24, 1974, p. 225-238.
- van Dijke, M. I. J., and Sorbie, K. S., 2001, The effects of wettability on three-phase flow in porous media—basic theory and network modeling results, SCA 2001-36: Proceedings of the International Symposium of the Society of Core Analysts, Sept. 17-19, Edinburgh, Scotland.
- Wang, J. L., Gupta, A., Vaidya, R. N., Bulau, J. R., and Honarpour, M. M., 1997, Prediction of electrical and flow properties of reservoir rocks of varying wettability characteristics, SCA 1997-26: Proceedings of the International Symposium of the Society of Core Analysts, Sept. 7-10, Calgary, Alberta, Canada.
- Warren, J. E., and Price, H. S., 1961, Flow in heterogeneous porous media: Soc. Pet. Eng. Journal, Sept., p. 153-169.
- Watfa, M., and Nurmi, R., 1987, Calculation of saturation, secondary porosity and producibility in complex Middle East carbonate reservoirs, paper CC; *in*, 28th Annual Logging Symposium Transactions: Society of Professional Well Log Analysts, 24 p.
- Watney, W. L., Guy, W. J., and Byrnes, A. P., 2001, Characterization of the Mississippian Osage chat in south-central Kansas: American Association of Petroleum Geologists Bulletin, v. 85, no. 1.
- Weber, K. J., 1982, Influence of common sedimentary structures on fluid flow in reservoir models: Journal of Petroleum Technology, v. 32, p. 665-672.

## **National Energy Technology Laboratory**

626 Cochrans Mill Road  
P.O. Box 10940  
Pittsburgh, PA 15236-0940

3610 Collins Ferry Road  
P.O. Box 880  
Morgantown, WV 26507-0880

One West Third Street, Suite 1400  
Tulsa, OK 74103-3519

1450 Queen Avenue SW  
Albany, OR 97321-2198

2175 University Ave. South  
Suite 201  
Fairbanks, AK 99709

Visit the NETL website at:  
[www.netl.doe.gov](http://www.netl.doe.gov)

Customer Service:  
1-800-553-7681

